Analytical methods for predicting load-displacement behaviour of piles

Thesis submitted for the degree of Doctor of Philosophy in the Faculty of science University of Durham

Salma Fidel Hashem Ali

Mechanics Research Group

School of Engineering and Computing Sciences

Durham University

Abstract

This thesis presents new methods for predicting pile response under different loading and soil conditions. The new methods offer practs engineers with a simple, quick and reliable tool for designing piles and ensuring that both safety and serviceability requirements are satisfied.

In this thesis, an energy-based analytical approach for determining the dynamic response of piles subjected to dynamic loads is presented. The kinematic and potential energies of the pile-foundation system are minimized by a variational principle to obtain the governing equations of the pile-foundation system, along with the appropriate boundary conditions. Comparison with field data demonstrates the success of the new approach for predicting the resonant frequencies of laterally loaded piles.

Energy-based methods are also developed for piles subjected to combined static loading. These methods are formulated for different constitutive models: linear-elastic, non-linear elastic and elasto-plastic models. In addition to energy-based methods, simple similarity methods have been developed to predict pile displacements. In the similarity methods, the load-displacement curve of a pile foundation can be obtained directly by scaling the stress-strain response obtained from a triaxial test on a representative soil sample. Linear scaling factors are presented and extensive verification is carried out against field data, centrifuge models and nonlinear finite element analysis.

Key words: laterally loaded pile, linear elastic soil, axial loaded pile, nonlinear elastic soil, elasto plastic soil, energy method.

Declaration

This thesis submitted to Durham University for Doctor of Philosophy degree. The work described in this thesis was carried out in the School of Engineering and Computing Sciences, under the supervision of Dr Ashraf Osman. I hereby declare that no part of this thesis has been submitted or used for any other degree or other qualification. All of the work shown here is my own unless referenced to the contrary in the text.

Acknowledgements

Firstly, I would like to thank Allah who has enabled me to complete this thesis. I am deeply indebted to Dr Ashraf Osman for his outstanding guidance and encouragement during my studies. I would also like to thank Professor David Toll, and Professor Roger Crouch and for his valuable advice. I would like to express gratefulness to my colleagues Tom Birchall, Asem Alnoaemy and Syazwan.

I gratefully acknowledge my beloved parents, my sisters Mona, Khadija and Fawzia and my brother Ashraf for their love and support.

Finally, my dearest husband Basher and my children deserve the biggest thanks for their encouragement and support.

Contents

List of Figures

List of Tables

Nomenclature

A pile cross section area

A_p area of the pile base

AA constant obtained experimentally

A_s cross-section area of the pile

A_y non dimensional coefficients that relate to applied lateral load H.

a_s area of the pile surface

B foundation width

c cohesion of soil which is equal to zero in sand

D pile diameter

a, b, c and d constants

E_L soil modulus at the tip of the pile

E_p Young's modulus of pile

E_s secant young modulus

E_t tangent young modulus

e length of the pile above the ground level

F free energy

D dissipated energy

H horizontal load

I_p second moment of area

$I_{HM}, I_{MM}, I_{FH}\ and\ I_H$ influence factors.

$I_{UH}, I_{UM}, I_{\theta H}, I_{UF}$ and $I_{\theta M}$ Poulos dimensionless deformation factors for pile in homogenous soil

$I'_{UH}, I'_{UM}, I'_{\theta H}, I'_{UF}$ and $I'_{\theta M}$ Poulos dimensionless deformation factors for pile in non-homogenous soil

I_{hj} factor of displacement due to uniform shear on element j

I_{hb} factor of displacement due to uniform load on the base

G shear modulus of soil

G^* product of $G(1 + 3v/4)$

G_s base shear modulus

k strength gradient with z

k_0 ratio between horizontal effective stress and vertical effective stress

K bulk modulus

K_h coefficient of subgrade reaction

i imaginary number

L pile length

M_0 moment applied to pile at surface

M_u ultimate bending moment in a pile

m rate of increase of soil shear modulus with depth

m^* product of $m\ \left(1+\frac{3}{4}\nu\right)$

m_p pile masses

m_s soil masses

n constants obtained experimentally

n_h rate of increase of soil elastic modulus.

Nc, Nq and N_γ bearing capacity factors

r_0 radius of the pile

r_m magic radius

$p0$ overburden pressure at the base level

P_b load transfer by the base

P_s load transfer by the shaft

P_t axial load on the top of pile

p_j and p_b shear stress on element j and vertical stress on the base

p uniform stress

Q_0 lateral load

Q_u ultimate lateral load

q_b shear stress at the base of pile

$(\Delta q_s)_u$ ultimate bearing capacity

S_{u_0} undrained shear strength at surface

S_u undrained shear strength with depth

T kinetic energy

u lateral displacement of pile at surface

u_r lateral pile- soil displacement in *r* direction

u_θ lateral pile- soil displacement in θ direction

u_z lateral pile- soil displacement in *z* direction

v_r axial pile- soil displacement in *r* direction

v_θ axial pile- soil displacement in θ direction

v_z axial pile- soil displacement in z direction

V vertical load

w settlement at radius r

U_a, V_a and W radial, vertical and circumferential incremental of displacements

U lateral deformation

U_{ef} lateral displacement for fixed head pile

U potential energy

$u_k^{(1)}$, $u_k^{(2)}$, $v_k^{(1)}$ and $v_k^{(2)}$ are the 0^{th} and L^{th} order cosine and L^{th} Order sine harmonic coefficients of variable U_a and V_a

w_b base displacement

w_s settlement of the pile shaft

w_t combined deformation

z_f distance to point of virtual fixity

FDM finite difference method

FEM finite element method

BEM boundary element method

Greek symbols

τ_s shear stress along the shaft pile

γ shear strain

γ' effective unit weight of cohesion less soil

θ rotation deformation for free head pile

υ Poisson's ratio

η geometric coefficient

v_h and v_∞ settlement of the pile in horizontal of any depth h and in semi-infinite mass respectively

ε_f deviator strain

$\gamma_1, \gamma_2, \ldots \ldots and\ \gamma_6$ coefficient of displacements

σ_{ij} stress components

ε_{ij} strain components

ε^p plastic strain

ε^e elastic strain

ϕ_r decay in soil displacement at r direction

ϕ_θ decay in soil displacement at r direction

λ Lame's constant

θ rotation deformation of pile

$\overline{\Delta\lambda}$ deviatoric plastic strain

ρ_s soil density

ω circular frequency

ψ rate of variation of the shear modulus with depth

$\alpha_1, \alpha_2, \alpha_3, \alpha_4$ individual solutions of the differential equations

$\prod$ total energy

1 Introduction

1.1 Introduction

The rising use of both, offshore piles and of high structures such as bridges has increased the importance of the study of the behaviour of laterally loaded piles. Recently, because of rising energy demands there is an increasing use of wind farms and oil platforms. Now there are approximately 3500 oil platforms around the world. In addition the cost of offshore piles is high, perhaps reaching £250,000 for a single wind farm. Generally, the cost varies according to the depth of the installation, Figure 1.1 shows examples of the usage of piles for a wind farm and for an oil platform.

(a)

(b)

Figure 1.1: (a) The Bouri Offshore Field, Libya www.libya.spe.org , (b) Wind farm of Lake Erie, Ohio www.ubergizmo.com

However, offshore foundations are subjected to a combination of environmental forces such as waves, currents, wind and possibly earthquakes. These forces are usually more hostile than those on conventional onshore structures. In the offshore case the lateral load is usually a substantial fraction of the vertical load, and the overturning moment is also very large compared to those found in the design of onshore structures. Furthermore, there is often a major cyclic component of both vertical and horizontal loads. Compared to onshore foundations, offshore foundations are usually very large. Because of this large scale, the variation of soil properties and the depth of the foundation are significant, and need to be accounted for (Reese and Van Impe 2001; Haldar and Sivakumar., 2009; Basu et al., 2008; Basu et al., 2009).

Figure 1.2: Collapse of platform due to hurricane www.offshore-mag.com

Although there is an increasing use of offshore piles, there are many uncertainties associated with their installation and operational performance. For instance, the lateral interaction between soil and pile is complex, since the load-deflection behaviour is non-linear, except in the case of very small loads (Farrell et al., 2000; Gavin et al., 2008; Khemakhem et al., 2010). Also the cyclic nature of the loading makes it even more non-linear as the properties of the soil change during repeated loading.

In the offshore piling industry, the accurate prediction of pile deflection is an one important aim of geotechnical engineers, often carried out using 3D numerical analysis. However, such

analysis is expensive and needs time for computing. Therefore, there is a need for a tool that provides practising engineers with simple and accurate analysis of the performance of piles.

1.2 Aims of the research

The aim of this thesis is to develop simple methods that can be used by engineers to predict pile deformation and failure under different loads to address some of the problems highlighted above. The main objectives of the thesis are as follows:

1. To develop analytical solutions based on an energy approach to predict the deformations of a pile under static and dynamic lateral loads that takes into account the variation of soil stiffness with strain. Then to validate this solution with field data and 3D finite element analysis.
2. To develop other methods (analytical solutions) to calculate deformation under static and cyclic axial, lateral and combined loads for piles.
3. To establish the failure envelopes for piles under combined loads.

1.3 Outlines of the thesis

This research is presented in eight chapters as follows:

Chapter 2 gives brief reviews of the literature concerning the behaviour of a pile embedded in linear soil and nonlinear elastic soil, concentrating on modelling and current methods for pile analysis.

Chapter 3 introduces the analytical solution based on energy method that is used to estimate pile deformation due to static horizontal loads, where the soil behaviour is modelled as linear elastic. This analytical solution is extended to predict lateral load piles and better predictions of the resonant frequency.

Chapter 4 considers the behaviour of a single pile in nonlinear soil subjected to lateral loading, where soil stiffness is assumed to depend on the strain and stress levels. A single pile subjected to lateral cyclic loads is considered in this chapter. The results are successfully validated with previous studies and finite element modelling carried out in this thesis.

Chapter 5 is similar to Chapter 4 in that it considers an analytical solution for an axially loaded pile in nonlinear soil to calculate pile deflection, and cyclic axial load is also considered. Here then the results are validated with 3D finite element analysis, carried out in this thesis and in previous work.

In Chapter 6 a new method to predict pile displacement using triaxial test data is presented, where the load-displacement response can be derived from a stress-strain curve using a simple calculation. This method is far quicker and simpler than 3D numerical analysis. The technique is not intended to replace advanced numerical methods, but to provide a tool which is simple enough to be used in preliminary design calculations, whilst capturing the important influence of soil non-linearity.

In Chapter 7 finite element analysis to estimate the ultimate load of a pile is present. The analysis considers different variations of shear strength with depth and different pile geometries.

Chapter 8 concludes and summarises the calculation of pile deflection due to different types of loading using different methods. Suggestions for future work are given.

2 Literature Review

Introduction

Extensive research has been conducted into pile-soil deformation under different types of loads. Designers of pile foundations have to satisfy two requirements: (i) the pile needs to withstand applied loads without triggering structural or soil failure, and (ii) the induced displacements should not affect functionality of the supported structure. In this chapter, a review is conducted of different existing analytical methods for predicting ultimate collapse loads in foundations, with the emphasis on deep foundations. Different methods for predicting displacements will also be reviewed. This chapter compares different design assumptions with real soil behaviour. Since it is not possible to cover every aspect of soil behaviour, only some of the most important issues are briefly discussed here.

2.1 Predicting ultimate load analyses in foundations

Different solutions related to the bearing capacity of foundations have been developed by researchers. Most of these studies have focused on shallow foundations. For example, the failure envelope of a shallow foundation was calculated by Salencon and Pecker (1995a, 1995b) under static and dynamic loads. They assumed that the shallow foundation is resting on the surface of a homogeneous soil and that it was subjected to an inclined, eccentric load. Such studies have been extended to include different shapes of foundation and different constitutive models for soil (Meyerhof, 1951; Meyerhof, 1953; Shield, 1955; Cox et al., 1961; Brinch Hansen, 1970; Randolph and Puzrin, 2003).

Thirty years ago, significant attention was paid to the vertical bearing capacity of shallow foundations on homogenous soil by considering different shapes of different constitutive models of soil. The shear strength in most of those studied was assumed to increase linearly with depth. The effect of lateral and overturning loads was also reported by many researchers (Davis and Booker, 1973; Houlsby and Wroth, 1983; Bransby and Randolph, 1998; Ukritchon et al., 1998; Bransby et al., 1999; Butterfield and Ticof, 1979; Taiebat and Carter, 2010).

An extensive analysis of strip and circular footings was carried out by Gourvenec et al., (2003) where the surface foundation is subjected to undrained loads (vertical, horizontal or moment). In their study, 2D and 3D finite element analyses were used in order to estimate the bearing capacity. The soil was taken to follow the Tresca model and the undrained shear strength was assumed to vary linearly with depth.

The bearing capacity of offshore foundations has been studied by Bransby and Randolph (1998), Taiebat and Carter (2000), Taiebat and Carter (2002a &b), Gourvenec and Randolph (2003), and Gourvenec and Barnett (2011) where they applied 3D finite element analyses to the problem of offshore circular foundations resting on homogenous and cohesive soil, where the foundations were taken to be fully connected to the soil and were subjected to combined loads. This was extended by Gourvenec (2007) who used finite element analysis to obtain the failure envelope of offshore shallow foundations with peripheral skirts installed into the seabed. The shallow foundation was subjected to combined loading and assumed to be fully connected with the soil. Undrained conditions were assumed. Studies carried out by Houlsby and Puzrin (1999) and Taiebat and Carter (2002a and 2002b) based on finite element analysis assumed the foundation was free to be separated from the soil, and the soils in both studies were taken to be uniform.

2.1.1 Calculation of the ultimate load of a piled foundation

1. Pile subjected to horizontal load

Randolph and Houlsby (1984) developed solutions for a laterally loaded pile embedded in Tresca material. The upper bound and lower bound limit theorems were used to predict collapse loads. Figure 2.1 shows the soil movement around the pile.

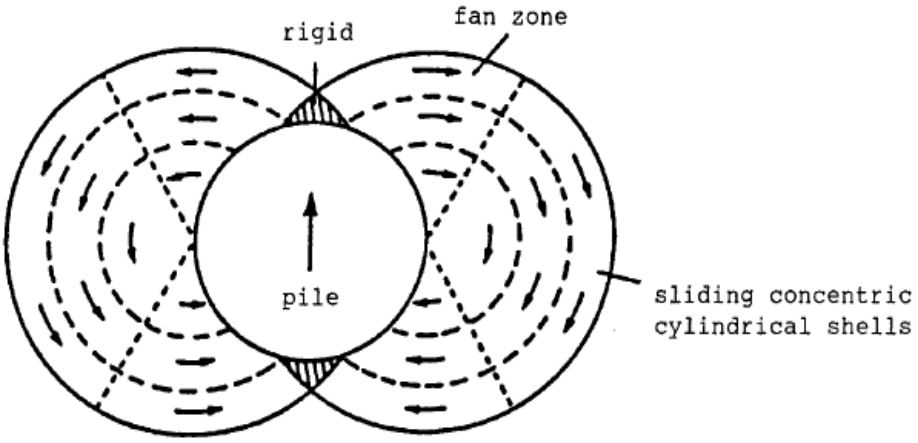

Figure 2.1: Soil movement around pile loaded laterally (Davies, 1987 from Randolph and Houlsby, 1984)

2. Pile subjected to axial load

Kezdi (1975) stated failure of piles depends on many factors such as the shear strength of soil surrounding the pile, the pile geometry and the material of the pile. Lambe and Whitman (1969) assumed that the axial capacity of piles can be calculated as follows:

$$P = P_p + P_s \tag{2.1}$$

where P represents pile capacity, P_p and P_s are pile base and shaft resistances respectively, and

$$P_p = A_p(\Delta q_s)_u \tag{2.2}$$

$$(\Delta q_s)_u = cN_c + \frac{\gamma D N_\gamma}{2} + \gamma d N_q \tag{2.3}$$

$$P_s = \int_0^L \Delta L \, a_s \, S_s \tag{2.4}$$

A_p is area of pile base, $(\Delta q_s)_u$ denotes ultimate bearing capacity, is cohesion term of soil which is equal to zero in sand, ΔL is an increment of pile length, a_s is area of the pile surface in ΔL, d denotes the depth of the base of the pile, N_q and N_γ are dimensionless factors that depend only on friction angle of the soil, D is the pile diameter, γ is the unit weight of the soil and S_s represents unit shaft resistance. Four patterns of failure zones due to axial load assumed by Vesic (1963) are shown in Figure 2.2.

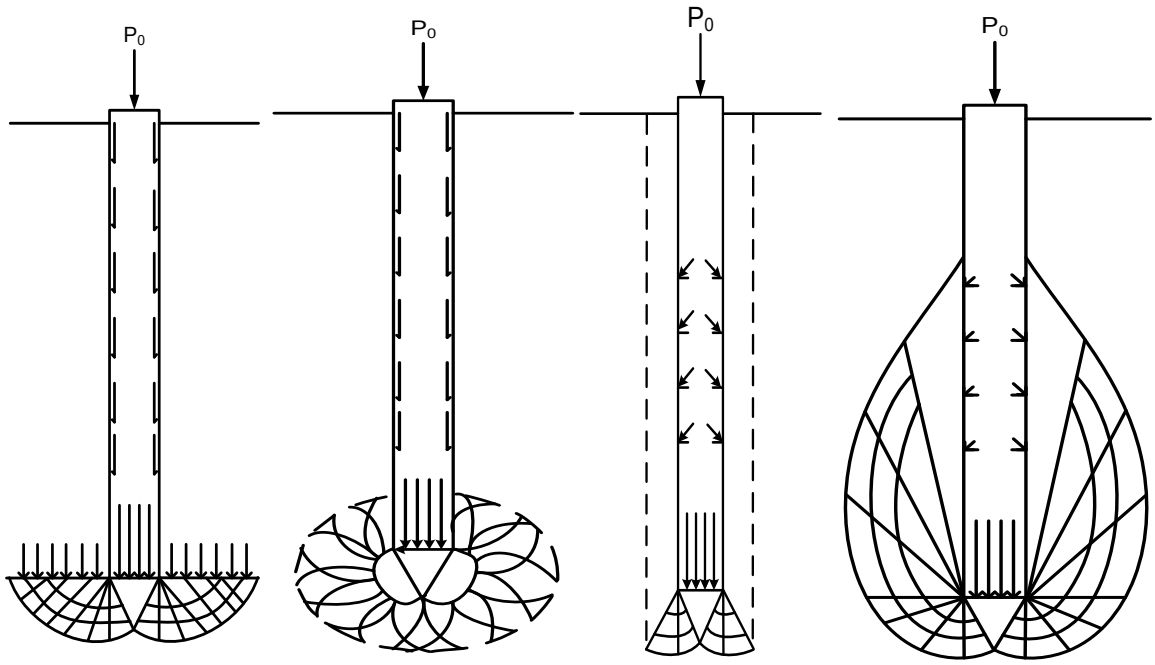

Figure 2.2: Failure mechanism of axial loaded pile (after Davies, 1987 from Vesic, 1963)

2.2 Analytical methods for calculation of pile displacement

2.2.1 Laterally loaded piles

Many researchers have developed methods over the past fifty years to describe the behaviour of elastic foundations subjected to axial and lateral loads. Several authors such as Poulos (1971), Banerjee (1978), Randolph (1981) and Verruijt et al. (1989) have detailed various models that can be used to analyse laterally loaded piles, where the pile can be modelled as a flexible beam. The major difference among these models is how the soil behaviour is treated.

In some analytical methods, the soil is treated as a series of independent non-linear springs, and the simplest model is that produced by Winkler (1867) which considers the soil as a set of springs. Several solutions based on the Winkler method have been reported in the literature (Gieser 1953; Barbar 1953; McClelland and Focht 1956, Matlok and Resse 1961, Wood 1979). The ground is modelled by a series of elastic springs that represent ground deflection, where the spring constant describes the soil's stiffness relative to the acting load. The beam deflection is governed by a linear differential equation of fourth order, where the deflection of the beam, bending moment, displacement and shear force can be obtained by inserting input parameters such as elastic modulus, beam geometry, the load applied and the spring constant of the foundation into the model. The spring constants are determined empirically. These methods are used for both cases of linear homogenous soil and nonlinear heterogeneous soil around the pile. Figures 2.3 and 2.4 show a beam on an elastic foundation and a laterally loaded pile against a bed of springs.

The beam-on-foundation concept has been adopted to apply to piles subjected to lateral loads. The main reason for this is that the pile behaves as a flexible beam when acted upon by lateral load. While the beam foundation can be rotated by 90°, the problem of laterally loaded piles is more complicated due to the nonlinear behaviour of soil in the field, especially near the top of the pile (Matlock et al., 1960; Reese 1971).

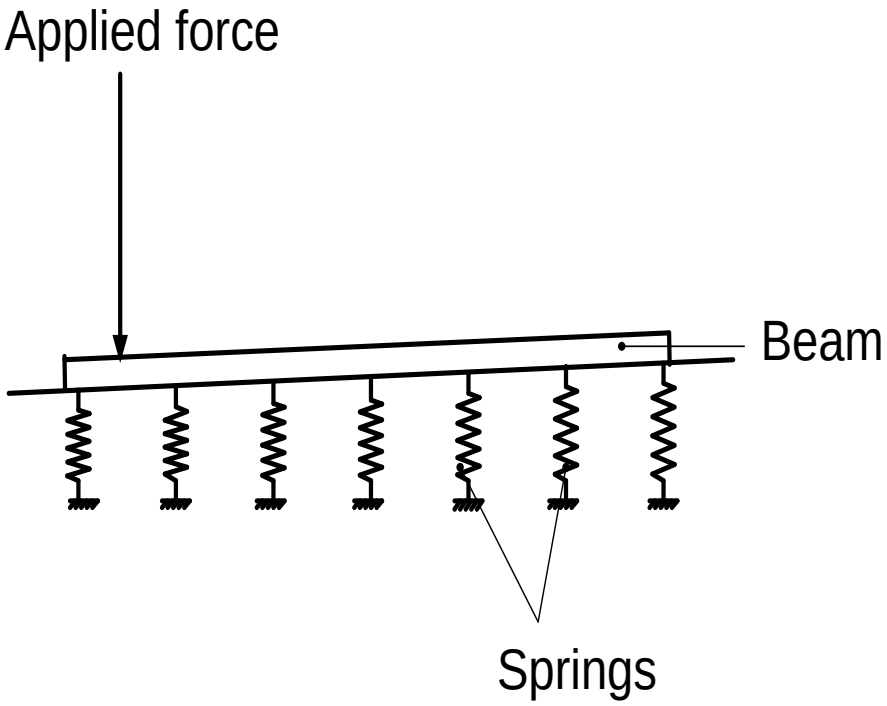

Figure 2.3: Beam on an elastic foundation (Basu et al. 2008)

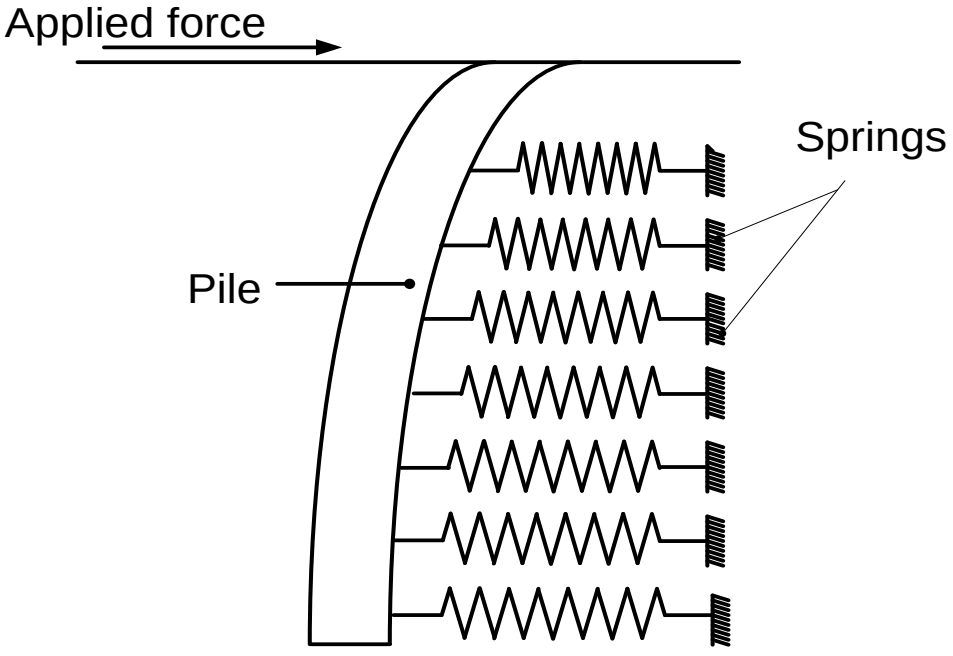

Figure 2.4: Laterally loaded pile in a bed of springs (Basu et al. 2008)

An empirical method has been commonly used to predict pile deformation due to horizontal loads, called the $p - y$ method, which presumes that the pile is an Euler-Bernoulli beam and that the soil works as a series of springs, where p represents the soil resistance and y is the pile deflection. The spring model has been developed to match soil response to actual load-displacement (Cox et al., 1974; Ashour and Norris., 2000; Basu et al., 2009; McGann and Mackenzie-Helnwein, 2011). In the case of three dimensions the $p - y$ method allows the response of the pile to be calculated where the non-linearity of the soil is taken into account (Anderson et al., 1999). Ashour and Norris (2000) developed a method in which there was a division into thin slices and the resistance of the soil was obtained by using the p - y curve for each slice against its deflection. Poulos and Davies (1980), Basu et al. (2008), Fleming et al. (2008), Moller and Christiansen (2011), Huang (2011) and Heidari et al. (2013) all assumed that the $p - y$ curves for a single pile can be developed for use among groups of piles, where the value of p will be reduced due to the interaction between piles leading to reductions in soil resistance.

One of the common approaches for calculating the ultimate displacement due to soil yielding is the beam-on-foundation approach, where the soil is treated as plastic and its lateral capacity can be determined from its resistance (Poulos et al., 1980). Unfortunately, this method fails to predict pile response since the resistance of soil, which is used in the $p - y$ analysis is developed empirically and is fitted to numerical analysis results to meet the field results. The other disadvantage of the p - y curve is that a curve developed for a specific site is not suitable for another site. In other words, each site needs its own p - y curve depending on the properties of the soil there, as well as a load pile test in order to predict lateral pile response accurately. This method is therefore expensive because each site needs a pile load test (Anderson et al., 2003; Basu et al., 2008). An analytical solution based on an energy based method resulting in a set of governing equations and boundary conditions that represent the deformation of pile and soil under static lateral load has been used by Sun (1994) (homogenous soil linear elastic) and Basu et al. (2008, 2009) (multi-layered nonlinear and linear elastic soil). These equations were solved numerically using a finite difference method, while Das and Sargand (1999) used the same method to predict the deformation of a pile in homogenous linear elastic soil under dynamic lateral loads.

In order to predict pile displacement due to lateral load, three approaches can be used: the cantilever method, Winkler's method and the elastic continuum method. The cantilever method was developed by Davisson and Robinson (1965) and Lee (1968), in this method, the soil reaction is ignored and the simple cantilever theory is used to calculate the deformation. For a floating pile (where the base of the pile is free to move under external load, see Figure 2.5a).

$$u = \frac{Q_0\left(e + z_f\right)^3}{3E_p I_p} \tag{2.5}$$

For a clamped pile (where the base of the pile is fixed, see Figure 2.5b)

$$u = \frac{Q_0\left(e+z_f\right)^3}{12E_p I_p} \tag{2.6}$$

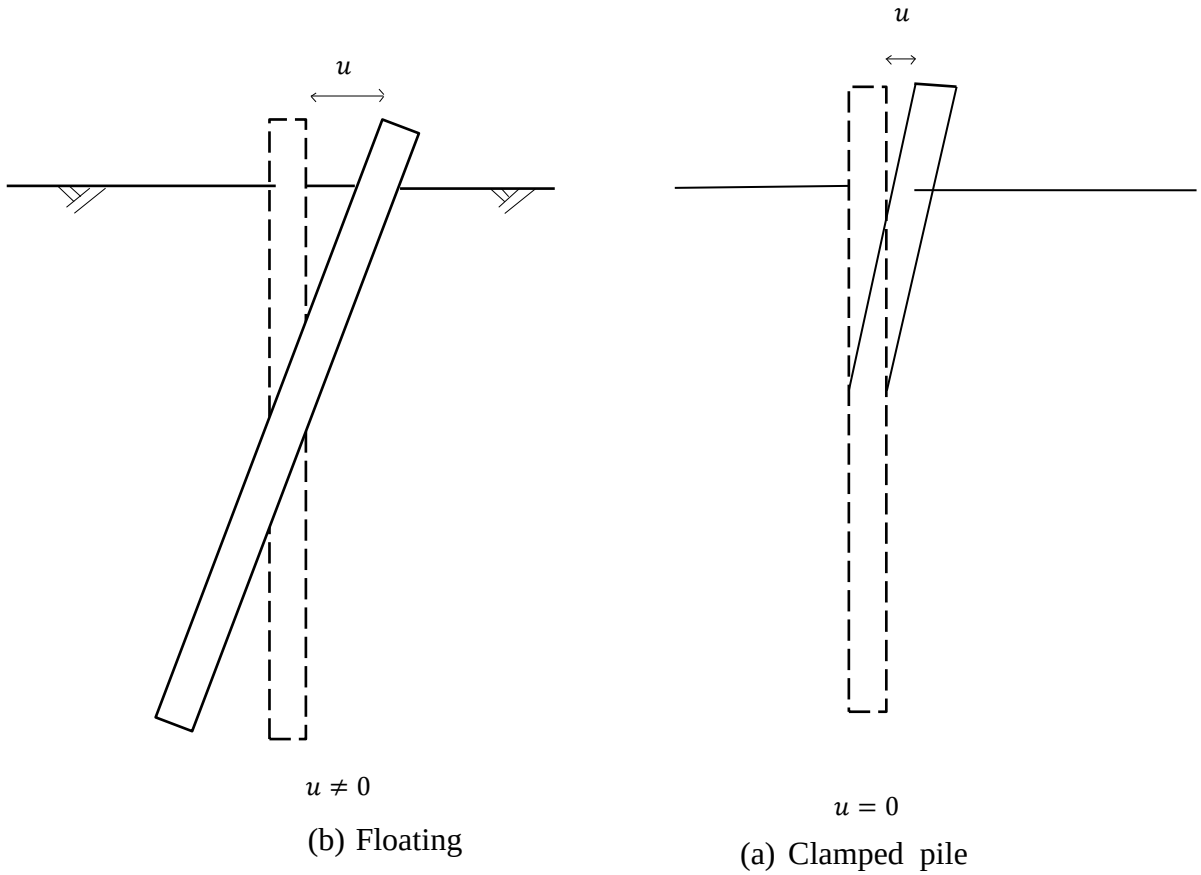

(b) Floating (a) Clamped pile

Figure 2.5: Deformation of rigid pile under lateral load

where e is the length of the pile above the ground level, u represent lateral displacement of the pile, Q_0 represents the lateral load, E_p the elastic modulus of pile, I_p is a second moment of area of pile and z_f is a distance to point of virtual fixity a point at a certain depth below ground surface where the piles are assumed fixed without movement under lateral load. Figure 2.6 shows z_f.

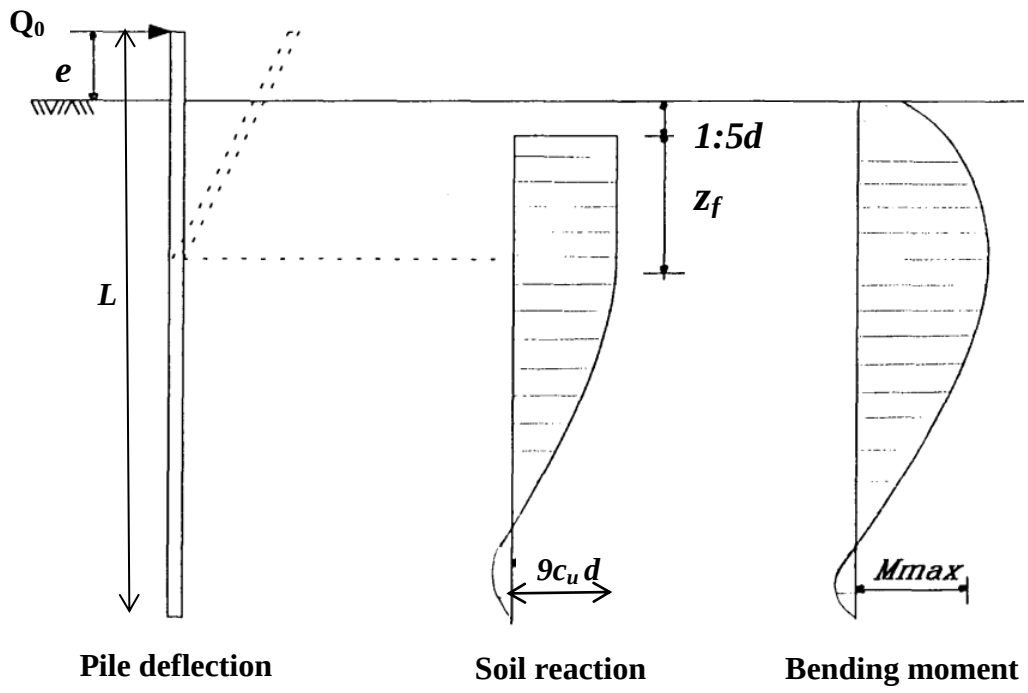

Figure 2.6: Laterally loaded pile (after Broms, 1964a)

In addition to Winkler's approach, several methods which treat the soil as an elastic continuum approach have been developed (Poulos (1971a, b, c, 1974, 1980), Banerjee and Davis (1978), Butterfield and Banerjee (1971) and Randolph (1981)). A summary of some these methods are given below.

- **Poulos's method (1971)**

This method considers the pile as a thin rectangular strip with constant flexural stiffness embedded vertically in a homogenous isotropic semi-infinite elastic medium. The pile is assumed to be fully connected with the soil. The horizontal shear stress between the pile and

the soil is ignored in order to obtain a simple solution. The pile is divided into elements but the top and bottom elements of the pile are not counted. The deformation for all central elements can be described as

$$u = \frac{B}{E_s\, I_s/p} \tag{2.7}$$

where u represents lateral displacement of the pile, p is uniform stress, E_s is elastic modulus of soil, I_s describes the influence factor of dimensionless soil deformation and B is the width of the strip (as mentioned the pile is assumed to be a rectangular strip). Poulos solution can regarded as an extension to Mindlin's solution (1936)[1]The soil here is assumed to be a linear elastic material, and its modulus constant, Poulos predicts free pile head deflection under horizontal load and rotation as

$$u = \left(\frac{Q_0}{LE_s}\right) I_{UH} + \left(\frac{M_0}{E_s L^2}\right) I_{UM} \tag{2.8}$$

$$\theta = \left(\frac{Q_0}{E_s L^2}\right) I_{\theta H} + \left(\frac{M_0}{E_s L^3}\right) I_{\theta M} \tag{2.9}$$

and deformation for a fixed head pile in homogenous soil as

$$u_{ef} = \left(\frac{Q_0}{E_s L}\right) I_{UF}. \tag{2.10}$$

For non-homogenous soil, the displacement of a free head pile can be calculated as

$$u = \left(\frac{Q_0}{n_h L^2}\right)\left(I'_{UM} + \left(\frac{e}{L}\right) I'_{UM}\right) \tag{2.11}$$

[1] Mindlin's solution is the solution for the stresses and displacements in the case of a concentrated force in interior of semi-infinite elastic uniform isotropic solid.

$$\theta = \left(\frac{Q_0}{n_h L^3}\right)\left(I'_{\theta H} + \left(\frac{e}{L^4}\right) I'_{\theta H}\right) \quad (2.12)$$

and for a fixed head pile as

$$u_{ef}{}' = \left(\frac{Q_0}{n_h L^2}\right) I'_{UF} \quad (2.13)$$

where θ is rotation deformation for free head pile, e is the eccentricity of lateral load, u_{ef} is lateral displacement for fixed head pile in homogenous soil, I_{UH}, I_{UM}, $I_{\theta H}$, I_{UF} and $I_{\theta M}$ are Poulos's dimensionless deformation factors for a pile in homogenous soil, L denotes pile length, Q_0 is lateral load and M_0 represents bending moments, $u_{ef}{}'$ is lateral displacement for fixed head pile in non-homogenous soil I'_{UH}, I'_{UM}, $I'_{\theta H}$, I'_{UF} and $I'_{\theta M}$ are Poulos dimensionless deformation factors for a pile in non-homogenous soil and n_h is the rate of increase of soil elastic modulus.

- **Budhu and Davies' Method**

A set of equations to predict lateral deformation of free and fixed head of pile and rotation were developed by Budhu and Davies (1987 and 1988). These analyses are based on the *p-y* method for a laterally loaded pile in elasto-plastic soil. For a free head pile the displacements can be obtained by

$$u = \frac{Q_0}{n_h D^2} I_{UH} + \frac{M_0}{n_h D^3} I_{UM} \quad (2.14)$$

$$\theta = \frac{Q_0}{n_h D^3} I_{\theta H} + \frac{M_0}{n_h D^4} I_{\theta M}. \quad (2.15)$$

The displacement and the moment of a fixed pile head can be calculated by

$$u_{ef} = \frac{Q_0}{n_h D^2} I_{FH} \tag{2.16}$$

$$M_f = -Q_0 D I_{MF} \tag{2.17}$$

where the maximum moment estimated by $M_{max} = I_{MH}\, Q_0\, D$ that occurs at depth $l_m = 0.53\, D\, K^{2/9}$, and $I_{MH} = 0.3K^{2/9}$. I_{UH}, I_{UM}, $I_{\theta H}$, I_{HM} and I_{FH} are influence factors which are calculated as $I_{UH} = 3.2K^{-3/9}$, $I_{UM} = I_{\theta H} = 5.0K^{-5/9}$, $I_{\theta M} = 13.6K^{-7/9}$ and $I_{FH} = 1.4K^{-3/9}$. K is the stiffness ratio of the pile-soil which is calculated as $K = \frac{E_{ef}}{n_h d}$ and E_{ef} is the effective elastic modulus of pile $E_{ef} = \left(\frac{E_p I_p}{\pi {r_0}^4/4}\right)$, where r_0 is pile radius.

- **Randolph's method (1981)**

Randolph derived the response of a laterally loaded pile embedded in homogenous soil using finite element analysis as follows

$$u = 0.25 \frac{Q_0}{G^* r_0} \left(\frac{E_p}{G^*}\right)^{-\frac{1}{7}} + 0.27 \frac{M_0}{G^* {r_0}^2} \left(\frac{E_p}{G^*}\right)^{-\frac{3}{7}} \tag{2.18}$$

$$\theta = 0.27 \frac{Q_0}{G^* {r_0}^2} \left(\frac{E_p}{G^*}\right)^{-\frac{3}{7}} + 0.8 \frac{M_0}{G^* {r_0}^3} \left(\frac{E_p}{G^*}\right)^{-\frac{5}{7}} \tag{2.19}$$

where G is the shear modulus of soil, $G^* = G\left(1 + \frac{3}{4}\nu\right)$, ν is Poisson ratio, M_0 is bending moment. Equations (2.18 and 2.19) were modified to calculate the deformation in non-homogeneous soil for laterally loaded piles as

$$u = 0.54 \frac{Q_0}{m^* {r_0}^2} \left(\frac{E_p}{m^* r_0}\right)^{-\frac{3}{9}} + 0.6 \frac{M_0}{m^* {r_0}^3} \left(\frac{E_p}{m^* r_0}\right)^{-\frac{5}{9}}. \tag{2.20}$$

The rotation deformation for non-homogenous soil can be obtained as

$$\theta = 0.6\frac{Q_0}{m^* {r_0}^3}\left(\frac{E_p}{m^* r_0}\right)^{-\frac{5}{9}} + 1.13\frac{M_0}{m^* {r_0}^4}\left(\frac{E_p}{m^* r_0}\right)^{-\frac{7}{9}} \quad (2.21)$$

where m is the rate of increase of soil shear modulus with depth and m^* is the product of m and $\left(1+\frac{3}{4}\nu\right)$.

- **Banerjee and Davies's Method**

Deformations due to lateral and moments loads on a pile are presented by Banerjee and Davies (1978) using boundary element analysis and the following relationships are obtained;

For free head piles

$$u = \left(\frac{Q_0}{E_s L}\right) I_H + \left(\frac{M_0}{E_s L^2}\right) I_{HM} \quad (2.22)$$

$$\theta = \left(\frac{Q_0}{E_s L^2}\right) I_{HM} + \left(\frac{M_0}{E_s L^3}\right) I_{MM} . \quad (2.23)$$

Displacement of a fixed head pile is given as

$$u = \left(\frac{Q_0}{E_s L}\right) I_{FH} \quad (2.24)$$

where E_s is the soil modulus at the tip of the pile, and $I_{HM}, I_{MM}, I_{FH}\ and\ I_H$ represent the influence factors. The difference between Poulos and Banerjee & Davies's methods is that Poulos used an integral approach while Banerjee & Davies's used boundary element analysis in order to obtain the displacement of pile loaded laterally.

Broms's method

Broms (1964b) suggested two methods to predict the ultimate lateral resistance of soil according to type of soil and geometry and boundary conditions of the pile.

For cohesion-less soil, the ultimate lateral resistance of a soil for a short pile at any depth can be obtained as

$$Q_u = 3\gamma' z K_p \qquad (2.25a)$$

where γ' is the effective unit weight of cohesion-less soil, Q_u is ultimate lateral load K_p can be calculated as $K_p = \frac{1+\sin\emptyset'}{1-\sin\emptyset'}$ and $\emptyset'$ is the effective soil friction angle, this solution is suitable for soil with K_p approximately equal to 3. However, Fleming et al. (1985) presents a solution for the ultimate lateral resistance of soil that is suitable for cohesion-less soil when K_p is greater than 3 as

$$Q_u = {K_p}^2 \gamma'. \qquad (2.25b).$$

Broms (1964b) also suggested a calculation of the ultimate lateral load capacity for rigid free head piles in cohesion-less soil as

$$Q_u = \frac{0.5B\ L^3 K_p \gamma'}{e + L} \qquad (2.26)$$

For rigid fixed head piles as

$$Q_u = 1.5\ B\ \gamma\ L^2 K_p \qquad (2.27)$$

For flexible free head piles as

$$Q_u = \frac{M_u}{e + z_f} \tag{2.28}$$

and for flexible fixed head piles as

$$Q_u = \frac{2M_u}{e + z_f}. \tag{2.29a}$$

The lateral deflection can be obtained from the relationship

$$P_u = k_h u \tag{2.29b}$$

where k_h is the modulus of horizontal subgrade reaction and u is the lateral displacement, z_f is equal to 1.5 for granular soil or stiff clay and 3 for soft clay and silt from surface level, Broms (1981) then suggested an alternative solution to obtain the maximum moments and lateral resistance in cohesive soil for a free head rigid pile as follows

$$M_{max} = Q_0(e + 1.5B + 0.5f) \tag{2.30}$$

and for a fixed head rigid pile as

$$Q_u = \frac{2M_u}{1.5B + 0.5f} \tag{2.31}$$

The ultimate moments and lateral resistance in a cohesion-less soil for a flexible free head pile is

$$M_{max} = Q_0(e + 0.67f) \tag{2.32}$$

For a flexible fixed head pile the ultimate load is

$$Q_u = \frac{2M_u}{e + 0.54\sqrt{\frac{Q_u}{\gamma B K_p}}} \tag{2.33}$$

where f defined as $f = 0.82\sqrt{\frac{Q_0}{\gamma B K_p}}$.

Based on these relations Broms (1981) presented a chart to obtain ultimate moment and lateral resistance of soil.

Guo (2009) developed a closed-form solution to calculate the lateral displacement of a single pile and group of piles embedded in elasto-plastic soil. This solution was based on the uncoupled (plastic zone) and coupled (elastic zone) load transfer models (see Figure 7a), based on a model which developed by Guo (2006). Guo (2009) assumes that the soil modulus and limiting force profile between pile and soil linearly increases with depth. A load transfer model was used in the elastic state to predict the load-displacement response by adopting a simplified displacement field that results in the simplified stress field derived by Guo and Lee (2001) where the radial stress is assumed to be given by:

$$\sigma_{rr} = 2G_s u \frac{\gamma_b}{r_0} \frac{K_1(\gamma_b r/r_0)}{K_0(\gamma_b)} \cos\theta. \tag{2.34}$$

In this solution $\sigma_{\theta\theta}$ and σ_{zz} assumed to be zero, where $\sigma_{rr}, \sigma_{\theta\theta}$ and σ_{zz} are radial, tangent and vertical stresses respectively, G_s is soil shear modulus, θ is an angle between the line joining the centre of the pile cross section and direction of the loading, γ_b is a factor which can be determined by the relation $\gamma_b = k_1(r_0/l)$, $k_1 = 2.14$ for lateral load applied on the pile when the pile head level at the ground $(e = 0)$ and $K_i(\gamma_b)(i = 0{,}1)$ are modified Bessel functions of the second kind of order i.

The lateral displacement can be determined by

$$u = \frac{p}{k_0 z\, D} \tag{2.35}$$

Z is depth, D is pile diameter for circural pile and width for rectangular pile, p is force for unit depth, and $k_0 D$ can be calculated as:

$$k_0 D = \frac{3\pi G_s}{2}\left(2\gamma_b \frac{K_1(\gamma_b)}{K_0(\gamma_b)} - {\gamma_b}^2\left(\left(\frac{K_1(\gamma_b)}{K_0(\gamma_b)}\right)^2 - 1\right)\right) \tag{2.36}$$

Then elasto-plastic solution was use, the displacement at depth z was calculated as

$$u = \varpi z + u_t \qquad (2.37a)$$

u_t is pile head displacement and ϖ is rotation angle that can be calculated as

$$\varpi = \frac{A_r}{k_0 l} \frac{-2\left(2 + \frac{3e}{l}\right)}{\left(\left(2 + \frac{z_0}{l}\right)\left(\frac{2e}{l} + \frac{z_0}{l}\right) + 3\right)\left(1 - \frac{z_0}{l}\right)^2} \qquad (2.37b)$$

and A_r can be obtained from following chart (Figure 2.7b). Figure 2.8 shows pile deflection under lateral load.

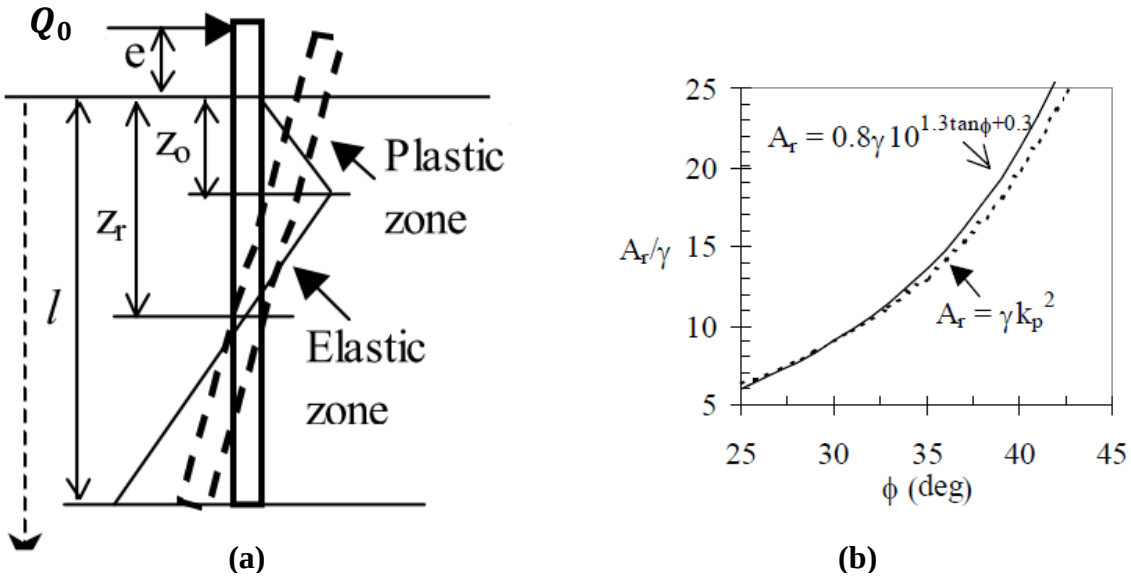

(a) **(b)**

Figure 2.7: (a) Pile soil system; (b) Gradient of the limiting force profile (from Guo, 2009)

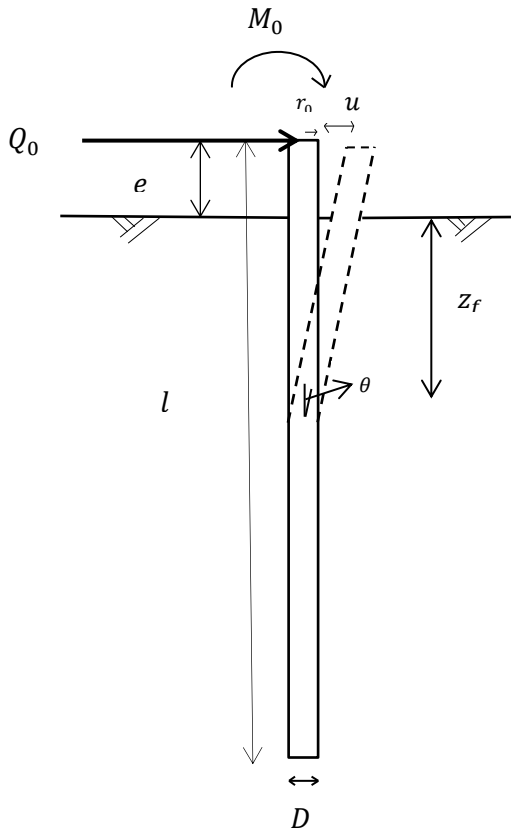

Figure 2.8: pile-soil system

2.2.2 Axially loaded pile

Several solutions for predicting the displacement of axially loaded piles are reported in the literature. Some of which are listed below:

- **Poulos and Davis's method**

Poulos and Davis (1968) presented analysis based on linear elastic theory to predict the behaviour of an incompressible single cylindrical floating pile in a semi-infinite mass and infinite layer under vertical load, for a wide range of ratios of length and diameter, and four values of Poisson's ratio. In this method the pile is divided in to n cylindrical elements as shown in Figure 2.9. Each element is subjected to uniform shear stress σ_{rz}, the circular base

of the pile having uniform vertical stress σ_{zz}, the initial analysis for shaft of the pile assumed to be rough while the base of the pile smooth, for incompressible pile each element has the same vertical displacements, the soil displacements due to shear stress at i^{th} element as shown in followed relationship

$$\mathrm{v}_s = \sum_{j=1}^{j=n} I_{ij}\sigma_{rz} + I_{ib}\sigma_{zz} \tag{2.38}$$

The displacement of pile due to uniform stress the base is

$$\mathrm{v}_b = \sum_{j=1}^{j=n} I_{bj}\sigma_{rz} + I_{bb}\sigma_{zz} \tag{2.39}$$

where I_{ij} is the factor of vertical displacement for i resulting from shear stress on element j, I_{ib} represents the vertical displacement factor for i resulting from uniform vertical stress acting the tip of the pile, I_{bj} is the factor of vertical displacement for the base resulting from shear stress on element j, v_s and v_b represent displacement in the shaft and the base of the pile. σ_{rz} and σ_{zz} are uniform shear loading and stress vertical stress on shaft and the base of the pile respectively. The displacement factors can be obtained from

$$I_{ij} = 4a \int_{(j-1)\delta}^{j\delta} \int_{0}^{\pi/2} pI \, d\theta dc \tag{2.40}$$

where δ represents the thickness of the element, and pI can be calculated according to Mindlin (1936) as

$$pI = \frac{1+v}{8\pi(1-v)E}\left[\frac{{z_1}^2}{{R_1}^3} + \frac{3-4v}{R_1} + \frac{5-12v+8v^2}{R} + \frac{(3-4v)z^2 - 2cz + 2c^2}{R^3} + \frac{6cz^2(z-c)}{R^5}\right] \tag{2.41}$$

where

$z = (i - 0.5)\delta + c,\ z_1 = (i - 0.5)\delta - c,\ R^2 = 4{r_0}^2 cos^2\theta + z^2$ and ${R_1}^2 = 4{r_0}^2 cos^2\theta + {z_1}^2$.

The influence factor of i point at the shaft due to uniform load in the base of the pile given by

$$I_{ib} = \int_0^{2\pi} \int_0^{a_b} pIr\ dr d\theta \qquad (2.42a)$$

where pI can be obtained from equation 2.41 however c, R^2 and ${R_1}^2$ calculated as

$$c = n\delta, R^2 = z^2 + {r_0}^2 + r^2 - 2rr_0\ \cos\theta \text{ and } {R_1}^2 = {z_1}^2 + {r_0}^2 + r^2 - 2rr_0\ \cos\theta$$

The calculation of displacement factor of centre of the base due to stress shear on element j calculated as

$$I_{bj} = 2\pi r_0 \int_{(j-1)\delta}^{j\delta} pI\ dc \qquad (2.42b)$$

where pI can be calculated using Equation 2.41 and $i = n + 0.5$, $R^2 = z^2 + {r_0}^2$ and ${R_1}^2 = {z_1}^2 + {r_0}^2$. The factor of vertical displacement for the base of the pile due to the load on the base is evaluated as

$$I_{bb} = \frac{\pi}{4} 2\pi \int_0^{a_b} pIr\ dr \qquad (2.42c)$$

where pI is obtained by inserting these values $i = n + 0.5, c = n\delta, R^2 = 4c^2 + r^2$ and $R_1 = r$

and r_0 is the radius of pile in Equation 2.41.Using the equilibrium condition we obtain

$$\sum_{j=1}^{j=n} \sigma_{rz}\pi\ r_0 \frac{L}{n} + \sigma_{zz}\pi \frac{{r_0}^2}{4} = P_t \qquad (2.43)$$

Poulos and Davis (1968) also presented Equation 2.44 to predict the vertical displacement for a unit applied load (P)

Moreover, Poulos and Davis (1968) proposed a solution for a floating pile in an infinite layer by assuming the shear stress distribution the independent of the depth of the layer. The deformation of the pile is estimated as

$$\mathrm{v}_h = \mathrm{v}_\infty - \left(\sum_{j=1}^{j=2} \sigma_{rz} I_{hj} + \sigma_{zz} I_{hb} \right) \tag{2.44}$$

where v_h is the settlement of a pile in a layer of any depth h, v_∞ is settlement of the pile in a semi-infinite mass, I_{hj} is the factor of displacement due to uniform shear on element j and I_{hb} represents the factor of displacement due to uniform load on the base.

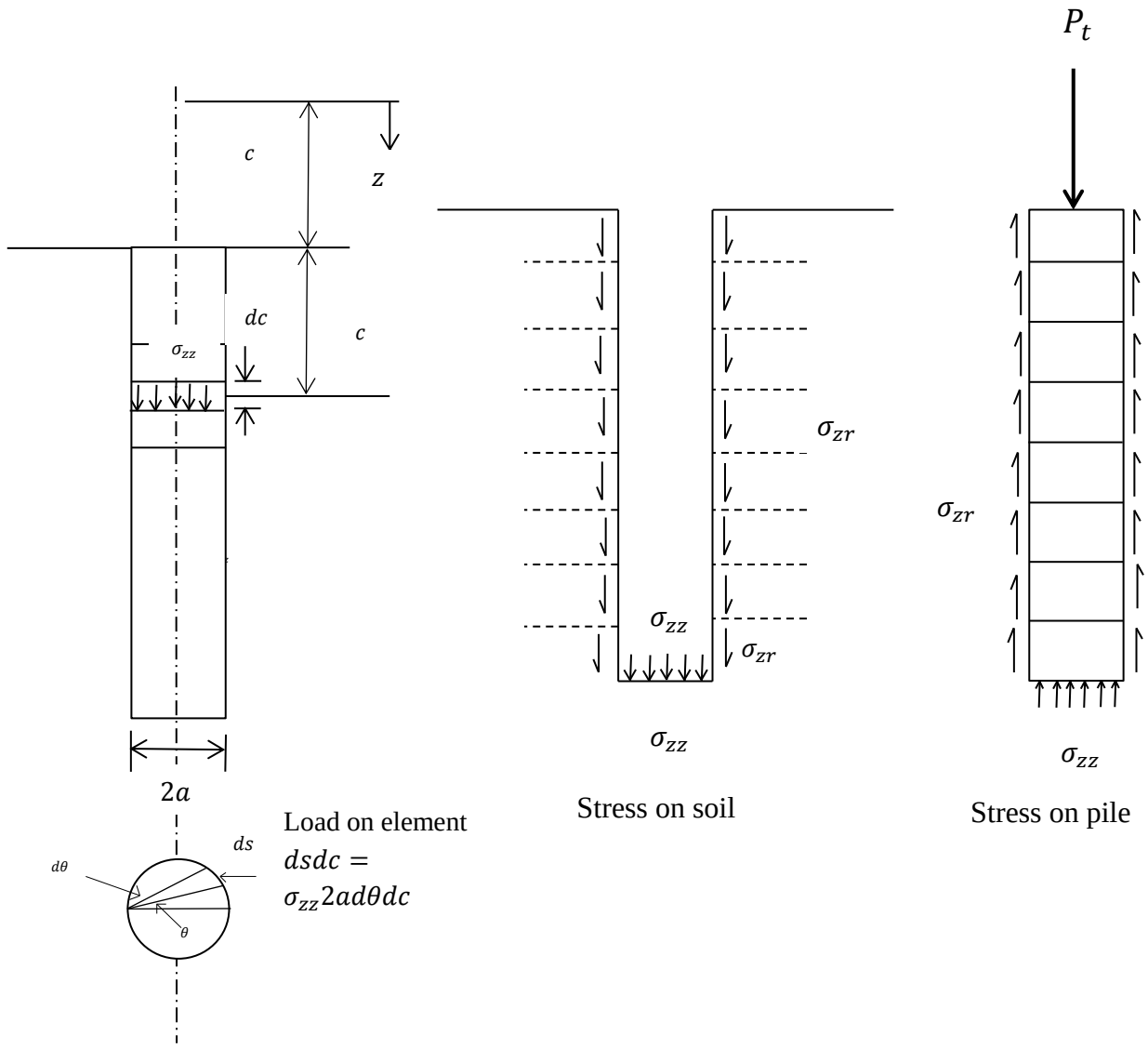

Figure 2.9: Stress acting on pile and adjacent soil (from Poulos & Davis, 1968)

- **Randolph and Wroth's method (1978)**

Randolph and Wroth (1978) explained that the analytical solution for deformation of piles should be usable for different pile geometries and soil stiffness, and the soil will deform due to the application of an axial load at the top of pile along and below the pile. The analysis of the axially loaded pile is based on a division of loads between the shaft and the base. Figure 2.10 shows the upper and lower soil layers and the separate deformation of these layers, where the plane AB is exploded to A_1B_1 and A_2B_2. The deformation around the shaft is modelled as a shearing of concentric soil cylinders. The shear stress around the pile will

increase when the pile is loaded, and will be greater than the increase of vertical stress. The vertical equilibrium of the soil element can be derived from Figure 2.10 as follows

The shaft pile response

$$\frac{d}{dr}(r\,\tau) + r\frac{d\sigma_z}{dz} = 0 \tag{2.45}$$

where $\frac{d}{dr}\tau$ represents the increment of shear stress, $\frac{d\sigma_z}{dz}$ is the vertical total stress increment and r is the radius of circular slice which is concentric with the pile. τ_s represents the shear stress along the shaft pile and τ is the shear stress at distance r. When the axial load is applied to the pile the shear stress in the shaft of the pile will be greater than the vertical stress so Equation 2.45 becomes

$$\frac{d}{dr}(\tau\,r) = 0. \tag{2.46}$$

By integrating Equation (2.46) the shear stress on the pile shaft will be obtained when $r = r_0$ as

$$\tau = \tau_s\frac{r_0}{r} \tag{2.47}$$

The shear strain is

$$\gamma = \frac{\tau}{G} = \frac{d\mathrm{v}_r}{dz} + \frac{d\mathrm{v}_z}{dr} \tag{2.48}$$

where v_r represents the radial displacement of soil, v_z represents the vertical displacement of the soil, γ is the shear strain and G is the shear modulus of soil. Based on Randolph and Wroth (1978) the vertical displacement is larger than the radial displacement, so Equation 2.48 becomes

$$\gamma = \frac{\tau}{G} = \frac{d\mathrm{v}_z}{dr} \tag{2.49}$$

where

$$d\mathrm{v}_z = \frac{\tau}{G}\, dr$$

Since $\tau = \tau_s r_{0/r}$ hence

$$\mathrm{v}_s = \frac{\tau_s r_0}{G} \int_{r_0}^{r_m} \frac{dr}{r} \tag{2.50}$$

where v_s is the shaft pile displacement and r_m is the magic radius (at which the ground settlement is zero) that can be calculated from $r_m = 2.5L(1 - v)$

$$\mathrm{v}_s = \frac{\tau_s r_0}{G} ln\left(\frac{r_m}{r_0}\right) = \frac{\tau_s r_0}{G}\zeta = \frac{P_s}{2\pi LG}\,\zeta \tag{2.51}$$

where $\zeta = ln\left({}^{r_m}/_{r_0}\right)$.

The base pile response

Soil below the pile will deform because the pile acts as a rigid punch and the deformation of the soil at the base of the pile will decrease with r when the vertical stress σ_z increases (Randolph & Wroth, 1978). Randolph and Wroth expresses the settlement at radius r as

$$\mathrm{v} = \mathrm{v}_s - \frac{\tau_s r_0}{G} \ln\left(\frac{r}{r_0}\right) \tag{2.52}$$

Where v is the settlement at radius r. Timoshenko and Goodier (1987) had described the displacement at the base of the pile as

$$\mathrm{v}_b = \frac{P_b(1-\upsilon)}{4\,G_s\,r_0}\eta \tag{2.53}$$

where P_b represents the shear stress under the pile, G_s is the base shear modulus, υ is the Poisson's ratio and η is base enlargement ratio, equal to 1.

The head pile response

For vertical equilibrium

$$P_t = P_b + P_s \tag{2.54}$$

where P_t is the axial load on the top of the pile, $P_b = q_b\,A_s$, q_b is the shear stress at the base of pile and $P_s = \tau_s A_s$, and A_s is the cross-section of area of the pile.

To predict the accurate displacement of the soil-pile system due to pure vertical load, the response of the shaft and the base of the pile must be combined

$$\mathrm{v}_t = \mathrm{v}_s = \mathrm{v}_b$$

$$\frac{P_t}{G\,r_0\mathrm{v}_t} = \frac{P_b}{G\,r_0\mathrm{v}_b} + \frac{P_s}{G\,r_0\mathrm{v}_s} \tag{2.55}$$

$$\frac{P_t}{G\,r_0\mathrm{v}_t} = \frac{4}{\eta(1-\nu)} + \frac{2\pi L}{\zeta\,r_0} \tag{2.56}$$

where v_t is the combined deformation, v_s is settlement of the pile shaft, v_b is the base displacement, P_t represents total vertically loaded pile, η is geometric factor which equal to 1 and $\zeta = \ln\left(\frac{r_m}{r_0}\right)$.

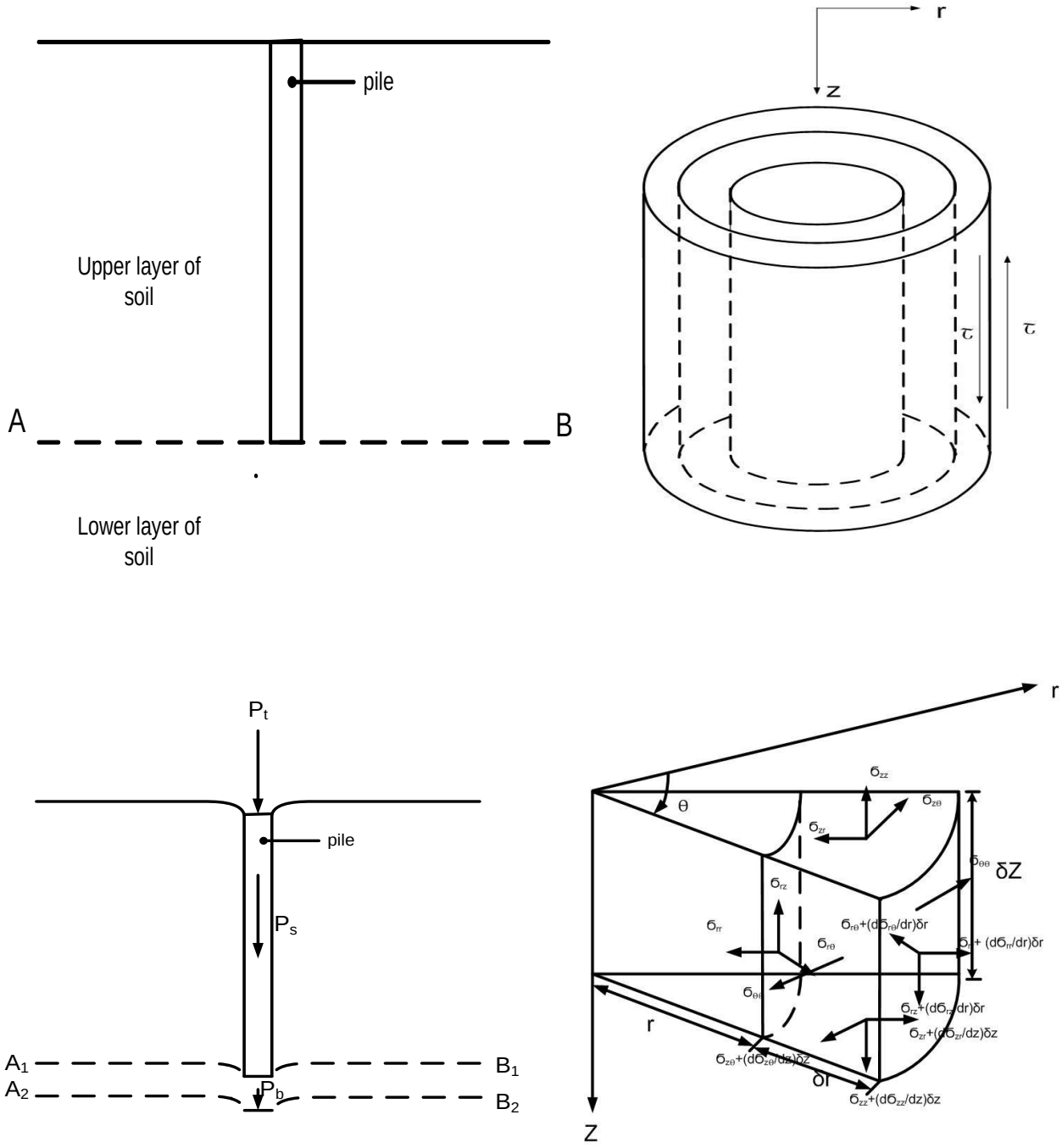

Figure 2.10: Analysis of pile by uncoupling of loads carried by the shaft and base (after Randolph and Wroth 1978).

2.3 Discretised continuum approach (numerical method)

Unlike the beam-on-foundation method, the discretised continuum approach treats the surrounding soil in three dimensions. Several numerical methods are used to estimate the pile deflection in 3 directions with different pile geometry and different constitutive models: finite element method, finite difference method and boundary element method (Poulos, 1971a), Poulos (1971b), Banerjee and Davies (1978), Budhu and Davies (1988), Basack & Dey (2012), Georgiadis et al (2013), Verruijt et al. (1989) and Basu et al. (2009).

2.3.1 Laterally loaded pile

The finite element method has been used to calculate pile displacement for different pile geometries in uniform and multi-layered soil and with different constitutive models of soil and for single pile and group of piles (Comodromos & Papadopoulou, 2012; Verruijt & Kooijman, 1989; Randolph, 1981; Bransby 1999; McGann et al 2011; Georgiadis et al. 2013)

The boundary element method has been used to analyse the behaviour of a pile under dynamic loading, although the accuracy of numerical dynamic solutions depends on frequency parameters (Kaynia. 1982; Sen, et al. 1985; Banerjee, et al. 1987). The boundary element method tackles pile-soil interaction by dividing the pile into slices and modelling the interaction between pile slices and the soil by using the solution proposed by Mindlin.

Various authors (Sun, 1994; Zhang et al. 2000; Guo and Lee, 2001) have found solutions which are based on energy approaches to determine lateral pile deflection at depth (analytical solutions). However, the disadvantage of these methods is that they assume the displacement in the radial and tangent directions are the same that gives a stiffer soil response compared with the response of the soil in reality.

Cox, et al. (1974), Ashour and Norris (2000) and Basu, et al. (2009) obtained solutions for the responses of laterally loaded piles by developing an analysis for multi-layered elastic

media. Displacements in the pile-soil system are derived from functions which vary in the three directions. The governing differential equations are derived using Hamilton's principle for pile deflections in different soil layers. The response of a pile group embedded in non-homogenous elastic linear soil subjected to lateral load was developed by Salgado et al., (2014) using semi-analytical approach based on the displacements of the soil mass at any point around a pile is tying the with the displacement pile themselves, the governing equation here obtained by minimizing and variations the potential energy.

Sun (1994) calculated the response of a pile in linear elastic soil under static horizontal load while Das and Sargand (1999) have used the Vlasov energy method to analyse the dynamic lateral loading that acts on the pile. This method is based on strain-stress relations to calculate the potential energy for the soil column and surrounding soil, then inserting them through Hamilton's principle. The energy method can be used for both static and dynamic analysis, and Vallabhan and Das (1991a) have modified the Vlasov energy method for the static analysis of beams on elastic foundations. Vallabhan and Das used a variational method to obtain the equilibrium configuration. The finite difference method is used to solve the differential equation for soil displacement in Verruijt and Kooijman (1989) and Basu, et al. (2009). Basu, et al. (2009) developed an advanced continuum-based method to analyse laterally loaded piles by considering soil displacement decay when the distance from the pile increases. They assumed the direction of soil displacement is consistent with the direction of the load, the constitutive model of the soil in his study was linear elastic. They also explained that, by using the variational principle, the governing differential equations for pile and soil displacements can be derived.

Sun (1994) predicted the deflection of a laterally loaded pile in homogenous soil using an energy based method, and used the same dimensionless displacement function of soil $\phi(r)$ in radial and tangent displacements(u_r and u_θ), meaning that displacement must be in the load direction. However, Basu et al., (2009) improved Sun's analysis by assuming the soil as multi-layered instead of a single layer, and the value of soil displacement was taken not only in the load direction, but also had a component perpendicular to the load direction, which meant that $u_r \neq u_\theta$; in other words $\phi(r) \neq \phi_r \neq \phi_\theta$, where ϕ_r is the dimensionless

displacement function of soil in the radial direction, and ϕ_θ represents a dimensionless displacement function of soil in the tangential direction (more details in Chapter 3).

Das and Sargand (1999) calculated displacement along the pile, and supposing that the soil displacement will be in the load direction and parallel to it (using Sun (1994) assumption but for dynamic load instead of static load), the soil displacement found from this method is larger than real displacements. The main point of this study is that to obtain a realistic result using the Basu et al. (2009) assumption, the pile here subjected to dynamic lateral load, and an analytical method suggested to analyse deformation data for laterally loaded piles depends on the energy conservation of the pile-soil system.

2.3.2 Axially loaded pile

The continuum approach treats the surrounding soil in three dimensions for the analysis of axially and laterally loaded piles, because in nature, the soil interacts with the pile in three dimensions. Three numerical techniques are widely used in the analysis of piles, namely the finite element method (FEM) (Randolph, 1981; Brown et al., 1989; Trochanis et al., 1991; Carter and Kulhawy, 1992; Bransby and Springman 1996; Bransby, 1999), the boundary element method (BEM) (Banerjee and Davies, 1978; Budhu and Davies, 1988; Basack and Dey, 2011, 2012) and the finite difference method (Ng and Zhang, 2001; Klar and Frydman, 2002; Basu et al., 2008 and Haldar and Sivakumar Babu, 2012). The disadvantage of the FE method is that it usually takes a longer time for computing compared with the FD method.

Analytical solutions such as those developed by Butterfield and Banerjee (1971), and Poulos and Davis (1968), are widely used in engineering practice. These solutions treat the soil as a linear elastic material. Vallabhan and Mustafa, (1996) developed solutions for displacement of a pile embedded into two-layered soil. This analysis was expanded by Lee and Xiao (1999), Salgado et al. (2007) and Seo et al. (2009) to multi-layered soil. In this thesis the response of a pile in non-uniform soil is considered, where the elastic moduli G and λ (Lame's constant) are varied in three directions, and both are functions of stress and strain. As stress and strain decay with increases in the length of radial direction, the soil stiffness

(G) increases. In other words, soil stiffness degrades with increasing strain, so G and λ vary in radial and depth directions. The soil in reality is not uniform, and the stiffness in the soil varies in all directions. Thus, studies which consider soil as linear elastic are not suitable for predicting real structural behaviour during working loads.

2.4 Soil behaviour

In order to model pile response accurately, an appropriate constitutive model is needed. However, soil behaviour is complex so it is difficult to find a single constitutive model that describes the soil behaviour. For example the undrained strength of soils depends on a number of factors such as the failure mode, strain rate, stress history, and soil anisotropy as well as the mode of loading effects of stress-strain non-linearity. These factors make the undrained strength dependent on test type (Koutsoftas and Ladd, 1985; Kulhawy and Mayne, 1990), a summary of some these factors (such as stress history, hysteric behaviour of soil) which affect the response of a pile can be explained as follows

2.4.1 Stress history

The term 'recent stress history' has been used by Atkinson et al. (1990) to define the previous stress path and the time spent at a constant stress state before an imposed change in stress. A series of laboratory stress path tests on London clay samples made by Atkinson et al. (1990) to investigate the effect of current state, the recent stress history and the sudden change in the different directions on soil stiffness. They stated that at small strain (of the order 0.01%) the stiffness at $\theta = 180^o$ is larger than stiffness of the order $\theta = 0^o$, and stiffness for $\theta = 90^o$ falls between those $\theta = 0^o$ and $\theta = 180^o$. This study was extended in Stallebrass (1990) and Stallebrass and Taylor (1997). Figure 2.11shows the stiffness-stress response for different rotations ($\theta = 0^o, 90^o, -90^o$ and 180^o), from this experiment we can concluded that as engineering to apply the load depends on the sequence of the load application the response is different.

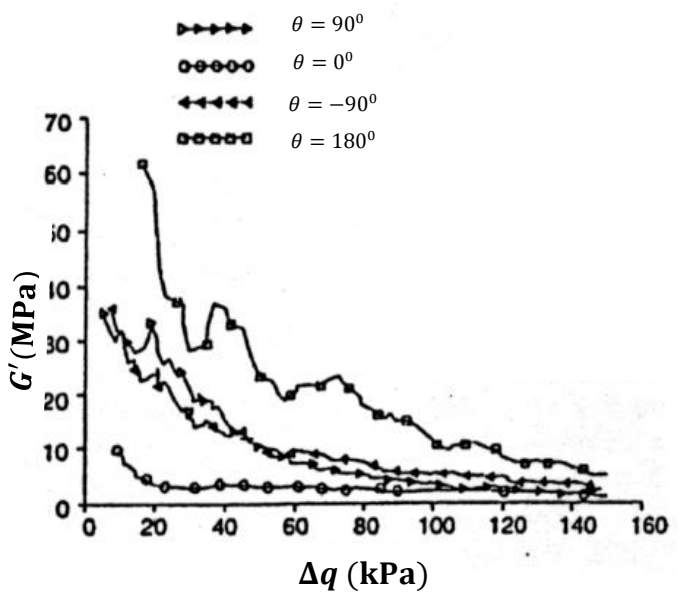

Figure 2.11: The effect of recent stress on soil stiffness (from Stallebrass and Taylor, 1997)

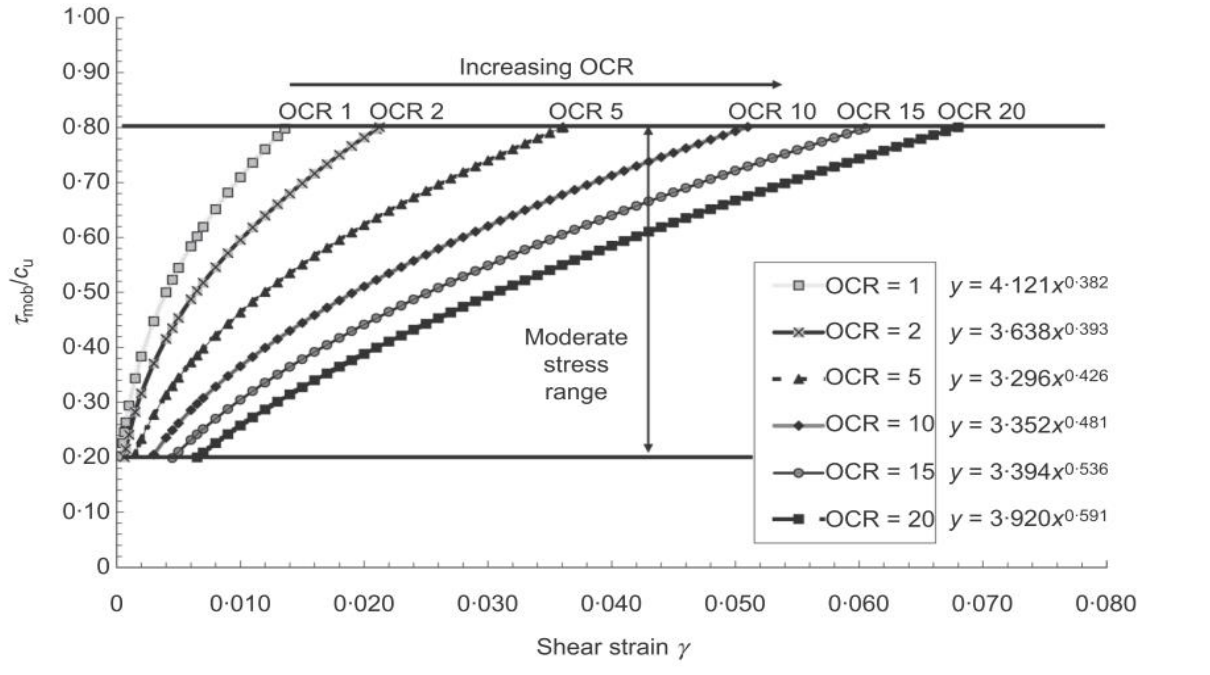

Figure 2.12: Stress-strain curve with different over consolidation ratio (Burland et al. (1996) modified by Vardanega & Bolton (2011b).

Vardanega & Bolton (2011c) tested a samples of natural London clay in order to investigate the relationship between the mobilisation strain is and depth. They stated that mobilisation strain increases with decreasing depth and also increases with OCR. Figure 2.12 shows the response of Todi clay for different over consolidation ratios (OCRs).

2.4.2 Hysteretic behaviour of soil

Hysteretic behaviour can be observed in an unloading and reloading cycle in an undrained triaxial test as shown in Figure 2.13. Wood (1990) illustrated that in a loading-unloading-reloading loop, the stress-strain relationship is not unique because of the inelastic response due to energy being dissipated in a closed load cycle. An experiment carried out by Jardine et al. (1984) showed that the pure elastic region did not exceed 0.1% of strain. Figure 2.13 shows the strain-stress response of dense sand resulting from cyclic triaxial test (Biarez and Hicher, 1994).

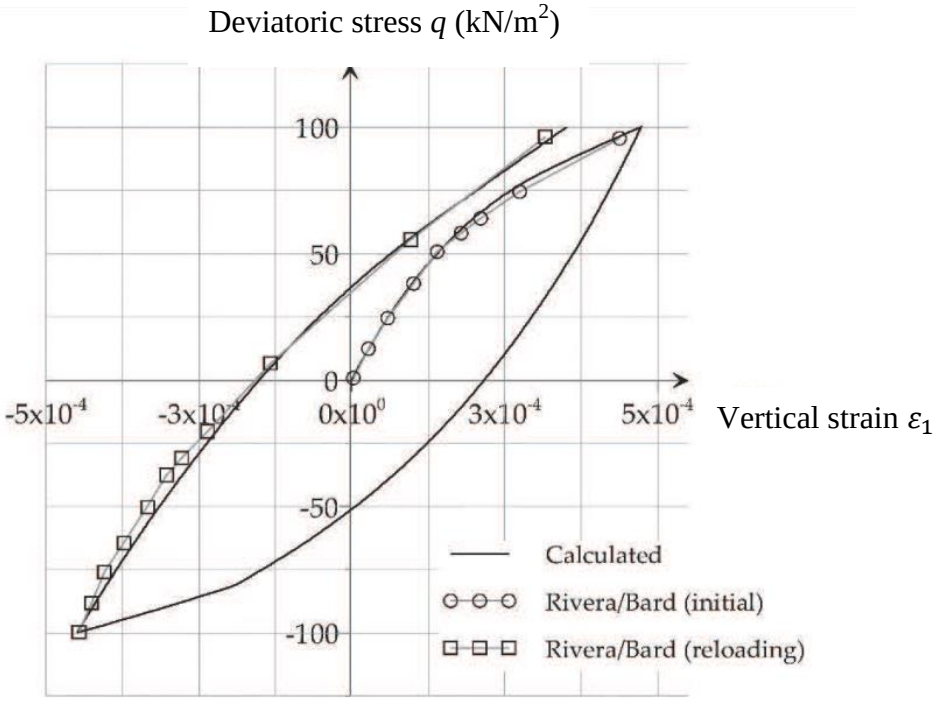

Figure 2.13: Hysteresis loop for dense Huston sand resulting from drained triaxial test (from Biarez & Hicher, 1994)

2.4.3 Nonlinear behaviour of soil

Atkinson (2000) stated that for loading structures the decay of the soil stiffness varies with strain, where the stiffness of soil is high at very small strain level and decreases with the increase in strain. This decay differs according to the type of material. Soil behaviour has been studied by many researchers using triaxial tests and the results show that high stiffness occurs when shear strain is less than 10^{-5} (Jardine et al., 1984; Burland, 1990; Atkinson and Sallfors, 1991; Houlsby and Wroth, 1991; Osman et al., 2007). There are some factors that affect small strain stiffness G_{max}, such as mean effective stress, void ratio, stress history, rate of loading, soil plasticity for silts and clays, stress anisotropy for sands, and effective confining stress (Drnevich and Massarsch, 1979; Hardin, 1978; Hardin and Drnevich, 1972; Lo Presti et al., 1996; Vucetic, 1994; Yamashita et al., 2003). A power law can be used to describe the decay of stiffness with the increase of strain (Bolton and Whittle, 1999; Bolton et al., 1993; Gunn, 1992). A simple power law has been used by Gunn (1993), where the soil is assumed to be nonlinear-elastic, perfectly plastic and with a Tresca yield surface.

Two parameters (A and n) that have been obtained experimentally (by using a pressuremeter test), are used to describe the variation of shear stress with strain as follows

$$q = A\left(\varepsilon_q\right)^n \tag{2.57}$$

where q represents equivalent shear stress, ε_q is deviator shear strain. Gunn (1993) stated that this model is valid to predict undrained displacement but is unsuitable for determining the response of soil under cyclic loads because it cannot capture the change of soil stiffness during unloading. Atkinson (2000) shows the decay of stiffness with strain and concludes that the stiffness-strain curve can be divided into three regions as shown in Figure 2.14. The first region represents the very small strain where the stiffness is almost constant, the second region (small strain) starts from ε_0 till $\varepsilon = 0.1\%$, in this region the stiffness decay rapidly and in large strain the stiffness is the smallest, where the soil stiffness is high at small strain and decrease with large strain (Atkinson, 2000). Figure 2.15 shows the degradation of stiffness with increasing of strain for different types of clay.

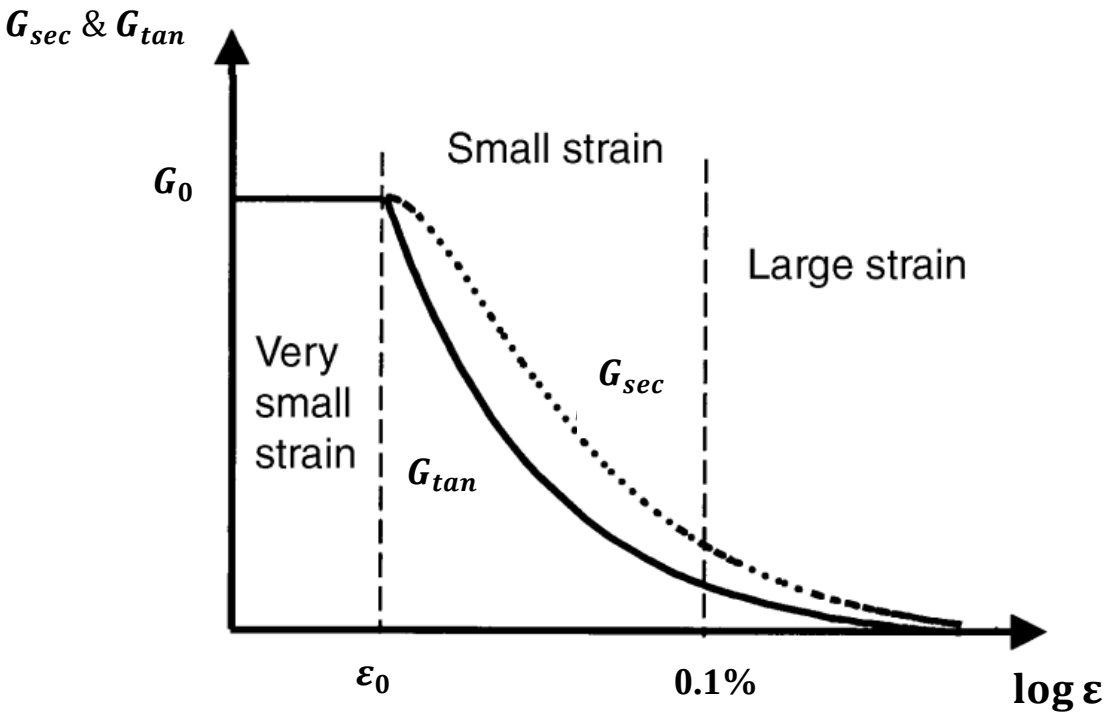

Figure 2.14: The variation of normalizing shear secant with logarithmic strain $\varepsilon_q$or normalized displacement (after Atkinson, 2000)

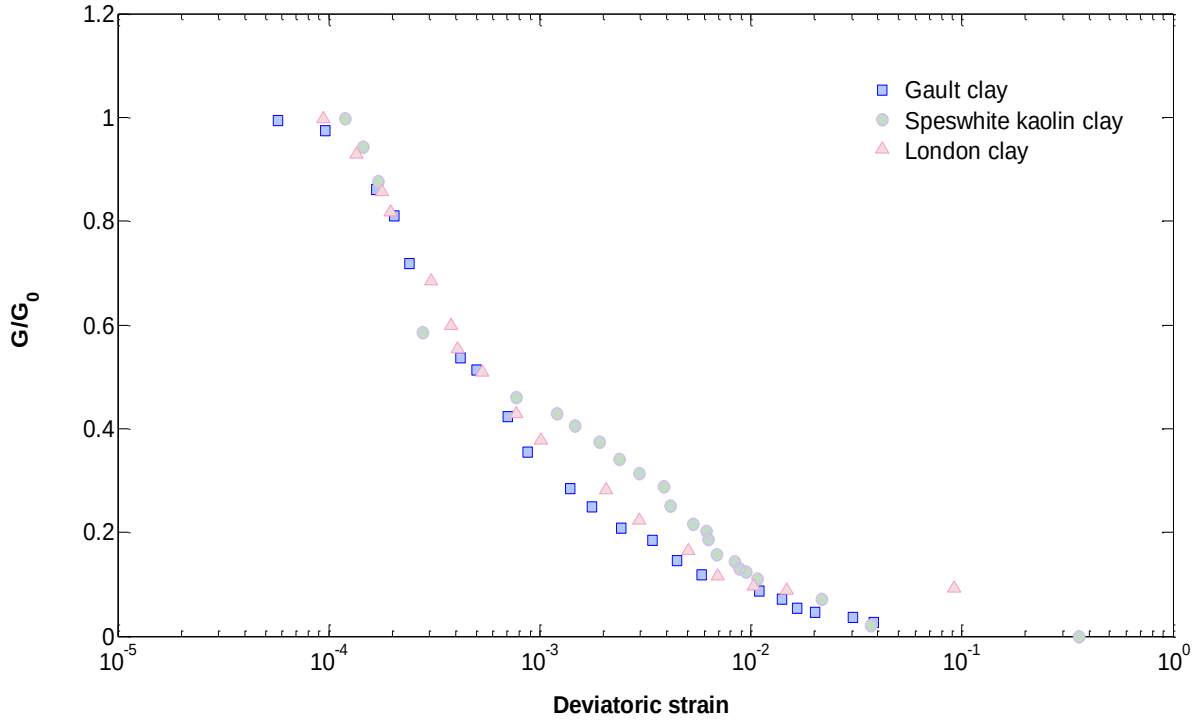

Figure 2.15: Degradation of tangent with deviatoric strain (after Dasari, 1996)

2.5 Soil plasticity

Once strain increases to exceed yield stress the material becomes plastic and will not return to original state after load removed. Several models have been used to model soil plasticity. In elasto-perfectly plastic models, the stress remains constant beyond the yield stress point with an increase strain, see Figure 2.16b. Similar to elasto-perfectly plastic material, the strains hardening models behaves as linear elastic before yield stress, and become plastic beyond the yield point and the stress increases with strain, see Figure 2.16c. In the strain softening model, the material behaves as elastic to yield followed by a dropping stress, as shown in Figure 2.16d.

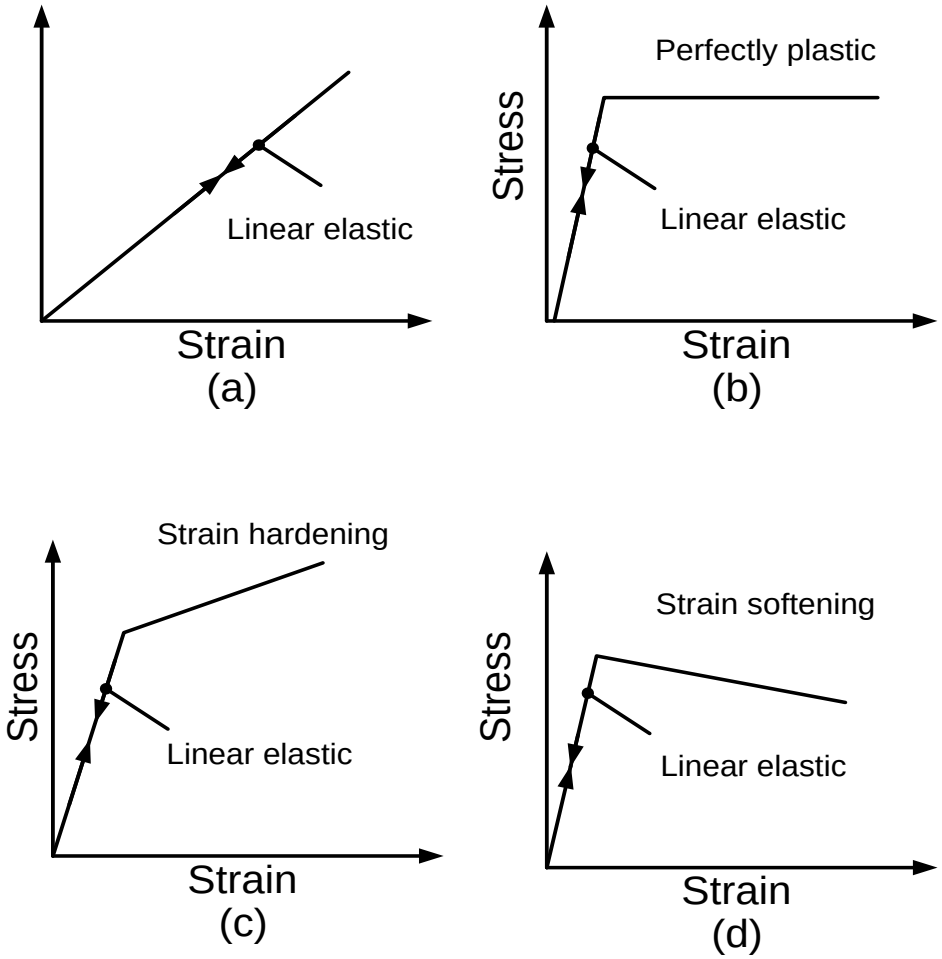

Figure 2.16: Different soil models (a) Linear elastic model; (b) linear elastic perfectly plastic model; (c) linear elastic strain hardening model; (d) linear elastic strain softening model (after Elhakim, 2005)

Plasticity occurs when the stress reaches the yield surface $f(\sigma_{ij}) = 0$, where f is a yield function that governs each element of material and this function depends only on stress components (σ_{ij}). The yield function for perfectly plastic material depends on the stress component rather the strain component. When $f(\sigma_{ij}) < 0$ the material is elastic.

Two terms have been used to describe the plastic flow: yield and failure. Yield is the change of the material from an elastic response while failure means that the material is continuing to plastically deform at constant stress. Perfectly- plastic models such as Drucker-Prager, Mohr-Coulomb, Von-mises and Tresca are often used in practice. The wide use of these models is due to the fact that only a few parameters are needed to describe plasticity.

Tresca yield criterion

Tresca assumed that yield takes place when the maximum shear stress is equal to *k* where *k* is the limit value, in other words the maximum difference between principal stresses taken in pairs must equal to 2*k* or twice the undrained soil shear strength $2S_u$ (measured in a triaxial test).

$$(\sigma_1 - \sigma_3) = 2\,S_u \tag{2.58}$$

where S_u is undrained shear strength, σ_1 is maximum principal stress and σ_3 is minimum principal stress (Tresca, 1869), see Figure 2.17.

Von-mises yield criterion

Von-mises (1913) modified the Tresca yield criterion, where he assumed the surface yield is a smooth yield function instead of one with corners, these corners implying singularities in the yield function that lead to difficulties in numerical analysis. The yield surface in the Von - mesis model is plotted as a circular cylinder in principal stress space as, shown in Figure 2.18. The failure occurs in Von-mises criterion when the energy of distortion reaches the

same energy for yield or it failed in uniaxial tension. This model has been widely used in case of undrained soils and metals (Von Mises, 1913; Potts and Zdravkovic, 1999), the relationship between undrained shear strength and main principal stresses can be expressed as

$$S_u = \sqrt{\frac{1}{8}((\sigma_1 - \sigma_2)^2 + (\sigma_1 - \sigma_3)^2 + (\sigma_2 - \sigma_3)^2)}. \quad (2.59)$$

Mohr-Coulomb yield criterion

Mohr-Coulomb assumes that the plastic deformation takes place when the shear stress reaches an amount that depends linearly upon the material cohesion and normal stress σ.

This model is considered as the best model for anisotropic pressure-sensitive soil, since this model agrees well with experimental studies. On the other hand, because of singularities this model is not mathematically convenient (Coulomb, 1773). The yield "surface" in case of one dimension is defined by a linear line between shear stress τ and normal or effective stress σ' is calculated as

$$\tau = \sigma' \tan \phi' \ . \quad (2.60)$$

where ϕ' represents the angle of internal friction of soil (see Figure 2.17).

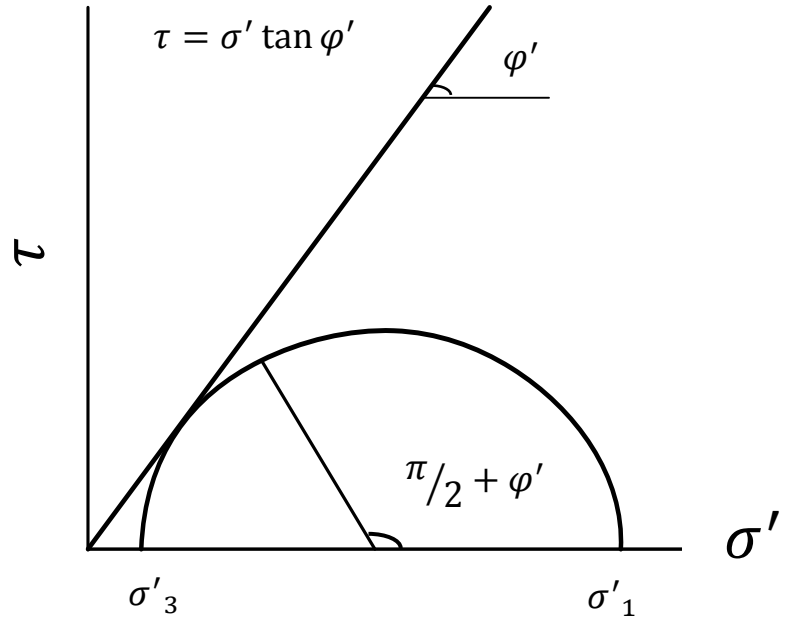

Figure 2.17: Mohr Coulomb circle of stress

Drucker-Prager yield criterion

The Drucker-Prager et al. (1952) yield criterion plots as a cone in effective stress space, and is a pressure-dependent model. The yielding surface of this criterion depends on the cohesion and the material internal friction angle. This criterion is a modification of the Coulomb yield criterion but avoids the singularity problem co and is similar to the Von-Mises yield criterion, see Figure 2.18. Von-mises and Drucker-Prager models are commonly used for elasto- plastic analyses (Drucker et al. 1952).

The differences between the four models mentioned above are their shapes in the deviatoric plan, the strength is related to the difference between major and minor stresses.

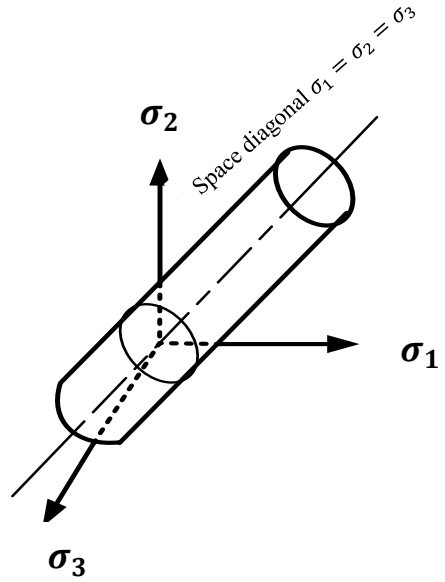

Von-mesis yield criterion

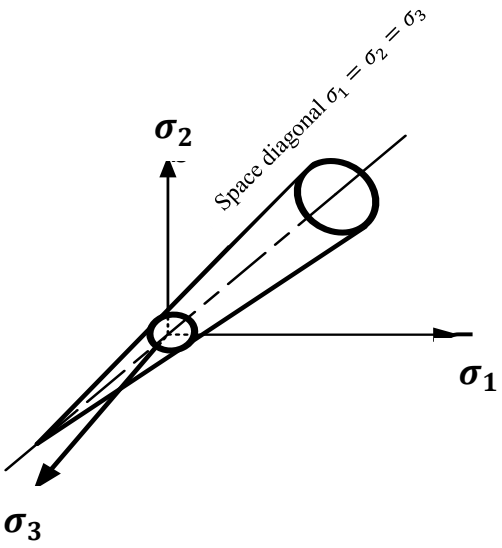

Drucker-Prager yield criterion

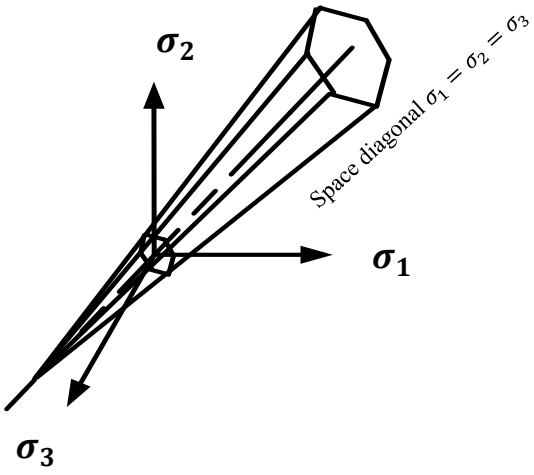

Coulomb yield criterion

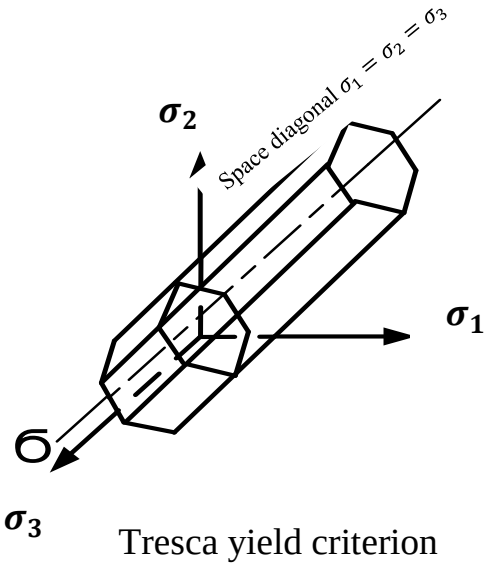

Tresca yield criterion

Figure 2.18: Different yield criteria (after Potts and Zdravkovic, 1999)

2.6 Similarity method for foundation analysis

A similarity approach is presented in Atkinson (2000), which is a simple method to predict structural displacement in geotechnics. The analysis is based on the straining of undrained

soil in a triaxial test, related to ground movement. In this approach, Atkinson (2000) used elastic solutions to link the load and displacement via secant stiffness. His solution allows nonlinear soil to be considered. Atkinson (2000) suggested that the decay in soil stiffness with strain level and the decay in foundation stiffness with normalised displacement take the same form.

Using the stress-strain response resulting from a triaxial test, the soil secant stiffness G_{sec} can be obtained, and then the soil secant stiffness is plotted against the deviatoric strain. The soil stiffness-strain curve can be converted directly into a stiffness-displacement curve by scaling the x-axis (the strain axis) using a linear scaling factor. Once the displacement is known together with the corresponding secant stiffness, the lateral load Q_0 can then be calculated from the conventional linear elastic solution for axial and lateral loads.

Atkinson (2000) obtained a strain scaling factor for vertical displacement by assuming $\alpha_v = \frac{\left({}^{u_v}/_{D}\right)}{\varepsilon_a} = 3$, where v is vertical displacement, D denotes foundation diameter and ε_a is compressive strain. The former method was extended by Osman et al. (2007), where a similarity method was developed for circular shallow foundations and which coefficients for circular foundations subjected to vertical, horizontal and moment loads were derived. The calculation in this approach can give quicker and simpler results than numerical analysis. The technique is not intended to replace advanced numerical methods but to provide a tool which is simple enough for use in preliminary design calculations, whilst also capturing the important influence of soil non-linearity. There is no need for a large number of parameters in this method, and it is also cheaper than numerical analysis. Osman et al. (2007) obtained the coefficients of displacement for circular shallow foundations under undrained loads (horizontal and bending moment) using the similarity approach. The similarity method will be extended in this thesis to piled foundations under vertical and horizontal loads.

2.7 Summary

The literature review in this chapter has outlined the background to the types and failure mechanisms of piles. In doing so, existing methods that are used to analyse piles under different types of loads have been categorized based on analytical solution and numerical analysis. This analysis methods are suitable for specific problems; for example, in the case of laterally loaded pile, Winkler's method can be used for a clamped pile in cohesive and cohesion-less soil, while Poulos' method is most suitable for free rigid and fixed rigid pile in homogenous and heterogeneous soil. Budhu and Davies' method works for free and fixed head piles in elasto-plastic soil, whereas Randolph's method can be used for rigid and flexible piles in homogenous soil. Finally, Broms' method is most suitable for free and fixed of short pile in cohesion and cohesion-less soil. Nevertheless, in the case of axially loaded piles, Poulos and Davies' method is used for a floating pile in semi-infinite and infinite layers, while Randolph's method is used for piles in homogenous soil.

There is a need to develop tools that are suitable for modelling a large range of constitutive models of soil and different pile geometries. These tools should be simple and quick. Therefore, an analytical solution based on an energy method will be considered in this thesis, where the energy method has been used for the soil-structure problem. This method will be used to analyse the following:

- The deformation of a pile in linear elastic soil under lateral dynamic load.

- The displacement of a pile subjected to static lateral load; the shear modulus of soil, G assumed to vary linearly with depth.

- The response of a pile in nonlinear elastic soil under lateral, axial and combined loads.

There is also a need to develop a method using the similarity approach that can provide a powerful tool for estimating the stiffness and working displacements of a pile under combined loading. A calculation method is needed that is far quicker and simpler than numerical analysis. The technique is not intended to replace advanced numerical methods, but to provide a tool which is simple enough for use in preliminary design calculations, whilst capturing the important influence of soil non-linearity. The potential benefit to engineering practice of being able to apply the similarity principle is obvious.

3 The response of a laterally loaded pile in linear elastic soil

Introduction

Many factors can affect pile deflection due to lateral loads, such as soil properties, the pile - soil interaction (e.g. soil is fully connected to the pile or able to slip), the direction of the load, the pile material, geometry and stiffness. The resistance of the soil and lateral deflection should all be considered when designing vertical piles, whether a single pile or in a group of piles.

In this part of the thesis, an energy-based method has been developed to predict pile deformation. An analytical solution based on the energy method was used by several researchers (Vlasov and Leont'ev, 1966; Vallabhan and Das, 1991a; Basu, et al., 2009; Seo and Prezzi, 2007; Basu et al., 2008) to estimate laterally and axially loaded pile deformation for linear elastic soil. Independent functions describing the soil displacement have been used; these functions vary in vertical, radial and circumferential directions. The linear elastic analysis has been developed by employing variational principles and minimization of energy, called Hamilton's principle, to derive the governing equation and boundary conditions. Hamilton's equation can be expressed as

$$\int_{t_2}^{t_1}(\delta T - \delta U)dt + \int_{t_1}^{t_2} \delta W \, dt = 0 \qquad (3.1)$$

where T and U are the kinetic and potential energies of the pile and soil and W is work done by applying lateral load, t_1 and t_2 are the initial and final times of loading (Asik and Vallaban, 2001).

The governing equations for pile deflection are obtained by minimizing kinetic and potential energies. These governing equations can be solved either numerically or analytically once the boundary conditions are included. Each of the displacement components are expressed as a multiplication of one-dimensional functions when minimizing the energy, a set of one

dimensional equation is obtained. These equations are solved numerically, using the finite difference technique.

Sun (1994), and Das and Sargand (1999) developed an analysis based on energy methods to estimate the response of a laterally loaded pile due to static and dynamic loads. Both studies assume zero soil displacement perpendicular to the direction of the applied force and the resultant displacement vector at any point within the soil is taken to be parallel to the applied force. This artificial constraint leads to stiffer pile response as demonstrated by Basu et al. (2009). Sun (1994), and Das and Sargand (1999) assumed the displacement field in the soil as

$$u_r = u(z)\phi(r)\cos\theta \qquad (3.2a)$$

$$u_\theta = -u(z)\phi(r)\sin\ \theta \qquad (3.2b)$$

where $u(z)$ represents a displacement function with a dimension of length, and $\phi(r)$ is dimensionless soil displacement in the r direction.

Basu et al. (2009) suggests a more realistic displacement field which is described as:

$$u_r = u(z)\phi_r(r)\cos\theta \qquad (3.3a)$$

$$u_\theta = -u(z)\phi_\theta(r)\sin\ \theta \qquad (3.3b)$$

where $u(z)$ represents a displacement function with a dimension of length. $\phi_r(r)$ is dimensionless soil displacement in the radial direction (r), and ϕ_θ is dimensionless soil displacement in the tangent direction (θ) (see Figure 3.1). However, in the work of Basu et al. (2009) only static loads are considered and the soil stiffness is taken to be constant within the soil layer. Field data shows that the soil stiffness varies with depth and it is quite often that variation is described by a linear function. In this chapter the analysis will extend the energy-based method to deal with (i) stiffness variation with depth, (ii) dynamic lateral loads.

3.1 Response of a lateral loaded pile in elastic soil with stiffness varying linearly

Consider a circular pile with radius r_0 and length L. The pile is assumed to be vertical and embedded in an isotropic linear elastic medium which extends to infinity. The pile is perfectly connected to the surrounding soil, which means there is no separation at the interface between the soil and pile, and the head of the pile is located at the ground surface. The pile is subjected to a lateral load with a bending moment M_0 at the head of the pile. In this analysis, cylindrical coordinates (r, θ, z) have been chosen, and the downward direction is taken as positive (see Figure 3.1). The shear modulus of soil here varies linearly with depth, see Figure 3.3.

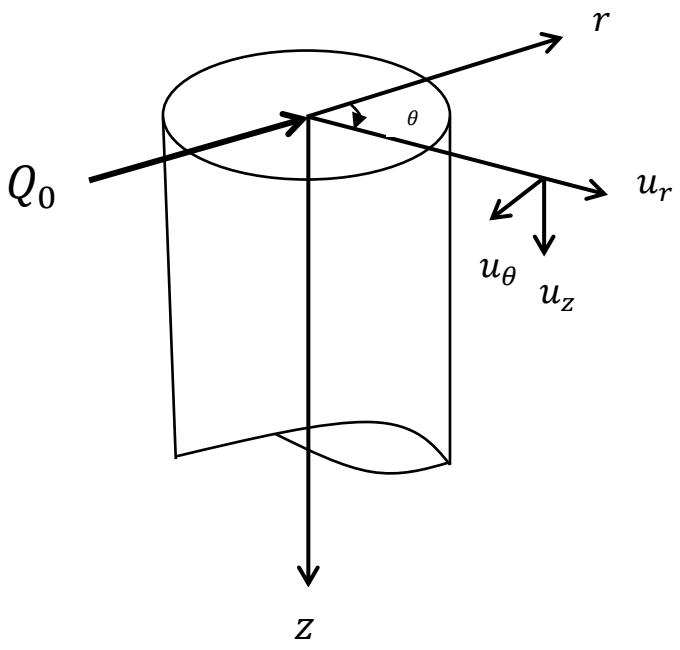

Figure 3.1: Cylindrical coordinate system and components of displacement at top of pile

3.1.1 Energy based approach

In this method, the deformation of the pile-soil system can be obtained using the energy approach. The variational method used here to minimize the potential energy allows us to estimate the governing equations. The pile-soil system is divided into three parts: the pile, the soil column below the pile, and the soil around the pile (see Figure 3.2). The governing equation and boundary conditions are obtained by minimizing the energy into three parts.

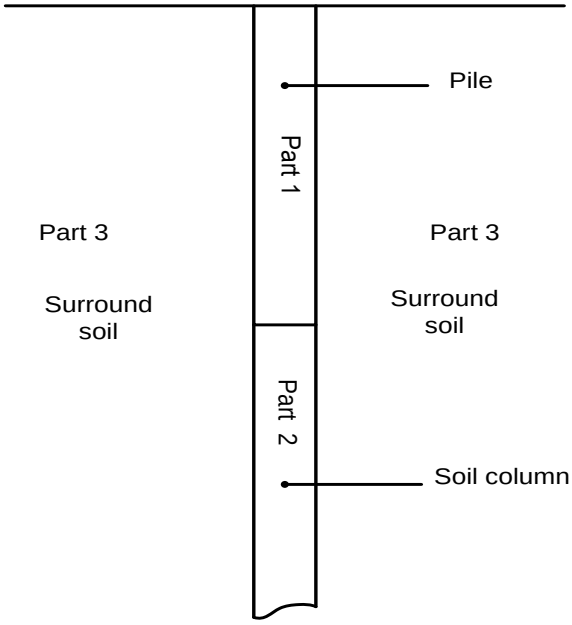

Figure 3.2: Zones of energy of the pile - soil system

Potential Energy

The lateral load acting on the top of the pile leads to lateral displacement of the pile-soil system, which causes potential and/or kinetic energies in the pile and surrounding elastic media (Sun, 1994). The potential energy of the pile and soil for both external and internal potential energies is given by

$$U = \frac{1}{2}\int_0^L E_P I_P \left(\frac{d^2u}{dz^2}\right)^2 dz + \frac{1}{2}\int_L^\infty \pi {r_0}^2\ G\left(\frac{du}{dz}\right)^2\ dz + \frac{1}{2}\int_{r_0}^\infty \int_0^{2\pi} \int_0^\infty (\sigma_{rr}\varepsilon_{rr} + \sigma_{\theta\theta}\varepsilon_{\theta\theta} + \sigma_{r\theta}\varepsilon_{r\theta} + \sigma_{rz}\varepsilon_{rz} + \sigma_{\theta z}\varepsilon_{\theta z})\, r dr d\theta dz \quad (3.4)$$

where u is the pile displacement, E_p represents the pile Young's modulus, I_p is the second moment of area, σ_{ij} and ε_{ij} are the stress and the strain in the soil, respectively and G is the shear modulus of soil which is assumed to change with depth (Figure 3.3) as follows:

$$G(z) = G_0 + \psi z. \tag{3.5}$$

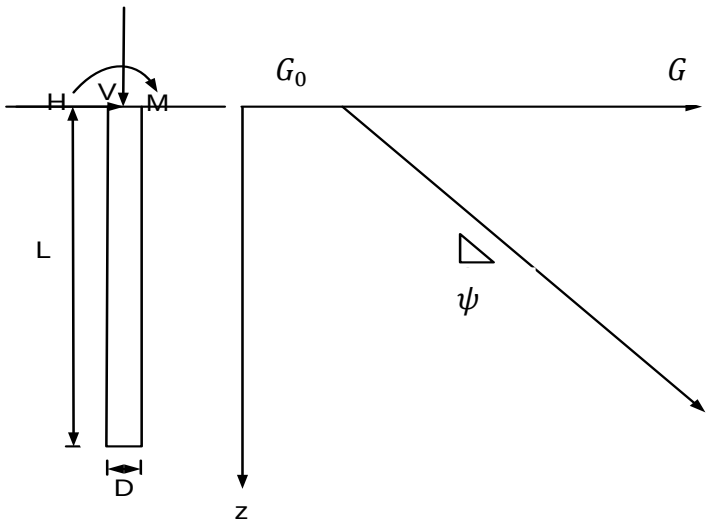

Figure 3.3: The shear modulus of soil vary linearly with depth

The first part of the integration represents the potential energy for the pile according to Bernoulli's theory

$$U = \frac{1}{2} Mk \tag{3.6}$$

where M is the bending moment, $M = E_p I_p \left(\frac{d^2u}{dz^2}\right)$, and k is the curvature, $k = \frac{d^2u}{dz^2}$ (Menaldi, et al., 2001).

The second part of the integration represents the internal potential energy of the soil column below the pile, which is calculated from L to infinity in the depth direction. The third part represents the internal potential energy of the surrounding soil. The strains are derived from displacements in cylindrical coordinates, and are described as follows:

$$\varepsilon_{rr} = \frac{du_r}{dr} \tag{3.7a}$$

$$\varepsilon_{\theta\theta} = \frac{1}{r}\left(u_r + \frac{du_\theta}{d\theta}\right) \tag{3.7b}$$

$$\varepsilon_{zz} = \frac{du_z}{dz} \tag{3.7c}$$

$$\varepsilon_{r\theta} = \frac{1}{2}\left(\frac{1}{r}\frac{\partial u_r}{\partial \theta} + \frac{\partial u_\theta}{\partial r} - \frac{u_\theta}{r}\right) \tag{3.7d}$$

$$\varepsilon_{\theta z} = \frac{1}{2}\left(\frac{\partial u_\theta}{\partial z} + \frac{1}{r}\frac{\partial u_z}{\partial \theta}\right) \tag{3.7e}$$

$$\varepsilon_{zr} = \frac{1}{2}\left(\frac{\partial u_r}{\partial z} + \frac{\partial u_z}{\partial r}\right) \tag{3.7f}$$

The stress components in cylindrical coordinates are given by

$$\sigma_{rr} = \lambda(\varepsilon_{rr}+\varepsilon_{\theta\theta}+\varepsilon_{zz}) + 2G\varepsilon_{rr} \tag{3.8a}$$

$$\sigma_{\theta\theta} = \lambda(\varepsilon_{rr}+\varepsilon_{\theta\theta}+\varepsilon_{zz}) + 2G\varepsilon_{\theta\theta} \tag{3.8b}$$

$$\sigma_{zz} = \lambda(\varepsilon_{rr}+\varepsilon_{\theta\theta}+\varepsilon_{zz}) + 2G\varepsilon_{z\,z} \tag{3.8c}$$

$$\sigma_{r\theta} = 2G\varepsilon_{r\theta} \tag{3.8d}$$

$$\sigma_{\theta z} = 2G\varepsilon_{\theta z} \tag{3.8e}$$

$$\sigma_{zr} = 2G\varepsilon_{zr} \tag{3.8f}$$

The governing equation is obtained by inserting the stress-strain relations into the potential energy Equation 3.4, and applying Hamilton's principle and the calculus of variations to obtain

$$\delta U = \left(E_p I_p \frac{d^2u}{dz^2}\delta\left(\frac{du}{dz}\right)\right) - \left[E_p I_p \frac{d^3u}{dz^3}\delta u\right]_0^L + \int_0^L E_p I_p \frac{d^4u}{dz^4}\delta u dz + \left[\pi {r_0}^2 G \frac{du}{dz}\delta u\right]_L^\infty$$
$$- \int_L^\infty \pi {r_0}^2 \left(G\frac{d^2u}{dz^2} + \frac{du}{dz}\frac{dG}{dz}\right)\delta u dz + \int_{r_0}^\infty r\left(\frac{d\phi_r}{dr}\right)^2 dr \int_0^\infty \pi(\lambda+2G)\, u\delta u dz$$
$$+ \int_0^\infty \pi(\lambda+3G)u^2 dz \int_{r_0}^\infty \left(\frac{\phi_r-\phi_\theta}{r}\right)\delta\phi_r dr + \int_0^\infty \pi(\lambda+2G)u^2\, dz \left[r\frac{d\phi_r}{dr}\delta\phi_r\right]_{r_0}^\infty$$
$$- \int_0^\infty \pi(\lambda+2G)u^2\, dz \int_{r_0}^\infty \left(r\frac{d^2\phi_r}{dr^2} + \frac{d\phi_r}{dr}\right)\delta\phi_r dr$$
$$+ \int_{r_0}^\infty r\left(\frac{\phi_r-\phi_\theta}{r}\right)^2 dr \int_0^\infty \pi(\lambda+3G)u\delta u dz$$
$$- \int_0^\infty \pi(\lambda+3G)\, u^2 dz \int_{r_0}^\infty \left(\frac{\phi_r-\phi_\theta}{r}\right)\delta\phi_\theta dr$$
$$+ \int_{r_0}^\infty r\left(\frac{d\phi_\theta}{dr}\right)^2 dr \int_0^\infty \pi G u\delta u dz + \int_0^\infty \pi G u^2\, dz \left[r\frac{d\phi_\theta}{dr}\right]_{r_0}^\infty$$
$$- \int_{r_0}^\infty \left(r\frac{d^2\phi_\theta}{dr^2} + \frac{d\phi_\theta}{dr}\right)\delta\phi_\theta dr + \int_0^\infty \pi G\left(\frac{du}{dz}\right)^2 dz \int_{r_0}^\infty r\phi_r\, \delta\phi_r dr$$
$$- \int_{r_0}^\infty r{\phi_r}^2\, dr \int_0^\infty \pi\left(G\frac{d^2u}{dz^2} + \frac{dG}{dz}\frac{du}{dz}\right)\delta u dz + \int_{r_0}^\infty r{\phi_r}^2\, dr \left[\pi G\frac{du}{dz}\delta u\right]_0^\infty$$
$$+ \int_0^\infty \pi G\left(\frac{du}{dz}\right)^2 dz \int_{r_0}^\infty r\phi_\theta\, \delta\phi_\theta dr + \int_{r_0}^\infty r{\phi_\theta}^2\, dr \left[\pi G\frac{du}{dz}\delta u\right]_0^\infty$$
$$- \int_0^\infty \pi G u^2\, dz \int_{r_0}^\infty \frac{d\phi_r}{dr}\delta\phi_\theta dr + \int_0^\infty \pi G u^2\, dz[(\phi_r-\phi_\theta)\delta\phi_\theta]_{r_0}^\infty$$
$$- \int_{r_0}^\infty r{\phi_\theta}^2\, dr \int_0^\infty \pi\left(G\frac{d^2u}{dz^2} + \frac{dG}{dz}\frac{du}{dz}\right)\delta u dz$$
$$+ \int_{r_0}^\infty (\phi_r-\phi_\theta)\frac{d\phi_r}{dr}dr \int_0^\infty \pi\lambda u\delta u dz + \int_0^\infty \pi\lambda u^2\, dz \int_{r_0}^\infty \frac{d\phi_\theta}{dr}\delta\phi_r dr$$
$$- \int_0^\infty \pi\lambda u^2\, dz \int_{r_0}^\infty \frac{d\phi_r}{dr}\delta\phi_\theta dr + \int_0^\infty \pi\lambda u^2\, dz[(\phi_r-\phi_\theta)\delta\phi_r]_{r_0}^\infty$$
$$+ \int_{r_0}^\infty (\phi_r-\phi_\theta)\frac{d\phi_\theta}{dr}dr \int_0^\infty 2\pi G u\delta u dz + \int_0^\infty \pi G u^2\, dz \int_{r_0}^\infty \frac{d\phi_\theta}{dr}\delta\phi_r dr \qquad (3.9)$$

3.1.2 The governing equation of the pile displacement for a static load

Governing equation that presents pile displacement can be obtained by collecting δu coefficients from Equation 3.9

For $0 \le z \le L$

$$E_p I_p \frac{d^4u}{dz^4} - C(G_0 + \psi z)\frac{d^2u}{dz^2} - C\psi\frac{du}{dz} + k(G_0 + \psi z)u = 0 \tag{3.10}$$

Governing equation for pile displacement at $L \leq z \leq \infty$

$$C_s(G_0 + \psi z)\frac{d^2u}{dz^2} + C_s\frac{du}{dz} + k(G_0 + \psi z)u = 0 \tag{3.11}$$

where

$$C = \pi\int_{r_0}^{\infty} r\left({\phi_r}^2 + {\phi_\theta}^2\right)dr$$

$$\begin{aligned} k = \pi\left(\frac{\lambda}{G} + 3\right)\int_{r_0}^{\infty} r\left(\frac{\phi_r - \phi_\theta}{r}\right)^2 dr \\ + \pi\left(\frac{\lambda}{G} + 2\right)\int_{r_0}^{\infty} r\left(\frac{d\phi_r}{dr}\right)^2 dr \\ + \pi\int_{r_0}^{\infty} r\left(\frac{d\phi_\theta}{dr}\right)^2 dr + 2\pi\frac{\lambda}{G}\int_{r_0}^{\infty}(\phi_r - \phi_\theta)\frac{d\phi_r}{dr}dr \\ + 2\pi\int_{r_0}^{\infty}(\phi_r - \phi_\theta)\frac{d\phi_\theta}{dr}dr \end{aligned}$$

$$C_s = \pi\int_{r_0}^{\infty} r\left({\phi_r}^2 + {\phi_\theta}^2\right)dr + \pi{r_0}^2$$

and ψ is the rate of variation of the shear modulus with depth. Governing equation of pile can be solved when boundary conditions are known which are obtained by collecting $\delta u \; and \; \delta\frac{du}{dz}$

For $z = 0$

$$\left(E_p I_p \frac{d^3u}{dz^3} - C(G_0 + \psi z)\frac{du}{dz} - Q_0\right)\delta u = 0 \tag{3.12}$$

$$\left(E_p I_p \frac{d^2u}{dz^2} + M_0\right)\delta\frac{du}{dz} = 0 \tag{3.13}$$

For $z = L$

$$\left(E_p I_p \frac{d^3u}{dz^3} - C(G_0 + \psi z)\frac{du}{dz}_{pile} + C_s(G_0 + \psi z)\frac{du}{dz}_{soil\ column}\right)\delta u = 0 \tag{3.14}$$

$$\left(E_p I_p \frac{d^2u}{dz^2}\right)\delta\frac{du}{dz} = 0 \tag{3.15}$$

For $z \to \infty$

$$\left(C_s[G_0 + \psi z]\frac{du}{dz}\right)\delta u = 0 \tag{3.16}$$

3.1.3 The governing equation of soil displacement for a static load

Governing equation for soil can be obtained by collecting coefficients that associated with $\delta\phi_r$ as follows:

$$r\frac{d^2\phi_r}{dr^2} + \frac{d\phi_r}{dr} - \left(\frac{\gamma_1}{r_0}\right)^2 r\phi_r - \gamma_2\frac{d\phi_\theta}{dr} - \gamma_3\frac{(\phi_r - \phi_\theta)}{r} = 0 \tag{3.17}$$

where

$$\left(\frac{\gamma_1}{r_0}\right)^2 = \frac{\int_0^\infty \pi G\left(\frac{du}{dz}\right)^2 dz}{\int_0^\infty \pi(\lambda + 2G)u^2 dz}$$

$$\gamma_2 = \frac{\int_0^\infty \pi(\lambda + G)u^2 dz}{\int_0^\infty \pi(\lambda + 2G)u^2\, dz}$$

$$\gamma_3 = \frac{\int_0^\infty \pi(\lambda + 3G)u^2 dz}{\int_0^\infty (\pi(\lambda + 2G)u^2 dz)}$$

By collecting the coefficients of $\delta\phi_\theta$ we get:

$$r\frac{d^2\phi_\theta}{dr^2} + \frac{d\phi_\theta}{dr} - \left(\frac{\gamma_4}{r_0}\right)^2 r\phi_\theta + \gamma_5\frac{d\phi_r}{dr} + \gamma_6\frac{(\phi_r - \phi_\theta)}{r} = 0 \tag{3.18}$$

where

$$\left(\frac{\gamma_4}{r_0}\right)^2 = \frac{\int_0^\infty \pi G \left(\frac{du}{dz}\right)^2 dz}{\int_0^\infty \pi G u^2 \, dz}$$

$$\gamma_5 = \frac{\int_0^\infty \pi(\lambda + G)u^2 dz}{\int_0^\infty \pi G u^2 \, dz}$$

$$\gamma_6 = \frac{\int_0^\infty \pi(\lambda + 3G)u^2 dz}{\int_0^\infty \pi G u^2 \, dz}$$

These governing equations can be solved using the boundary conditions

when $r = r_0$

$$\phi_r = 1 \qquad (3.19a)$$
$$\phi_\theta = 1$$

when $r \to \infty$

$$\phi_r = 0 \qquad (3.19b)$$
$$\phi_\theta = 0$$

All terms related to the variation of δu and $\delta\frac{\mathrm{du}}{\mathrm{dz}}$ at domain $\mathrm{L} \leq \mathrm{z} < \infty$ are equal to zero, but δu is not necessarily equal to zero, which gives the governing equation below the pile (Equation 3.10). For clamped pile, displacement at the tip of the pile equal to zero while the displacement under the pile in the case of a floating pile does not equal zero, so the general solution of the differential equation of the second order Equation 3.11 (at $L \leq z \leq \infty$) can be given in the form

$$u(z) = e^{-\sqrt{\frac{k}{C_s}}(z-L)} X(z) \qquad (3.20)$$

The second order equation can be written as

$$zu'' + (\chi + z)u' - \mu u = 0$$

and can be solved using a confluent hypergeometric function. By substituting Equation 3.20 into Equation 3.11 and introducing $Z = 2\sqrt{\frac{k}{C_s}}\left(\frac{G_0}{\psi} + z\right)$, it can be shown that X is governed by the confluent hypergeometric equation

$$Z\frac{d^2X}{dz^2} - Z\frac{dX}{dZ} + \frac{dX}{dZ} - \Upsilon X = 0 \tag{3.21}$$

where

$$\Upsilon = \frac{\psi\sqrt{kC_s}}{2\psi\sqrt{kC_s}} = 0.5.$$

The solution for X requires that it remains finite as $Z \to \infty$, therefore

$$X = AU(\Upsilon, 1, Z) \tag{3.22}$$

where A is a constant which can be determined from the pile displacement at $z=L$ and $U(\Upsilon, 1, Z)$ is the confluent hypergeometric function of second order.

At $L \leq z \leq \infty$

$$u(z) = u(z) = e^{-\sqrt{\frac{k}{C_s}}(z-L)} \frac{U\left(\Upsilon, 1, 2\sqrt{\frac{k}{C_s}}\left(\frac{G_0}{\psi}+z\right)\right)}{U\left(\Upsilon, 1, 2\sqrt{\frac{k}{C_s}}\left(\frac{G_0}{\psi}+L\right)\right)}. \tag{3.23}$$

The boundary condition at $(z = L)$ given by Equation 3.14 can be re-written as

$$E_p I_p \frac{d^3u}{dz^3} - C(G_0 + \psi z)\frac{du}{dz} - \chi u = 0 \tag{3.24}$$

where at $z = L$

$$\chi = \frac{\sqrt{kC_s}}{U(\Upsilon, 1, \mathrm{z})}\left(\frac{G_0}{\psi} + L\right)(1 + \psi U(\Upsilon + 1,2, Z) \tag{3.25}$$

Solution procedure

The solution of the governing differential equation for the floating pile displacement Equation 3.10 with the boundary conditions (Equations 3.12, 3.13, 3.14 and 3.15) follows procedure below

I. Assume initial values for γ_1 , ... and γ_6. In the author's experience, the values could be less than 0.001.

II. Calculate ϕ_r and ϕ_θ by solving Equations 3.17 and 3.18 simultaneously together with the boundary conditions given by Equation 3.23. The one dimensional finite difference technique can be used.

III. Calculate the coefficients C, k and C_s.

IV. Solve Equation 3.10 together with the boundary conditions given by Equations 3.12, 3.13, 3.14 and 3.15. One dimensional finite difference technique can be used here as well.

V. Insert the results obtained in IV to calculate the new values for γ_1 , ... and γ_6.

VI. Iterate until the difference between the new γ_1 , ... and γ_6 and the old values becomes negligible.

The procedure should be repeated until the relative error $\left(\gamma_i(new) - \gamma_i(old)\right)/\gamma_i(old)$ is less than the specified tolerance. A program written in Wolfram MATHEMATICA version 9.10 has been used here to solve this iterative procedure.

3.1.4 Comparison with static load solution

The validity of the proposed solution can be compared with other solutions for piles under static lateral loads. For uniform soil, by taking the limits when $\eta \to 0$, the displacement beneath a floating pile (Equation 3.20) at $(L \leq z \leq \infty)$ is reduced to

$$u(z) = e^{-\sqrt{\frac{k}{C_s}}(z-L)}. \tag{3.26}$$

and the quantity χ in Equation 3.12 reduces to

$$\chi = \sqrt{kC_s}G_0 \,. \tag{3.27}$$

Thus, the solution becomes similar to that derived by Basu et al. (2009) $(u = Ae^{-\alpha z} + Be^{\alpha z})$

For a pile embedded in non-uniform elastic soil, the stiffness of soil is assumed to change with depth according to this relation $(G = \eta z)$, Randolph (1981) derived algebraic expressions which allow the behaviour of flexible piles under lateral loading to be calculated, in terms of fundamental soil properties. These expressions are based on the results of finite element studies. The pile displacement at the ground surface is given by Equations 2.20 and 2.21. For the case of one layer soil, the pile head displacement is given by Equations 2.18 and 2.19, and the soil stiffness assumed to be constant. The proposed solution and previous work show that, the results are of the same order of magnitude, see Figures 3.4, 3.5, 3.6 and 3.7.

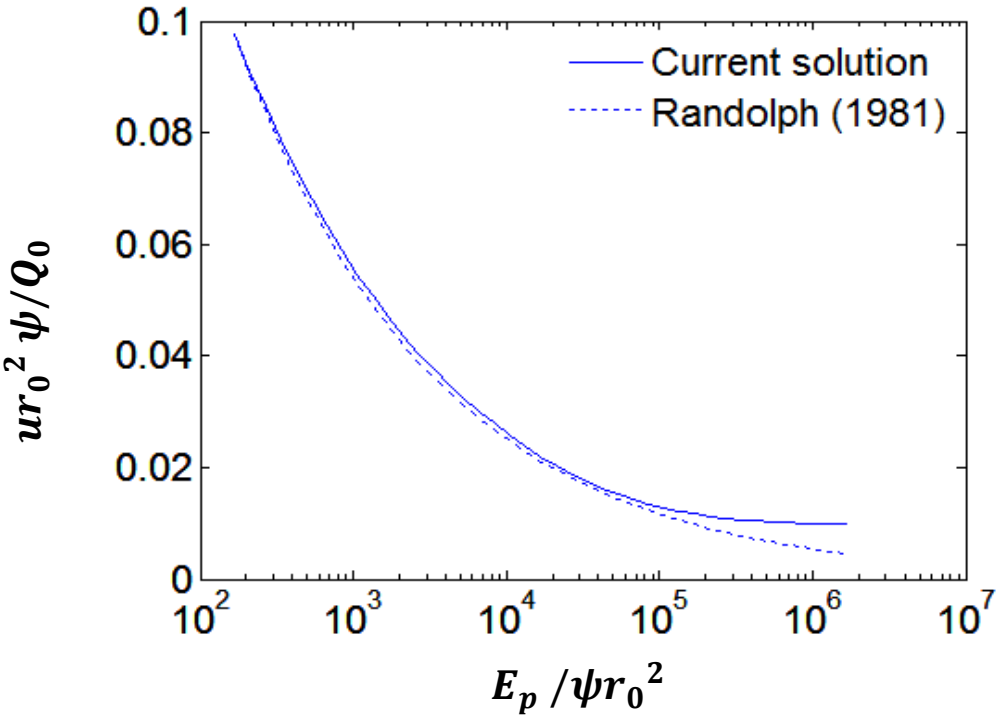

Figure 3.4: Variation of pile displacement under lateral load with stiffness ratio (uniform soil)

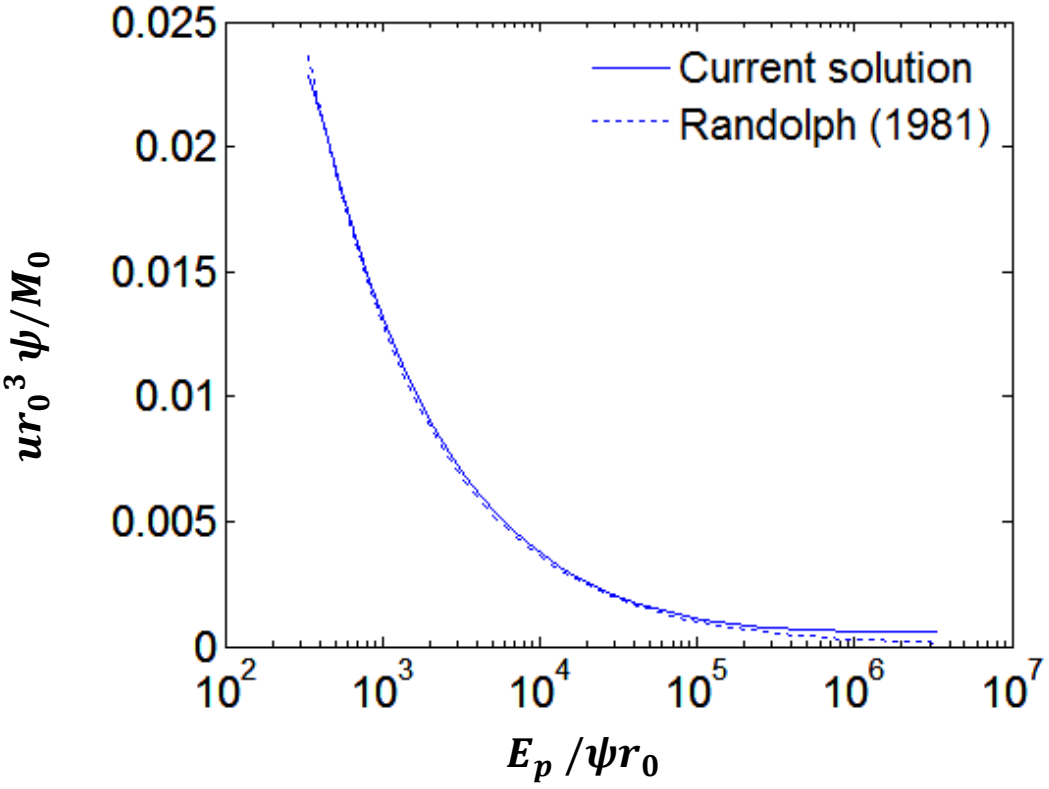

Figure 3.5: Variation of pile displacement under lateral moment with stiffness ratio (uniform soil)

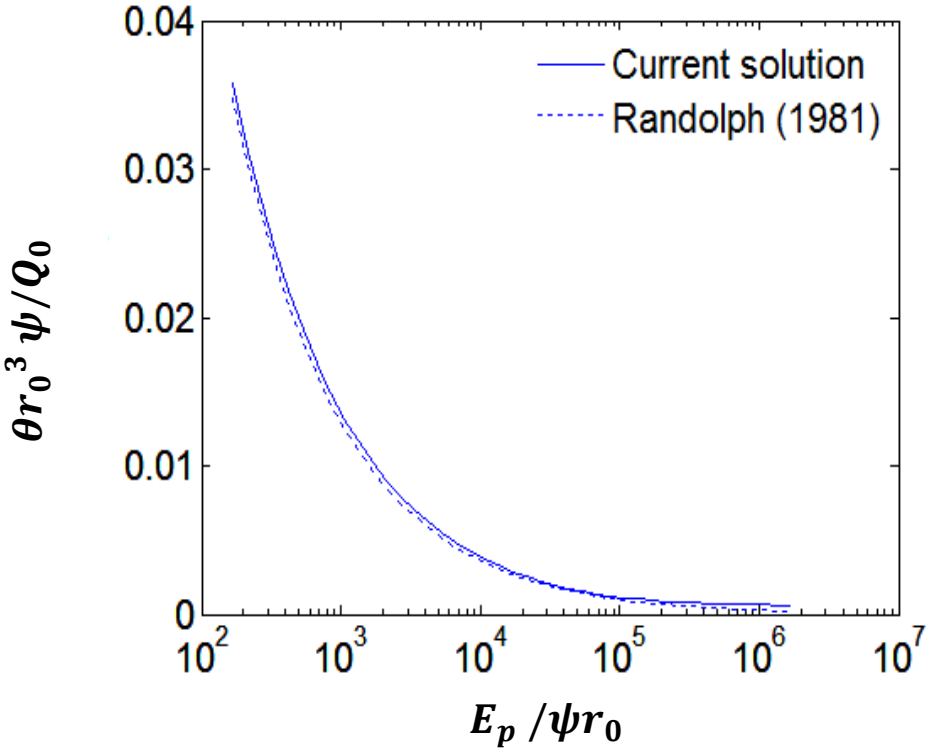

Figure 3.6: Variation of pile displacement under lateral load with stiffness ratio (non-uniform soil)

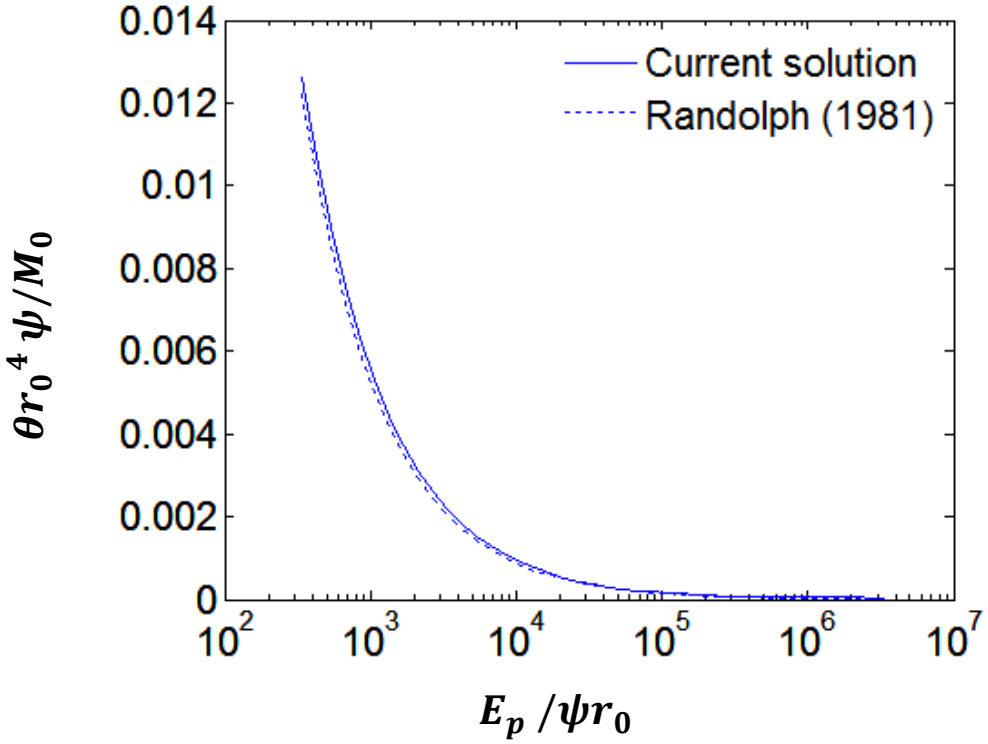

Figure 3.7: Variation of pile displacement under lateral moment with stiffness ratio (non-uniform soil)

3.2 Analysis of piles under dynamic lateral loads

There is a solution developed by Liu et al. (2014) this solution based on the energy approach to predict the response of pile in uniform isotropic linear elastic soil, the pile-soil system overlying on rigid rock base (see Figure 3.8). The pile is subjected to vertical propagating waves, and the Hamilton's principle has been used. However, in this thesis the pile is subject to lateral propagation waves, where the governing equations for pile and soil resulting from current study are different compared with Liu et al. (2014), although both studies are used the energy method to predict the dynamic pile response. Liu et al. (2014)'s assumption of the deformation field (Equations 3.28a-3.28c) could lead to high stiffness response as demonstrated by Basu et al. (2009), see Figure 3.13.

$$\mathrm{v}_r = \left(\mathrm{v}_f - \left(\mathrm{v}_f - \mathrm{v}\right)\phi\right)cos\theta \tag{3.28a}$$

$$\mathrm{v}_\theta = -\left(\mathrm{v}_f - \left(\mathrm{v}_f - \mathrm{v}\right)\phi\right)sin\theta \tag{3.28b}$$

$$\mathrm{v}_z = 0. \tag{3.28c}$$

and the governing equations and boundary conditions are obtained by minimizing the potential and kinetic energies as follows

$$E_P I_P \frac{d^4\mathrm{v}}{dz^4} - 2t\frac{d^2\mathrm{v}}{dz^2} + 4\lambda^4\mathrm{v} - \xi_p\mathrm{v}_f = 0 \tag{3.29}$$

Boundary conditions

When $z = 0$

$$\frac{d^2\mathrm{v}}{dz^2} = 0 \tag{3.30a}$$

$$E_P I_P \frac{d^3\mathrm{v}}{dz^3} - 2C\frac{d\mathrm{v}}{dz} = 0 \tag{3.30b}$$

When $z = L$

$$\frac{d^2\mathrm{v}}{dz^2} = 0 \tag{3.30c}$$

$$E_P I_P \frac{d^3 \mathrm{v}}{dz^3} - 2C \frac{d\mathrm{v}}{dz} + (2C + G_s A) \frac{d\mathrm{v}}{dz} = 0 \qquad (3.30d)$$

The governing equation for the soil

$$\frac{d^2\phi}{dr^2} + \frac{1}{r}\frac{d\phi}{dr} - \left(\frac{\gamma}{r_0}\right)^2 \phi = 0 \qquad (3.31)$$

$$\left(\frac{\gamma}{r_0}\right)^2 = \frac{2Gs \int_0^H \left(\frac{d\mathrm{v}}{dz} - \frac{d\mathrm{v}_f}{dz}\right)^2 dz - 2\rho \int_0^H \left(\frac{d\mathrm{v}}{dt} - \frac{d\mathrm{v}_f}{dt}\right)^2 dz}{(\eta^2 + 1) G_s \int_0^H (\mathrm{v} - \mathrm{v}_f)^2 \, dz} \qquad (3.32)$$

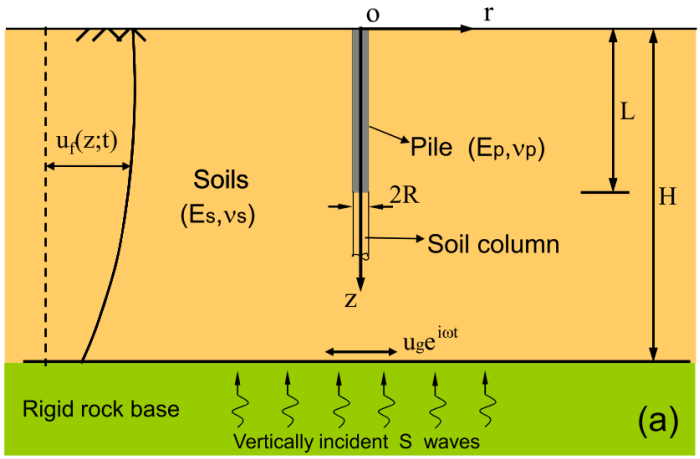

Figure 3.8: Piles under vertically propagating waves (from Liu et al., 2014)

In this thesis, the governing equation of the pile and the soil for a static load can be obtained by using potential energy and external energy. However, for the response of a laterally loaded pile subjected to a dynamic force, kinetic energy is involved and Hamilton's principle has been used. The potential energy of the pile-soil system is

$$\frac{1}{2}E_P I_P \int_0^L \left(\frac{d^2u}{dz^2}\right)^2 dz + \frac{\pi}{2}\int_0^\infty \int_{r_0}^\infty \left[(\lambda+2G)u^2\left(\frac{d\phi_r}{dr}\right)^2 + 2\lambda u^2 \frac{d\phi_r}{dr}\frac{(\phi_r-\phi_\theta)}{r} + (\lambda+3G)u^2\frac{(\phi_r-\phi_\theta)^2}{r^2} + Gu^2\left(\frac{d\phi_\theta}{dr}\right)^2 + G\left(\frac{du}{dz}\right)^2 {\phi_r}^2 + G\left(\frac{du}{dz}\right)^2 {\phi_\theta}^2 + 2Gu^2\frac{(\phi_r-\phi_\theta)}{r}\frac{d\phi_\theta}{dr}\right] r dr dz + \frac{\pi}{2}G\int_L^\infty \int_{r_0}^\infty \left(\frac{du}{dz}\right)^2 r dr dz = 0\,. \quad (3.33)$$

Equation 3.33 should be differentiated to minimize the potential energy for the equilibrium of the system. The set of equations below represents the differentiations of the potential energy equation, where it divides into three parts. The first part denotes the potential of the pile δU_1, the second part is the soil column under the pile δU_2, and the third part is the surrounding soil δU_3.

$$\delta U_{1=} \int_0^L E_P I_P \frac{d^2u}{dz^2}\delta\left(\frac{d^2u}{dz^2}\right)dz = \left[E_P I_P \frac{d^2u}{dz^2}\delta\left(\frac{du}{dz}\right)\right]_0^L - E_P I_P \int_0^L \frac{d^3u}{dz^3}\delta\frac{du}{dz}dz$$
$$= \left[E_P I_P \frac{d^2u}{dz^2}\delta\left(\frac{du}{dz}\right)\right]_0^L - \left[E_P I_P \frac{d^3u}{dz^3}\delta u\right]_0^L$$
$$- E_P I_P \int_0^L \frac{d^4u}{dz^4}\delta u dz \quad (3.34a)$$

$$\delta U_2 = \pi {r_0}^2 G \int_L^\infty \frac{du}{dz}\delta\left(\frac{du}{dz}\right)dz$$
$$= \left[\pi {r_0}^2 G\frac{du}{dz}\delta u\right]_L^\infty - \int_L^\infty \pi {r_0}^2\left(G\frac{d^2u}{dz^2}\right)\delta u dz \quad (3.34b)$$

$$\delta U_3 = \frac{\pi}{2}\int_0^\infty \int_{r_0}^\infty \left[(\lambda+2G)u\frac{d\phi_r}{dr}\delta u\frac{d\phi_r}{dr} + 2\lambda u\frac{d\phi_r}{dr}\frac{(\phi_r-\phi_\theta)}{r}\delta u + \lambda u^2\delta\left(\frac{d\phi_r}{dr}\frac{(\phi_r-\phi_\theta)}{r}\right) + (\lambda+3G)u\frac{(\phi_r-\phi_\theta)}{r}\delta u\left(\frac{(\phi_r-\phi_\theta)}{r}\right) + Gu\frac{d\phi_\theta}{dr}\delta\left(u\frac{d\phi_\theta}{dr}\right) + G\phi_r\frac{du}{dz}\delta\phi_r\frac{du}{dz} + G\phi_\theta\frac{du}{dz}\delta\left(\phi_\theta\frac{du}{dz}\right) + 2Gu\frac{(\phi_r-\phi_\theta)}{r}\frac{d\phi_\theta}{dr}\delta u + Gu^2\delta\left(\frac{(\phi_r-\phi_\theta)}{r}\frac{d\phi_\theta}{dr}\right)\right] r dr dz. \quad (3.34c)$$

Full details can be found in Appendix 3.5.

The kinetic energy of the pile - soil system, which is based on stresses and strains, is given by

$$T = \frac{1}{2}\int_0^L m_p \left(\frac{du}{dt}\right)^2 dz + \frac{1}{2}\int_L^\infty m_s \left(\frac{du}{dt}\right)^2 dz + \frac{1}{2}\int_0^{2\pi}\int_0^\infty\int_{r_0}^\infty \rho_s \left[\left(\frac{du_r}{dt}\right)^2 + \left(\frac{du_\theta}{dt}\right)^2\right] r dr d\theta dz \quad (3.35)$$

Where $G\ and\ \lambda$ are elastic modulus which are constant, m_p and m_s represent the pile and the soil masses, and ρ_s is soil density.

Similar to the potential energy, kinetic energy should be differentiated for the equilibrium system as follows:

$$\delta T = \pi {r_0}^2 \rho_p \int_{t_1}^{t_2}\int_0^L \frac{du}{dt}\delta\left(\frac{du}{dt}\right) dz dt + \pi {r_0}^2 \rho_s \int_{t_1}^{t_2}\int_{L\infty}^\infty \frac{du}{dt}\delta\frac{du}{dt} dz dt + \pi\rho_s \int_{t_1}^{t_2}\int_0^\infty\int_{r_0}^\infty \phi_r \frac{du}{dt}\delta\phi_r \frac{du}{dt} r dr dz dt + \pi\rho_s \int_{t_1}^{t_2}\int_0^\infty\int_{r_0}^\infty \phi_\theta \frac{du}{dt}\delta\phi_\theta \frac{du}{dt} r dr dz dt \quad (3.36)$$

Full details on differentiating potential and kinetic energies can be found in the Appendix.

3.2.1 Pile displacement

Governing equation pile displacement under lateral dynamic load represents as

$$E_P I_P \frac{d^4u}{dz^4} - C\frac{d^2u}{dz^2} + ku - S\frac{d^2u}{dt^2} = 0 \quad (3.37)$$

where

$$s_1 = \pi {r_0}^2 (\rho_P) \quad (3.38a)$$

$$s_2 = 2\pi\rho_s(m_1 + m_2) \tag{3.38b}$$

$$S = s_1 + s_2 \tag{3.38c}$$

$$m_1 = \int_R^\infty r\ {\phi_r}^2\ dr \tag{3.39a}$$

$$m_2 = \int_R^\infty r\ \ {\phi_\theta}^2\ \ \ \ \phi_\theta\ dr \tag{3.39b}$$

The boundary conditions for the governing equation of the free base pile are calculated by collecting δu and $\delta\frac{du}{dz}$ at $z = 0$.

$$\left(E_P I_P\ \frac{d^2u}{dz^2} + M_0\right)\delta\frac{du}{dz} = 0 \tag{3.40a}$$

$$\left(E_P I_P\ \frac{d^3u}{dz^3} - C\frac{du}{dz} - Q_0\right)\delta u = 0 \tag{3.40b}$$

at $z = L$

$$E_P I_P\ \frac{d^2u}{dz^2}\delta\frac{du}{dz} = 0 \tag{3.40c}$$

$$\left(E_P I_P\frac{d^3u}{dz^3} - C\frac{du}{dz}\Big|_{pile} + C_s\frac{du}{dz}\Big|_{soil\ column}\ \right)\delta u = 0. \tag{3.40d}$$

The domain below the pile will be considered as $L \le z \le \infty$ and we can write

$$C_s\frac{d^2u}{dz^2} - ku - S\frac{d^2u}{dt^2} = 0. \tag{3.41}$$

The fourth part of the governing (Equation 3.37) represents the lateral displacement as a function of time; for a linear system and harmonic force with frequency ω, the steady state response of the pile - soil system can be expressed as

$$u = \hat{u}\,(r,z)e^{-i\omega t} \tag{3.42a}$$

$$\frac{du}{dt} = -i\omega\hat{u}\,(r,z)e^{-i\omega t} \tag{3.42b}$$

$$\frac{d^2u}{dt^2} = -\omega^2\hat{u}\,(r,z)e^{-i\omega t} \tag{3.42c}$$

where i is the imaginary number $\left(\sqrt{-1}\right)$, $\hat{u}$ is the amplitude of pile displacement and ω represents a circular frequency. For the domain below the pile, similar to the case of static load, the pile displacements $u_1(l)$ at the connection point with the soil $u_2(l)$ are the same,

u_1 is a pile displacement in domain $0 \le z \le L$ and u_2 denotes soil displacement in domain $L \le z < \infty$

$u_1(l) = u_2(l)$

$u_1 = u_2 = Ae^{-\alpha z}$.

The boundary condition at $z = L$ is $u_2(L) = u_1(L)$

$u_1 = u_2 = Ae^{-\alpha l}$

Since

$A = \frac{u_1}{e^{-\alpha l}}$, hence $u_2 = \frac{u_1}{e^{-\alpha l}} \times e^{-\alpha z}$

$u_2 = u_1 \times e^{-\alpha(z-l)}$

$\frac{d^2u}{dz^2} = -\alpha^2 u_1 \times e^{-\alpha(z-l)}$.

The third part is with respect to time, so it changes to the frequency domain

$\frac{d^2u}{dt^2} = -\omega^2 u_1$.

Equation 3.36 then becomes

$$C_s\left(-\alpha^2 u_1 \times e^{-\alpha(z-l)}\right) - ku - S(-\omega^2 u_1) = 0 \tag{3.43}$$

$$\alpha = \sqrt{\frac{\mathrm{k} - \mathrm{S}\omega^2}{\mathrm{C_s}}}\,. \tag{3.44}$$

The governing equation will be

$$E_P I_P \ \frac{d^4u}{dz^4} - C\frac{d^2u}{dz^2} + (k - S\omega^2)u = 0. \tag{3.45}$$

The boundary condition equations for floating piles are then as follows

$z = 0$

$$\left(E_P I_P \ \frac{d^2u}{dz^2} + M_0\right)\delta\frac{du}{dz} = 0 \tag{3.46a}$$

$$\left(E_P I_P \ \frac{d^3u}{dz^3} - C\frac{du}{dz} - Q_0\right)\delta u = 0 \tag{3.46b}$$

at $z = L$,

$$E_P I_P \ \frac{d^2u}{dz^2}\delta\frac{du}{dz} = 0 \tag{3.46c}$$

$$E_P I_P \ \frac{d^3u}{dz^3} - C_s\frac{du}{dz} - \sqrt{(k - S\omega^2)C_s}u = 0. \tag{3.46d}$$

The boundary conditions for a clamped pile are as follows

at $z = 0$

$$\left(E_P I_P \ \frac{d^2u}{dz^2} + M_0\right)\delta\frac{du}{dz} = 0 \tag{3.47a}$$

$$\left(E_P I_P \frac{d^3u}{dz^3} - C\frac{du}{dz} - Q_0\right)\delta u = 0 \qquad (3.427b)$$

at $z = L$

$$u = 0 \qquad (3.47c)$$

$$\frac{du}{dz} = 0 \qquad (3.47d)$$

3.2.2 Soil displacement

By collecting $\delta\phi_r dr$ from differentiating potential and kinetic energies, the governing equation for static loading will be obtained

$$\int_{r0}^{\infty}\left[-m_{s1}\left(r\frac{d^2\phi_r}{dr^2} + \frac{d\phi_r}{dr}\right) + (m_{s2} + m_{s3})\frac{d\phi_\theta}{dr} + m_{s4}\left(\frac{\phi_r}{r} - \frac{\phi_\theta}{r}\right) + n_{s1} r\phi_r\right]\delta\phi_r dr = 0 \qquad (3.48)$$

where

$$m_{s1} = (\lambda + 2G)\int_0^{\infty} u^2\, dz \qquad (3.49a)$$

$$m_{s2} = G\int_0^{\infty} u^2\, dz \qquad (3.49b)$$

$$m_{s3} = \lambda\int_0^{\infty} u^2\, dz \qquad (3.49c)$$

$$m_{s4} = (\lambda + 3G)\int_0^{\infty} u^2\, dz \qquad (3.49d)$$

$$n_{s1} = G\int_0^{\infty}\left(\frac{du}{dz}\right)^2 dz \qquad (3.49e)$$

$$n_{s2} = \pi\rho_s\omega^2 \int_0^\infty u^2 dz. \tag{3.49f}$$

By dividing Equation 3.47 by $(-m_{s1}\ and\ r)$, the governing differential equation is obtained as follows

$$\left(\frac{d^2\phi_r}{dr^2} + \frac{1}{r}\frac{d\phi_r}{dr}\right) - \left(\left(\frac{\gamma_1}{r}\right)^2 + \left(\frac{\gamma_2}{r_0}\right)^2\right)\phi_r = \frac{\gamma_3}{r}\frac{d\phi_\theta}{dr} - \left(\frac{\gamma_1}{r}\right)^2 \phi_\theta \tag{3.50}$$

where

$$\gamma_1 = \sqrt{\frac{(\lambda + 3G)\int_0^\infty u^2\, dz}{(\lambda + 2G)\int_0^\infty u^2\, dz}} \tag{3.51a}$$

$$\gamma_2 = \sqrt{\frac{\pi\rho_s\omega^2 \int_0^\infty u^2 dz + G\int_0^\infty \left(\frac{du}{dz}\right)^2 dz}{(\lambda + 2G)\int_0^\infty u^2\, dz}}\, r_0 \tag{3.51b}$$

$$\gamma_3 = \sqrt{\frac{G\int_0^\infty u^2\, dz + \lambda\int_0^\infty u^2\, dz}{(\lambda + 2G)\int_0^\infty u^2\, dz}}. \tag{3.51c}$$

In the same way, by collecting $\delta\phi_\theta$ and dividing the term by $(m_{s2}r)$, we obtain

$$\left(\frac{d^2\phi_\theta}{dr^2} + \frac{1}{r}\frac{d\phi_\theta}{dr}\right) - \left(\left(\frac{\gamma_4}{r}\right)^2 + \left(\frac{\gamma_5}{r_0}\right)^2\right)\phi_\theta = \frac{\gamma_6}{r}\frac{d\phi_r}{dr} - \left(\frac{\gamma_1}{r}\right)^2 \phi_r \tag{3.52}$$

where

$$\gamma_4 = \sqrt{\frac{(\lambda + 3G)\int_0^\infty u^2\, dz}{G\int_0^\infty u^2\, dz}} \tag{3.53a}$$

$$\gamma_5 = \sqrt{\frac{\pi\rho_s\omega^2 \int_0^\infty u^2 dz + G\int_0^\infty \left(\frac{du}{dz}\right)^2 dz}{G\int_0^\infty u^2\, dz}}\, r_0 \tag{3.53b}$$

$$\gamma_6 = \sqrt{\frac{G\int_0^\infty u^2\,dz + \lambda\int_0^\infty u^2\,dz}{G\int_0^\infty u^2\,dz}}. \qquad (3.53c)$$

The boundary conditions for both governing equations are

$\phi_r(r) = 1$ when $r = r_0$ and $\phi(r) = 0$ when $r \to \infty$. Similarly $\phi_\theta = 1$ when $r = r_0$, and $\phi_\theta = 0$ when $r \to \infty$. The values of ϕ_r and ϕ_θ vary between 1 and zero.

3.2.3 Closed-form solution for pile displacement

The governing equation of the pile can be solved using a closed-form solution, the general solution of differential equations of pile displacement of the 4th order is

$$u = a\,\alpha_1 + b\,\alpha_2 + c\,\alpha_3 + d\alpha_4 \qquad (3.54)$$

where a, b, c and d are constants, and $\alpha_1, \alpha_2, \alpha_3\ and\ \alpha_4$ are the individual solutions of the differential equations.

a, b, c and d constants can be determined by solving the boundary conditions in a matrix form

$$[k]_{4\times4}.[U]_{4\times1} = [F]_{4\times1} \qquad (3.55)$$

The k matrix represents the boundary conditions, U describes the constants and F is the external load. The response of a laterally loaded pile depends on a number of factors, such as the soil properties and the pile geometry.

The governing equations of soil displacement can be solved by using the finite difference method (see Figure 3.9). These equations are mutually dependent, therefore, they must be solved concurrently using a central difference scheme. Then the governing equations can be written as

$$\frac{{\phi_r}^{i+1} - 2{\phi_r}^{i} + {\phi_r}^{i-1}}{\Delta r^2} + \frac{1}{r_i}\frac{{\phi_r}^{i+1} - {\phi_r}^{i-1}}{2\,\Delta r} - \left[\left(\frac{\gamma_1}{r_i}\right)^2 + \left(\frac{\gamma_2}{r_0}\right)^2\right]{\phi_r}^{i}$$
$$= \frac{{\gamma_3}^2}{r_i}\frac{{\phi_\theta}^{i+1} - {\phi_\theta}^{i-1}}{2\,\Delta r} - \left(\frac{\gamma_1}{r_j}\right)^2 {\phi_\theta}^{i} \qquad (3.56a)$$

$$\frac{{\phi_\theta}^{i+1} - 2{\phi_\theta}^{i} + {\phi_\theta}^{i-1}}{\Delta r^2} + \frac{1}{r_i}\frac{{\phi_\theta}^{i+1} - {\phi_\theta}^{i-1}}{2\,\Delta r} - \left[\left(\frac{\gamma_4}{r_i}\right)^2 + \left(\frac{\gamma_5}{r_0}\right)^2\right]{\phi_\theta}^{i}$$
$$= \frac{{\gamma_6}^2}{r_i}\frac{{\phi_r}^{i+1} - {\phi_r}^{i-1}}{2\,\Delta r} - \left(\frac{\gamma_4}{r_i}\right)^2 {\phi_r}^{i} \qquad (3.56b)$$

where i is the node i^{th} at r_i distance in radial axis; Δr represents the distance between two nodes and should be small for accuracy. The number of nodes is m.

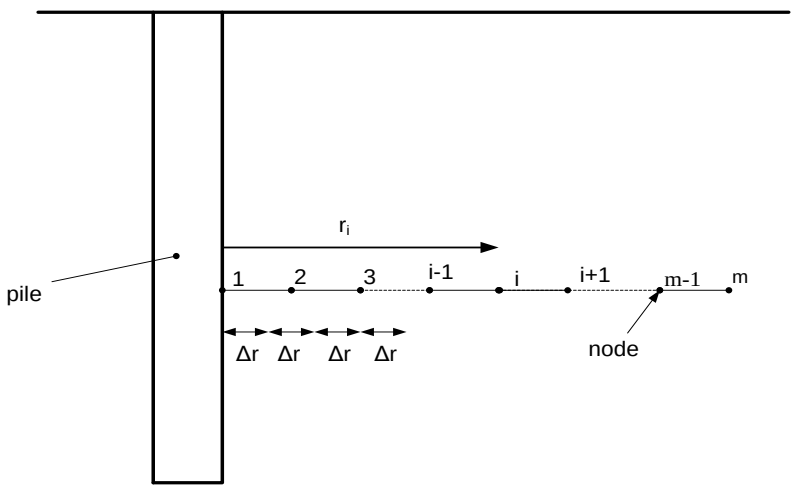

Figure 3.9: Finite difference discretisation for ϕ_r and ϕ_θ

The governing equation of soil has been calculated by assuming initial values for $\gamma_1, \gamma_2, \ldots\ldots\ldots and\ \gamma_6$ to calculate *C, k, m_1, m_2,.. m_6* to obtain $\phi_r\ and\ \phi_\theta$ the results for these variables can be inserted into the governing differential equation of the pile. Also, the iterative technique has been employed by obtaining the condition $\frac{\gamma_{old-}\gamma_{new}}{\gamma_{old}} = 0.001$, see Figure 3.10.

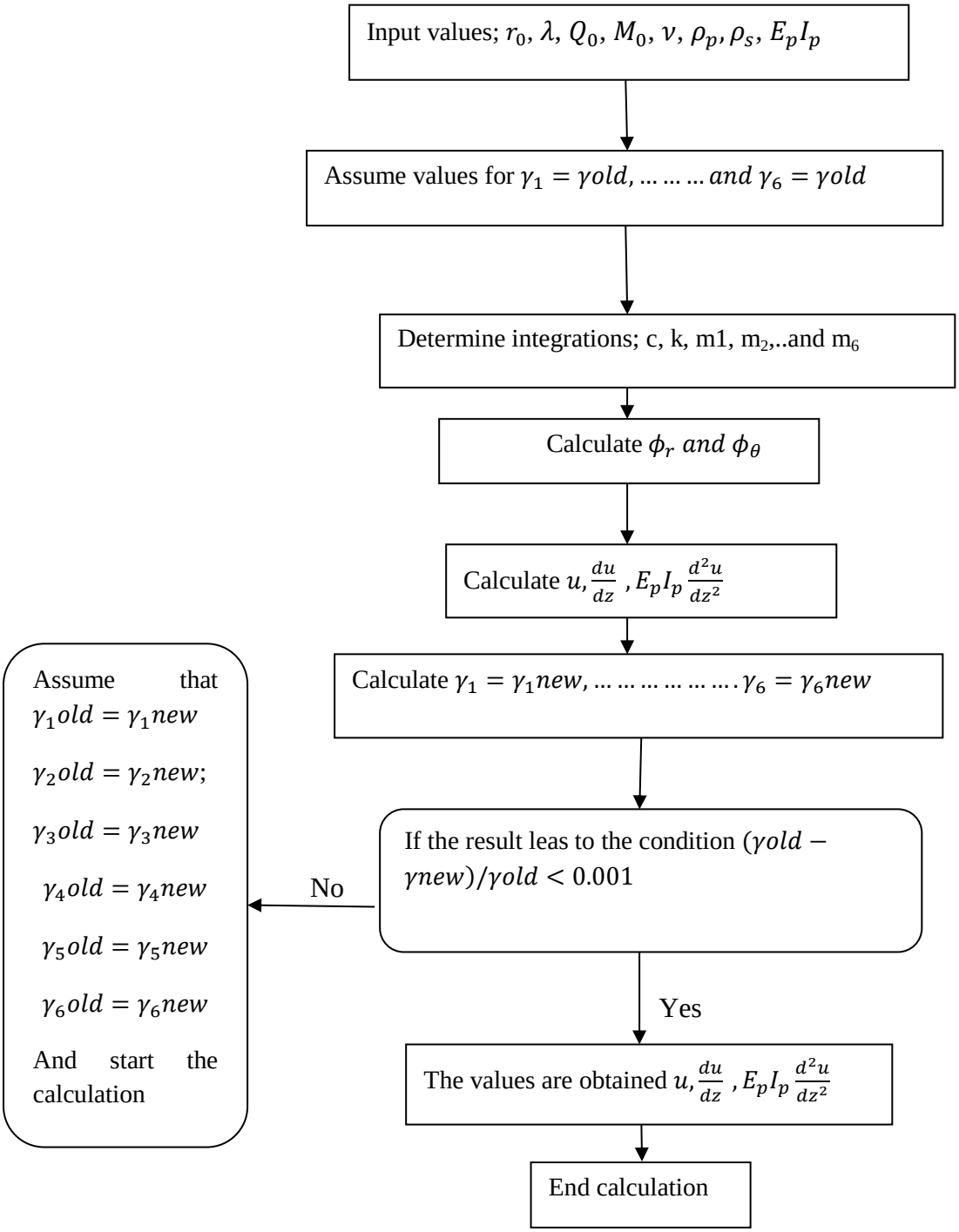

Figure 3.10: Solution flow chart

3.2.4 Comparison with field data and previous work

El-Marsafawi et al. (1992) tested a single concrete pile subjected to a horizontal vibration load. The pile, of length 7.5m and diameter 0.32m, was installed in homogenous sandy clay soil in Harbin (China). The Young's modulus of the pile being $1.96 \times 10^{10} N/m^2$. The exciting force applied to the top of the pile was given by

$$q_0(t) = m_e e\, \omega^2 \cos \omega t \tag{3.57}$$

where m_e is the mass of exciter which $(120kg)$, e is the length of the pile above the surface, and ω represents a circular frequency which is equal to $\omega = \frac{a_0\, V_s}{r_0}$, where a_0 is a function of the dimensionless frequency and V_s is the soil shear wave velocity, which is equal to $130m/s$ in the surface.

Figure 3.11 shows the single pile used in the experiment, where the normalized amplitudes are for three excitation intensities, $m_e.e = 96\ kg.mm$, $m_e.e = 1741kg.mm$ and $m_e.e = 259\ kg.mm$, where m_e represents the mass of the pile cap and e is the length of the pile between the bottom face of the pile cap and above the surface. The maximum normalized amplitudes were at frequencies 18, 17 and 15.6, respectively. The results of the present study were reasonable with the field data, as compared with those of Das and Sargand's analysis.

The frequency response at the head of the clamped pile is shown in Figure 3.12. Here, the ratio between the Young modulus for the pile and the soil is 1000 $\left(\frac{E_p}{E_s} = 1000\right)$. As shows in this figure, the present formulations gives the better prediction to resonant frequency compared with Das and Sargand (1999). The present study's assumptions leads to more accurate pile-soil prediction, because it assumed that soil displacement was not only occurs in the load direction as it assumed in Das and Sargand (1999), but that the soil mass displacement had components perpendicular to the load direction, which meant that $u_r \neq u_\theta$ whereas. Das and Sargand (1999) assumed that the radial and circumferential components of displacements are equal $\phi_r(r) = \phi_\theta(r) = \phi(r)$ Figure 3.12 shows the difference between these sets of assumptions. Figure 3.14 shows the dimensional frequency (a_0) plotted against the normalised displacement u(a_0)/u(a_0=0). This figure shows that Das and Sargand (1999) that the predicts higher resonant frequency compared this analytical solution. Comparing

Figure 3.14 with Figure 3.13, it could be concluded that Das and Sargand (1999) gives stiffer unrealistic response while the present solution can capture the resonant response of structures.

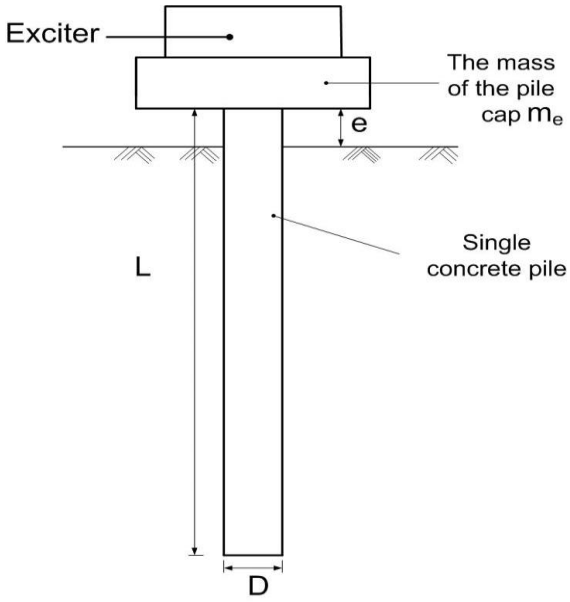

Figure 3.11: Single concrete pile subjected to a lateral load (El-Marsafawi, 1992)

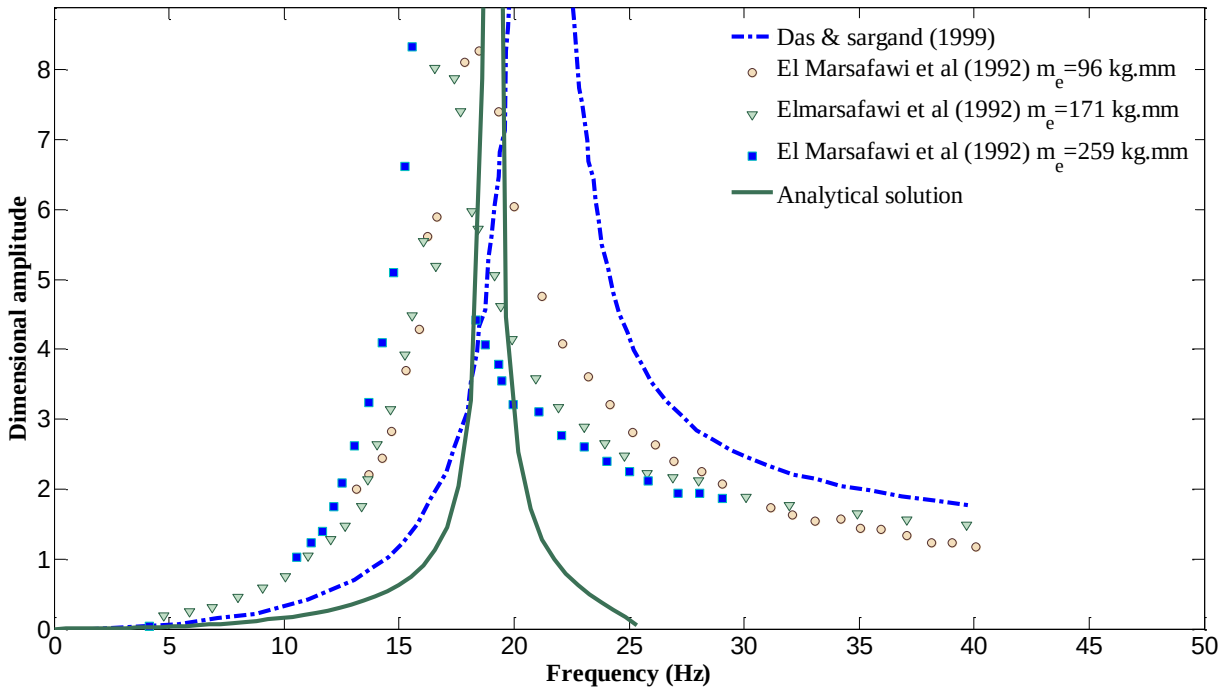

Figure 3.12: Dimensionless displacement of the top of the pile at different frequenci

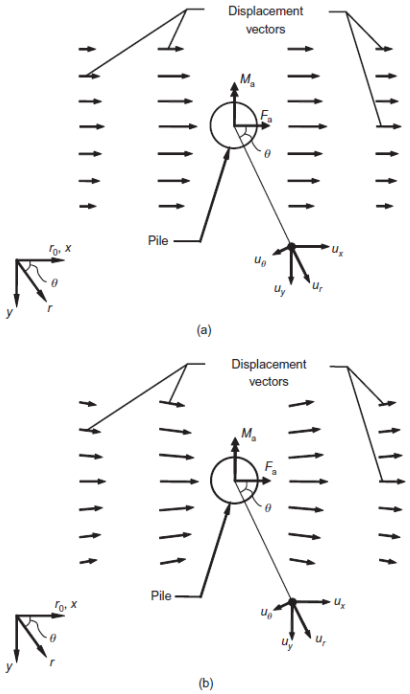

Figure 3.13: Laterally loaded pile displacement according to Sun's (1994) and Basu, et al.'s assumptions (after Basu, et al., 2009)

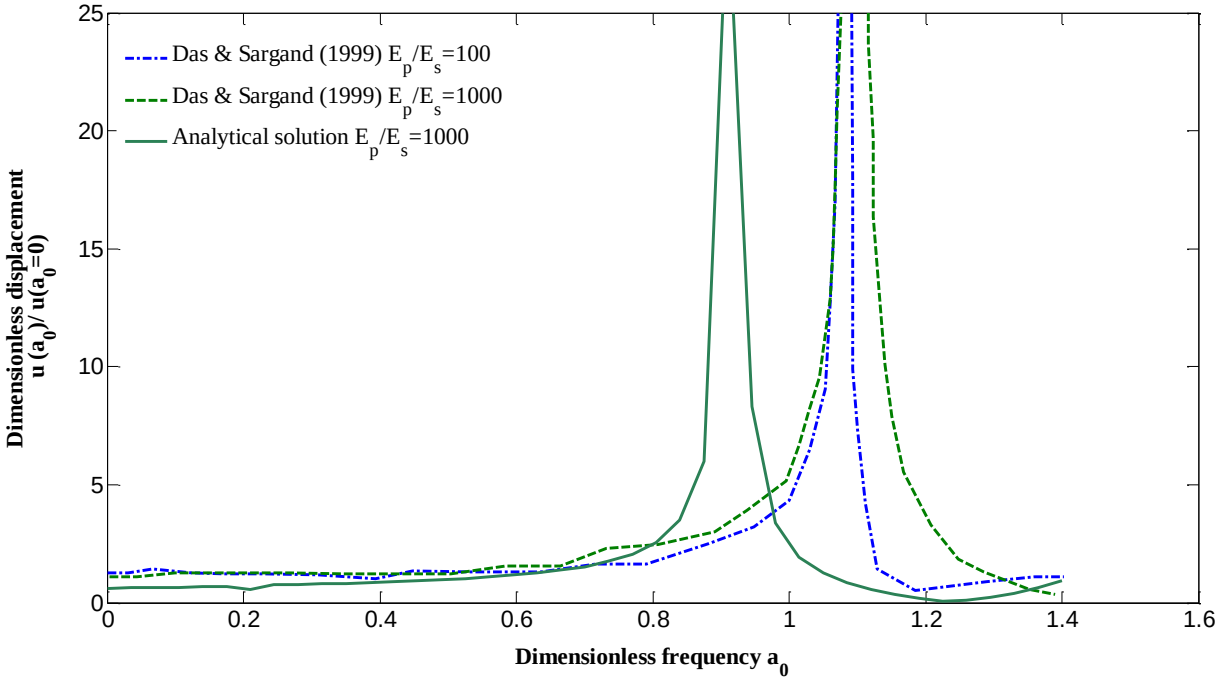

Figure 3.14: Horizontal response of the single pile

3.3 Summary

- The displacement of a single circular pile under static lateral load is presented in this chapter using anenergy based approach. The shear modulus of soil in this analysis is assumed to vary linearly with depth. The differential equations governing the displacements of the pile-soil system are obtained using variational principles.

- The response of a pile in linear elastic soil subjected to harmonic lateral load has also been studied using the same technique presented in the case of static load. In both cases, the more realistic displacement field introduced by Basu et al. (2009) has been used to give more accurate results, instead of the displacement field used by Sun (1994) and Das & Sargand (1999), where they assumed zero soil displacement perpendicular to the direction of the applied force and the resultant displacement vector at any point within the soil is taken to be parallel to the applied force.

- The results of the analyses in this chapter are reliable and reasonable compared with field data and finite element analysis.

3.4 Appendix

The stress-strain relationships is used to calculate potential energy as follows

$$\sigma_{rr}\varepsilon_{rr} = (\lambda + 2G)\left(u\frac{d\phi_r}{dr}\right)^2 + \lambda\frac{u^2}{r}\cos^2\theta(\phi_r - \phi_\theta) \tag{3.58a}$$

$$\sigma_{\theta\theta}\varepsilon_{\theta\theta} = (\lambda + 2G)\left[\left(\frac{u}{r}\phi_r\cos\theta\right)^2 - \frac{u^2}{r}\phi_r\phi_\theta\cos\theta + \left(\frac{u}{r}\phi_\theta\cos\theta\right)\right)^2 + \left(\frac{u^2}{r}\frac{d\phi_r}{dr}\cos\theta^2\,(\phi_r - \phi_\theta)\right)\right] \tag{3.58b}$$

$$\sigma_{r\theta}\varepsilon_{r\theta} = G\left[\left(\frac{u}{r}\phi_r\sin\theta\right)^2 + \left(u\frac{d\phi_\theta}{dr}\sin\theta\right)^2 + \left(\frac{u}{r}\phi_\theta\sin\theta\right)^2 + 2\frac{u^2}{r}\phi_r\frac{d\phi_\theta}{dr}\sin\theta^2 - 2\frac{u^2}{r^2}\phi_\theta\phi_r\sin\theta^2 - 2\frac{u^2}{r}\frac{d\phi_\theta}{dr}\phi_\theta\sin\theta^2\right] \tag{3.58c}$$

$$\sigma_{zr}\varepsilon_{zr} = G\left(\frac{du}{dz}\phi_r\cos\theta\right)^2 \tag{3.58d}$$

$$\sigma_{\theta z}\varepsilon_{\theta z} = G\left(-\frac{du}{dz}\phi_\theta\sin\theta\right)^2 \tag{3.58e}$$

Potential energy

The potential energy equation can be obtained by inserting equations (3. 58a-3. 58e) in equation 3.4.

$$U = \frac{1}{2}E_P I_P\int_0^L\left(\frac{d^2u}{dz^2}\right)^2 dz + \frac{\pi}{2}\int_0^\infty\int_{r_0}^\infty\left[(\lambda + 2G)u^2\left(\frac{d\phi_r}{dr}\right)^2 + 2\lambda u^2\frac{d\phi_r}{dr}\frac{(\phi_r - \phi_\theta)}{r} + (\lambda + 3G)u^2\frac{(\phi_r - \phi_\theta)^2}{r^2} + Gu^2\left(\frac{d\phi_\theta}{dr}\right)^2 + G\left(\frac{du}{dz}\right)^2{\phi_r}^2 + G\left(\frac{du}{dz}\right)^2{\phi_\theta}^2 + 2Gu^2\frac{(\phi_r - \phi_\theta)}{r}\frac{d\phi_\theta}{dr}\right]rdrdz + \frac{\pi}{2}G\int_L^\infty\int_{r_0}^\infty\left(\frac{du}{dz}\right)^2 rdrdz = 0 \tag{3.59}$$

$$U = \underbrace{\frac{1}{2}E_P I_P \int_0^L \left(\frac{d^2u}{dz^2}\right)^2 dz}_{\text{For pile}} + \underbrace{\frac{\pi}{2}G\int_L^\infty \int_{r_0}^\infty \left(\frac{du}{dz}\right)^2 r dr dz}_{\text{For soil column}}$$

$$+\frac{\pi}{2}\int_0^\infty \int_{r_0}^\infty \Bigg[(\lambda+2G)\frac{d\phi_r}{dr}\delta u\frac{d\phi_r}{dr} + 2\lambda u\frac{d\phi_r}{dr}\frac{(\phi_r-\phi_\theta)}{r}\delta u + (\lambda+3G)u^2\delta\frac{(\phi_r-\phi_\theta)^2}{r^2}$$
$$+ Gu\frac{d\phi_\theta}{dr}\delta\left(u\frac{d\phi_\theta}{dr}\right) + 2Gu^2\delta\frac{(\phi_r-\phi_\theta)}{r}\frac{d\phi_\theta}{dr} + G\phi_r\frac{du}{dz}\delta\phi_r\frac{du}{dz}$$
$$+ G\phi_\theta\frac{du}{dz}\delta\phi_\theta\frac{du}{dz}\Bigg] r dr dz$$

Soil around the pile

The following equation expresses the minimum potential energy,

$$\delta U = \frac{1}{2}E_p I_p \int_0^L \frac{d^2u}{dz^2}\delta\frac{d^2u}{dz^2}dz$$
$$+\frac{\pi}{2}\int_0^\infty \int_{r_0}^\infty \Bigg[(\lambda+2G)\frac{d\phi_r}{dr}\delta u\frac{d\phi_r}{dr} + 2\lambda u\frac{d\phi_r}{dr}\frac{(\phi_r-\phi_\theta)}{r}\delta u$$
$$+ (\lambda+3G)u^2\delta\frac{(\phi_r-\phi_\theta)^2}{r^2} + Gu\frac{d\phi_\theta}{dr}\delta\left(u\frac{d\phi_\theta}{dr}\right) + 2Gu^2\delta\frac{(\phi_r-\phi_\theta)}{r}\frac{d\phi_\theta}{dr}$$
$$+ G\phi_r\frac{du}{dz}\delta\phi_r\frac{du}{dz} + G\phi_\theta\frac{du}{dz}\delta\phi_\theta\frac{du}{dz}\Bigg] r dr dz + \frac{1}{2}{r_0}^2 G\int_L^\infty \int_0^\infty \frac{du}{dz}\delta\frac{du}{dz}dz$$
$$- Q_0 u_{z=0} - M_0\frac{du}{dz}_{z=0} \qquad (3.60)$$

$$\delta U = E_P I_P\left\{\left[\frac{d^3u}{dz^3}\delta u\right]_0^L - \int_0^L \frac{d^4u}{dz^4}\delta u dz\right\} - \pi {r_0}^2 G\left\{\left[\frac{du}{dz}\delta u\right]_L^\infty \int_L^\infty \left(\frac{d^2u}{dz^2}\right)\delta u dz\right\}$$

$$+\pi(\lambda+2G)\left\{\int_{r_0}^\infty r\left(\frac{d\phi_r}{dr}\right)^2 dr\int_0^\infty u\delta u dz + \int_0^\infty u^2\,dz\left[r\frac{d\phi}{dr}\delta\phi_r\right]_{r_0}^\infty\right.$$
$$\left. - \int_0^\infty u^2\,dz\int_{r_0}^\infty \left(r\frac{d^2\phi_r}{dr^2} + \frac{d\phi_r}{dr}\right)\delta\phi_r dr\right\}$$

$$+\pi\lambda\left\{\int_{r_0}^{\infty}(\phi_{r-}\phi_\theta)\frac{d\phi_r}{dr}dr\int_0^{\infty}u\delta udz+\int_0^{\infty}u^2dz\int_{r_0}^{\infty}\frac{d\phi_\theta}{dr}\delta\,\phi_r dr\right.$$
$$\left.-\int_0^{\infty}u^2dz\int_{r_0}^{\infty}\frac{d\phi_r}{dr}\delta\phi_\theta dr+\int_0^{\infty}u^2\,dz[(\phi_{r-}\phi_\theta)\delta\phi_r]_{r_0}^{\infty}\right\}$$

$$+\pi\,(\lambda+3G)\left\{\int_{r_0}^{\infty}r\left(\frac{\phi_r-\phi_\theta}{r}\right)^2dr\int_0^{\infty}u\delta udz+\int_{r_0}^{\infty}\left(\frac{\phi_r-\phi_\theta}{r}\right)\delta\phi_r dr\int_0^{\infty}u^2\,dz\right.$$
$$\left.-\int_0^{\infty}u^2\,dz\int_{r_0}^{\infty}\left(\frac{\phi_r-\phi_\theta}{r}\right)\delta\phi_\theta\,dr\right\}$$

$$+\pi G\left\{\int_{r_0}^{\infty}r\left(\frac{d\phi_\theta}{dr}\right)^2dr\int_0^{\infty}u\delta udz+\int_0^{\infty}u^2dz\left[r\frac{d\phi_\theta}{dr}\delta\phi_\theta\right]_{r_0}^{\infty}\right.$$
$$-\int_0^{\infty}u^2\,dz\int_{r_0}^{\infty}\left(r\frac{d^2\phi_\theta}{dr^2}+\frac{d\phi_\theta}{dr}\right)\delta\phi_\theta\,dr+\int_0^{\infty}\left(\frac{du}{dz}\right)^2dz\int_{r_0}^{\infty}r\phi_r\,\delta\phi_r dr$$
$$+\int_{r_0}^{\infty}r{\phi_r}^2\,dr\left[\frac{du}{dz}\delta u\right]_0^{\infty}-\int_{r_0}^{\infty}r{\phi_r}^2\,dr\int_0^{\infty}\left(\frac{d^2u}{dz^2}\right)\delta udz+\int_0^{\infty}\left(\frac{du}{dz}\right)^2dz\int_{r_0}^{\infty}r\phi_\theta\,\delta\phi_\theta dr$$
$$+\int_{r_0}^{\infty}r{\phi_\theta}^2\,dr\left[\frac{du}{dz}\delta u\right]_0^{\infty}-\int_{r_0}^{\infty}r{\phi_\theta}^2\,dr\int_0^{\infty}\left(\frac{d^2u}{dz^2}\right)\delta udz$$
$$+\int_{r_0}^{\infty}(\phi_{r-}\phi_\theta)\frac{d\phi_\theta}{dr}dr\int_0^{\infty}u\delta udz+\int_0^{\infty}u^2\,dz\int_{r_0}^{\infty}\frac{d\phi_\theta}{dr}\delta\,\phi_r dr-\int_0^{\infty}u^2\,dz\int_{r_0}^{\infty}\frac{d\phi_r}{dr}\delta\,\phi_\theta dr$$
$$\left.+\int_0^{\infty}u^2\,dz[(\phi_{r-}\phi_\theta)\delta\phi_\theta]_{r_0}^{\infty}\right\}-Q_0u_{z=0}$$
$$-M_0\frac{du}{dz}_{z=0}\qquad(3.61)$$

Kinetic energy

The equations below describe the differentiation of the kinetic energy

Kinetic energy

The equations below describe the differentiation of the kinetic energy

$$T=\underbrace{\frac{1}{2}\pi{r_0}^2\rho_p\int_{t_1}^{t_2}\int_0^{L}\left(\frac{du}{dt}\right)^2dz\,dt}_{\text{Pile}}+\underbrace{\frac{1}{2}m_s\int_{t_1}^{t_2}\int_L^{\infty}\left(\frac{du}{dt}\right)^2dz\,dt}_{\text{soil column}}$$

$$\underbrace{+\frac{1}{2}\int_0^{2\pi}\int_0^{\infty}\int_{r_0}^{\infty}\rho_s\left[\left(\frac{du_r}{dt}\right)^2+\left(\frac{du_\theta}{dt}\right)^2\right]rdrd\theta dz}_{\text{Soil around the pile}}\qquad(3.62)$$

$$\delta T = \pi {r_0}^2 \rho_p \int_{t_1}^{t_2} \int_0^L \frac{du}{dt} \delta \left(\frac{du}{dt}\right) dz dt + \pi {r_0}^2 \rho_s \int_{t_1}^{t_2} \int_{L\infty}^{\infty} \frac{du}{dt} \delta \frac{du}{dt} dz dt + \pi \rho_s \int_{t_1}^{t_2} \int_0^{\infty} \int_{r_0}^{\infty} \phi_r \frac{du}{dt} \delta \phi_r \frac{du}{dt} r dr dz dt + \pi \rho_s \int_{t_1}^{t_2} \int_0^{\infty} \int_{r_0}^{\infty} \phi_\theta \frac{du}{dt} \delta \phi_\theta \frac{du}{dt} r dr dz dt \quad (3.63a)$$

$$\delta T = \left\{ \pi {r_0}^2 \rho_p \int_{t_1}^{t_2} \left[\frac{du}{dt} \delta u\right]_{t_1}^{t_2} dt - \pi {r_0}^2 \rho_p \int_{t_1}^{t_2} \int_0^L \frac{d^2u}{dt^2} \delta u dz\, dt \right\} + \left\{ \pi {r_0}^2 \rho_s \int_{t_1}^{t_2} \left[\frac{du}{dt} \delta u\right]_{t_1}^{t_2} dt - \pi {r_0}^2 \rho_s \int_{t_1}^{t_2} \int_L^{\infty} \frac{d^2u}{dt^2} \delta u dz\, dt \right\} + \left\{ \pi \rho_s \int_0^{\infty} \left[\frac{du}{dt} \delta u\right]_{t_1}^{t_2} dz \int_{r_0}^{\infty} r\, {\phi_r}^2 dr - \pi \rho_s \int_{t_1}^{t_2} \int_0^{\infty} \frac{d^2u}{dt^2} \delta u dz dt \int_{r_0}^{\infty} r\, {\phi_r}^2 dr + \pi \rho_s \int_{t_1}^{t_2} \int_0^{\infty} \left(\frac{du}{dt}\right)^2 dz dt \int_{r_0}^{\infty} r\, \phi_r \delta \phi_r dr + \pi \rho_s \int_0^{\infty} \left[\frac{du}{dt} \delta u\right]_{t_1}^{t_2} dz \int_{r_0}^{\infty} r\, {\phi_\theta}^2 dr - \pi \rho_s \int_{t_1}^{t_2} \int_0^{\infty} \frac{d^2u}{dt^2} \delta u dz dt \int_{r_0}^{\infty} r\, {\phi_\theta}^2 dr + \pi \rho_s \int_{t_1}^{t_2} \int_0^{\infty} \left(\frac{du}{dt}\right)^2 dz dt \int_{r_0}^{\infty} r\, \phi_\theta \delta \phi_\theta dr \right\} \quad (3.63b)$$

By inserting potential and kinetic energies in Hamilton's principle the governing equations and boundary condition for pile soil system can be obtained

$$\delta \Pi = \int_{t_1}^{t_2} (\delta T - \delta U) dt + \int_{t_1}^{t_2} \delta W dt = 0 \quad (3.64)$$

$$\delta\Pi = \left\{\pi {r_0}^2 \rho_p \int_{t_1}^{t_2} \left[\frac{du}{dt}\delta u\right]_{t_1}^{t_2} dt - \pi {r_0}^2 \rho_p \int_{t_1}^{t_2}\int_0^L \frac{d^2u}{dt^2}\delta u dz\, dt\right\}$$
$$+ \left\{\pi {r_0}^2 \rho_s \int_{t_1}^{t_2} \left[\frac{du}{dt}\delta u\right]_{t_1}^{t_2} dt - \pi {r_0}^2 \rho_s \int_{t_1}^{t_2}\int_L^\infty \frac{d^2u}{dt^2}\delta u dz\, dt\right\}$$
$$- \left(E_P I_P \left\{\left[\frac{d^3u}{dz^{\,3}}\delta u\right]_0^L - \int_0^L \frac{d^4u}{dz^{\,4}}\delta u dz\right\}\right.$$
$$- \pi {r_0}^2 G \left\{\left[\frac{du}{dz}\delta u\right]_L^\infty \int_L^\infty \left(\frac{d^2u}{dz^2}\right)\delta u dz\right\}$$
$$+ \pi(\lambda + 2G)\left\{\int_{r_0}^\infty r\left(\frac{d\phi_r}{dr}\right)^2 dr \int_0^\infty u\delta u dz + \int_0^\infty u^2\, dz\left[r\frac{d\phi}{dr}\delta\phi_r\right]_{r_0}^\infty\right.$$
$$\left. - \int_0^\infty u^2\, dz \int_{r_0}^\infty \left(r\frac{d^2\phi_r}{dr^2} + \frac{d\phi_r}{dr}\right)\delta\phi_r dr\right\}$$
$$+ \pi\lambda\left\{\int_{r_0}^\infty (\phi_{r-}\phi_\theta)\frac{d\phi_r}{dr}dr \int_0^\infty u\delta u dz + \int_0^\infty u^2 dz \int_{r_0}^\infty \frac{d\phi_\theta}{dr}\delta\,\phi_r dr\right.$$
$$\left. - \int_0^\infty u^2 dz \int_{r_0}^\infty \frac{d\phi_r}{dr}\delta\phi_\theta dr + \int_0^\infty u^2\, dz[(\phi_{r-}\phi_\theta)\delta\phi_r]_{r_0}^\infty\right\}$$
$$+ \pi\,(\lambda$$
$$+ 3G)\left\{\int_{r_0}^\infty r\left(\frac{\phi_r - \phi_\theta}{r}\right)^2 dr \int_0^\infty u\delta u dz + \int_{r_0}^\infty \left(\frac{\phi_r - \phi_\theta}{r}\right)\delta\phi_r dr \int_0^\infty u^2\, dz\right.$$
$$\left. - \int_0^\infty u^2\, dz \int_{r_0}^\infty \left(\frac{\phi_r - \phi_\theta}{r}\right)\delta\phi_\theta\, dr\right\}$$
$$+ \pi G\left\{\int_{r_0}^\infty r\left(\frac{d\phi_\theta}{dr}\right)^2 dr \int_0^\infty u\delta u dz + \int_0^\infty u^2 dz\left[r\frac{d\phi_\theta}{dr}\delta\phi_\theta\right]_{r_0}^\infty\right.$$
$$- \int_0^\infty u^2\, dz \int_{r_0}^\infty \left(r\frac{d^2\phi_\theta}{dr^2} + \frac{d\phi_\theta}{dr}\right)\delta\phi_\theta\, dr + \int_0^\infty \left(\frac{du}{dz}\right)^2 dz \int_{r_0}^\infty r\phi_r\,\delta\phi_r dr$$
$$+ \int_{r_0}^\infty r{\phi_r}^2\, dr\left[\frac{du}{dz}\delta u\right]_0^\infty - \int_{r_0}^\infty r{\phi_r}^2\, dr \int_0^\infty \left(\frac{d^2u}{dz^2}\right)\delta u dz$$
$$+ \int_0^\infty \left(\frac{du}{dz}\right)^2 dz \int_{r_0}^\infty r\phi_\theta\,\delta\phi_\theta dr + \int_{r_0}^\infty r{\phi_\theta}^2\, dr\left[\frac{du}{dz}\delta u\right]_0^\infty$$
$$- \int_{r_0}^\infty r{\phi_\theta}^2\, dr \int_0^\infty \left(\frac{d^2u}{dz^2}\right)\delta u dz$$
$$+ \int_{r_0}^\infty (\phi_{r-}\phi_\theta)\frac{d\phi_\theta}{dr}dr \int_0^\infty u\delta u dz + \int_0^\infty u^2\, dz \int_{r_0}^\infty \frac{d\phi_\theta}{dr}\delta\,\phi_r dr$$
$$\left.\left. - \int_0^\infty u^2\, dz \int_{r_0}^\infty \frac{d\phi_r}{dr}\delta\,\phi_\theta dr + \int_0^\infty u^2\, dz[(\phi_{r-}\phi_\theta)\delta\phi_\theta]_{r_0}^\infty\right\}\right) + Q_0 u_{z=0}$$
$$- M_0 \frac{du}{dz}_{z=0} \qquad (3.65)$$

The following equations give the solutions for the governing equation of pile displacement

$$u = A\,e^{-\alpha_1 z} + Be^{\alpha_1 z} + Ce^{-\alpha_2 z} + De^{\alpha_2 z} \tag{3.66}$$

The boundary conditions at the surface

1. $E_p I_p \frac{d^3 u_1}{dz^3} - c_1 \frac{du_1}{dz} - Q_0 = 0$

$$E_p I_p(-\alpha_1{}^3 A_1 e^{-\alpha_1 z_1} + \alpha_1{}^3 B_1 e^{\alpha_1 z_1} - \alpha_2{}^3 C_1 e^{-\alpha_2 z_1} + \alpha_2{}^3 D_1 e^{\alpha_2 z_1}) - c_1[-\alpha_1 A_1 e^{-\alpha_1 z_1} + \alpha_1 B e^{\alpha_1 z_1} - \alpha_2 C_1 e^{-\alpha_2 z_1} + \alpha_2 D_1 e^{\alpha_2 z_1}] = Q_0$$

$$\left(c_1\alpha_1 - E_p I_p\,\alpha_1{}^3\right)A_1 + \left(E_p I_p\,\alpha_1{}^3 - c_1\alpha_1\right)B_1 + \left(c_1\alpha_2 - E_p I_p\,\alpha_2{}^3\right)C_1 + \left(E_p I_p\,\alpha_2{}^3 - c_1\alpha_2\right)D_1 = Q_0 \tag{3.67a}$$

2. $E_p I_p \frac{d^2 u}{dz^2} + M_0 = 0$

$$E_p I_p\,\alpha_1{}^2 A_1 + E_p I_p\,\alpha_1{}^2 B_1 + E_p I_p\,\alpha_2{}^2 C_1 + E_p I_p\,\alpha_2{}^2 D_1 = -M_0 \tag{3.67b}$$

The boundary condition at z=L

3. $u_1 = 0$

$$A_1 e^{-\alpha_1 z_1} + B_1 e^{\alpha_1 z_1} + C_1 e^{-\alpha_2 z_1} + D_1 e^{\alpha_2 z_1} = 0 \tag{3.67c}$$

4. $u_1{}' = 0$

$$-\alpha_1 A_1 e^{-\alpha_1 z_1} + \alpha_1 B_1 e^{\alpha_1 z_1} - \alpha_2 C_1 e^{-\alpha_2 z_1} + \alpha_2 D_1 e^{\alpha_2 z_1} = 0 \tag{3.67d}$$

where

$$\alpha_1 = \frac{\sqrt{\frac{CG}{2E_p I_p} - \frac{\sqrt{C^2G^2 - 4\,E_p I_p\,kG + 4\,E_p I_p\,C_s\omega^2}}{E_p I_p}}}{\sqrt{2E_p I_p}} \tag{3.68a}$$

$$\alpha_2 = \frac{\sqrt{\frac{CG}{2E_p I_p} + \frac{\sqrt{C^2G^2 - 4\,E_p I_p\,kG + 4\,E_p I_p\,C_s\omega^2}}{E_p I_p}}}{\sqrt{2E_p I_p}} \tag{3.68b}$$

4 Lateral Pile Displacement in Nonlinear Soil

Introduction

Most solutions that have been used to predict the deformation of a pile under different loads treat the soil as a linear elastic material in order to simplify the calculations. However, in reality the behaviour of soil is highly nonlinear and soil stiffness depends on the stress and strain levels. In this chapter, a new method, based on an energy approach, to predict the displacement of a pile in nonlinear soil is presented. Unlike the assumptions made in the previous chapter, the soil moduli (λ and G) are not treated as constants but assumed to vary in radial, circumference and depth directions according to the strain and stress levels. A simple power law has been assumed to describe the variation of the soil stiffness. These solutions have been developed for static and cyclic loading. Comparison has been made with finite element analysis, field data, centrifuge tests and other published analytical methods.

4.1 Lateral pile displacement in nonlinear soil

4.1.1 Problem definition

Clays behave in a nonlinear manner at a very wide range of shear strain, whereas soil behaves as an linear elastic material only at a very small strain $\varepsilon < 10^{-4}$ (Atkinson, 2000). Thus, a power law can be used to describe the stress-strain behaviour of soil (Gunn, 1993; Bolton & Whittle, 1999). The decay of soil stiffness with strain can be expressed as

$$G = G_0 \left(\frac{\varepsilon_q}{\varepsilon_{q_0}} \right)^n \tag{4.1}$$

$$G = a \, {\varepsilon_q}^n \tag{4.2}$$

where $a = \frac{G_0}{{\varepsilon_{q_0}}^n}$, a is a constant determined empirically, n describes soil nonlinearity which is equal to (-0.5) according to the experimental data analysed by Osman et al. (2007) (see Figure 4.1), ε_q represents the deviatoric strain and ε_{q_0} is the maximum deviatoric strain with linear elastic behaviour which is equal to 10^{-5}. Soil stiffness is estimated by calculating strain at each location, then using the power law.

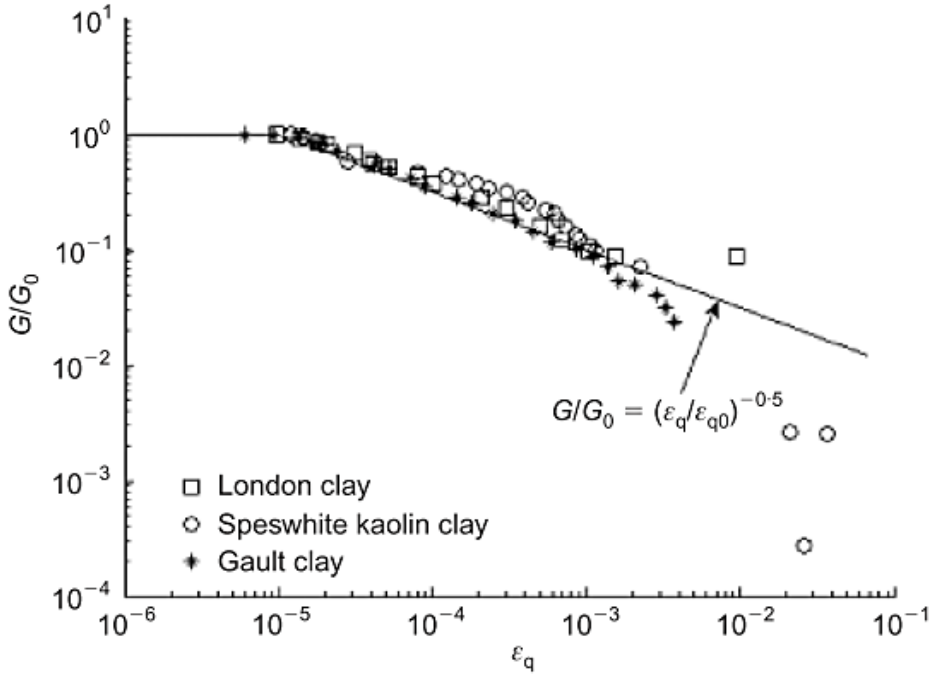

Figure 4.1: Logarithmic scale of degradation of tangent stiffness with strain level (data adopted by Osman et al. 2007 after Dassari, 1996)

4.1.2 Energy variation method for pile

Potential energy

The potential energy of the pile and the soil is given by

$$U = \frac{1}{2}\int_0^L E_P I_P \left(\frac{d^2u}{dz^2}\right)^2 dz + \frac{1}{2}\int_L^\infty \pi {r_0}^2\ G\left(\frac{du}{dz}\right)^2\ dz + \frac{1}{2}\int_{r_0}^\infty \int_0^{2\pi} \int_0^\infty (\sigma_{rr}\varepsilon_{rr} + \sigma_{\theta\theta}\varepsilon_{\theta\theta} + \sigma_{r\theta}\varepsilon_{r\theta} + \sigma_{rz}\varepsilon_{rz} + \sigma_{\theta z}\varepsilon_{\theta z})\, r dr d\theta dz. \quad (4.3)$$

The variations $\delta u, \delta\phi_r$ and $\delta\phi_\theta$ are functions of $u(z), \phi_r(r)$ and $\phi_\theta(r)$ and are independent. To obtain the pile governing equation, from folloing equation (4.4) all terms associated with $\delta u, \delta\frac{du}{dz}$ will be collected. Furthermore, the terms that are related to $\delta\phi_r$ and $\delta\phi_\theta$ will be collected to get the governing equation of the soil.

$$\delta U = \int_0^L E_P I_P \left(\frac{d^2u}{dz^2}\right)\delta\left(\frac{d^2u}{dz^2}\right)dz + \int_L^\infty \pi {r_0}^2\ G\left(\frac{du}{dz}\right)\delta\ \left(\frac{du}{dz}\right)\ dz$$
$$+ \int_0^\infty \int_{r0}^\infty \int_0^{2\pi} \Bigg[(\lambda+2G)u\delta u\left(\frac{d\phi_r}{dr}\right)^2 cos^2\theta + 2\lambda u\delta u\frac{d\phi_r}{dr}\frac{(\phi_{r-}\phi_\theta)}{r}cos^2\theta$$
$$+ (\lambda+2G)u^2cos^2\theta\left(\frac{d\phi_r}{dr}\right)\delta\left(\frac{d\phi_r}{dr}\right) + Gu\delta u\left(\frac{d\phi_\theta}{dr}\right)^2 sin^2\theta + Gcos^2\theta{\phi_r}^2\frac{du}{dz}\delta\frac{du}{dz}$$
$$+ Gsin^2\theta{\phi_\theta}^2\frac{du}{dz}\delta\frac{du}{dz} + Gu^2sin^2\theta\frac{1}{r}\left(\frac{d\phi_\theta}{dr}\right)\delta\phi_r - Gu^2sin^2\theta\left(\frac{d\phi_\theta}{dr}\right)\delta\phi_\theta$$
$$+ \lambda u^2cos^2\theta\frac{(\phi_r-\phi_\theta)}{r}\delta\left(\frac{d\phi_r}{dr}\right) + \lambda u^2cos^2\theta\frac{1}{r}\frac{d\phi_r}{dr}\delta\phi_r - \lambda u^2cos^2\theta\frac{1}{r}\frac{d\phi_r}{dr}\delta\phi_\theta$$
$$+ G\,u\delta u\,sin^2\theta\frac{1}{r}(\phi_r-\phi_\theta)^2 + Gu^2sin^2\theta\frac{1}{r^2}(\phi_r-\phi_\theta)\delta\phi_r$$
$$+ (\lambda+2G)u\delta ucos^2\theta\frac{1}{r^2}(\phi_r-\phi_\theta)^2 - Gu^2sin^2\theta\frac{1}{r^2}(\phi_r-\phi_\theta)\delta\phi_\theta$$
$$+ (\lambda+2G)u^2cos^2\theta\frac{1}{r^2}(\phi_r-\phi_\theta)^2\delta\phi_r - (\lambda+2G)u^2cos^2\theta\frac{1}{r^2}(\phi_r-\phi_\theta)^2\delta\phi_\theta$$
$$+ 2Gsin^2\theta u\delta u\frac{(\phi_r-\phi_\theta)}{r}\frac{d\phi_\theta}{dr} + Gu^2sin^2\theta\left(\frac{d\phi_\theta}{dr}\right)\delta\left(\frac{d\phi_\theta}{dr}\right)$$
$$+ Gu^2sin^2\theta\frac{(\phi_r-\phi_\theta)}{r}\delta\left(\frac{d\phi_\theta}{dr}\right) + Gcos^2\theta\left(\frac{du}{dz}\right)^2\phi_r\delta\phi_r$$
$$+ Gsin^2\theta\left(\frac{du}{dz}\right)^2\phi_\theta\delta\phi_\theta\Bigg]rdrd\theta dz - Q_0\delta u_{z=0} + M_0\,\delta\left(\frac{du}{dz}\right)_{z=0} = 0 \qquad (4.4)$$

Soil displacement

To form the soil governing equation, all terms that are associated with ϕ_r over domain $r_0 \le r < \infty$ must be summed and the sum equalize to zero.

$$\int_0^{\infty}\int_{r0}^{\infty}\int_0^{2\pi}\Big[(\lambda+2G)u^2cos^2\theta\left(\frac{d\phi_r}{dr}\right)\delta\left(\frac{d\phi_r}{dr}\right)+Gu^2sin^2\theta\frac{1}{r}\left(\frac{d\phi_\theta}{dr}\right)\delta\phi_r$$
$$+\lambda u^2cos^2\theta\frac{(\phi_r-\phi_\theta)}{r}\delta\left(\frac{d\phi_r}{dr}\right)+\lambda u^2cos^2\theta\frac{1}{r}\frac{d\phi_r}{dr}\delta\phi_r$$
$$+Gu^2sin^2\theta\frac{1}{r^2}(\phi_r-\phi_\theta)\delta\phi_r+(\lambda+2G)u^2cos^2\theta\frac{1}{r^2}(\phi_r-\phi_\theta)^2\delta\phi_r$$
$$+Gcos^2\theta\left(\frac{du}{dz}\right)^2\phi_r\delta\phi_r\Big]rdrd\theta dz=0. \quad (4.5)$$

By simplifying Equation 4.5 we get

$$\int_{r_0}^{\infty}\Big(m_{s1}\left(\frac{d\phi_r}{dr}\right)\delta\left(\frac{d\phi_r}{dr}\right)+m_{s3}\frac{1}{r}(\phi_r-\phi_\theta)\delta\left(\frac{d\phi_r}{dr}\right)+m_{s3}\frac{1}{r}\frac{d\phi_r}{dr}\delta\phi_r+m_{s1}\frac{1}{r^2}(\phi_r-\phi_\theta)\delta\phi_r$$
$$+m_{s2}\frac{1}{r^2}(\phi_r-\phi_\theta)\delta\phi_r+m_{s2}\frac{1}{r}\left(\frac{d\phi_\theta}{dr}\right)\delta\phi_r+n_{s1}\phi_r\delta\phi_r\Big)dr=0 \quad (4.6)$$

where $n_{s1}, n_{s2}, m_{s1}, m_{s2}\ and\ m_{s3}$ for homogenous soil are represented as follows:

$$m_{s1}(r)=\int_0^{\infty}\int_0^{2\pi}(\lambda+2G)u^2cos^2\,\theta rd\theta dz \quad (4.7a)$$

$$m_{s2}(r)=\int_0^{\infty}\int_0^{2\pi}Gu^2sin^2\,\theta\, rd\theta dz \quad (4.7b)$$

$$m_{s3}(r)=\int_0^{\infty}\int_0^{2\pi}\lambda\, u^2cos^2\,\theta rd\theta dz \quad (4.7c)$$

$$n_{s1}(r)=\int_0^{\infty}\int_0^{2\pi}G\left(\frac{du}{dz}\right)^2cos^2\,\theta rd\theta dz \quad (4.7d)$$

For multilayer soil the summation of $n_{s1}, n_{s2}, m_{s1}, m_{s2}\ and\ m_{s3}$ will be considered. i represents the number of layers and n is the last layer number.

$$m_{s1}(r)=\sum_{i=1}^{n}\int_{H_{i-1}}^{H_i}\int_0^{2\pi}(\lambda_i+2G_i){u_i}^2cos^2\,\theta rd\theta dz \quad (4.8a)$$

$$m_{s2}(r) = \sum_{i=1}^{n} \int_{H_{i-1}0}^{H_i} \int_0^{2\pi} G_i {u_i}^2 sin^2\,\theta\; r d\theta dz \tag{4.8b}$$

$$m_{s3}(r) = \sum_{i=1}^{n} \int_0^{\infty} \int_0^{2\pi} \lambda_i\, {u_i}^2 cos^2\,\theta r d\theta dz \tag{4.8c}$$

$$n_{s1}(r) = \sum_{i=1}^{n} \int_0^{\infty} \int_0^{2\pi} G_i \left(\frac{du_i}{dz}\right)^2 cos^2\,\theta r d\theta dz \tag{4.8d}$$

$$n_{s2}(r) = \sum_{i=1}^{n} \int_0^{\infty} \int_0^{2\pi} G_i \left(\frac{du_i}{dz}\right)^2 sin^2\,\theta r d\theta dz. \tag{4.8e}$$

Equation 4.9 below is a simplified version of Equation 4.6 using integration by parts of the terms that comprise $\delta\left(\frac{d\phi_r}{dr}\right)$. The governing equation can then be obtained by dividing the resulting equation by $(-m_{s1})$.

$$\frac{d^2\phi_r}{dr^2} + \frac{1}{m_{s1}}\frac{dm_{s1}}{dr}\frac{d\phi_r}{dr} - \left\{\frac{1}{r^2}\frac{m_{s1}+m_{s2}+m_{s3}}{m_{s1}} - \frac{1}{r}\frac{1}{m_{s1}}\frac{dm_{s3}}{dr} + \frac{n_{s1}}{m_{s1}}\right\}\phi_r = \frac{m_{s2}+m_{s3}}{m_{s1}}\frac{1}{r}\frac{d\phi_\theta}{dr} - \left\{\frac{1}{r^2}\frac{m_{s1}+m_{s2}+m_{s3}}{m_{s1}} - \frac{1}{r}\frac{1}{m_{s1}}\frac{dm_{s3}}{dr}\right\}\phi_\theta. \tag{4.9}$$

In order to derive the governing equation for soil, terms related to ϕ_θ in the circumferential directional must be collected.

$$\int_0^{\infty}\int_{r0}^{\infty}\int_0^{2\pi}\Bigg[-Gu^2 sin^2\theta\left(\frac{d\phi_\theta}{dr}\right)\delta\phi_\theta - \lambda u^2 cos^2\theta\frac{1}{r}\frac{d\phi_r}{dr}\delta\phi_\theta - Gu^2 sin^2\theta\frac{1}{r^2}(\phi_r - \phi_\theta)\delta\phi_\theta - (\lambda+2G)u^2 cos^2\theta\frac{1}{r^2}(\phi_r-\phi_\theta)^2\delta\phi_\theta + Gu^2 sin^2\theta\left(\frac{d\phi_\theta}{dr}\right)\delta\left(\frac{d\phi_\theta}{dr}\right) + Gu^2 sin^2\theta\frac{(\phi_r-\phi_\theta)}{r}\delta\left(\frac{d\phi_\theta}{dr}\right) + Gsin^2\theta\left(\frac{du}{dz}\right)^2\phi_\theta\delta\phi_\theta\Bigg] r dr d\theta dz = 0. \tag{4.10}$$

Then Equation 4.10 is simplified as

$$\int_{r_0}^{\infty}\left(-m_{s2}\left(\frac{d\phi_\theta}{dr}\right)\delta\left(\frac{d\phi_\theta}{dr}\right)-m_{s3}\frac{1}{r}\frac{d\phi_r}{dr}\delta\phi_\theta-m_{s2}\frac{1}{r^2}(\phi_r-\phi_\theta)\delta\phi_\theta-m_{s1}\frac{1}{r^2}(\phi_r-\phi_\theta)^2\delta\phi_\theta\right.$$
$$\left.+m_{s2}\left(\frac{d\phi_\theta}{dr}\right)\delta\left(\frac{d\phi_\theta}{dr}\right)+m_{s2}\frac{(\phi_r-\phi_\theta)}{r}\delta\left(\frac{d\phi_\theta}{dr}\right)+n_{s2}\phi_\theta\delta\phi_\theta\right)dr=0 \qquad (4.11)$$

Dividing Equation 4.11 by $(-m_{s2})$ gives

$$\frac{d^2\phi_\theta}{dr^2}+\frac{1}{m_{s2}}\frac{dm_{s2}}{dr}\frac{d\phi_\theta}{dr}-\left\{\frac{1}{r^2}\frac{m_{s1}}{m_{s2}}+\frac{1}{r}\frac{1}{m_{s2}}\frac{dm_{s2}}{dr}+\frac{n_{s2}}{m_{s2}}\right\}\phi_\theta$$
$$=-\frac{m_{s2}+m_{s3}}{m_{s2}}\frac{1}{r}\frac{d\phi_r}{dr}-\left\{\frac{1}{r^2}\frac{m_{s1}}{m_{s2}}+\frac{1}{r}\frac{1}{m_{s2}}\frac{dm_{s2}}{dr}\right\}\phi_r. \qquad (4.12)$$

n_{s2} for homogenous and non-homogenous soil respectively is denoted as

$$n_{s2}(r)=\int_0^{\infty}\int_0^{2\pi}G\left(\frac{du}{dz}\right)^2 sin^2\,\theta r d\theta dz \qquad (4.13a)$$

$$n_{s2}(r)=\sum_{i=1}^{n}\int_0^{\infty}\int_0^{2\pi}G_i\left(\frac{du_i}{dz}\right)^2 sin^2\,\theta r d\theta dz. \qquad (4.13b)$$

The boundary conditions for the soil are

$$\phi_r=1 \text{ at } r=r_0 \qquad (4.14a)$$

$$\phi_r=0 \text{ at } r\to\infty \qquad (4.14b)$$

$$\phi_\theta=1 \text{ at } r=r_0 \qquad (4.14c)$$

$$\phi_\theta=0 \text{ at } r\to\infty. \qquad (4.14d)$$

the governing equations of soil can then be rewritten as

$$\frac{d^2\phi_r}{dr^2}+y_1\frac{d\phi_r}{dr}-y_2\phi_r=y_3\frac{d\phi_\theta}{dr}-y_4\phi_\theta \qquad (4.15)$$

$$\frac{d^2\phi_\theta}{dr^2}+y_5\frac{d\phi_\theta}{dr}-y_6\phi_\theta=-y_7\frac{d\phi_r}{dr}-y_8\phi_r \qquad (4.16)$$

where

$$y_1 = \frac{1}{m_{s1}}\frac{dm_{s1}}{dr} \tag{4.17a}$$

$$y_2 = \frac{1}{r^2}\frac{(m_{s1}+m_{s2}+m_{s3})}{m_{s1}} - \frac{1}{r}\frac{1}{m_{s1}}\frac{dm_{s3}}{dr} + \frac{n_{s1}}{m_{s1}} \tag{4.17b}$$

$$y_3 = \frac{1}{r}\frac{(m_{s2}+m_{s3})}{m_{s1}} \tag{4.17c}$$

$$y_4 = \frac{1}{r^2}\frac{(m_{s1}+m_{s2}+m_{s3})}{m_{s1}} - \frac{1}{r}\frac{1}{m_{s1}}\frac{dm_{s3}}{dr} \tag{4.17d}$$

$$y_5 = \frac{1}{m_{s2}}\frac{dm_{s2}}{dr} \tag{4.17e}$$

$$y_6 = \frac{1}{r^2}\frac{m_{s1}}{m_{s2}} + \frac{1}{r}\frac{1}{m_{s2}}\frac{dm_{s2}}{dr} + \frac{n_{s2}}{m_{s2}} \tag{4.17f}$$

$$y_7 = \frac{1}{r}\frac{(m_{s2}+m_{s3})}{m_{s2}} \tag{4.17g}$$

$$y_8 = \frac{1}{r^2}\frac{m_{s1}}{m_{s2}} + \frac{1}{r}\frac{1}{m_{s2}}\frac{dm_{s2}}{dr}. \tag{4.17h}$$

These equationshave been solved in this study using MATLAB..

Pile displacement

In a similar manner the governing equation of piles installed in nonlinear soil can be obtained by collecting terms that are associated with δu and $\delta\left(\frac{du}{dz}\right)$ for $(0 \le z \le L)$ from the potential energy (Equation 4.4), then equating them to zero.

$$\int_0^L E_P I_P \left(\frac{d^2u}{dz^2}\right)\delta\left(\frac{d^2u}{dz^2}\right)dz + \int_L^\infty \pi {r_0}^2\ G\left(\frac{du}{dz}\right)\delta\ \left(\frac{du}{dz}\right)\ dz$$
$$+ \int_0^\infty \int_{r0}^\infty \int_0^{2\pi} \Bigg[(\lambda + 2G)u\delta u\left(\frac{d\phi_r}{dr}\right)^2 cos^2\theta + 2\lambda u\delta u\frac{d\phi_r}{dr}\frac{(\phi_{r-}\phi_\theta)}{r}cos^2\theta$$
$$+ Gu\delta u\left(\frac{d\phi_\theta}{dr}\right)^2 sin^2\theta + Gcos^2\theta{\phi_r}^2\frac{du}{dz}\delta\frac{du}{dz} + Gsin^2\theta{\phi_\theta}^2\frac{du}{dz}\delta\frac{du}{dz}$$
$$+ G\,u\delta u\,sin^2\theta\frac{1}{r}\left(\phi_r - \phi_\theta\right)^2 + (\lambda + 2G)u\delta ucos^2\theta\frac{1}{r^2}\left(\phi_r - \phi_\theta\right)^2\Bigg] rdrd\theta dz$$
$$- Q_0\delta u_{z=0} + M_0\ \delta\left(\frac{du}{dz}\right)_{z=0} = 0. \qquad (4.18)$$

The governing equation becomes

$$E_P I_P\frac{d^4u}{dz^4} - C\frac{du}{dz} + ku = 0 \qquad (4.19)$$

where

$$C = \int_{r_0}^\infty \int_0^{2\pi} G_{si}\left({\phi_r}^2 cos^2\theta + {\phi_\theta}^2 sin^2\theta\right)rd\theta dr \qquad (4.20a)$$

where i denotes the layer number from the surface level pile length

$$C_s = \int_{r_0}^\infty \int_0^{2\pi} G_{sj}\left({\phi_r}^2 cos^2\theta + {\phi_\theta}^2 sin^2\theta\right)rd\theta dr \qquad (4.20b)$$

and where j represents the layer number from pile length to infinity.

In addition for Equation 4.19

$$k = \int_{r_0}^\infty \int_0^{2\pi}\Bigg((\lambda + G)\left(\frac{d\phi_r}{dr}\right)^2 cos^2\theta + 2\lambda\frac{1}{r}\frac{d\phi_r}{dr}(\phi_r - \phi_\theta)cos^2\theta + (\lambda + G)\frac{(\phi_r - \phi_\theta)^2}{r^2}cos^2\theta$$
$$+ G\frac{(\phi_r - \phi_\theta)^2}{r^2}sin^2\theta + 2G\frac{(\phi_r - \phi_\theta)}{r}\frac{d\phi_\theta}{dr}sin^2\theta$$
$$+ G\left(\frac{d\phi_\theta}{dr}\right)^2 sin^2\theta\Bigg)rd\theta dr. \qquad (4.20c)$$

The fourth order differential Equation 4.19 can be solved using a central finite difference scheme (see Section 5.8)). Equation 4.20 becomes

$$E_p I_p \left(\frac{u_{i-2} - 4u_{i-1} + 6u_i - 4u_{i+1} + u_{i+2}}{\Delta z^4}\right) + C\left(\frac{-u_{i-1} + u_{i+1}}{\Delta z}\right) + m\, u_i = 0 \qquad (4.21)$$

where i denotes the i^{th} node in z direction, and Δz is the distance between two nodes. At each point in the soil domain, G and λ have been calculated (see Figure 4.2).

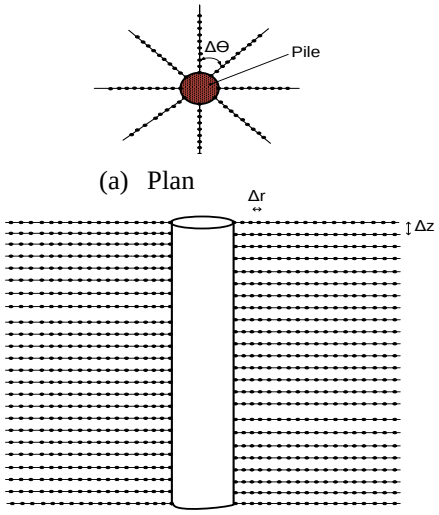

Figure 4.2: Discretization of the soil

The pile deflection equation can be solved when the soil parameters k and C are known however these parameters depend on the unknown dimensionless soil functions, $\phi_r and\ \phi_\theta$, which can be estimated by calculating $y_1, y_2, y_3, y_4, y_5, y_6, y_7$ and y_8. The soil deformation is calculated in radial and circumference directions, then calculated in the depth direction. To obtain the soil displacement the initial numbers of these values, $y_1, y_2, y_3, y_4, y_5, y_6, y_7$ and y_8 must be assumed. Then they are inserted into Equations 4.9 and 4.12, from which the soil parameters k and C are obtained as a result of the pile displacement. New values of $y_1, y_2, y_3, y_4, y_5, y_6, y_7$ and y_8 can then be inserted into Equations 4.9 and 4.12 to evaluate ϕ_r and ϕ_θ, which are then inserted into Equation 4.19 to obtain displacement u, so an iteration technique is needed to the condition $\left(\frac{y_{old} - y_{new}}{y_{old}}\right) > 0.001$. Figure 4.3 shows the flow chart of the solution procedure

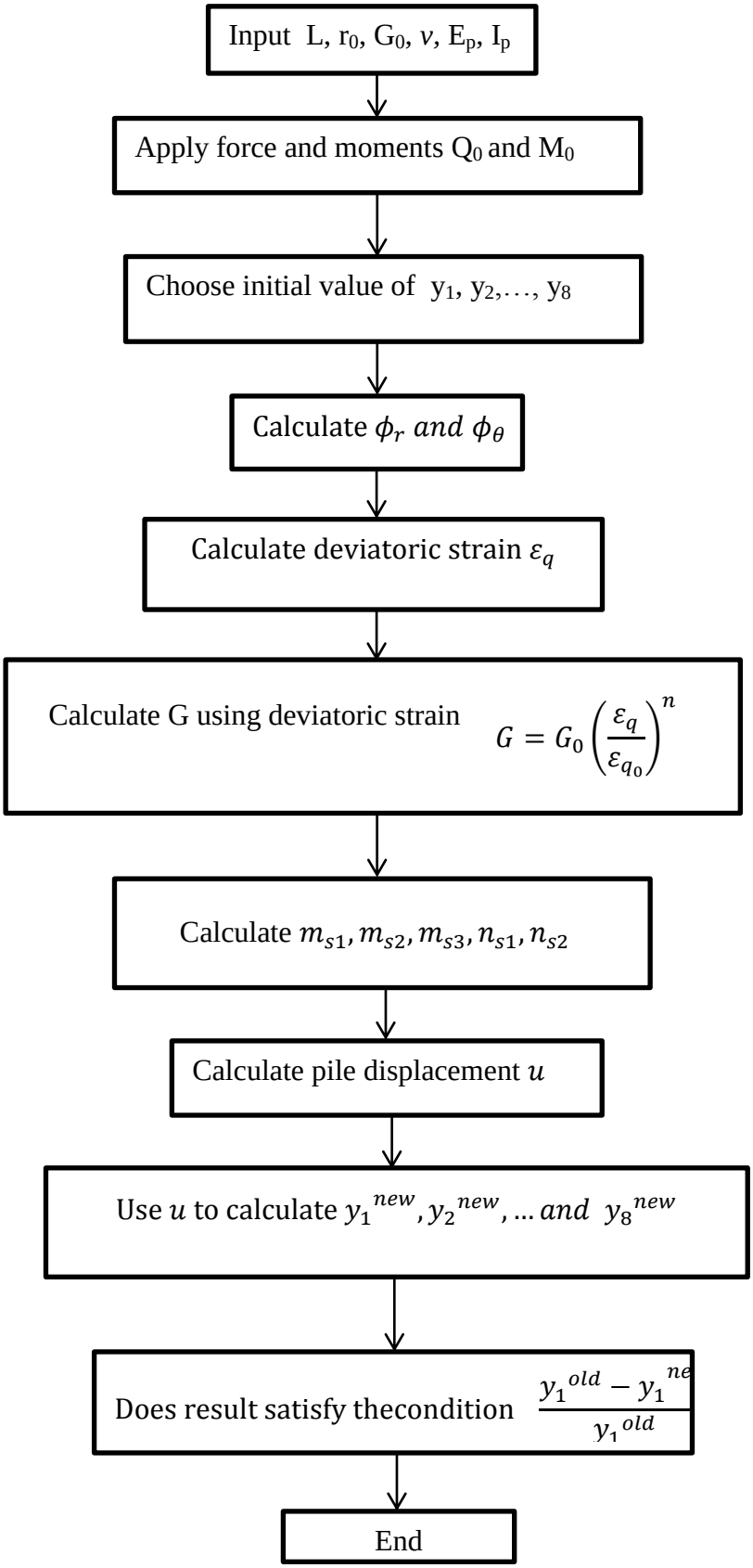

Figure 4.3: Flow chart for the iterative scheme to predict pile displacement

4.2 Alternative stiffness function

In the previous section, the energy based solution was derived assuming that the soil stiffness is a function of the strain only. However, as shown by Richart et al. (1970), the shear modulus should depend on the effective stress. The variation of stiffness with stress and strain is modelled by the constitutive relationship of Atkinson and Sallfors(1991) and Atkinson, (2000) as follows:

$$G = G_0 \left(\frac{\varepsilon_q}{\varepsilon_{q_0}} \right)^b \tag{4.22}$$

where G_0 is given by:

$$G_0 = A \left(\frac{P'}{P_a} \right)^n {R_0}^m \tag{4.23}$$

where P_a is the reference pressure, equal to 1 kPa, n, A and R_0 are constants obtained

experimentlly, where $n = 0.65$, $A = 2000$, $R_0 = 1$ and $m = 0.2$ for normal consolidation. P' denotes the effective mean stress which is equal to $P' = \frac{(\sigma_{rr}' + \sigma_{\theta\theta}' + \sigma_{zz}')}{3}$, $\sigma_{rr}', \sigma_{\theta\theta}'$ and σ_{zz}' being the principal effective stresses

4.3 Comparison with the finite element method

3D finite element analysis is discussed in this part of the thesis (using ABAQUS 6.10 software) to predict the response of a pile subjected to lateral load. The soil is assumed to be uniform and the size of the mesh here needs to ensure that all displacement fields are contained within the mesh boundary. The mesh radius is equal to 15 D and 20 D depth, where D is pile diameter. 3649 quadratic hexahedral elements and 354 quadratic wedge elements have been used (see Figure 4.4). The pile geometry is 1m radius and 20 m length, the pile elastic modulus $E_p = 1.15$ GPa and the initial soil stiffness $G_0 = 1.13$ MPa.

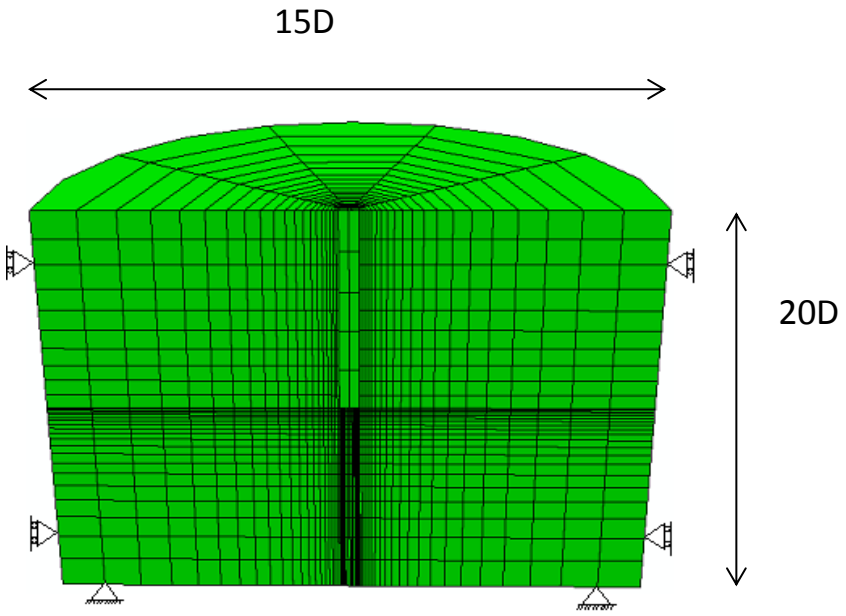

Figure 4.4: Finite element mesh

Figure 4.5 shows that the mean stress has little effect on the lateral response of piles. Therefore its effect can be ignored for practical purposes.

Figure 4.6 shows that predictions of the energy-based method for lateral displacements in piles are in excellent agreement with the finite element analysis.

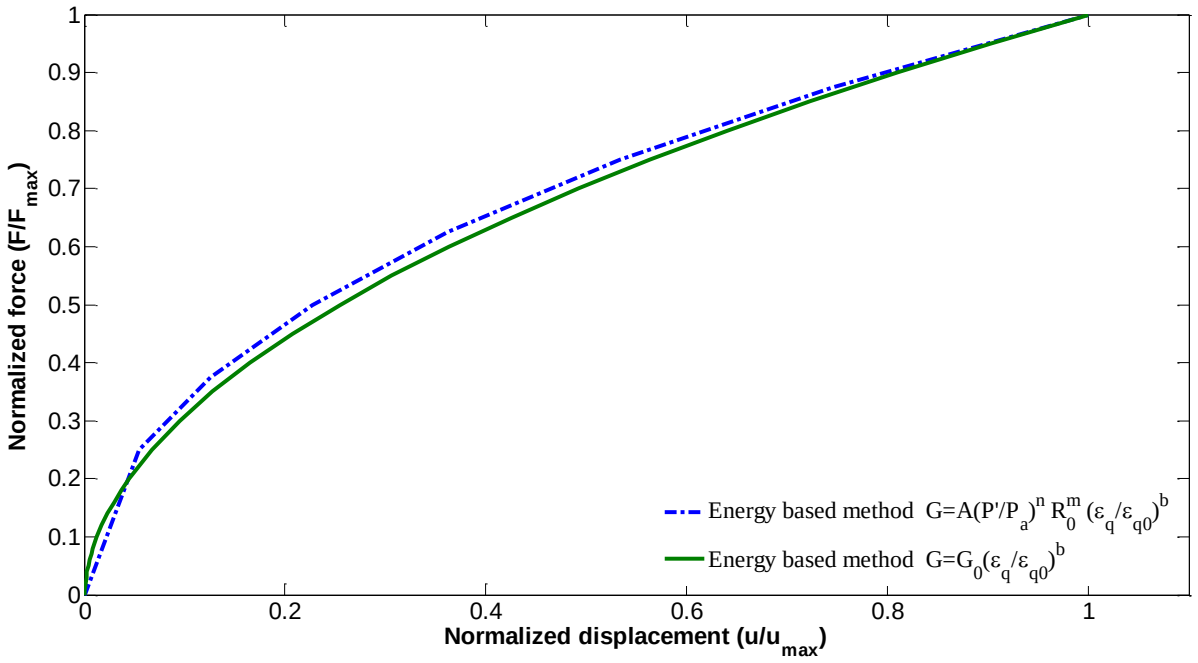

Figure 4.5: Response of the pile subjected to lateral load

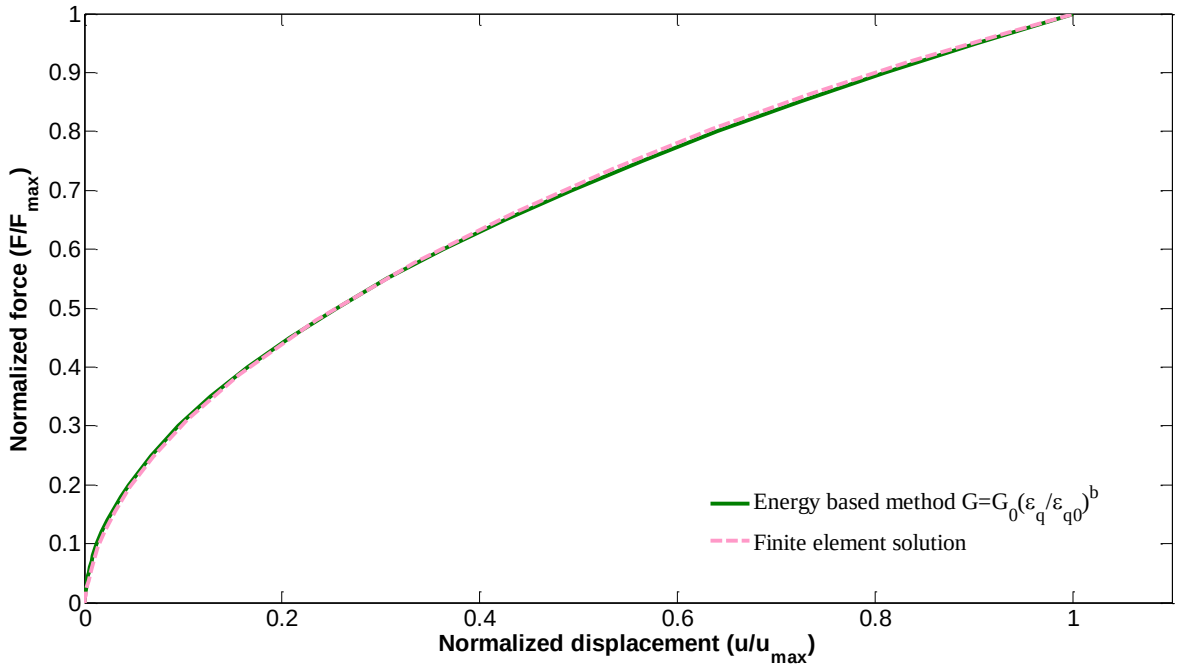

Figure 4.6: Deformation of the pile head due to lateral load

4.4 Comparison with field data

4.4.1 Phillips and Lehane (1998)

The analytical solution has also been validated against field data from a pile tests at greenfield sites near Dublin city centre, as reported by Phillips and Lehane (1998). In this case history, two steel piles were driven into stiff glacial till. A series of lateral loads were applied to the free top of the piles. The stiff glacial till contained 0.2 m of granular fill over 1.2 m of brown boulder clay, lying on black boulder clay (see Figure 4.7), n is a constant obtained experimentlly equal to -0.5, and each layer was divided into a number of sub-layers so that degradation of the moduli could be calculated in an accurate way. The average undrained shear strength for the brown boulder clay was 100 kPa while for the black boulder clay layer was between 350kPa and 600 kPa. Here the average undrained shear stress was used. The shear modulus for each layer was calculated following the empirical formula suggested by Atkinson (2000). For stiff clay, the initial stiffness of the soil can be related to the undrained shear strength as $\frac{E_{u0}}{2S_u} = 1000$ (see Atkinson, 2000), where E_0 is the initial Young's modulus and $E_0 = 3G$.

The two steel piles were H-piles ($203 \times 203 \times 46\ kg/m$) and the pile length was 5 m. The distance between the two piles (A & B) was 2 m. Three static load tests were performed and the initial two loads were denoted as LT1 and LT2, while the ultimate load was applied in the third test, denoted as LT3 (more than 220kN). The deformation here is supposed to be controlled by the average soil stiffness. Figure 4.8 shows the observed displacement of the pile head plotted against applied load compared with the prediction obtained using the analytical solution detailed in Section 4.1. This figure demonstrates that the analytical solution gives consistent results compared with field data. For pile displacement less than 30 mm, the analytical solution slightly overestimates the lateral load but by less than 20%.

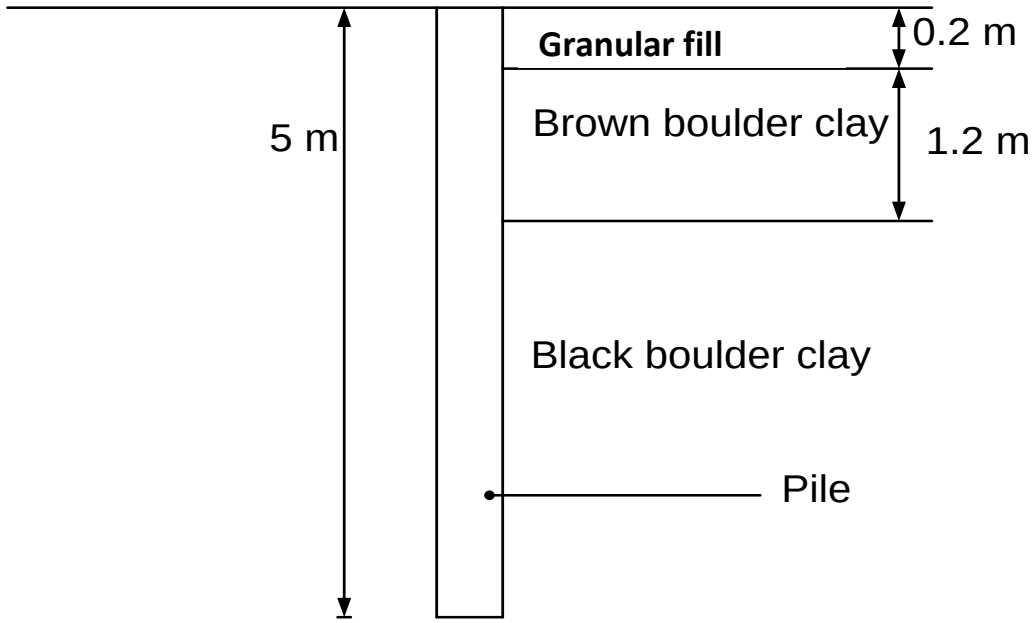

Figure 4.7: Stratigraphy of the site

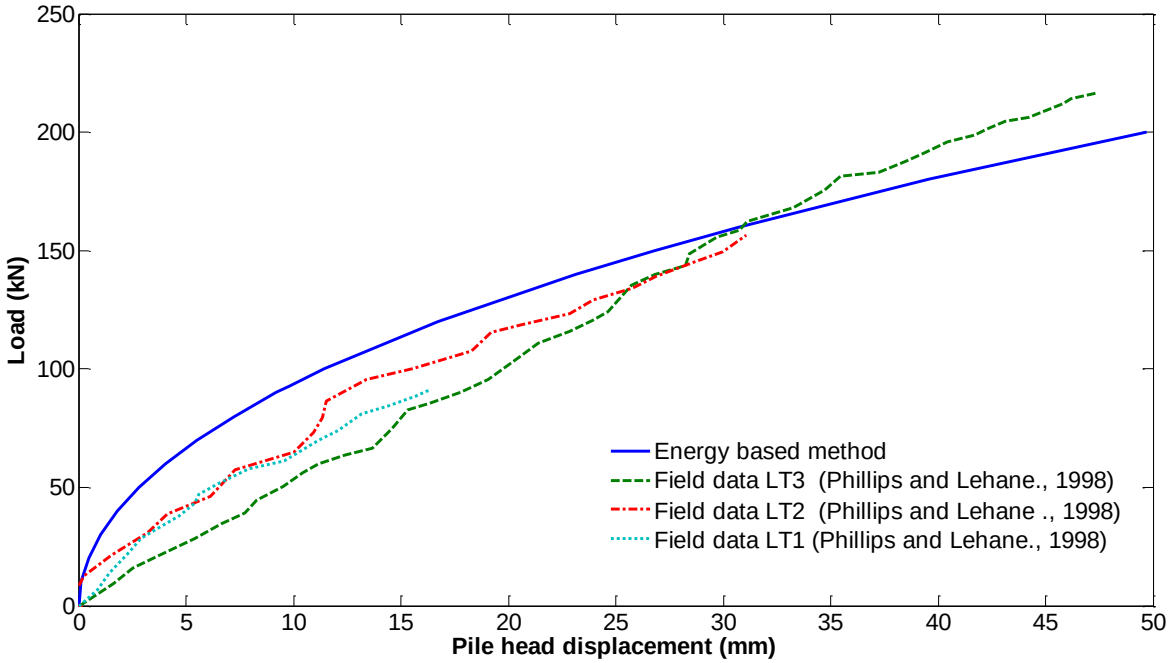

Figure 4.8: Load versus pile head displacement comparison with Phillips and Lehan (1998)

4.5 Comparison with centrifuge tests

4.5.1 Ilyas et al. (2004) tests

The analytical solution was also compared with centrifuge tests carried out by Ilyas et al. (2004). The centrifuge test was for piles embedded in kaolin clay, where the pile cross section was square. This area was modified to a circlular cross section area.

The pile was hollow, square and made from aluminium. A series of tests were applied to different pile cross sections. The experiment was conducted at 70 g, with a pile width of 0.84 m and 14.7 m in the prototype. The flexural rigidity $E_p I_p$ was equal to 922 kNm^2, the soil stiffness of soil derived from triaxial test carried out by Atkinson (2000). The shear strength of soil (normal consolidation soil) can be obtained from relationship stated by Wood (1990) ${S_u}/{\sigma_v'} = 0.21$, where S_u is shear strength of soil and σ_v' is vertical effective stress. Once S_u is known we can calculate Young modulus from relation carried out by Atkinson (2000) for soft soil ${E_{u0}}/{2S_u} = 2000$, and shear modulus of calculated from $E_u = 3G$, the initial shear modulus of soil for first layer as $G_{01} = 19.11$ MPa, for second layer is $G_{02} = 38.2$ MPa, for third layer $G_{03} = 57.33$ MPa, and $G_{04} = 76.44$ MPa.

A series of tests for a single pile and a group of piles were carried out. The response of a single laterally loaded pile for experiment and analytical analysis was validated. These comparisons demonstrate clearly that the analytical solution can be used as a useful approximation for the piles performance. The slight discrepancies between the predicted performace and the measured beformance could be attributed to the approximation in modelling the stress-strain response (see Figure 4.9).

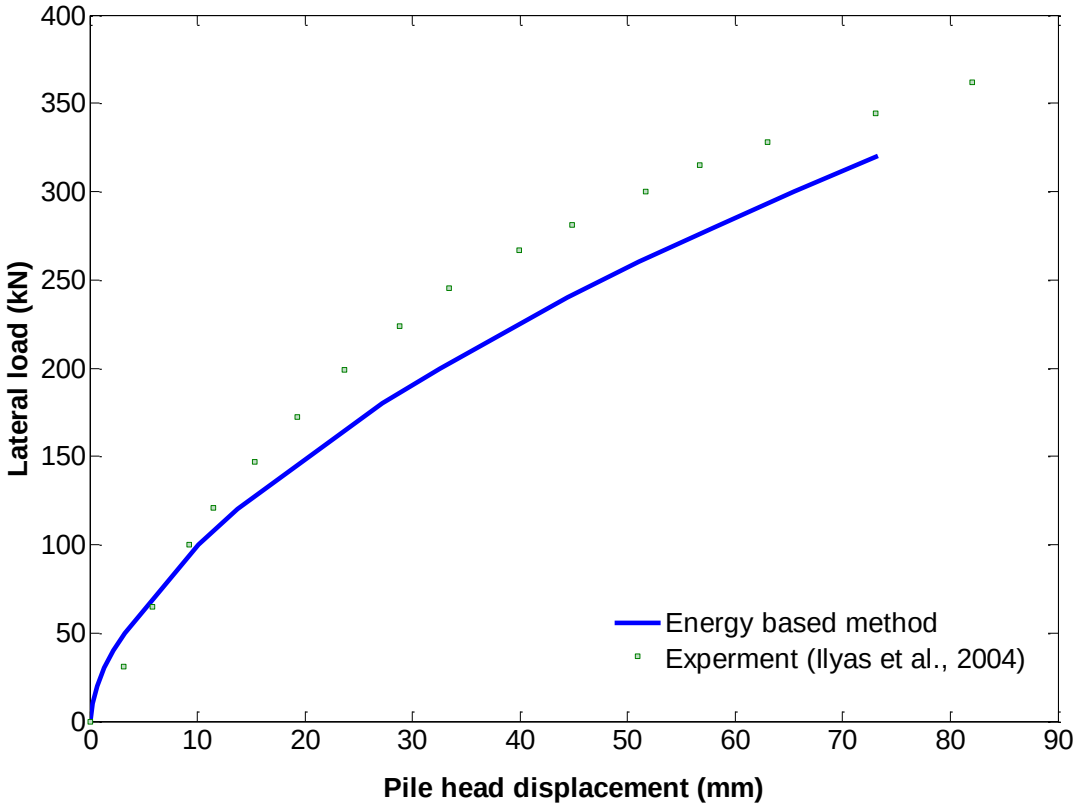

Figure 4.9: The pile-soil deformation comparison with centrifuge tests

4.5.2 Khemakhem et al. (2010) tests

Khemakhem et al. (2010) carried out a centrifuge test, where the pile was manufactured to simulate at 50g a prototype steel pile with a diameter of 0.9 m and length of 16 m. The thickness of the pile was 1 mm and the bending stiffness of the pile was $E_p I_p$ 38100 MNm^2. The experiment was designed for variable lateral loading in order to estimate the pile head displacement. Figure 4.10 indicates that at a very small load (0-60 kN) the displacement increases linearly. However, at load $>$ 60 kN there is a significant change in slope as the load-displacement curve is slightly higher in the analytical solution based on the energy method than the result from test 1 of Kemakem et al. (2010) as shown in Figure 4.10. The analytical solution shows a softer response compared with the experimental data particularly at the initial stage of loading. These results indicate that more appropriate functions to describe the stress-strain response might be needed.

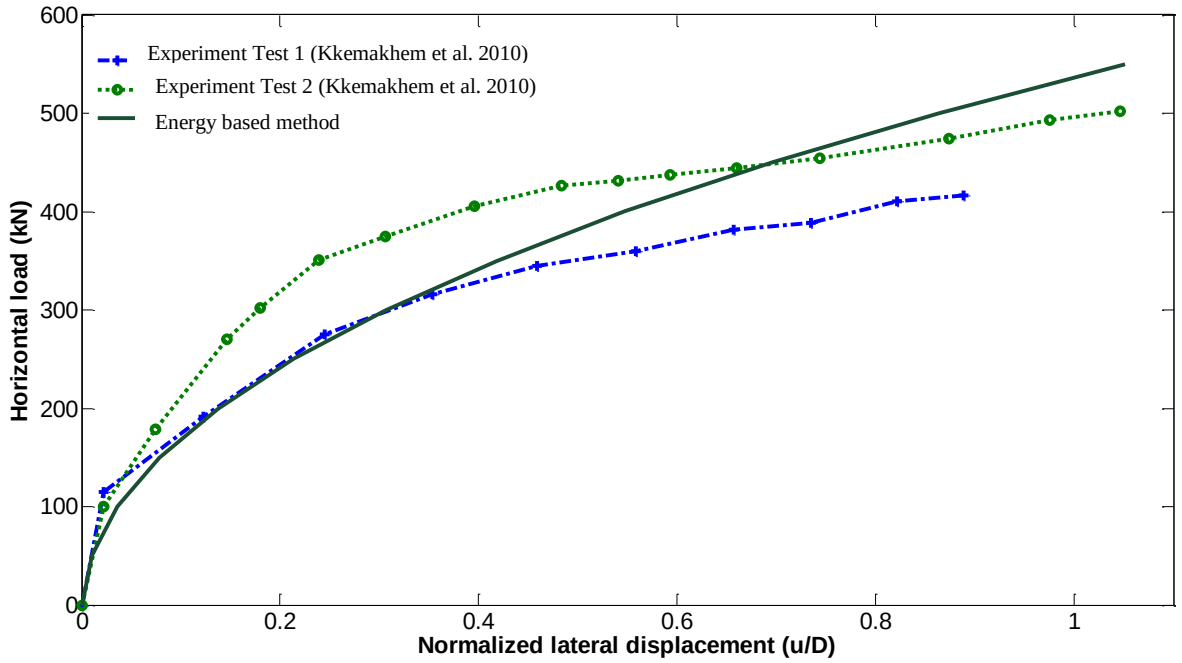

Figure 4.10: Response of laterally loaded piles comparison with Khemakhem et al. (2010)

4.6 Comparison with published numerical analysis

4.6.1 Allotey and El Naggar (2008)

A numerical analysis of lateral cyclic nonlinear soil-pile response was carried out by Allotey and El Naggar (2008) using a beam on nonlinear Winkler foundation model (BNWF dynamic model), where the model was compression-dominant, used to model the pile-soil interaction. This model has been produced to predict the response of pile for four main parts: the backbone curve, the standard reload curve, the general unload curve and the direct reload curve. The advantage of using the BNWF model is its ability to account for cyclic soil degradation and reduced radiation damping due to increased soil nonlinearity. Allotey and El Naggar (2008) simulated a reinforced concrete pile of length 12 m and diameter 600 mm embedded in uniform stiff clay. The undrained shear strength was 50 kPa. Six tests with different assumptions were undertaken. Case C is considered here, which assumed full connection between the pile and the soil. Here, the one type of test assumed that there was no

gap between the pile and the soil. Figure 4.11 shows the load-deflection response from the numerical analysis and compares it to the analytical solution. The displacement is overestimated by 10% at loads ranging from 0 to 70kN, but overall, there is a good agreement between the backbone curve of Allotey and El Naggar (2008) and the proposed analytical solution.

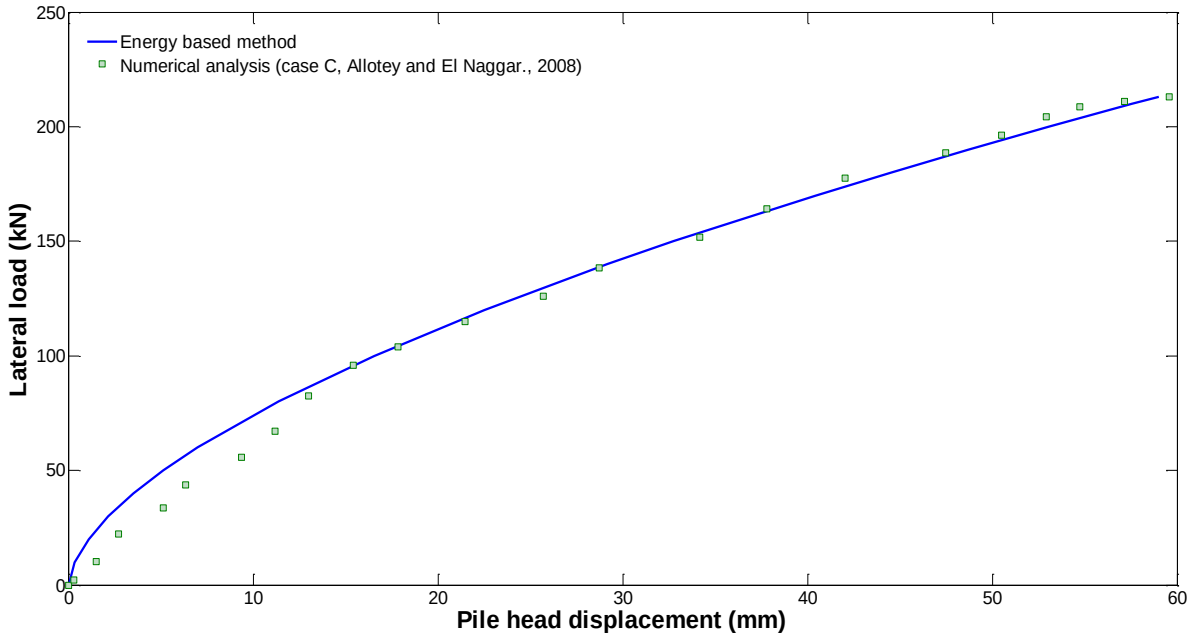

Figure 4.11: Load-displacement response: comparison with allotey and El Naggar (2008)

4.7 Modelling the pile subjected to lateral cyclic load

To predict the response of soil due to cyclic loading, an empirical model for undrained soil can be used which is based on Masing's rules (Masing, 1926) and Pyke (1975) and can be sumarrised as:

(a) the shear modulus on each loading reversal assumes a value equal to initial tangent modulus of the intial loading (back-boned) curve. (b) the shape of the unloading or reloading curves is the same as that backbone curve. (c) the unload-reload curves should follow the backbone curve if the maximum amplitude of shear

strain is exceeded. (d) the current unloading or reloading curve intersects the curve described by a previous unloading or reloading curve (Puzrin et al., 1995)

The stress follows the previous unloading or reloading curve. The stiffness of the soil during unloading-reloading can be expressed as

$$G = a\left(\frac{\Delta\varepsilon_q}{2}\right)^n \tag{4.24}$$

where $\Delta\varepsilon_q$ is accumulated of deviatoric strain relative to the previous stress reversal state

$\Delta\varepsilon_q = \sqrt{\frac{2}{3}\Delta\varepsilon_{ij}\Delta\varepsilon_{ij}}$ where $\Delta\varepsilon_{ij} = {\varepsilon_{ij}}^r - \varepsilon_{ij}$ and ${\varepsilon_{ij}}^r$ is the strain tensor at the reversal point.

The reversal point for undrained soil can be estimated by the change in accumulateddeviatoric strain because the volumetric strain is taken to be zero in the case of undrained soil. The soil stiffness when $\varepsilon_q = 10^{-5}$ is taken to be constant.

4.7.1 Comparison with field data

Phillips and Lehane (1998) reported three cyclic loading tests (unloading-reloading) performed on a pile. More details about soil properties and pile geometry are mentioned in Section 4.4.1. The load here was increased regularly by 10 kN each time. The maximum loads for LT1, LT2 and LT3 were 91 kN, 156 kN and 215 kN, respectively. The analytical solution has been used to make a comparison with the field data. The cyclic load-displacement is shown in Figure 4.12. This figure demonstrates that the energy-based method can be used to estimate the pile behaviour in this situation as well.

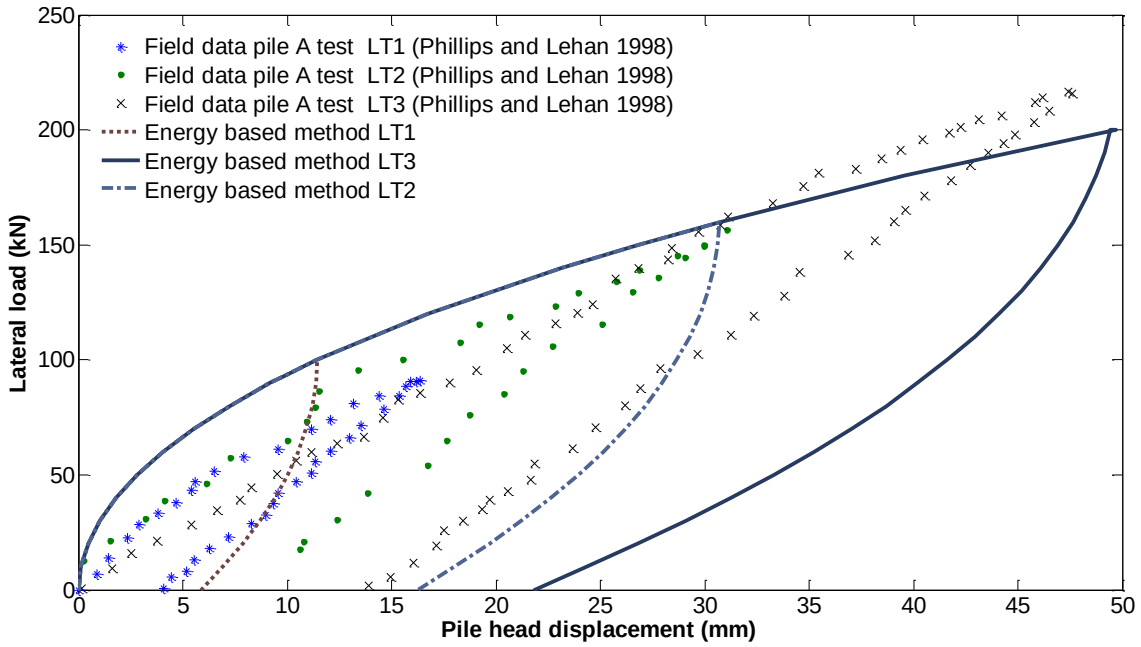

Figure 4.12: Cyclic lateral load versus pile horizontal displacement

4.7.2 Comparison with published numerical analysis

A numerical study carried out by Allotey and El Naggar (2008) predicted the response of a pile subjected to cyclic lateral load. The BNWF model was used (more details were given in Section 4.6.1). A very good agreement between the numerical analysis and analytical solution is shown in Figure 4.13.

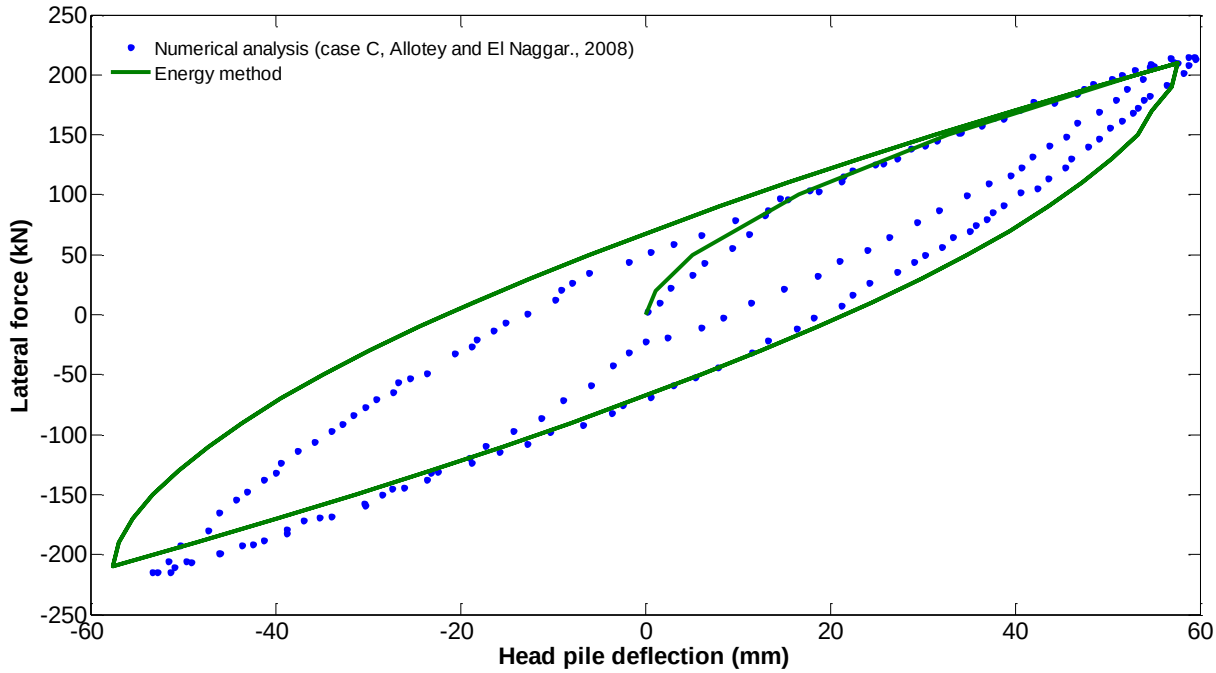

Figure 4.13: Lateral pile displacement resulting from numerical analysis

4.8 Summary

- An analytical solution based on an energy method has been developed to predict pile-soil displacements, where the soil is assumed to be nonlinear elastic (soil parameters vary in radial, tangential and depth directions).

- Governing equations for pile and soil have been obtained by applying the variational principle to the potential energy. The soil stiffness is expressed as a function of strain $G(\varepsilon)$, and as a function of the stress and the strain $G(\sigma, \varepsilon)$.

- The analysis in this chapter has considered static and cyclic lateral loads.

- Comparisons have been made with the finite element method, field data and centrifuge tests.

5 The response of a pile under axial and combined loads in nonlinear soil

Introduction

In Chapter 4, the development of an analytical approach based on the energy method was illustrated for laterally loaded piles. In this chapter, an energy-based solution is presented for axially loaded piles and for piles subjected to combined axial, lateral and moment loading. Piles under both static and cyclic loads are considered.

5.1 Axially loaded pile in a nonlinear elastic soil

5 .1.1 Basic assumptions

As the horizontal and tangential strains are very small in an axially loaded pile, both displacements can be neglected (Salgado et al., 2007). For a circular pile there are two functions that can be considered, v (z) and $\phi(r)$, where v(z) is vertical displacements at depth z and $\phi(r)$ represents dimensionless functions describing the variation of soil displacements in the radial direction.

The vertical displacement at any point of the soil is represented as a function in (r, z).

$$\mathrm{v}_r = 0 \qquad (5.1a)$$

$$\mathrm{v}_\theta = 0 \qquad (5.1b)$$

$$\mathrm{v}_z(r,z) = \phi(r)\, u\,(z). \qquad (5.1c)$$

For the same cross-sectional area of the pile $\phi(r) = 1$ when $r = 0\ to\ r_0$, while $\phi(r) = 0$ when $r \to \infty$, which explains the decay of $\phi(r)$ with an increase in the radial direction.

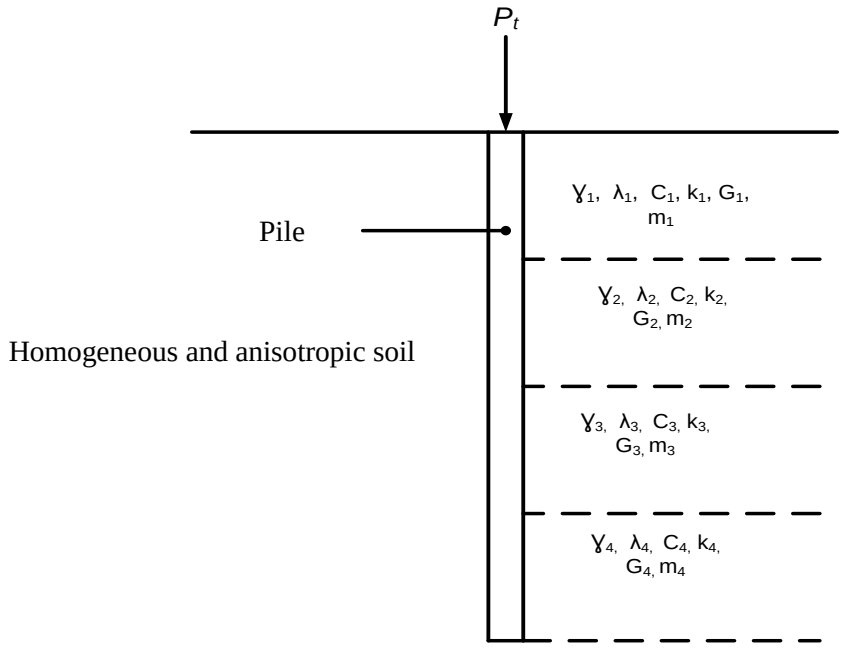

Figure 5.1: An axially loaded pile in a homogeneous nonlinear elastic medium

5.1.2 Potential energy

The vertical load acting on the top of the pile leads to the vertical displacement of the pile-soil system, which results in potential energy in the pile and the surrounding elastic medium. The total potential energy of the pile and the soil is a summation of internal potential energy and external potential energy (Basu et al., 2008), which is given as

$$U = \frac{1}{2} E_p A_p \int_0^L \left(\frac{d\mathrm{v}}{dz}\right)^2 dz + \frac{1}{2}\int_{r_0}^{\infty} \sigma_{ij}\varepsilon_{ij}\, dr + \frac{1}{2}\int_0^{\infty} \sigma_{ij}\varepsilon_{ij}\ dr - \mathrm{v}\, P_{t\ at\ z=0} \tag{5.2}$$

where E_p denotes the elastic Young modulus of the pile, A_p denotes the cross-section area of the pile, v represents the vertical displacement, and $\sigma_{ij,}\varepsilon_{ij}$ are stress and strain components respectively.

The first term of the equation represents pile potential pile energy, the second and third terms are potential energy from the surrounding soil and the soil below the pile respectively, and P_t is the vertical load. By inserting the nonlinear stress-strain relationships into Equation 5.2, the potential energy equation becomes

$$U = \frac{1}{2}E_pA_p\int_0^L\left(\frac{d\mathrm{v}}{dz}\right)^2dz + \pi\int_0^L\int_{r_0}^{\infty}\left((\lambda+2G)\left(\phi\frac{d\mathrm{v}}{dz}\right)^2 + G\left(\mathrm{v}\frac{d\phi}{dr}\right)^2\right)rdrdz$$
$$+ \pi\int_L^{\infty}\int_0^{\infty}\left((\lambda+2G)\left(\phi\frac{d\mathrm{v}}{dz}\right)^2 + G\left(\mathrm{v}\frac{d\phi}{dr}\right)^2\right)rdrdz - \mathrm{v}P_{t\,(z=0).} \qquad (5.3)$$

The variational principle has been used to calculate δU and δW, where δU and δW are potential and external energies respectively (Vallabhan and Mustafa, 1996; Lee and Xiao, 1999). As a result, the governing equations of the pile-soil system are obtained by minimizing the potential energy of soil and pile.

The expression of potential energy contains different functions, such as $\mathrm{v}(z)$, $\phi(r)$, $\left(\frac{d\mathrm{v}(z)}{dz}\right)$ and $\left(\frac{d\phi(r)}{dr}\right)$, so by minimizing the potential energy we get:

$$\delta\Pi = \left[A(\mathrm{v})\delta\mathrm{v} + B(\mathrm{v})\delta\left(\frac{d\mathrm{v}}{dz}\right)\right] + [C(\phi)\delta\varphi] = 0. \qquad (5.4)$$

A, B and C are terms associated with variations $\delta\mathrm{v}$, $\delta\left(\frac{d\mathrm{v}}{dz}\right)$ and $\delta\phi$, and the variation of Equation 5.3 becomes

$$\delta U = \frac{1}{2}E_pA_p\int_0^L\frac{d\mathrm{v}}{dz}\delta\frac{d\mathrm{v}}{dz}dz + \pi\int_0^L\int_{r_0}^{\infty}\left((\lambda+2G)\left(\phi\frac{d\mathrm{v}}{dz}\delta\phi\frac{d\mathrm{v}}{dz}\right) + G\left(\mathrm{v}\frac{d\phi}{dr}\delta\mathrm{v}\frac{d\phi}{dr}\right)\right)rdrdz$$
$$+ \pi\int_L^{\infty}\int_0^{\infty}\left((\lambda+2G)\left(\phi\frac{d\mathrm{v}}{dz}\delta\phi\frac{d\mathrm{v}}{dz}\right) + G\left(\mathrm{v}\frac{d\phi}{dr}\delta\mathrm{v}\frac{d\phi}{dr}\right)\right)rdrdz - \mathrm{v}P_{t\,(z=0)}$$
$$= 0. \qquad (5.5)$$

The governing equation of the pile is obtained for $0 < z < L$ by collecting terms associated with δudz, $\delta\frac{d\mathrm{v}}{dz}dz$ and its derivative, $\delta\mathrm{v}$ and $\delta\frac{d\mathrm{v}}{dz} \neq 0$. The governing equation is obtained as follows:

$$k\frac{d^2\mathrm{v}}{dz^2} + C\frac{d\mathrm{v}}{dz} + m\mathrm{v} = 0 \qquad (5.6)$$

where

$$C = 2\pi \int_{r_0}^{\infty} r[(\lambda + 2G)\,\phi^2]\,dr \tag{5.7a}$$

$$k = E_p I_p + 2\pi \int_{r_0}^{\infty} r[(\lambda + 2G)\,\phi^2]\,dr \tag{5.7b}$$

$$m = -2\pi \int_{r_0}^{\infty} r\,G\,\left(\frac{d\phi}{dr}\right)^2 dr. \tag{5.7c}$$

For this study, the tip of a pile is assumed to be clamped, which means that the displacement and the curvature are equal to zero at the base of the pile. The boundary conditions are obtained by collecting δv and $\delta\frac{\mathrm{dv}}{dz}$ at the head of the pile $(z = 0)$.

$$s\frac{\mathrm{dv}}{dz} + P_t = 0 \tag{5.8}$$

where

$$s = -E_p A_p - 2\pi \int_{r_0}^{\infty} r\,[\lambda + G(2 + \phi^2)]\,dr. \tag{5.9}$$

The displacement at the tip of the pile $z = L$.

$$\mathrm{v} = 0. \tag{5.10}$$

Similar to the solution of pile governing equation in Chapetr 4, the second order differential Equation 5.6 can be solved using cental finite difference scheme (see appendix).

5.2 Response of the pile subject to vertical load

5.2.1 Soil displacement

Collecting the terms of $\delta\varphi\ dr$ for $r_0 \leq r \leq \infty$, the governing equation of soil is

$$r\ \frac{d^2\phi}{dr^2} + \gamma_1 \frac{d\phi}{dr} + \gamma_2\ \phi = 0 \tag{5.11}$$

where

$$\gamma_1 = \frac{\int_0^L G + r\ G}{\int_0^L G} \tag{5.12a}$$

$$\gamma_2 = \frac{-\int_0^L (\lambda + 2G)\left(\frac{d\mathrm{v}}{dz}\right)^2}{\int_0^L G\ \mathrm{v}^2}. \tag{5.12b}$$

This governing equation for the soil has been solved numerically using the finite difference method (MATLAB 7.12). Similar to the calculation of the pile displacement in Chapter 4, the pile displacement is solved using the central finite element technique.

5.3 Iterative solution scheme

The pile deflection equation can be solved when the soil parameters $k,\ C$ and m are known; however, these parameters depend on the unknown dimensionless soil function ϕ, which can be estimated by calculating $\gamma_1\ and\ \gamma_2$.

Soil displacement is obtained when the initial numbers of these values, $\gamma_1\ and\ \gamma_2$, are inserted into Equation 5.11, from which the soil parameters k, C and m are obtained as a result of the pile displacement. New values of $\gamma_1\ and\ \gamma_2$ (Equations 5.12a and 5.12b) are determined and then inserted into Equation 5.11 to evaluate ϕ, then v, so an iteration

technique is needed to obtain the condition $\left(\frac{\gamma_{old}-\gamma_{new}}{\gamma_{old}}\right) > 0.001$. Figure 5.2 shows the flow chart of the solution procedure.

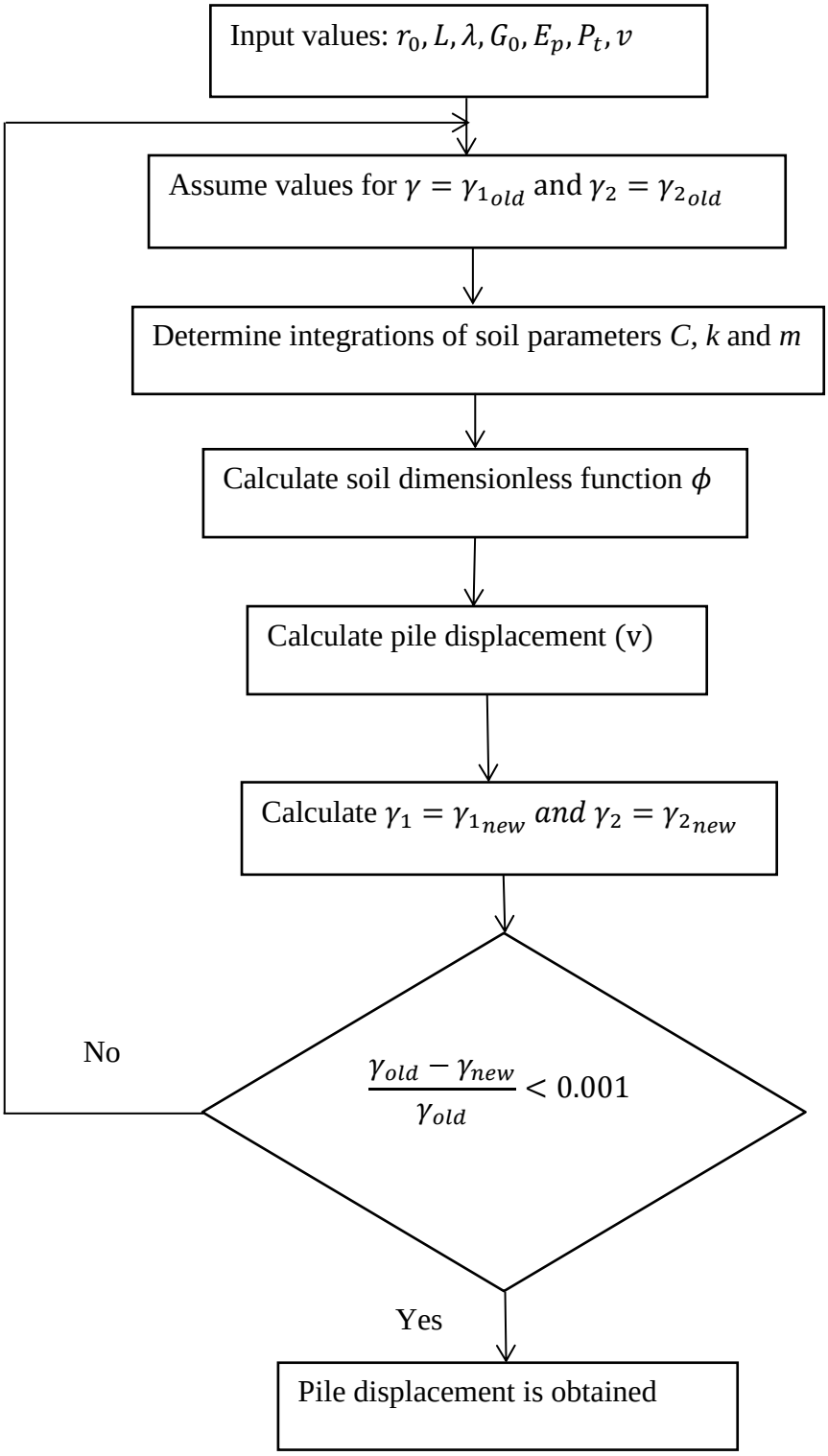

Figure 5.2: Flow chart for the iterative scheme to predict the reponse of pile under axial load

5.4 Comparison with field data

Two case histories were used to validate the results of the analytical solutions, both from the city of Dublin. Farrell et al. (1998) tested piles at Trinity College Dublin (TCD), which is located between River Liffey and River Dodder. This area was also investigated by Long and Menkiti (2007), and Gavin et al. (2008), who tested two compression piles and a tension pile about 2 km south of Dublin city centre. The geology of the area was investigated by Long and Menkiti (2007), who classified the layers into four categories: upper brown, upper black, lower brown, and black boulder clay, these lying on a limestone bed.

An undrained triaxial compression test was conducted in order to determine the undrained shear strength of the black boulder clay, which was 450kPa. Moreover, Phillips and Lehane (1998), and Long and Menkiti (2007), determined that the average undrained strength for upper brown boulder clay (UBrBC) was 100kPa, and between 350kPa and 600kPa for upper black boulder clay (UBkBC). For this analysis, an average undrained strength of 450kPa was adopted.

As mentioned in this study, Lame's modulus and shear modulus vary in nonlinear soil and pile responses calculated by assuming the soil as homogenous. Long and Menkiti (2007) reported $G_0 = 98$ MPa for the first layer and $G_0 = 83$ MPa for the second layer. The degradations of soil stiffness for upper brown and upper black boulder clay are shown in Figures 5.3 and 5.4. The initial soil stiffness used in the calculation was taken from Long's study, and was also calculated using the power law relation, Equation (4.2).

$$G = a\left(\varepsilon_q\right)^b \tag{5.13}$$

where a is a constant value, ε_q donates deviatoric strain, and b represents a constant. Following Osman et al. (2007), $b = -0.5$ fits the undrained data well.

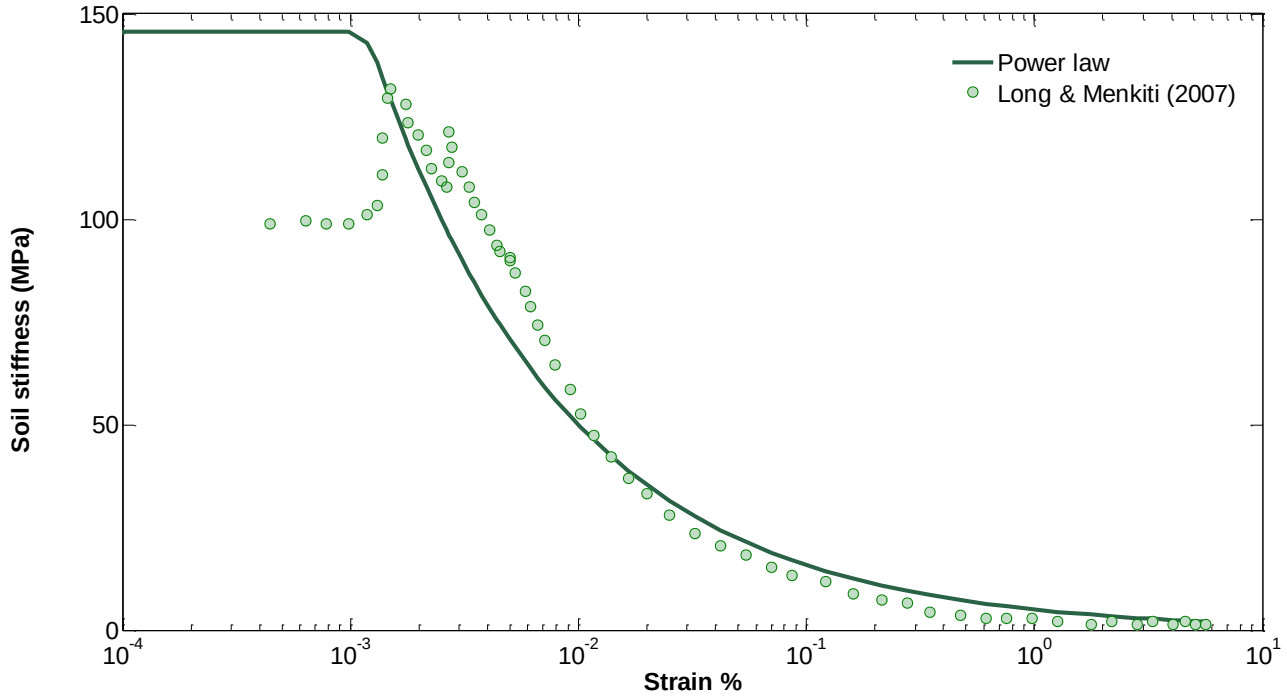

Figure 5.3: Variation of soil stiffness with strains for upper brown boulder clay

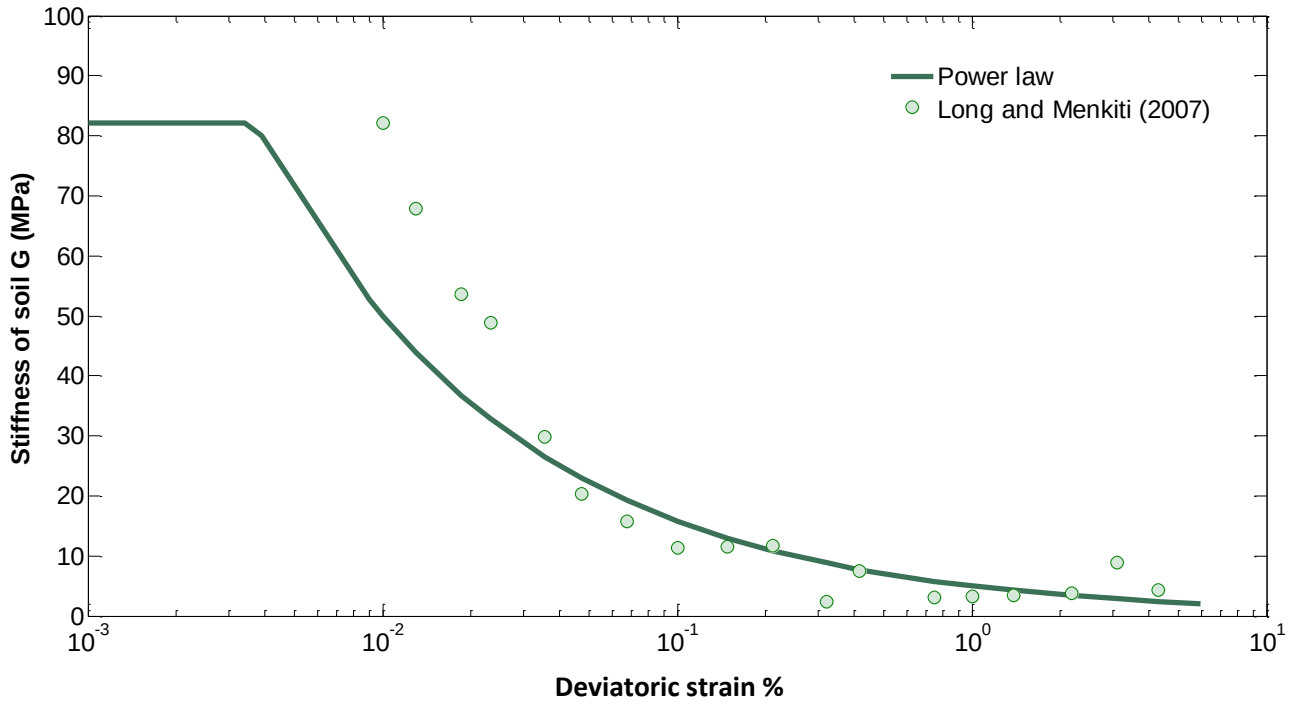

Figure 5.4: Variation of soil stiffness with strains for upper black boulder clay

5.4.1 Farrell et al. (1998)

Site location

Many investigations into Dublin boulder clay (DBC) have been reported. Much of the data has been obtained from the Dublin Port Tunnel (DPT) project and shaft WA2 sites, which cover approximately 10-12 square kilometres.

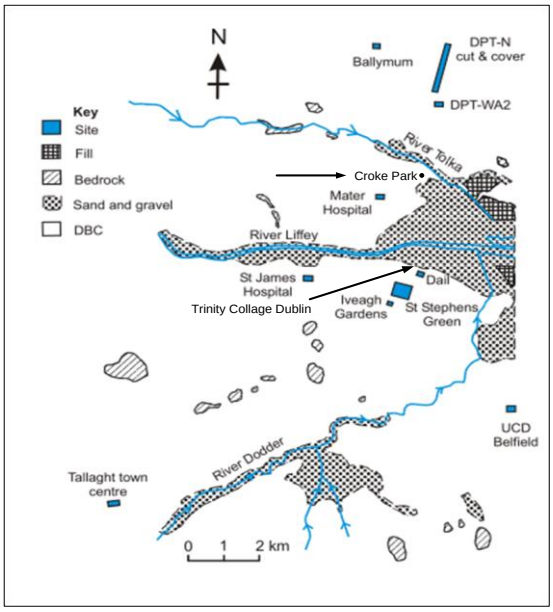

Figure 5.5: Location sites in Dublin (Long & Menkiti, 2007)

Field test

Fieldwork was also carried out by Farrell et al. (1995) at TCD. A steel driven pile 0.273 m in diameter and 7.5 m in length, a close end tubular pile, was embedded in the boulder clay. The thickness of the cross-section was 1 mm (0.001m) (see Figure 5.6).

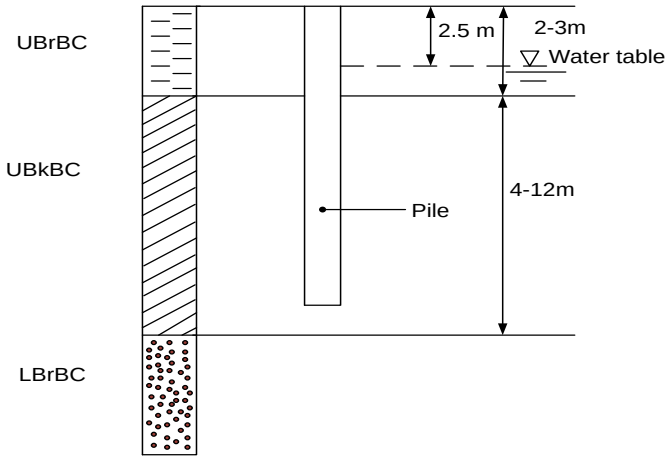

Figure 5.6: Soil profile at TCD in Dublin

A series of axial loads were applied to the pile in order to obtain a pile-soil deformation. The initial undrained shear strength S_u in the first layer was 110 kPa, and 300 kPa in the second and third layers (Long & Menkiti, 2007). The results were then compared with analytical solutions. Figure 5.7 shows axial load versus observed and predicted pile head deflection. This figure shows that the energy-based method prediction fits well with the field measurements.

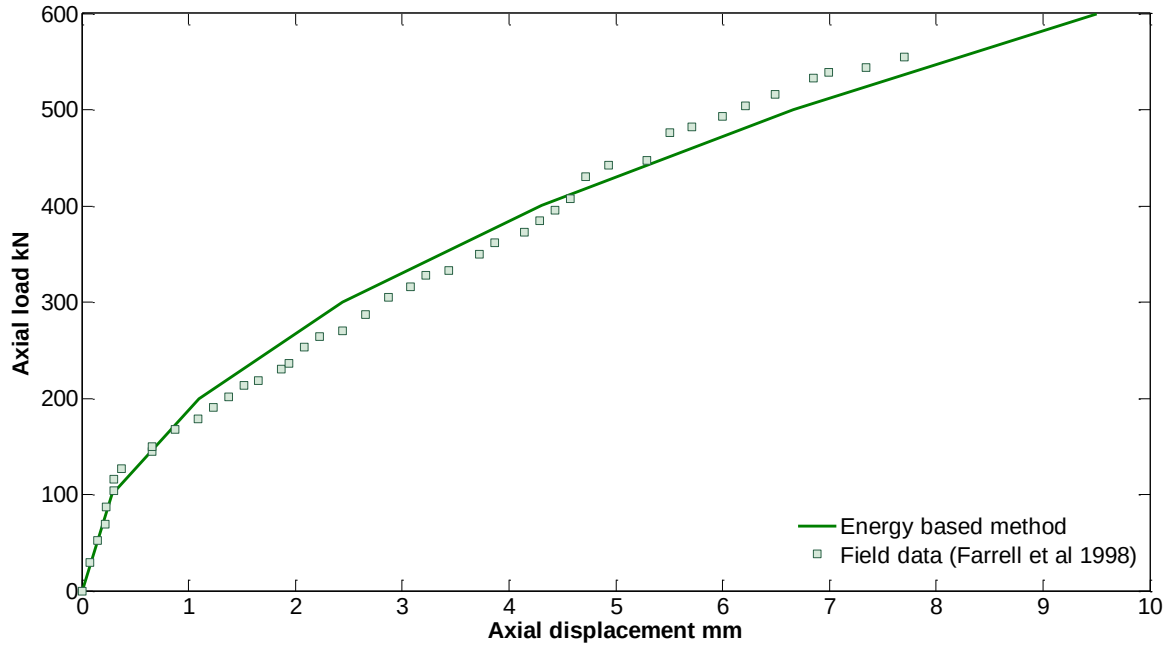

Figure 5.7: Response of the head of the axially loaded pile

Farrell et al. (1998) also reported results from unload-reload applied on the head of the pile. The displacement increased linearly from 0-100 kN, then there was a significant increase of pile displacement at loads greater than 100kN. The results were validated with deformations resulting from the analytical solution based on the energy method, where the corresponds of displacement were measured from the previous load reversal point. Figure 5.8 shows an unload-reload cycle compared with the analytical solution using Masing's rule (1926). Although, there are discrepancies between the measured and predicted response, the energy based method appears to provide quick initial estimates of pile reponse. Therefore, it could provides engineers with a useful tool for initial design of piles.

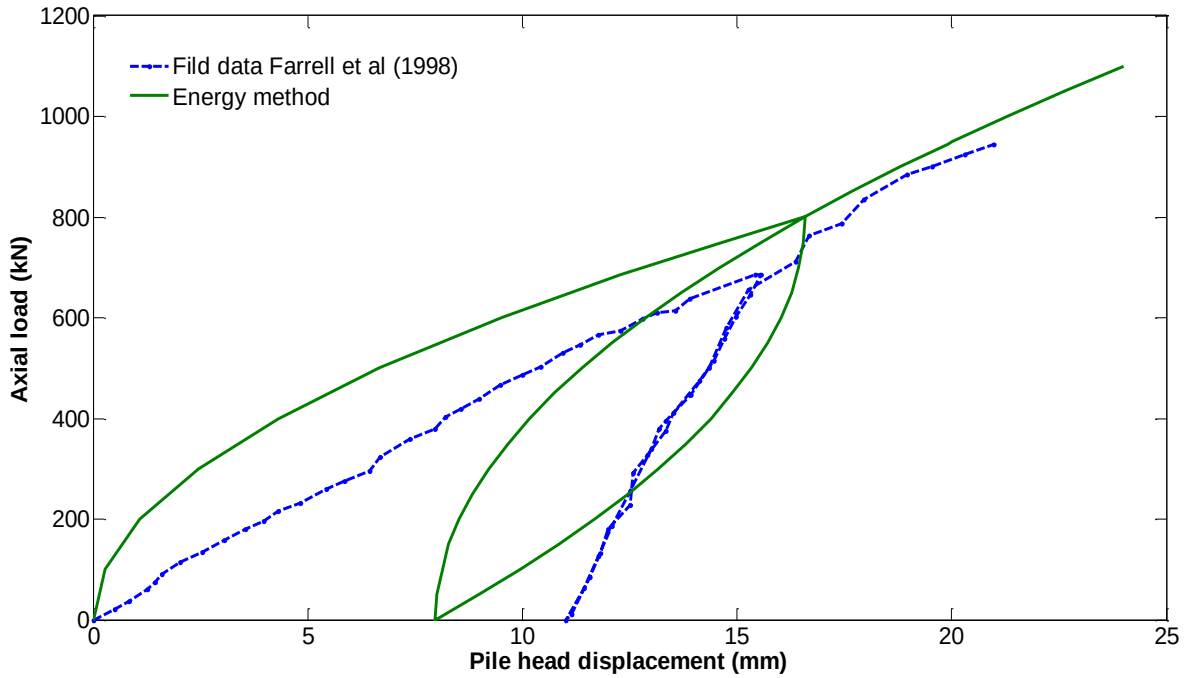

Figure 5.8: Cycle axial load

5.4.2 Gavin et al. (2008) piles test

Site location

Three piles were installed at the site located 2 km south of Dublin city centre (see Figure 5.9). The geology of Dublin has been described in the previous Section (5.4.1), and Figure 5.10 shows the geological cross section with installed piles.

The ground level of the soil is +4 m0D. The thickness of these layers varies in Dublin and the surrounding area. Undrained shear strength was estimated for a number of samples. Other soil properties were also measured, such as water content, liquid and plastic limits (see Figure 5.11).

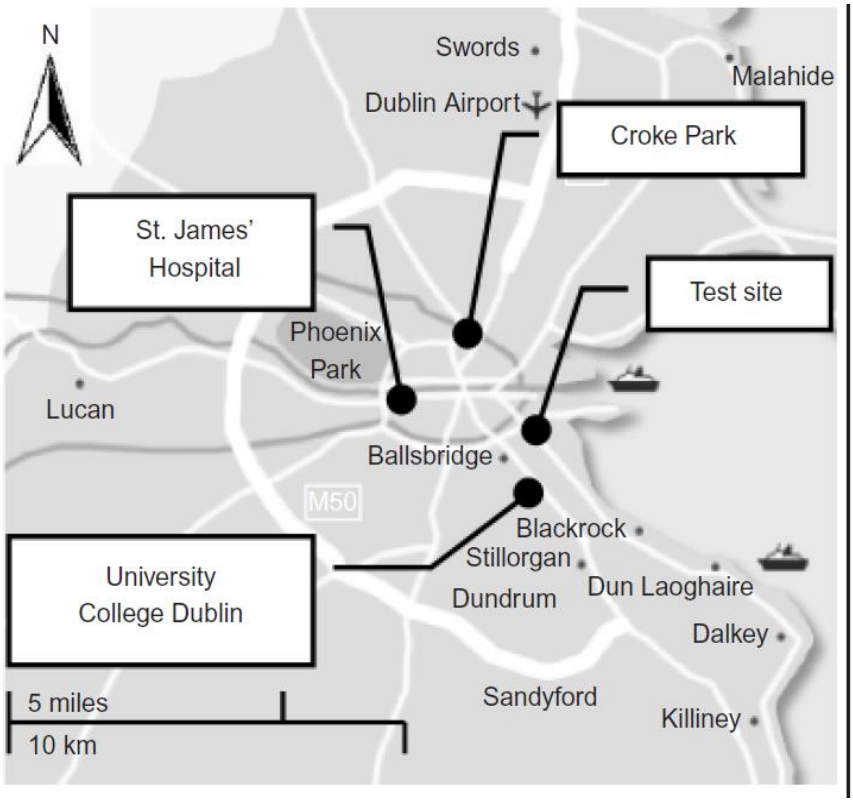

Figure 5.9: Location of pile test in DBC (Gavin et al., 2008)

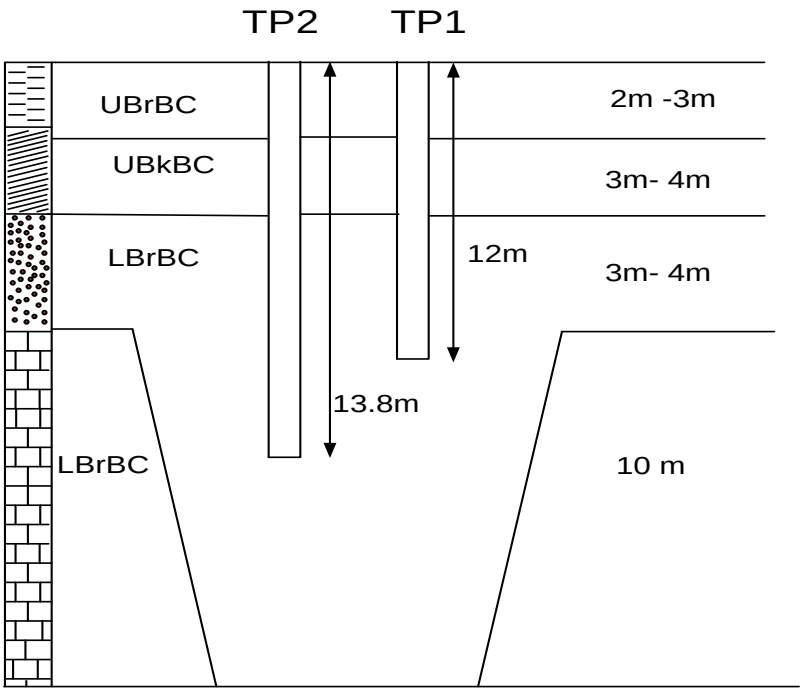

Figure 5.10: Geological cross section (Gavin et al., 2008)

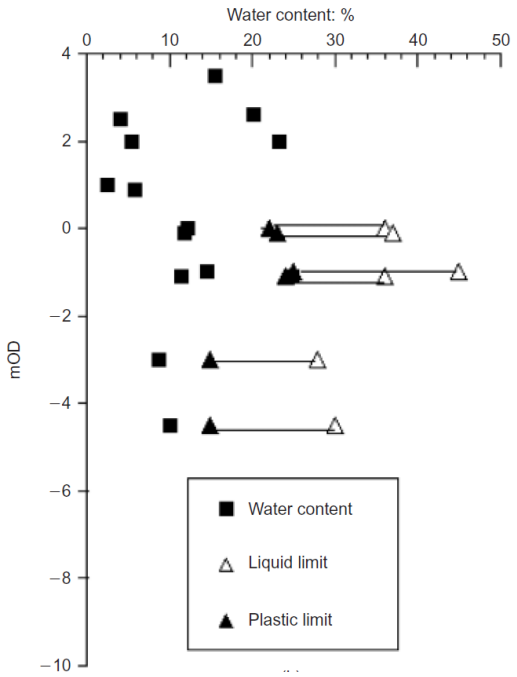

Figure 5.11: Water content and plastic limits at the site (Gavin et al., 2008)

Field test

Non-displacement pile tests were carried out by Gavin et al. (2008) to estimate the displacement of three piles subjected to monotonic and cyclic load at a site near Dublin city centre. The three pile diameters were 762 mm. Pile TP1 was 12 m in length and TP2 was 13.8 m in length and they were loaded in compression, while TP3 was loaded in tension. Only TP1 and TP2 are considered in this study.

Figure 5.12 shows the vertical displacement versus the axial force (TP1 and TP2). The load-displacement curve of the TP2 test results from the energy based method again fit well with the field data

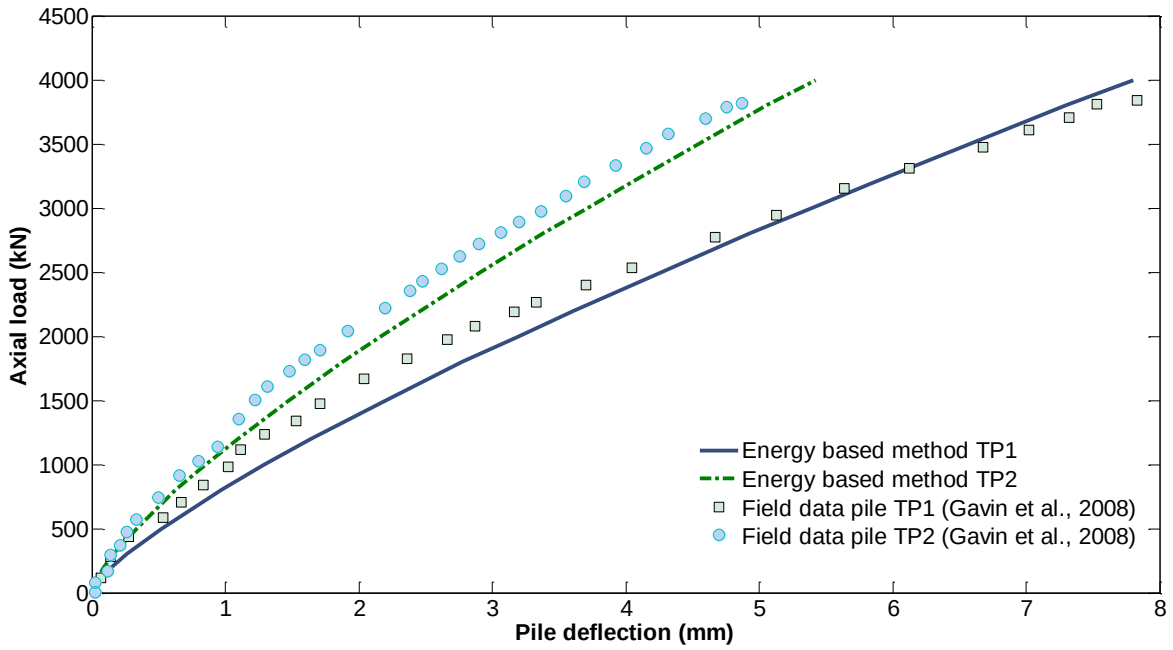

Figure 5.12: Response of the head of the axially loaded pile

5.4.3 Comparison with field data and the energy based method for linear elastic soil

Russo (2004) reported a test on a steel pile of 0.1 m diameter and 19 m length, installed in multilayered soil in Naples, Italy. The elastic modulus of the pile was 27 GPa, the soil

thickness of the first layer was 12 m and the Young's modulus was 50 MPa. The second layer thickness was 9m and the Young's modulus was 117 MPa. The Poisson's ratio for both layers was 0.3 and the elastic modulus of the pile was 27 GPa (see Figure 5.13). A series of loads were applied to the top of the pile.

Figure 5.14 compares the energy-based method with the field data. A comparison with the linear elastic solution of Salgado et al. (2007) is also shown in this figure. In the energy-based method, the soil stiffness is modelled as a function of strain using the power law of Equation 5.13. This figure illustrates clearly the superiority of the new energy-based method to the elastic methods which are widely used in practice. The predictions of the simple energy-based method fit well with the field data.

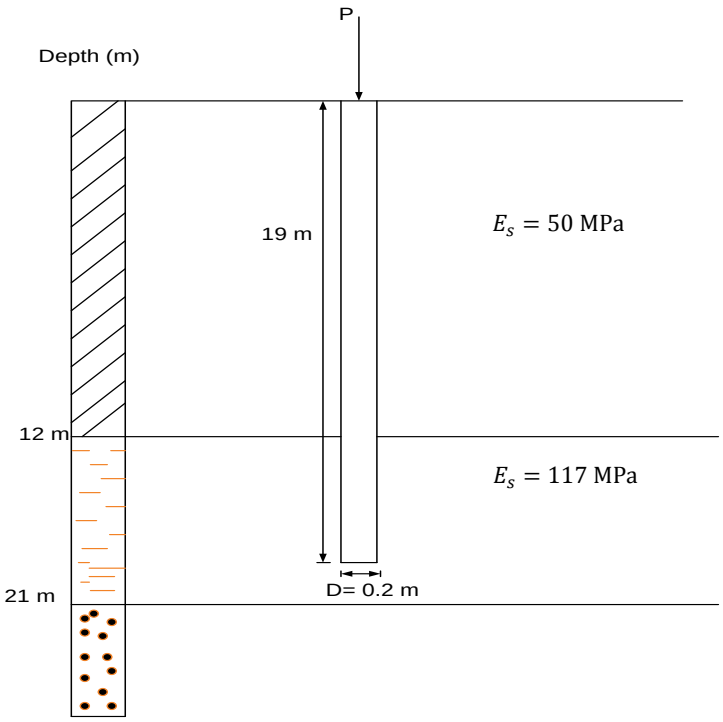

Figure 5.13: Cross-section area of the site

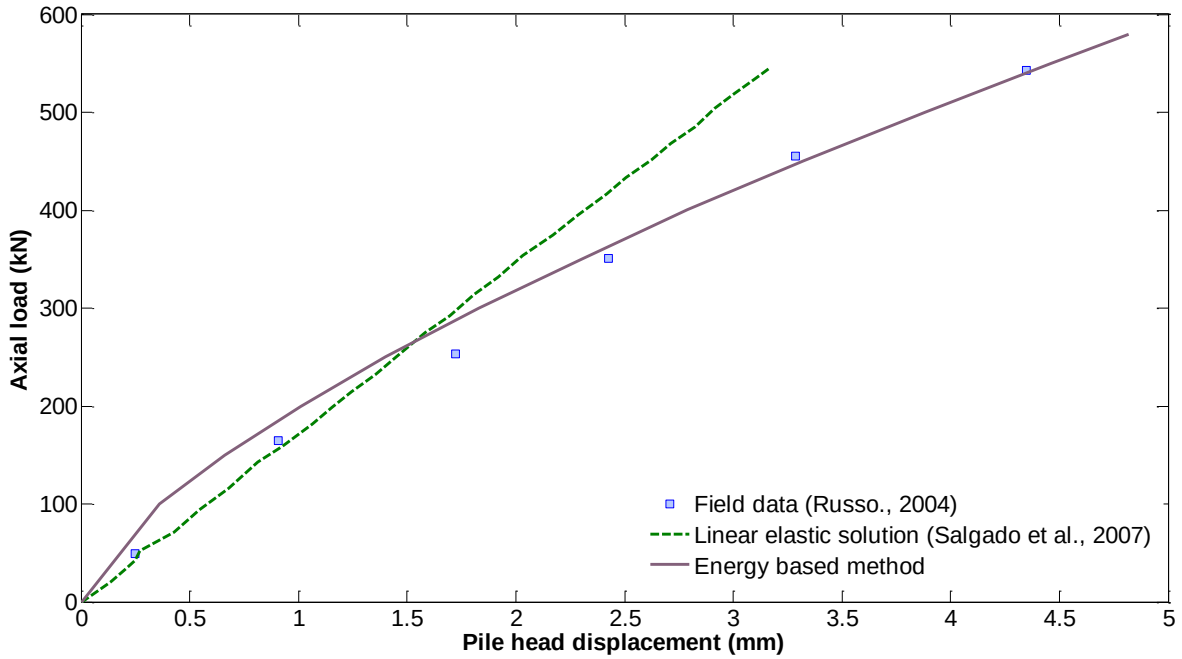

Figure 5.14: Response of the pile due to axial load

5.4.4 McCabe and Lehane pile test (2006)

McCabe and Lehane (2006) investigated a single pile and group of piles embedded in a site located 10 km north east of Belfast city centre in Northern Ireland and 2 km south east of Hollywood village. Figures 5.15 and 5.17 show a location map and the classification of the geology. Triaxial and odometer tests were made to estimate soil stiffness, water content, and undrained shear stress, which varied with depth (Figure 5.16).

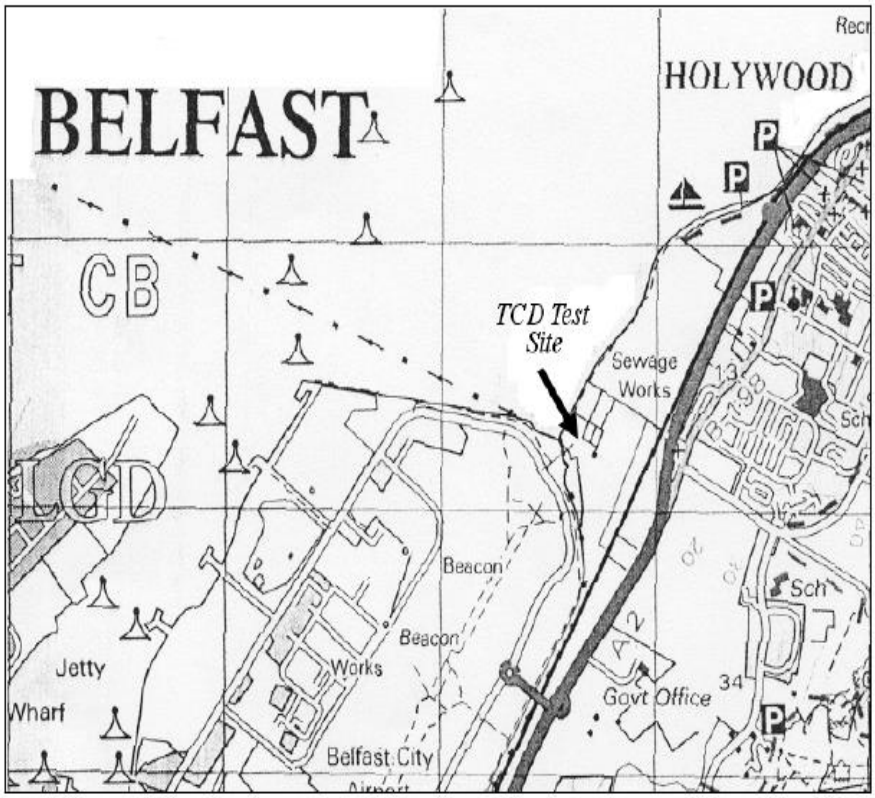

Figure 5.15: Site location map (from McCabe and Lehane (2006) & Lehan et al.(2003))

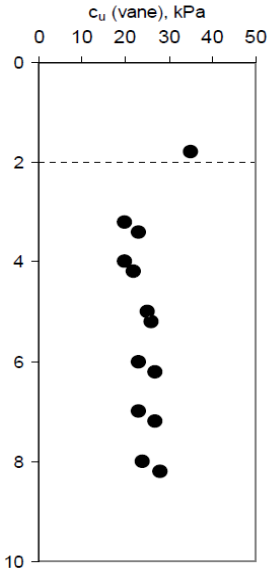

Figure 5.16: Undrained shear stress(from McCabe and Lehane (2006) & Lehan et al.(2003))

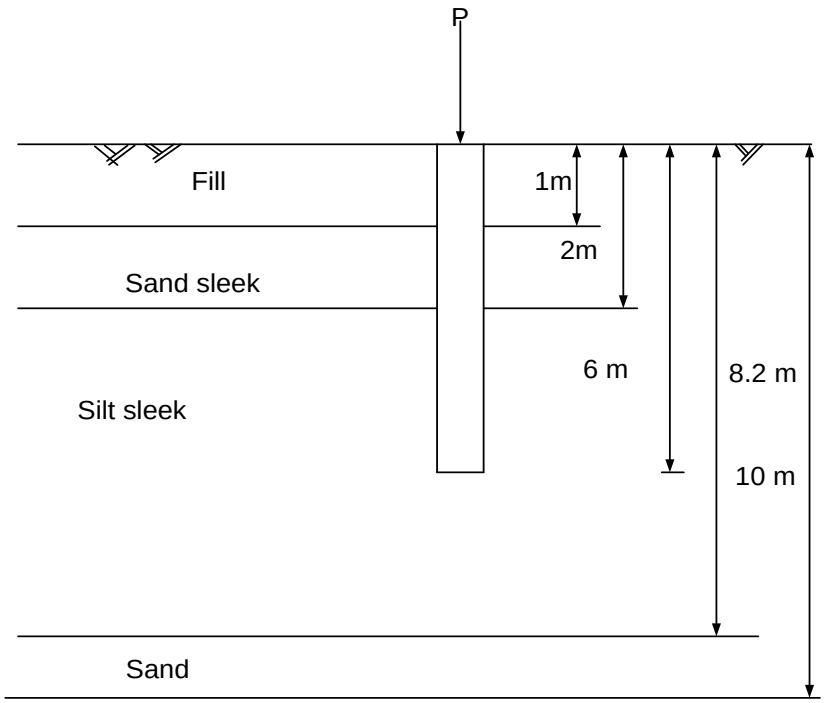

Figure 5.17: Cross section area of the pile

Three piles were tested as a group and a single pile acted by an axial static load. The cross section of the pile was square with a width of 250 mm and a pile length of 6 m. A square pile was treated as a circular pile of an equivalent area. These piles were embedded in multilayer soil. The initial soil stiffness was calculated using undrained shear strength (Lehane et al., 2003). Figure 5.18 the energy-based method overpredict the vertical displacements at high loads (i.e. 60- 70kN). This is might be due to the simple nonlinear elastic power law which is used to model the soil. This model does not account for plasticity at small strain .

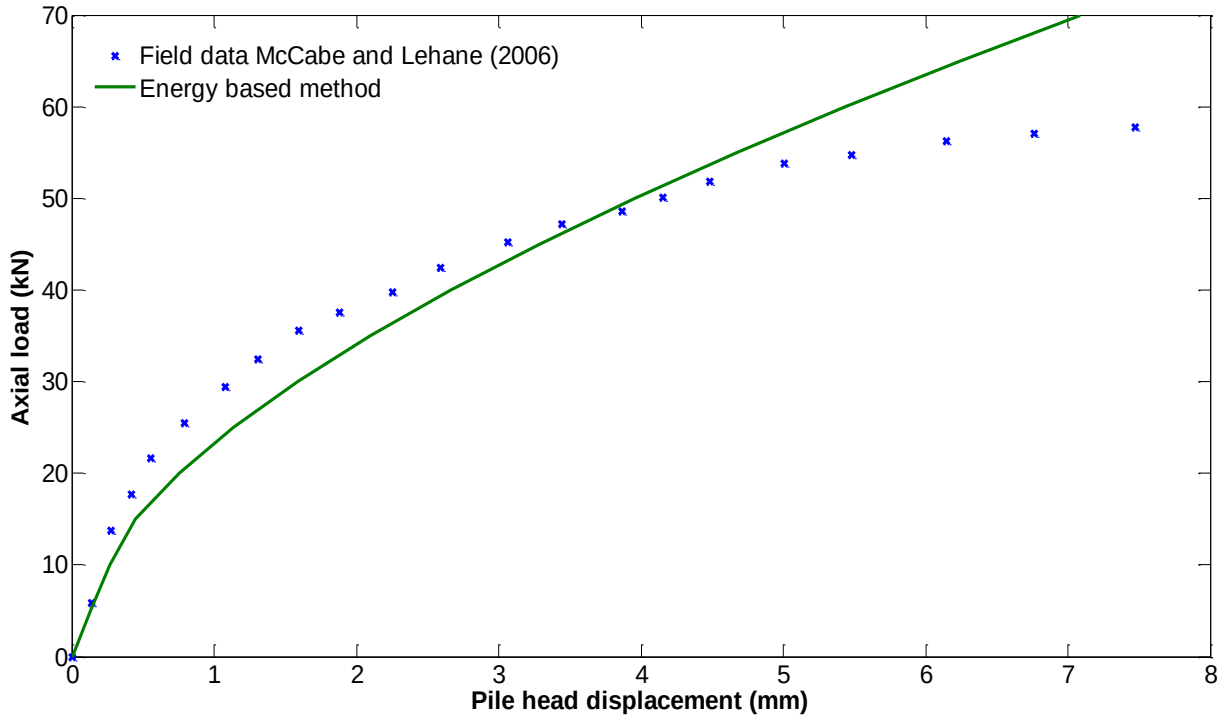

Figure 5.18: Pile head displacement

5.5 Comparison with finite element analysis

A nonlinear finite element analysis was also carried out using ABAQUS software to predict the deformation of an axially loaded pile. Tresca yield criterion with strain hardening function was adopted in the analysis, and in this study the pile was assumed to be perfectly rough, so the soil and the pile are taken to be fully connected. The size of the finite element model is 15D and 20D depth, the pile diameter is 0.5 m and 20 m length, and the mesh comprises 16108 hexahedral elements and 72807 nodes (Figure 5.19). The initial soil stiffness is $G_0$13 MPa. The hardening function was chosen so that the stress-strain curve in a simulated triaxial compression test is governed by Equation 2.62 where q is the deviatoric stress and ε_q is deviatoric strain, a and n are constants. The values of the constants were taken as $a = 100$, and $n = 0.5$. The same pile geometry and soil properties were inserted into the analytical solution. Figure 5.20 shows the good fit between the finite element analysis and the energy-based method for the case of a pile under pure vertical load. A good fit was also observed for the case of purely horizontal load (Figure 5.22).

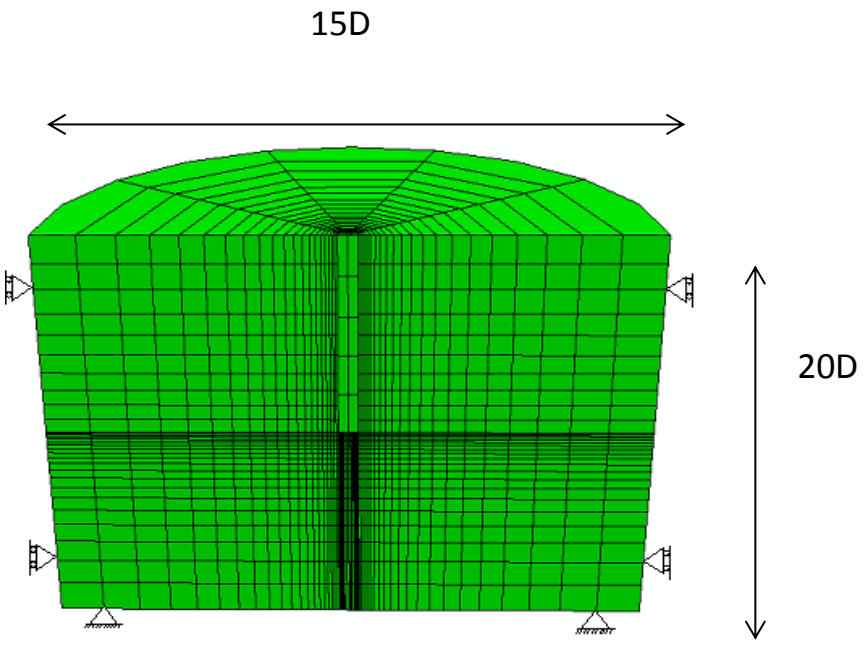

Figure 5.19: Finite element mesh

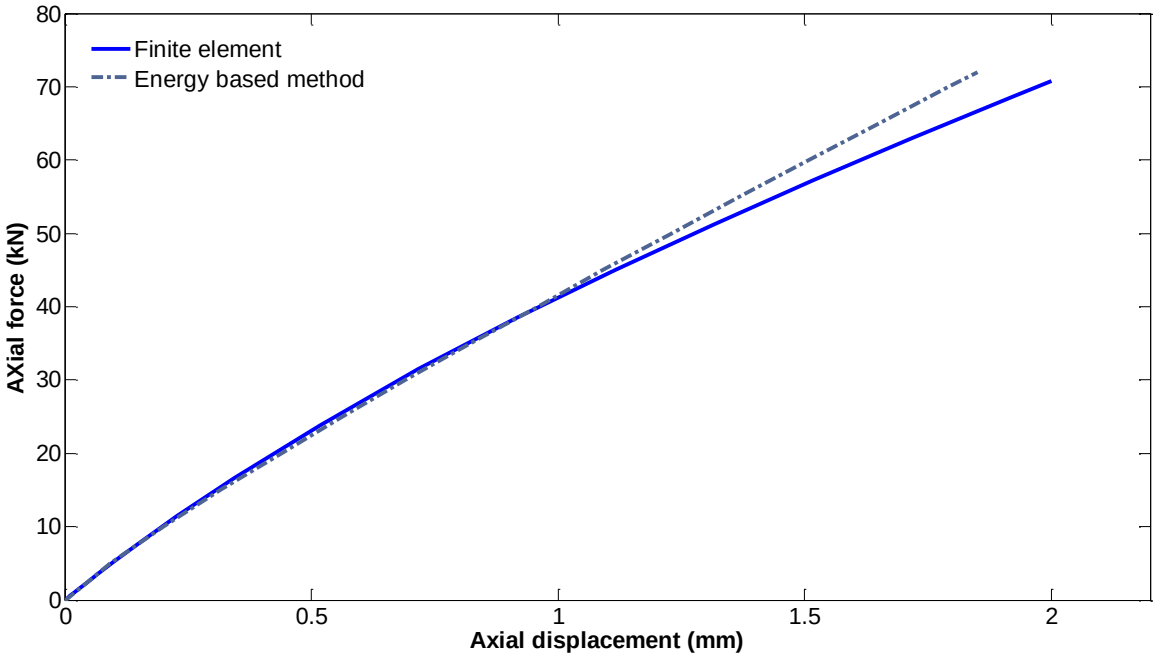

Figure 5.20: Pile deflection resulting from numerical analysis

5.6 The response of a pile subjected to combined load

To predict the deformation of pile embedded in nonlinear elastic soil subjected to combined loads, an axial load is assumed to be applied first, then a lateral load is applied. This is typical in the installation of offshore foundations (e.g. foundations of wind turbines), which are initially subjected to self-weight before exposure to wind, wave and other lateral loads.

5.6.1 Comparison with finite element analysis

Finite element modelling was carried out to simulate the response of piles subjected first to vertical load followed by a horizontal load. The same finite element model used in Section 5.5 was used with the pile is subjected first to a vertical load of 80 kN, then followed by a lateral load (50kN). Figure 5.21 shows the comparison between the finite element analysis and the energy based method for pile under lateral. As can be seen in Figure 5.22, the energy-based method is capable of replicating the pile response under combined vertical and horizontal loads.

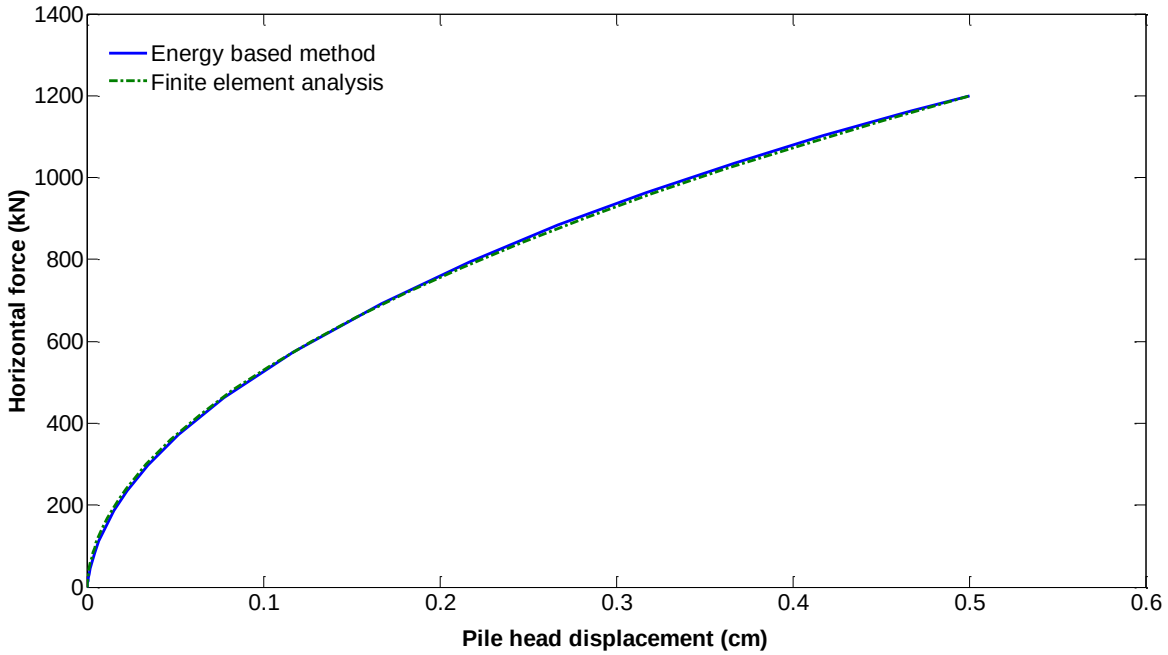

Figure 5.21: Lateral pile displacement resulting from numerical analysis and energy method

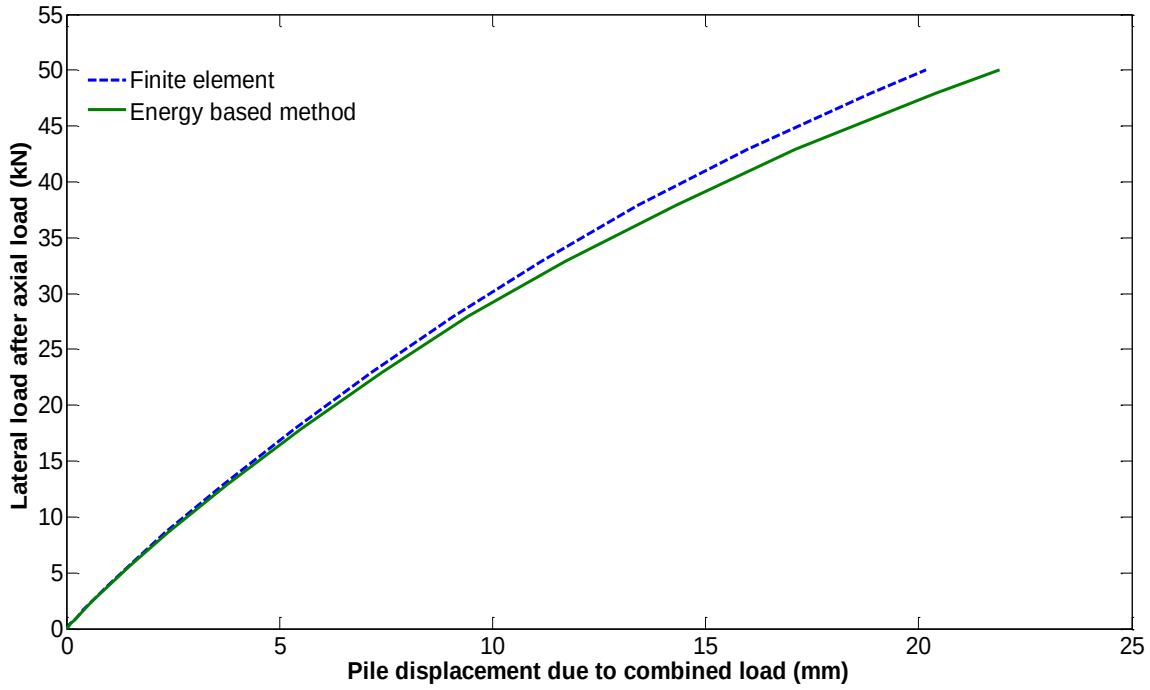

Figure 5.22: Pile displacement due to combined load

5.6.2 Comparison with field data

In order to further validate the energy method for combined loads, comparison is now made with field data. Phillips and Lehane (2004) carried out field trials on a pile in a site located on the outskirts of Belfast city. A reinforced concrete pile, 10 m length and 350 mm square, was cast in multilayered soil. Very stiff fill was located 1 m below ground level, a layer of sand sleech with a thickness of 1 m was located under the first layer, 6.5m of silt sleech lay over the sand, and the average undrained shear stress was 20 kPa. Figure 5.23 shows pile displacement due to pure lateral loads. This figure also shows a comparison between the field data reported by Phillips and Lehane and the analytical solution based on the energy method, the result shows good agreement with field data.

Figure 5.24 shows deformation of the pile due to combined loads. The load is applied in two steps: axial load is applied firstly followed by a horizontal load. This figure shows the results for the second step of loading. In this figure, the prediction of the analytical solution is compared with the field data of Phillips and Lehane (2004). At small loads 0-30kN, both the proposed solution and field data shows almost the same deformation. However, the analytical

solution slightly overestimates the displacements at loads between 25kN-65kN and underestimates the displacement at loads between 65kN-75kN compared with the energy based method.

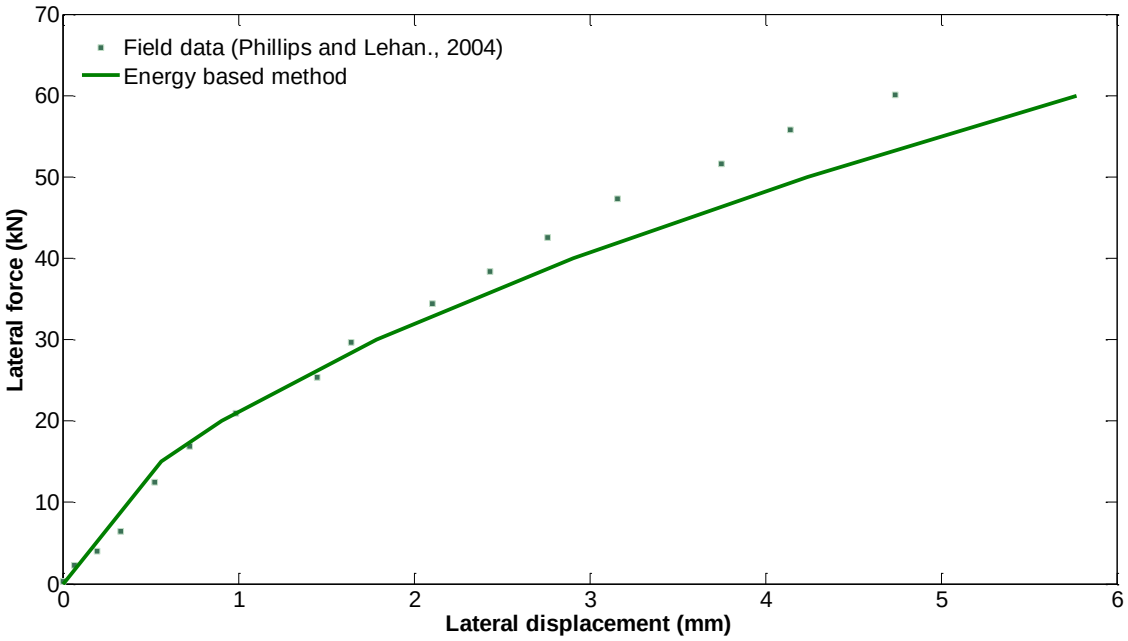

Figure 5.23: Response of the pile

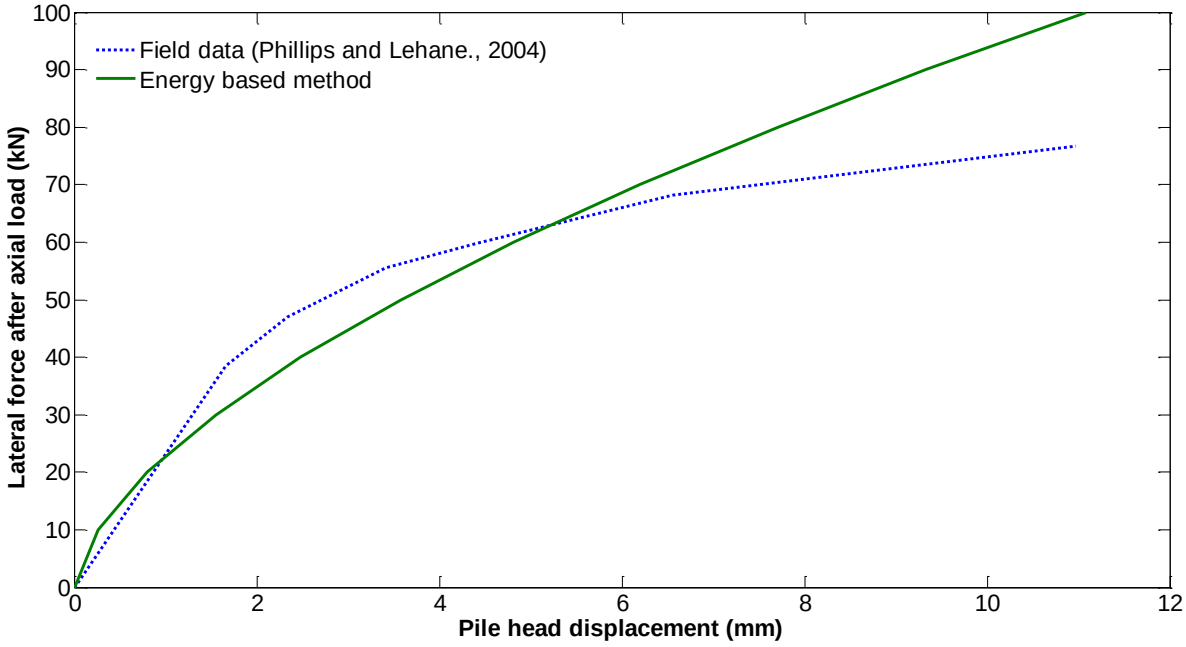

Figure 5.24: Pile deflection due to combined loads

5.7 Summary

- The energy-based method has been extended to axially loaded piles and to piles under combined loading.

- Comparison with field data and finite element analysis demonstrates the success of the proposed energy-based method in predicting pile displacements.

5.8 Appendix

A laterally loaded pile is embedded in homogenous soil. The pile is clamped and the elastic parameters $(G(r,\theta),\lambda(r,\theta))$ vary in three directions. The governing equation has been solved using the finite difference method. To obtain an accurate result C and k will be calculated for different depths and the depth will be divided by nodes i in the z direction. The total nodes are n the length between nodes (Δz). The governing equation will be determined for each node, C and k calculate in the middle between two nodes. The central difference method has been used to combine 2 boundary conditions equations in one line in the matrix. In this thesis, the soil is homogeneous but because of soil nonlinearity the soil will be divided into layers. The stiffness and the displacement for each layer will be determined. In other words if the thickness of the layer is 1m, the displacement will be calculated for each 1 cm along the pile.

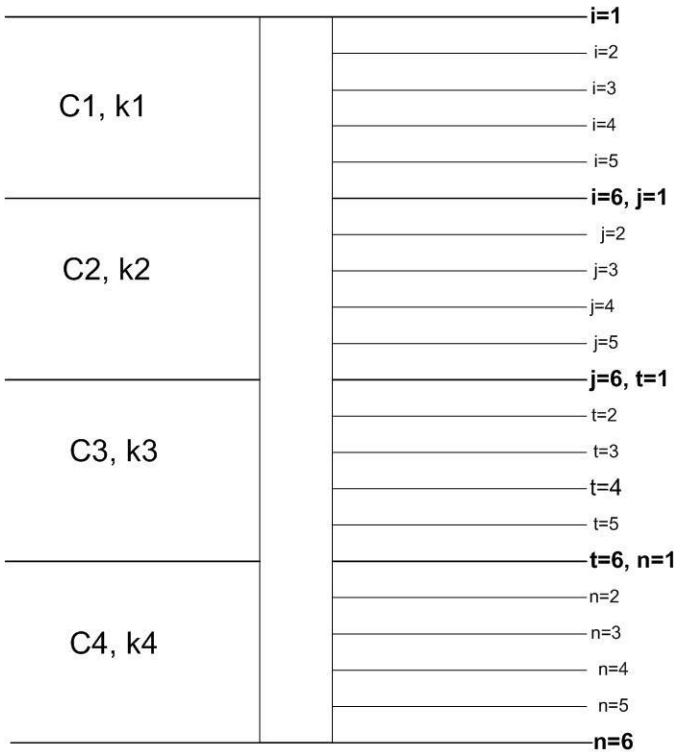

This method has been used for pile loaded laterally and axially, so we assume the displacement as *(u)* .

The governing equation

$$E_P I_P \frac{d^4u}{dz^4} - C\frac{d^2u}{dz^2} + ku = 0 \quad (5.14)$$

The boundary conditions at $i = 1$ and $z = 0$ are

$$E_P I_P \frac{d^2u}{dz^2} + M_0 = 0 \quad (5.15)$$

$$E_P I_P \frac{d^3u}{dz^3} - C\frac{du}{dz} = Q_0 \quad (5.16)$$

Both boundary conditions were used to find out $u_0\ and\ u_{-1}$ then inserting them into Governing equation at $i = 1$.

Equation 5.15 becomes

$$E_p I_p \left[\frac{u_0 - 2u_1 + u_2}{\Delta z^2}\right] = -M_0 \quad (5.17)$$

From equation 5.17

$$u_0 = \frac{-M_0 \Delta z^2}{E_p I_p} + 2u_1 - u_2 \quad (5.18)$$

Equation 5.16 becomes

$$E_p I_p \left[\frac{-u_{-1} + 2u_0 - 2u_2 + u_3}{2\Delta z^3}\right] - C\left[\frac{-u_0 + u_2}{2\Delta z}\right] = Q_0 \quad (5.19)$$

From equation 5.19 by inserting u_0 We can obtain u_{-1}

$A = E_p I_p$

$$\frac{d^2u}{dz^2} = \frac{u_0 - 2u_1 + u_2}{dz^2}$$

$$A\frac{d^2u}{dz^2} = -M_0$$

$$A\left(\frac{u_0 - 2u_1 + u_2}{dz^2}\right) = -M_0$$

$$u_0 = \frac{-M_0 dz^2}{A} + 2u_1 - u_2$$

$$\frac{du}{dz} = \frac{-u_0 + u_2}{2dz}$$

$$\frac{d^3u}{dz^3} = \frac{-u_{-1} + 2u_0 - 2u_2 + u_3}{2dz^3}$$

$$\frac{d^3u}{dz^3} = \frac{-u_{-1} + 2\left[\frac{-M_0 dz^2}{A} + 2u_1 - u_2\right] - 2u_2 + u_3}{2dz^3}$$

$$A\frac{d^3u}{dz^3} - C\frac{du}{dz} = Q$$

$$A\left(\frac{-u_{-1} + \frac{-2M_0 dz^2}{A} + 4u_1 - 4u_2 + u_3}{2dz^3}\right) - C_1\left(\frac{-u_0 + u_2}{2dz}\right) = Q$$

$$A\left(\frac{-u_{-1} + \frac{-2M_0 dz^2}{A} + 4u_1 - 4u_2 + u_3}{2dz^3}\right) = C_1\left(\frac{\frac{M_0 dz^2}{A} - 2u_1 + 2u_2}{2dz}\right) + Q$$

$$\left(-u_{-1} + \frac{-2M_0 dz^2}{A} + 4u_1 - 4u_2 + u_3\right) = \frac{2dz^3}{A}\left[C_1\left(\frac{\frac{M_0 dz^2}{A} - 2u_1 + 2u_2}{2dz}\right) + Q\right]$$

$$u_{-1} = constant + u_1\left(\frac{2C_1 dz^2}{A} + 4\right) + u_2\left(\frac{-2C_1 dz^2}{A} - 4\right) + u_3 \qquad (5.20)$$

$$constant = -\left(\frac{2Qdz^3}{A} + \frac{C_1 dz^4 M_0}{A^2} + \frac{2dz^2 M_0}{A}\right)$$

When $i = 1$

$$A\frac{d^4u}{dz^4} - C_1\frac{d^2u}{dz^2} + ku = 0$$

$$\frac{d^4u}{dz^4} = \frac{u_{-1} - 4u_0 + 6u_1 - 4u_2 + u_3}{dz^4}$$

$$\frac{A}{dz^4}\left(constant + u_1\left(\frac{2C_1dz^2}{A} + 4\right) + u_2\left(\frac{-2C_1dz^2}{A} - 4\right) + u_3 - 4\left[\frac{-M_0dz^2}{A} + 2u_1 - u_2\right] + 6u_1 - 4u_2 + u_3\right) + C_1\frac{M_0}{A} + ku_1 = 0$$

$$u_1\left(\frac{2A}{dz^4} + \frac{2C_1}{dz^2} + k\right) + u_2\left(\frac{-4A}{dz^4} - \frac{2C_1}{dz^2}\right) + u_3\left(\frac{2A}{dz^4}\right) = \frac{2Q_0}{dz} - \frac{2M_0}{dz^2} \qquad (5.21a)$$

When $i = 2$

$$A\frac{d^4u}{dz^4} - C_1\frac{d^2u}{dz^2} + ku = 0$$

$$\frac{d^4u}{dz^4} = \frac{u_0 - 4u_1 + 6u_2 - 4u_3 + u_4}{dz^4}$$

$$\frac{d^4u}{dz^4} = \frac{\frac{-M_0dz^2}{A} - 2u_1 + 5u_2 - 4u_3 + u_4}{dz^4}$$

$$\frac{d^2u}{dz^2} = \frac{u_1 - 2u_2 + u_3}{dz^2}$$

$$u_1\left(\frac{-2A}{dz^4} - \frac{C_1}{dz^2}\right) + u_2\left(\frac{5A}{dz^4} + \frac{2C_1}{dz^2} + k_1\right) + u_3\left(\frac{-4A}{dz^4} - \frac{C_1}{dz^2}\right) + u_4\left(\frac{A}{dz^4}\right) = \frac{M_0}{dz^2} \qquad (5.21b)$$

When $i = 3$

$$A\frac{d^4u}{dz^4} - C_1\frac{d^2u}{dz^2} + ku = 0$$

$$\frac{d^4u}{dz^4} = \frac{u_1 - 4u_2 + 6u_3 - 4u_4 + u_5}{dz^4}$$

$$\frac{d^2u}{dz^2} = \frac{u_2 - 2u_3 + u_4}{dz^2}$$

$$u_1\left(\frac{A}{dz^4}\right) + u_2\left(\frac{-4A}{dz^4} - \frac{C_1}{dz^2}\right) + u_3\left(\frac{6A}{dz^4} + \frac{2C_1}{dz^2} + k_1\right) + u_4\left(\frac{-4A}{dz^4} - \frac{C_1}{dz^2}\right) + u_5\left(\frac{A}{dz^4}\right) = 0 \qquad (5.21c)$$

When $i = 4$

$$A\frac{d^4u}{dz^4} - C_1\frac{d^2u}{dz^2} + ku = 0$$

$$\frac{d^4u}{dz^4} = \frac{u_2 - 4u_3 + 6u_4 - 4u_5 + u_6}{dz^4}$$

$$\frac{d^2u}{dz^2} = \frac{u_3 - 2u_4 + u_5}{dz^2}$$

$$u_2\left(\frac{A}{dz^4}\right) + u_3\left(\frac{-4A}{dz^4} - \frac{C_1}{dz^2}\right) + u_4\left(\frac{6A}{dz^4} + \frac{2C_1}{dz^2} + k_1\right) + u_5\left(\frac{-4A}{dz^4} - \frac{C_1}{dz^2}\right) + u_6\left(\frac{A}{dz^4}\right) = 0 \qquad (5.21d)$$

When $i = 5$

$$A\frac{d^4u}{dz^4} - C_1\frac{d^2u}{dz^2} + ku = 0$$

$$\frac{d^4u}{dz^4} = \frac{u_3 - 4u_4 + 6u_5 - 4u_6 + g_2}{dz^4}$$

$$\frac{d^2u}{dz^2} = \frac{u_4 - 2u_5 + u_6}{dz^2}$$

$$A\frac{d^4u}{dz^4} - C_1\frac{d^2u}{dz^2} + ku = 0$$

$$\frac{d^4u}{dz^4} = \frac{u_3 - 4u_4 + 6u_5 - 4u_6 + g_2}{dz^4}$$

$$\frac{d^2u}{dz^2} = \frac{u_4 - 2u_5 + u_6}{dz^2}$$

$$u_3\left(\frac{A}{dz^4}\right) + u_4\left(\frac{-4A}{dz^4} - \frac{C_1}{dz^2}\right) + u_5\left(\frac{6A}{dz^4} + \frac{2C_1}{dz^2} + k\right) + u_6\left(\frac{-4A}{dz^4} - \frac{C_1}{dz^2}\right) + g_2\left(\frac{A}{dz^4}\right) = 0 \qquad (5.21e)$$

When $i = 6,\ j = 1$

$$u_6 - g_1 = 0 \qquad (5.22a)$$

When $j = 2$

$$A\frac{d^2g}{dz^2} - C_2\frac{d^2g}{dz^2} + k_1g = 0$$

$$A\left(\frac{u_5 - 4g_1 + 6g_2 - 4g_3 + g_4}{dz^4}\right) - C_2\left(\frac{g_1 - 2g_2 + g_3}{dz^2}\right) + k_2g_2 = 0$$

$$u_5\left(\frac{A}{dz^4}\right) + g_1\left(\frac{-4A}{dz^4} - \frac{C_2}{dz^2}\right) + g_2\left(\frac{6A}{dz^4} + \frac{2C_2}{dz^2} + k_2\right) + g_3\left(\frac{-4A}{dz^4} - \frac{C_2}{dz^2}\right) + g_4\left(\frac{A}{dz^4}\right) = 0 \qquad (5.22b)$$

When $j = 3$

$$g_1\left(\frac{A}{dz^4}\right) + g_2\left(\frac{-4A}{dz^4} - \frac{C_2}{dz^2}\right) + g_3\left(\frac{6A}{dz^4} + \frac{2C_2}{dz^2} + k_2\right) + g_4\left(\frac{-4A}{dz^4} - \frac{C_2}{dz^2}\right) + g_5\left(\frac{A}{dz^4}\right) = 0 \qquad (5.22c)$$

When $j = 4$

$$g_2\left(\frac{A}{dz^4}\right) + g_3\left(\frac{-4A}{dz^4} - \frac{C_2}{dz^2}\right) + g_4\left(\frac{6A}{dz^4} + \frac{2C_2}{dz^2} + k_2\right) + g_5\left(\frac{-4A}{dz^4} - \frac{C_2}{dz^2}\right) + g_6\left(\frac{A}{dz^4}\right) = 0 \quad (5.22d)$$

When $j = 5$

$$g_3\left(\frac{A}{dz^4}\right) + g_4\left(\frac{-4A}{dz^4} - \frac{C_2}{dz^2}\right) + g_5\left(\frac{6A}{dz^4} + \frac{2C_2}{dz^2} + k_2\right) + g_6\left(\frac{-4A}{dz^4} - \frac{C_2}{dz^2}\right) + f_2\left(\frac{A}{dz^4}\right) = 0 \quad (2.22e)$$

When $j = 6, n = 1$

$$g_6 - f_1 = 0 \quad (5.23a)$$

When $n = 2$

$$g_5\left(\frac{A}{dz^4}\right) + f_1\left(\frac{-4A}{dz^4} - \frac{C_3}{dz^2}\right) + f_2\left(\frac{6A}{dz^4} + \frac{2C_3}{dz^2} + k_3\right) + f_3\left(\frac{-4A}{dz^4} - \frac{C_3}{dz^2}\right) + f_4\left(\frac{A}{dz^4}\right) = 0 \quad (5.23b)$$

When $n = 3$

$$f_1\left(\frac{A}{dz^4}\right) + f_2\left(\frac{-4A}{dz^4} - \frac{C_3}{dz^2}\right) + f_3\left(\frac{6A}{dz^4} + \frac{2C_3}{dz^2} + k_3\right) + f_4\left(\frac{-4A}{dz^4} - \frac{C_3}{dz^2}\right) + f_5\left(\frac{A}{dz^4}\right) = 0 \quad (5.23c)$$

When $n = 4$

$$f_2\left(\frac{A}{dz^4}\right) + f_3\left(\frac{-4A}{dz^4} - \frac{C_3}{dz^2}\right) + f_4\left(\frac{6A}{dz^4} + \frac{2C_3}{dz^2} + k_3\right) + f_5\left(\frac{-4A}{dz^4} - \frac{C_3}{dz^2}\right) + f_6\left(\frac{A}{dz^4}\right) = 0 \quad (5.23d)$$

When $n = 5$

$$f_3\left(\frac{A}{dz^4}\right)+f_4\left(\frac{-4A}{dz^4}-\frac{C_3}{dz^2}\right)+f_5\left(\frac{6A}{dz^4}+\frac{2C_3}{dz^2}+k_3\right)+f_6\left(\frac{-4A}{dz^4}-\frac{C_3}{dz^2}\right)+t_2\left(\frac{A}{dz^4}\right)=0 \quad (5.23e)$$

When $n=6, m=1$

$$f_6-t_1=0 \quad (5.24a)$$

$m=2$

$$f_5\left(\frac{A}{dz^4}\right)+t_1\left(\frac{-4A}{dz^4}-\frac{C_4}{dz^2}\right)+t_2\left(\frac{6A}{dz^4}+\frac{2C_4}{dz^2}+k_4\right)+t_3\left(\frac{-4A}{dz^4}-\frac{C_4}{dz^2}\right)+t_4\left(\frac{A}{dz^4}\right)=0 \quad (5.24b)$$

$m=3$

$$t_1\left(\frac{A}{dz^4}\right)+t_2\left(\frac{-4A}{dz^4}-\frac{C_4}{dz^2}\right)+t_3\left(\frac{6A}{dz^4}+\frac{2C_4}{dz^2}+k_4\right)+t_4\left(\frac{-4A}{dz^4}-\frac{C_4}{dz^2}\right)+t_5\left(\frac{A}{dz^4}\right)=0 \quad (5.24c)$$

$m=4$

$$t_2\left(\frac{A}{dz^4}\right)+t_3\left(\frac{-4A}{dz^4}-\frac{C_4}{dz^2}\right)+t_4\left(\frac{6A}{dz^4}+\frac{2C_4}{dz^2}+k_4\right)+t_5\left(\frac{-4A}{dz^4}-\frac{C_4}{dz^2}\right)+t_6\left(\frac{A}{dz^4}\right)=0 \quad (5.24d)$$

$m=5$

$$t_3\left(\frac{A}{dz^4}\right)+t_4\left(\frac{-4A}{dz^4}-\frac{C_4}{dz^2}\right)+t_5\left(\frac{5A}{dz^4}+\frac{2C_4}{dz^2}+k_4\right)+t_6\left(\frac{-2A}{dz^4}-\frac{C_4}{dz^2}\right)=0 \quad (5.24e)$$

$m=6$

$$t_6=0 \quad (5.24f)$$

6 Similarity Method

Introduction

The response of a pile under pure axial load and pure lateral load in elasto-plastic soil has been investigated using a similarity method which is based on elasticity theory. This method can provide a powerful tool which enables advanced element test data (quantifying soil non-linearity) to be used to estimate the stiffness and working displacements of a pile under combined loading. It yields a calculation method that is far quicker and simpler than numerical analysis. The technique is not intended to replace advanced numerical methods but to provide a tool which is simple enough to be used in preliminary design calculations, whilst capturing the important influence of soil non-linearity.

A similarity method was first proposed by Atkinson (2000). This method assumes that the strain of undrained soil in a triaxial test is related to ground movement, where the decay in soil stiffness with strain takes the same shape as the decay in structure stiffness with normalized displacement. Atkinson (2000) explains the calculation method that allows non-linearity to be considered in the design based on elasticity theory; a summarization can be found in Figure 6.1.

Osman et al. (2007) extended the similarity method for circular shallow foundations and derived coefficients for circular foundations subjected to vertical, horizontal and moment loads. This chapter discusses how the similarity method has been extended to estimate the response of a pile under vertical and horizontal loads.

6.1 The calculation procedure in the similarity approach

6.1.1 Similarity approach for pile

A similarity method was used based on the secant stiffness below the foundation at settlement $\frac{u}{D}$ equal to secant stiffness resulting from the triaxial test compressive strain $\frac{u}{D} = \alpha\varepsilon_q$, where u is displacement, ε_q represents the deviatoric strain, and α is the coefficient of displacement

that must be obtained. These coefficients of displacement are different according to load direction. Figure 6.1 summarizes the similarity approach.

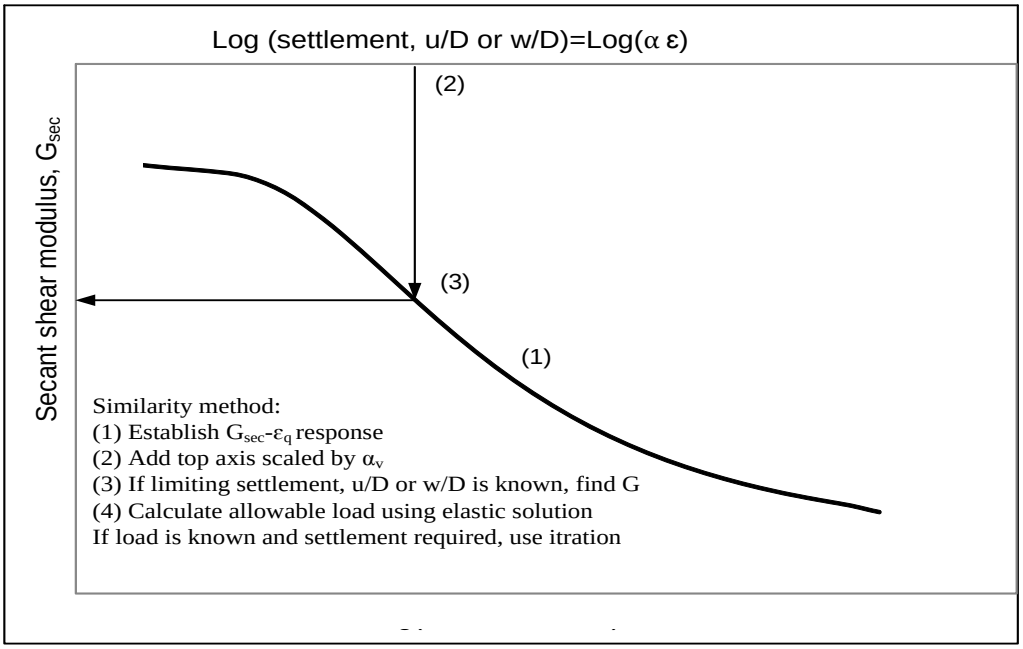

Figure 6.1: Illustration of Atkinson's method (Osman et al., 2007)

6.1.2 Similarity method for laterally loaded pile

Evaluating the load-displacement response of a laterally loaded pile using the similarity approach:

The response is obtained using the following steps:

1. The soil stress-strain data is obtained by performing a triaxial test on a representative soil sample.
2. The soil secant stiffness (G_{sec}) is calculated from the strain-stress curve:

$$G_{sec} = \frac{q}{3\varepsilon_q}$$

where q is the deviator stress and ε_q is deviatoric strain.

3. The soil secant stiffness is plotted against the deviatoric strain

4. The soil stiffness-strain curve can be converted directly into stiffness-displacement curve by scaling the x-axis (the strain axis) using a linear scaling factor α_h as follows:

$$\frac{u}{\mathrm{D}} = \alpha_h \varepsilon_q$$

where u represents lateral displacement and D is pile diameter.

5. Once the displacement is known together with the corresponding secant stiffness, the lateral load Q_0 can then be calculated from the conventional linear elastic solution for laterally loaded piles:

$$Q_0 = u\, G^* r_0 / \left(0.25\left(E_p/G^*\right)^{-1/7}\right)$$

where G^* product of $G_{sec}\,(1 + 3v/4)$ and E_p is Young's modulus of pile

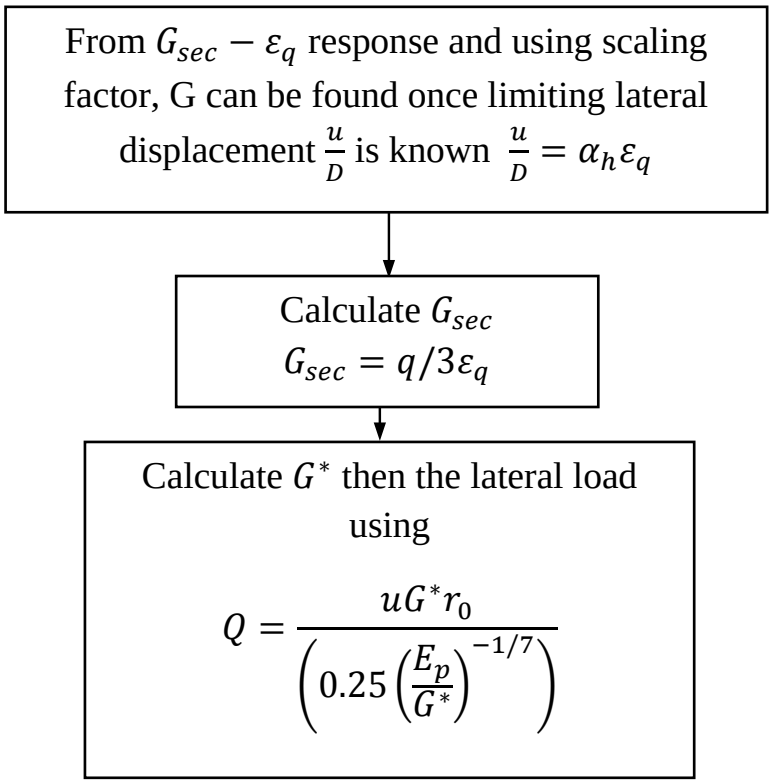

Figure 6.2: Flow chart for predicting the lateral load

6.2 Determination of the scaling parameters

In order to estimate the scaling parameters, a series of finite element analyses for axially and laterally loaded piles were carried out using ABAQUS 6.10 software (FEM). The Tresca model with strain hardening parameters was used to replicate soil nonlinearity. Figure 6.3 shows a typical response of a triaxial test using finite element software.

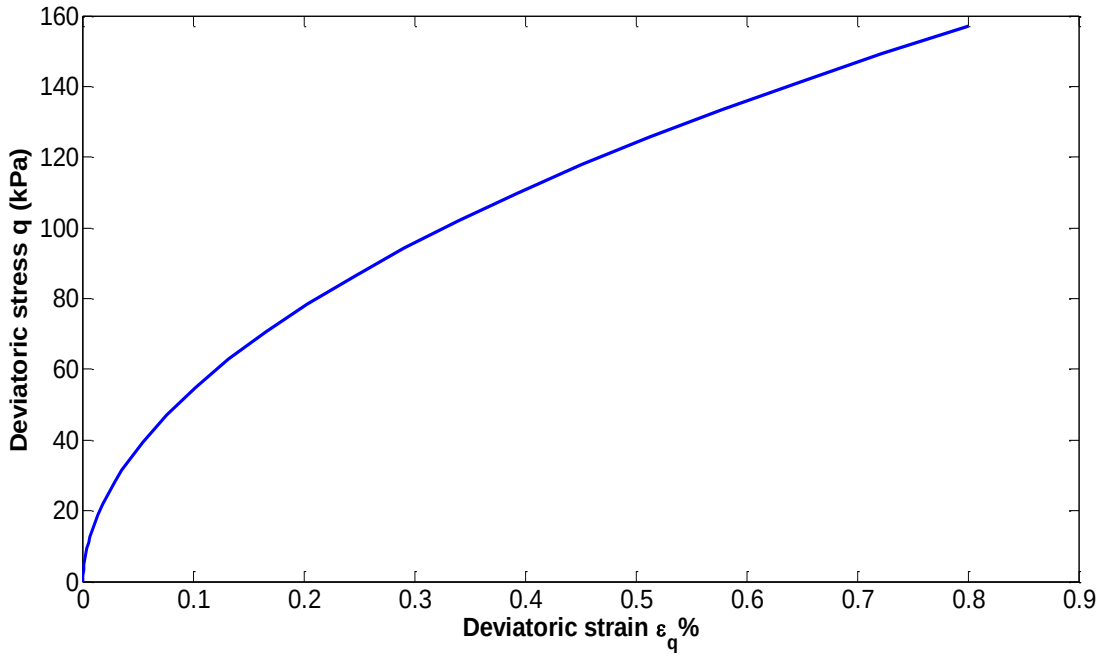

Figure 6.3: Response of triaxial test

6.2.1 Finite element mesh

Three dimensional finite element meshes were used to analyze piles with different geometries. Figure 6.4 shows the meshes with piles with different diameters *D* and lengths *L*. The dimensions, mesh depth, mesh size and element details are shown in Table 6.1. Displacement boundary conditions prevented the base of the mesh from moving. It was fixed in three directions in the flat diametrical plan on the front face and the circumference plane of the mesh prevented movement in z and x directions. The mesh was composed of second order reduced integration hexahedral elements. Smaller elements were used near the pile where the changes of stresses and strains were significant.

Table 6.1: Mesh size and element details

L/r_0	Mesh diameter	Mesh depth	Number of elements	Number of nodes	Type of elements
10	10 D	10 D	3649 354	17575	Quadratic hexahedral Quadratic wedges
20	30 D	30 D	16108	72807	Quadratic hexahedral
30	60 D	60 D	5503	25625	Quadratic hexahedral
40	40 D	40 D	9110	41210	Quadratic hexahedral

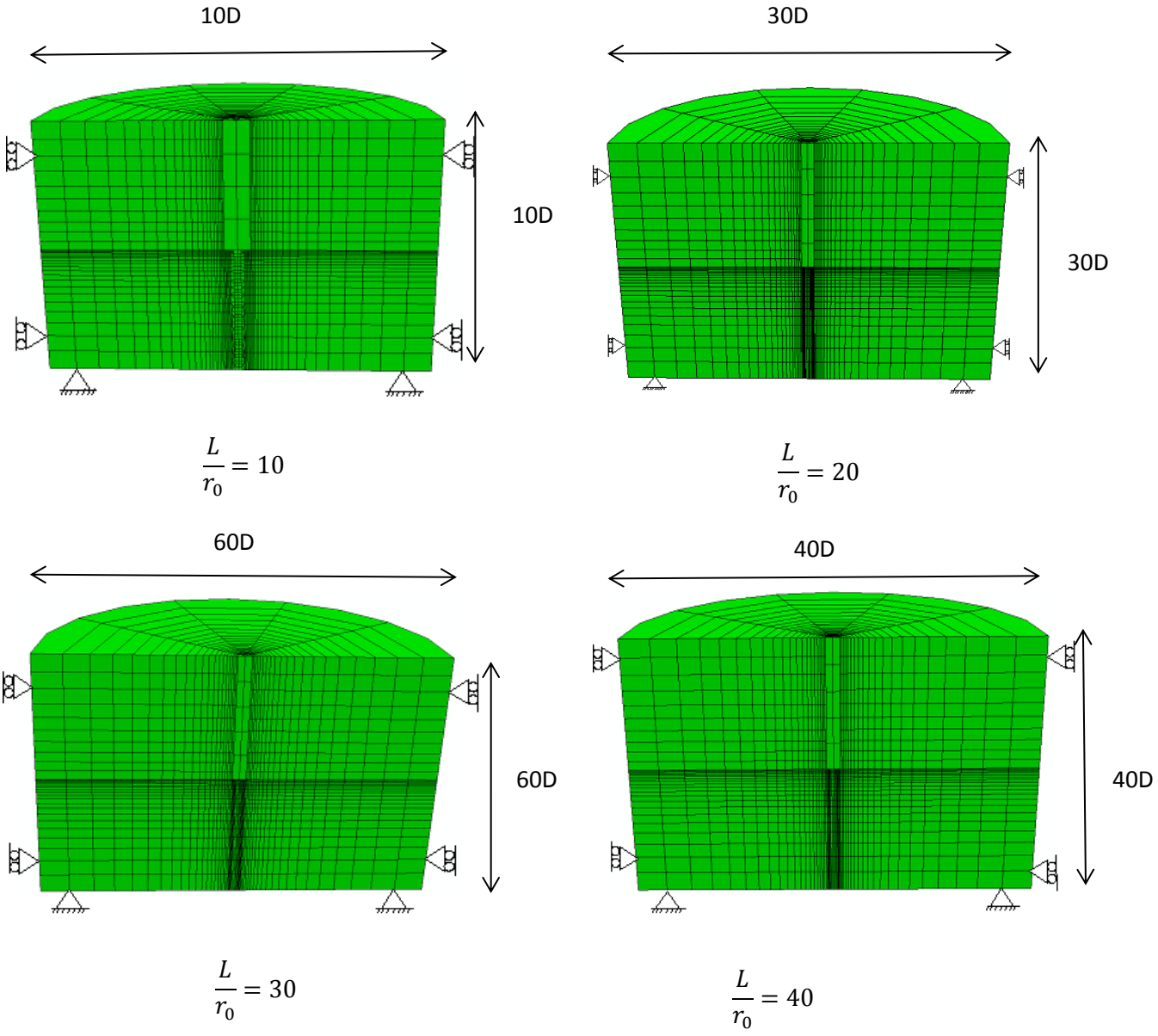

Figure 6.4: Geometries of the mesh for different pile geometries

Figures 6.5, 6.6 and 6.7 show the lateral displacement versus load obtained from finite element analysis for piles with length 10 m, 30 m and 40 m, radius 1 m, and curves calculated

using the similarity method with the stress–strain shown in Figure 6.3. These curves were obtained using different values for the scaling factor α_h. It can be seen that a scaling factor of $\alpha_h = 1$ fits better to the finite element results, as can be seen in Figure 6.8.

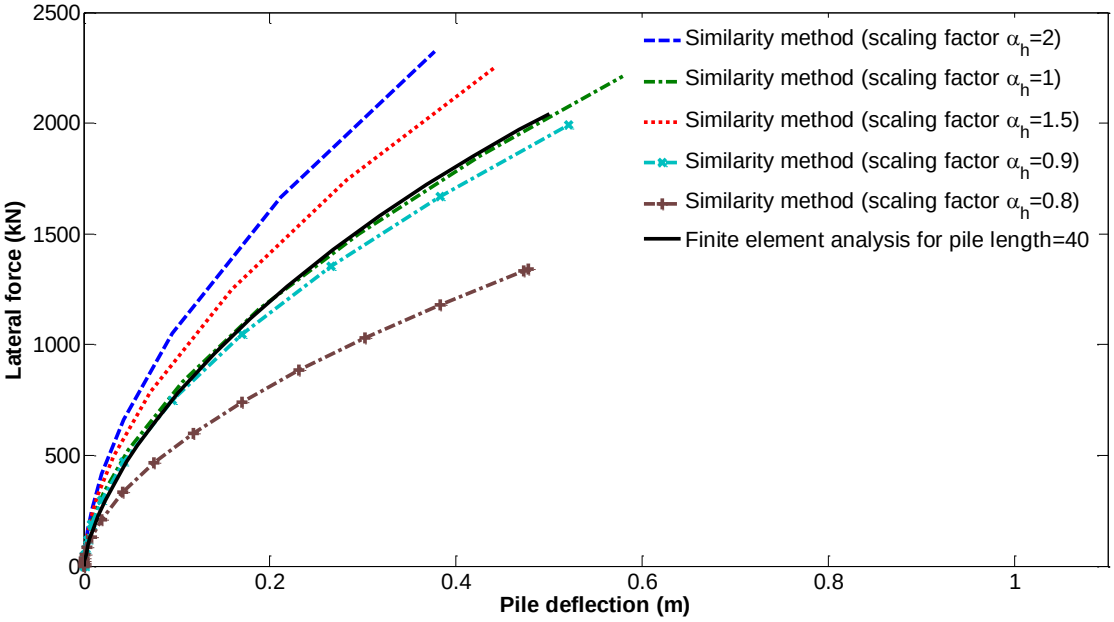

Figure 6.5: Response of laterally loaded pile with 40 m and load-displacement from triaxial test

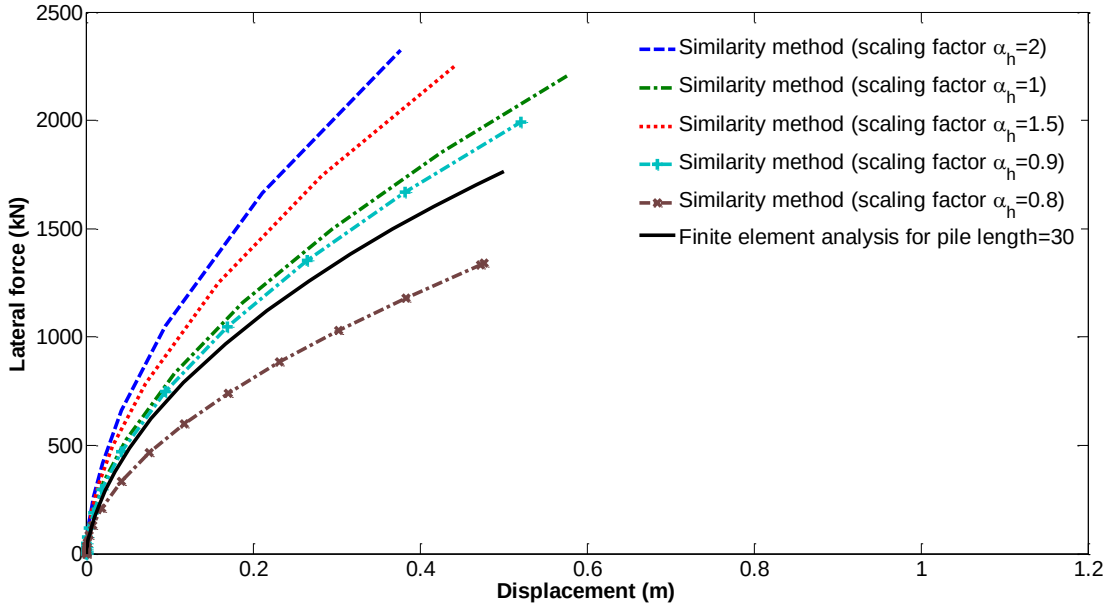

Figure 6.6: Response of laterally loaded pile with 30 m and load-displacement from triaxial test

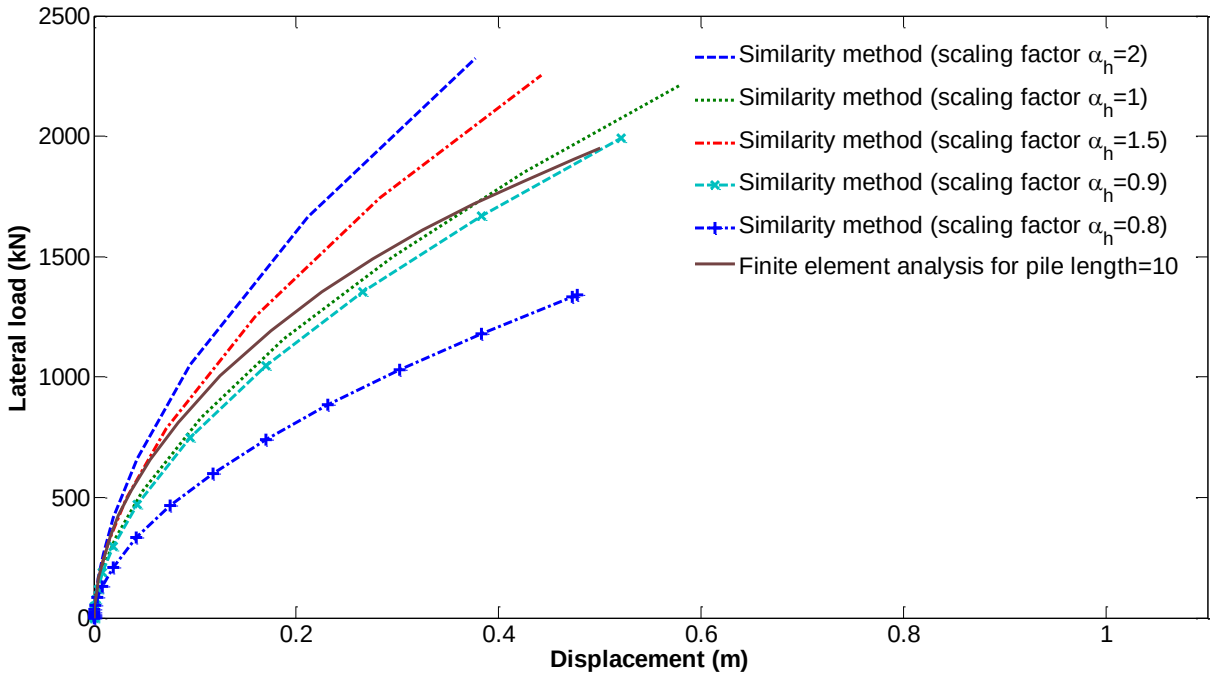

Figure 6.7: Response of laterally loaded pile with 10 m and load-displacement from triaxial test

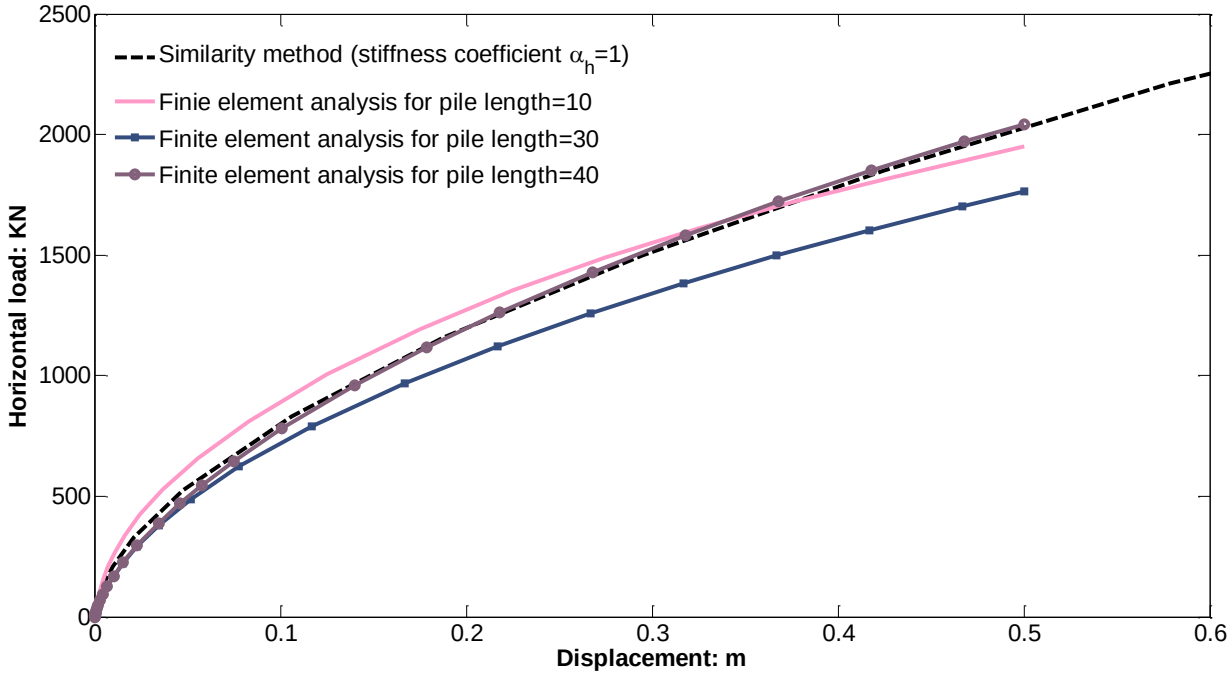

Figure 6.8: Comparison with FE analysis for laterally loaded pile

6.2.2 Similarity method for axially loaded pile

The method is performed using similar steps as laterally loaded piles. A scaling factor α_v is used to relate the deviatoric strain to the vertical displacement:

$$\frac{\mathrm{v}}{D} = \alpha_v \varepsilon_q$$

and the vertical load P_t is calculated using:

$$P_t = G_{sec}\,\mathrm{v}\left(\left(\frac{4}{\eta(1-v)}\right) + \frac{2\pi L}{\zeta r_0}\right)$$

where V represents vertical displacement, η geometric coefficient, $\zeta = ln\left(\frac{r_m}{r_0}\right)$ and r_m is the magic radius that can be calculated from $r_m = 2.5L(1-v)$. The scaling factor which gives the best fit is $\alpha_v = 0.6$

The responses of piles resulting from finite element and load-displacement derived from triaxial tests are shown in Figures 6.10, 6.11, 6.12 and 6.13 for piles with lengths of 10 m, 20 m, 30 m and 40 m, and a radius of 1 m, respectively. Regarding similarity analyses for different α_{v}, Figure 6.9 shows a flow chart that explains the similarity analyses. Figures 6.10, 6.11, 6.12 and 6.13 show the axial displacement versus load obtained from finite element analysis for piles with length 10 m, 20m, 30 m and 40 m, and a radius of 1 m. Curves calculated using the similarity method with the stress–strain response are shown in Figure 6.3. These curves were obtained using different values for the scaling factor α_{v}. It can be seen that a scaling factor of $\alpha_{\mathrm{v}} = 0.6$ fits better with to the finite element results, as can be seen in Figure 6.14.

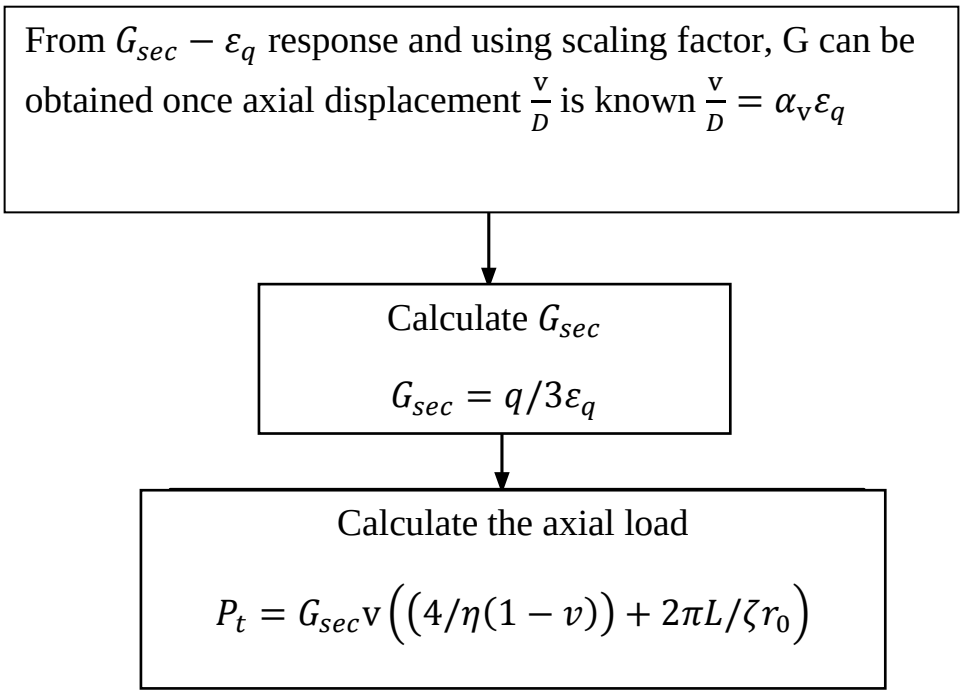

Figure 6.9: Flowchart of axially loaded pile

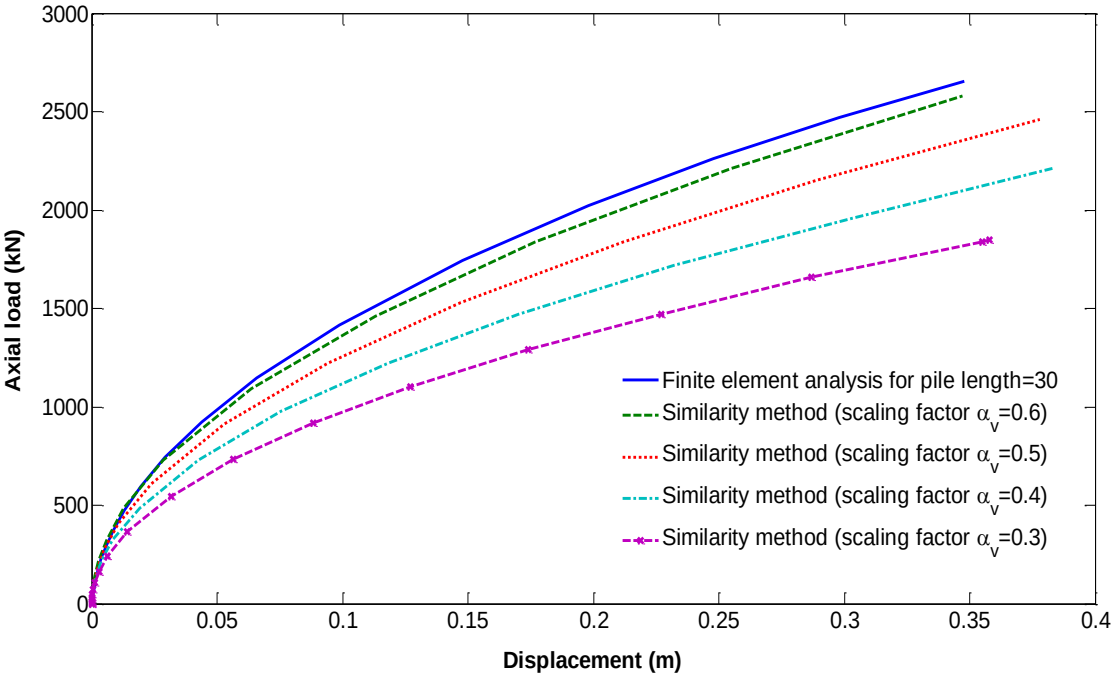

Figure 6.10: Response of axially loaded pile with length 10 m and load-displacement from triaxial test

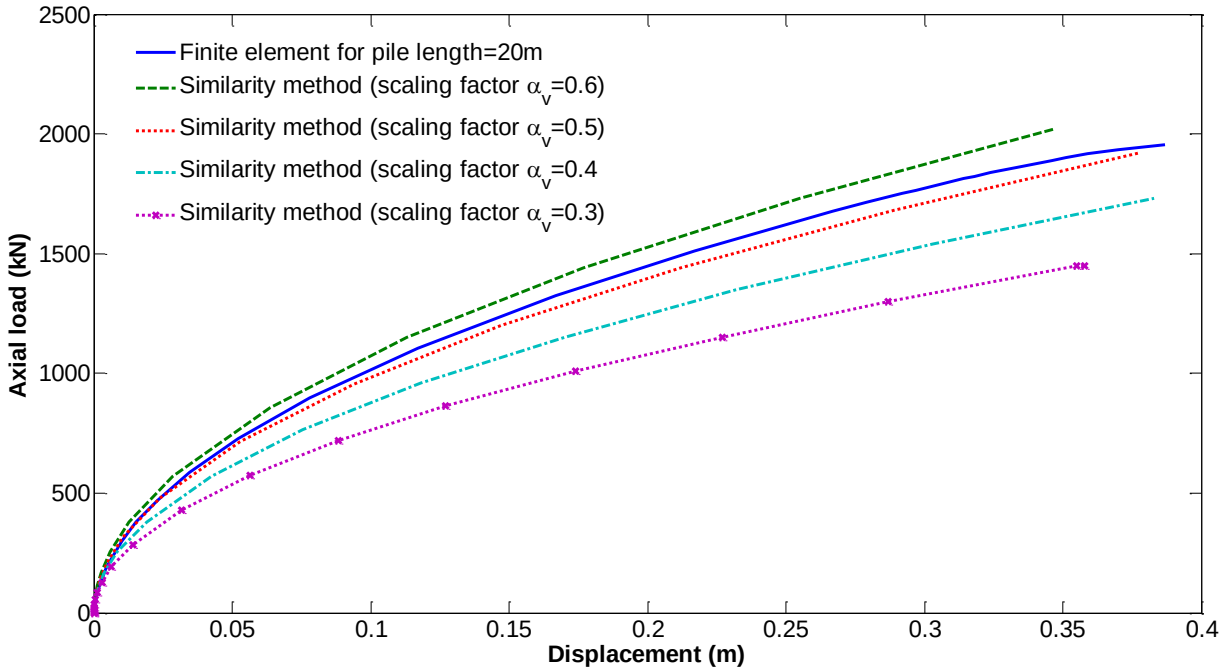

Figure 6.11: Response of axially loaded pile with length 20 m and load-displacement from triaxial test

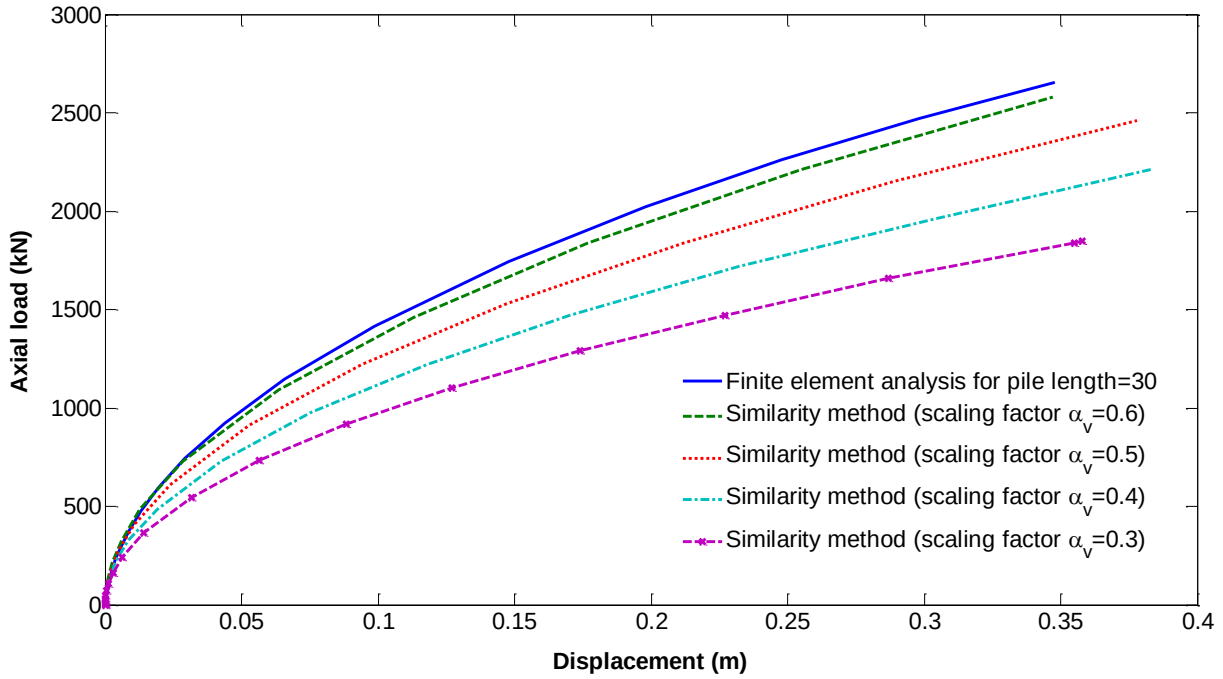

Figure 6.12: Response of axially loaded pile with length 30 m and load-displacement from triaxial test

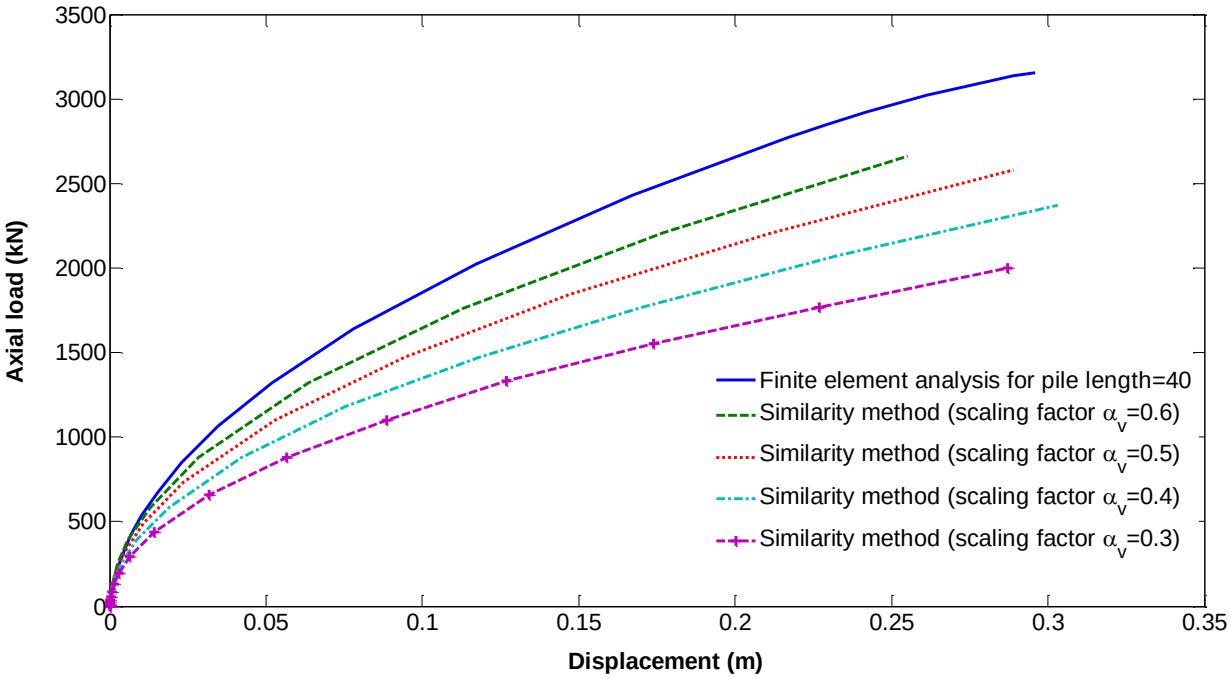

Figure 6.13: Response of axially loaded pile with length 40 m and load-displacement from triaxial test

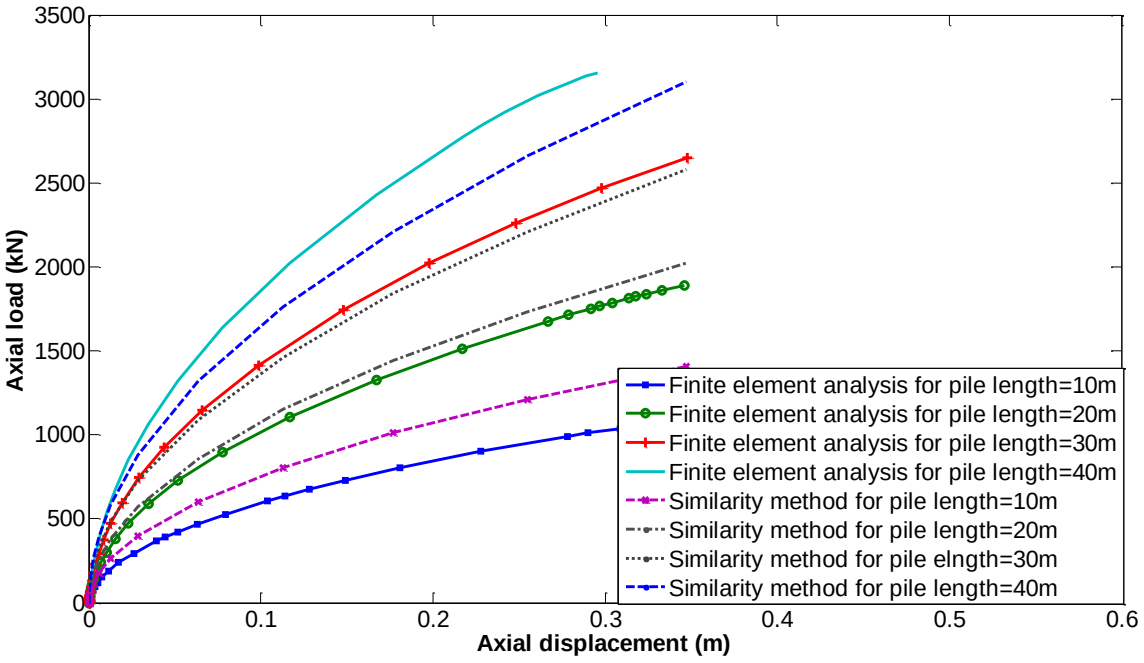

Figure 6.14: Comparison with FE analysis for axially loaded pile

6.3 Validation with field data

6.3.1 Comparison with Farrell et al. (1998)

A similarity method was used for comparison with field data obtained by Farrell et al. (1998), where a single steel pile in Dublin was subjected to an axial load. More details about the site location and field test can be found in Section 5.4.1. The comparison of field data using the similarity method (Figure 6.15) showed a very good agreement between both curves.

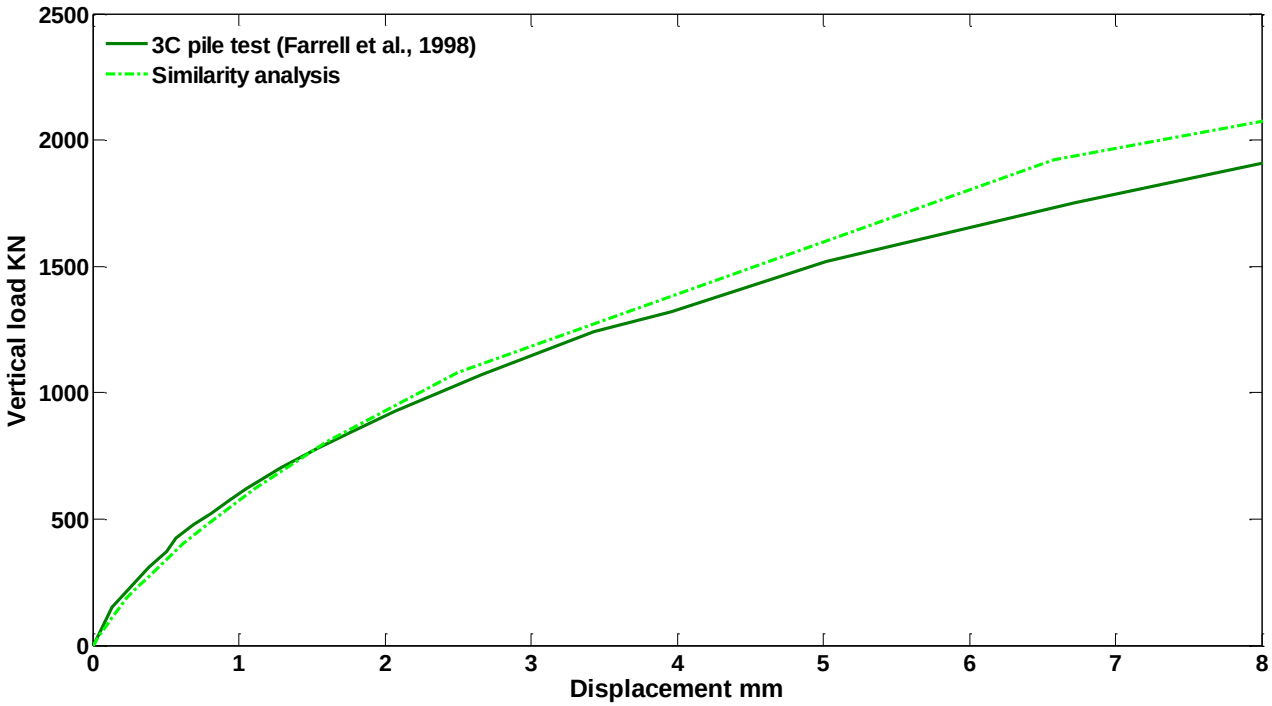

Figure 6.15: Deformation of pile and soil

6.3.2 Comparison with Gavin et al. (2008)

Site location

Analysis using a similarity method was validated with field data obtained by Gavin et al. (2008). The geology of Dublin, field test data and pile geometries have been described in the previous chapter, Section 5.4.2.

The load deformation curve has been compared with the similarity analysis. Figure 6.16 shows the vertical displacement versus the axial force, where for both piles (TP1 and TP2) at very small loading the displacement increases linearly. The load-displacement curves for TP1 and TP2 tests resulting from the similarity method and field data fit very well.

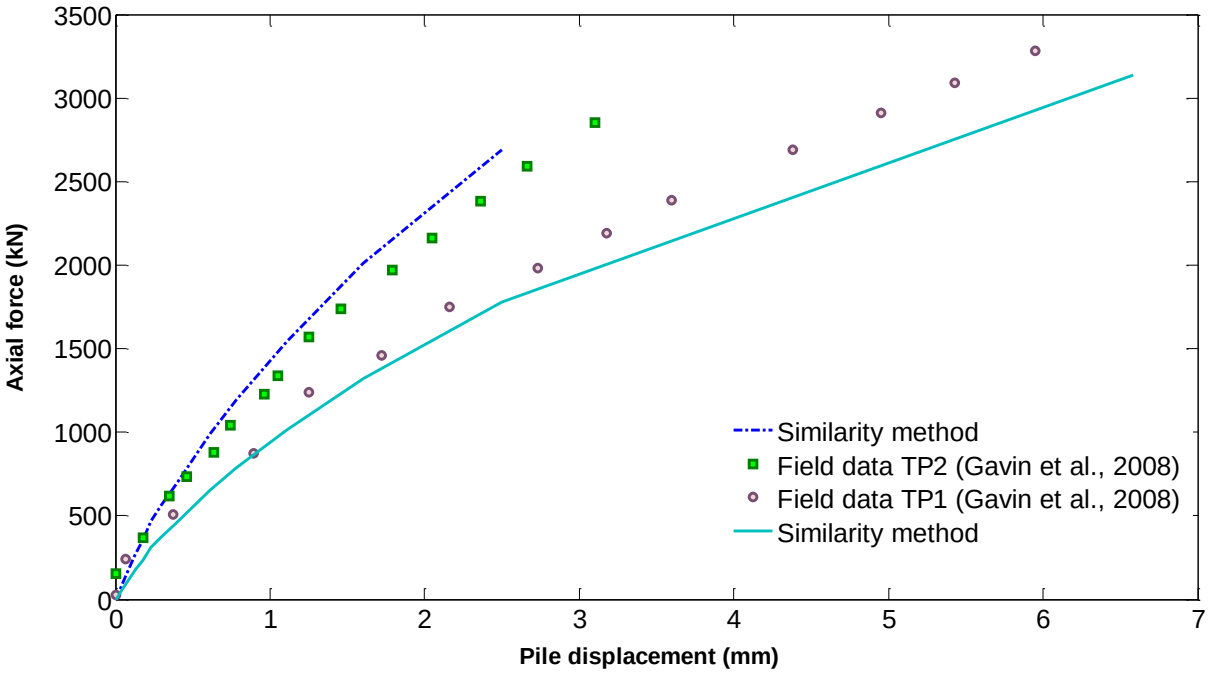

Figure 6.16: Deformation of pile and soil for Gavin et al. (2008)

6.3.3 Comparison with Looby et al. (1995)

Field test

Looby et al. (1995) used a pile test for both dynamic and monotonic loads. They applied a series of loads on a hollow steel pile with a diameter of 273 mm and a length of 9 m. The pile was driven into boulder clay. The thickness of the pile was 10 mm. Only the static load is considered in this comparison. Figure 6.17 shows the soil stratigraphy at the location, and the response of an axially loaded pile in the field compared with a similarity analysis is shown in Figure 6.18.

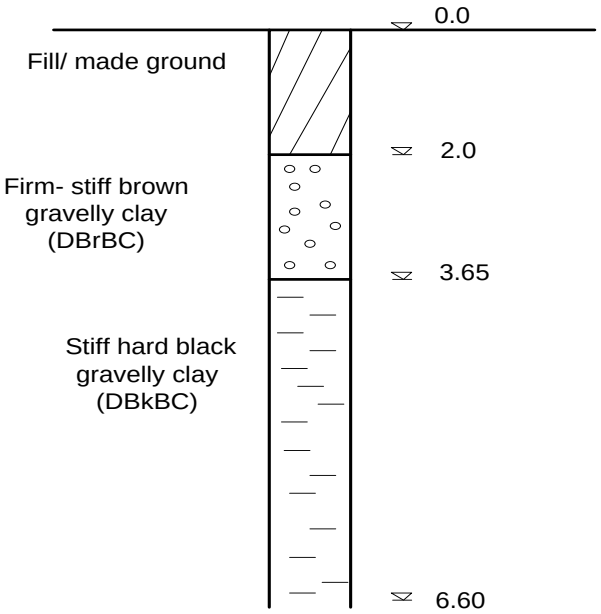

Figure 6.17: Soil stratigraphy at site in Loopy et al. (1995)

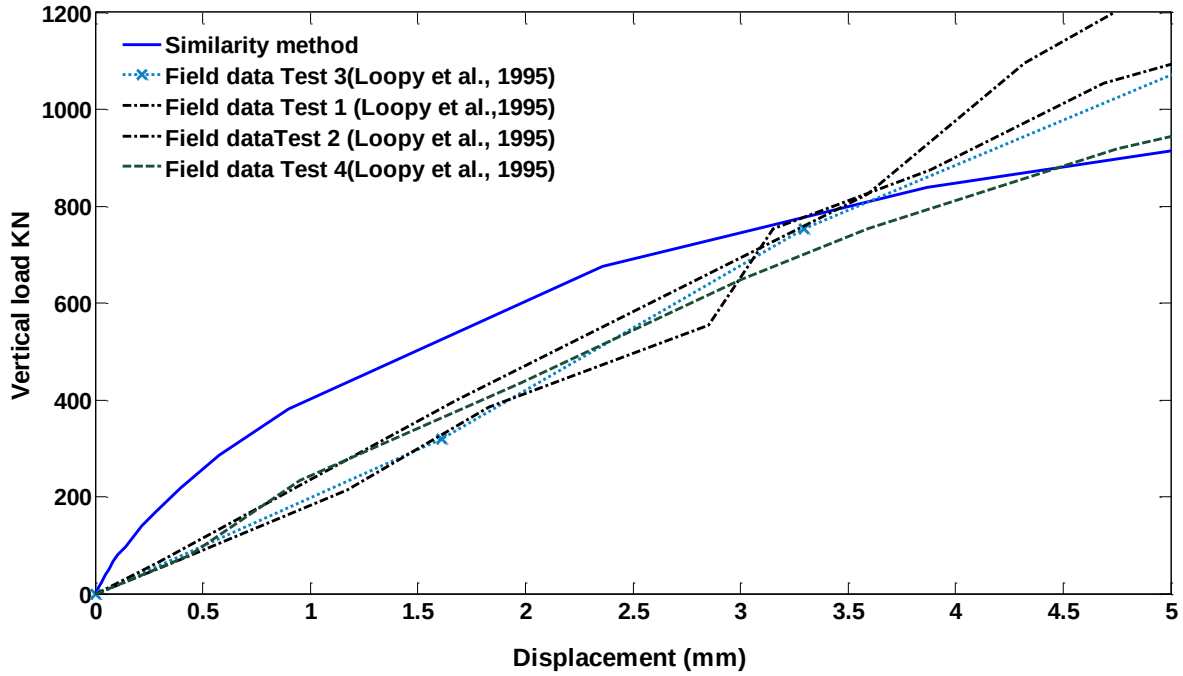

Figure 6.18: Deformation of pile and soil for Looby et al. (1995)

Figure 6.19 shows a comparison between the similarity analysis and all of the field data discussed above. It demonstrates that the nonlinear response of piles can be predicted using a relatively simple hand calculation.

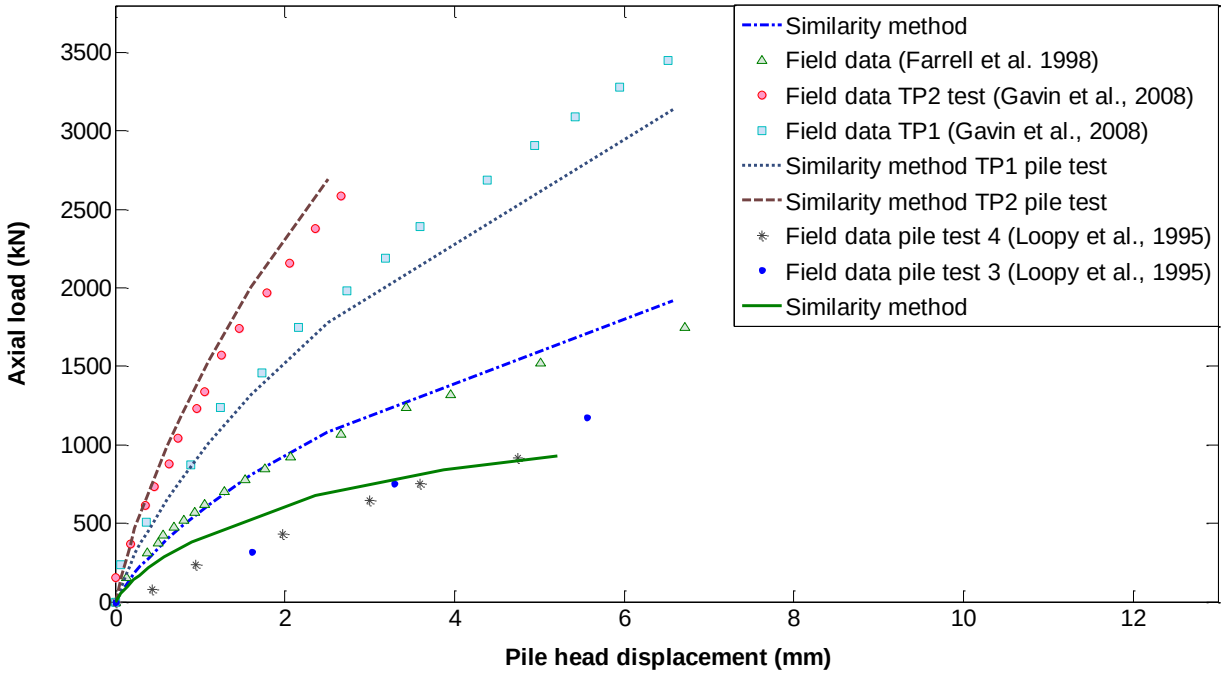

Figure 6.19: Similarity analysis for different axial loaded pile

6.4 Validation with centrifuge tests

A similarity analysis based on stress-strain data has been taken from the triaxial test carried out by Stallebrass and Taylor (1997) for kaolin clay (Figure 6.20). The experiment used the same type of soil. Khemakhem et al. (2010) carried out a centrifuge test, where a pile, manufactured to simulate at 50 g, was a prototype steel pile with a diameter of 0.9 m and a length of 16 m. The thickness of the pile was 1 mm and the bending stiffness of the pile was $E_p I_p$ 38100 MNm^2 .

The experiment was designed for variable lateral loading in order to estimate the pile displacement. Elastic soil was used and three tests were applied to the pile. Figure 6.21 shows, as expected, that the results from a finite element calculation of the triaxial test and for experiments carried out by Khemakhem et al. (2010) were comparable, where the displacement increases linearity from 0-150 kN, and the nonlinearity of soil occurs at a small loading (151 kN).

Moreover, a centrifuge test for square piles embedded in kaolin clay was carried out by Ilyas et al. (2004), where the pile cross section was square. This area was modified by finding the diameter of the pile by square area. The pile was hollow, square and made from aluminium.

A series of tests of different pile radiuses were reported by Ilyas et al. (2004). Their experiment was conducted at 70 g, with a pile width of 0.84 m and 14.7 m in the prototype. The flexural rigidity $E_p I_p$ was equal to $922\ kNm^2$. A series of tests for a single pile and group of piles were carried out. The response of a single laterally loaded pile for both experiments was validated with a simulation method derived from Stallebrass and Taylor (1997). These comparisons demonstrate clearly that a similarity approach can predict the performance of piles with reasonable accuracy, as can be seen in Figure 6.22.

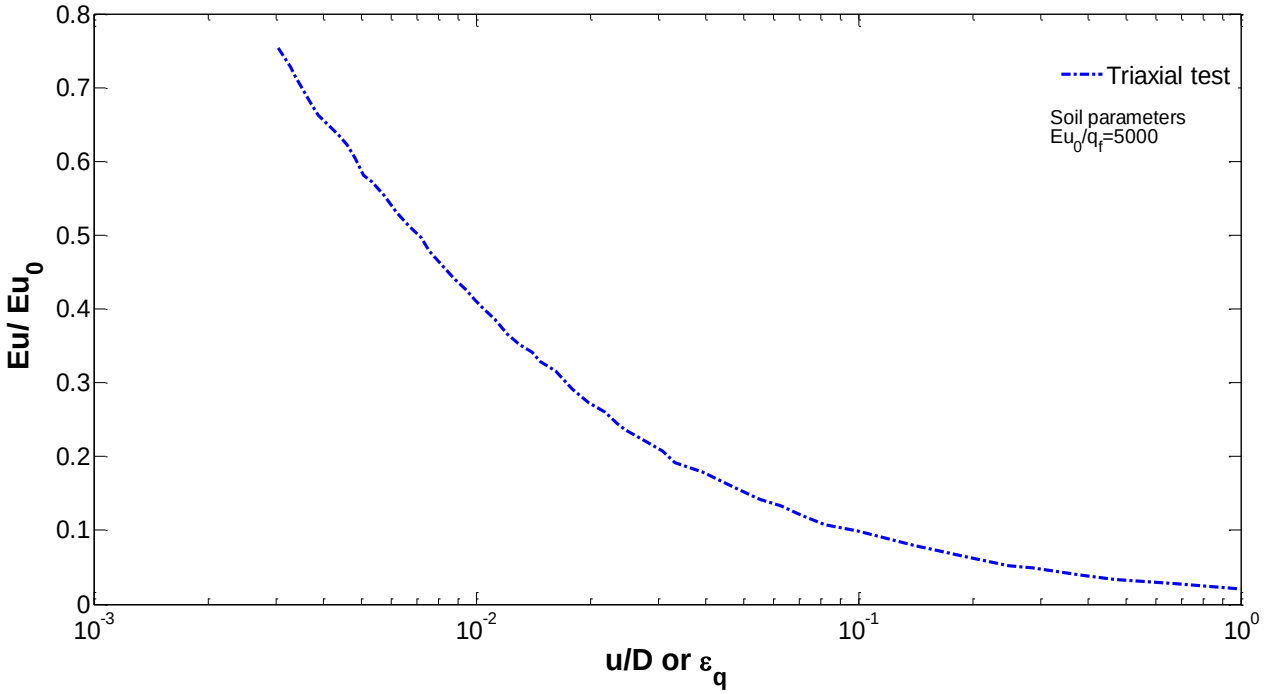

Figure 6.20: Triaxial test of kaolin clay (Stallebrass & Taylor, 1997)

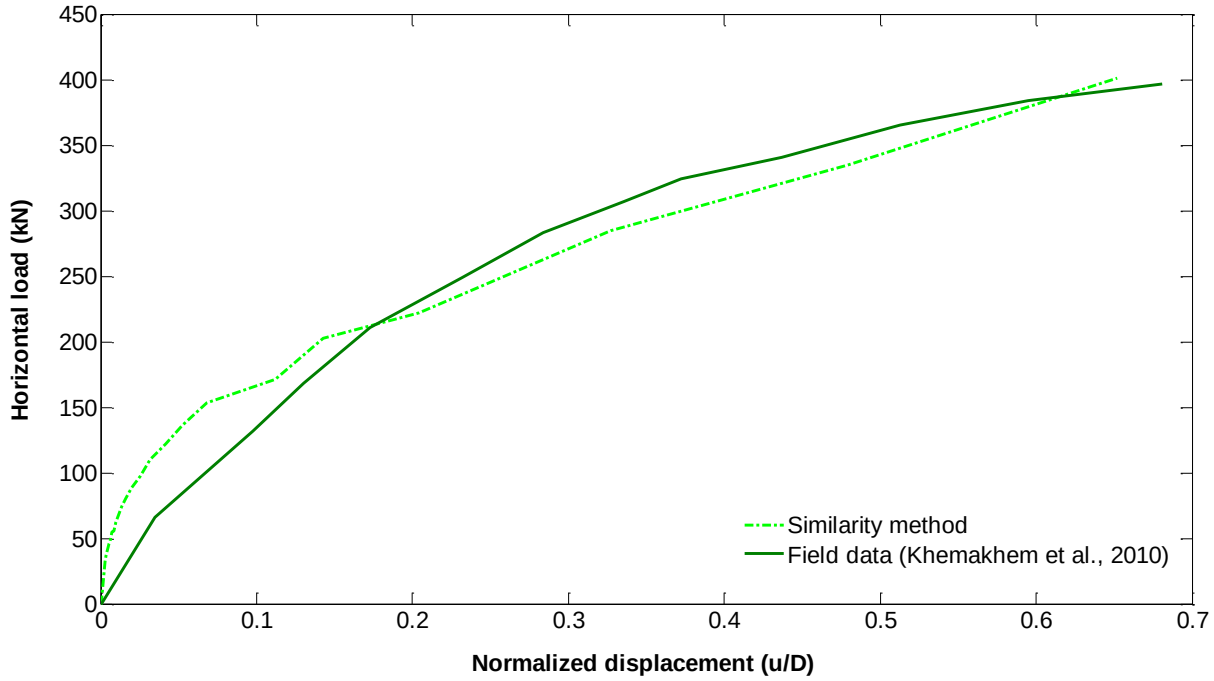

Figure 6.21: Similarity analysis of different laterally loaded pile

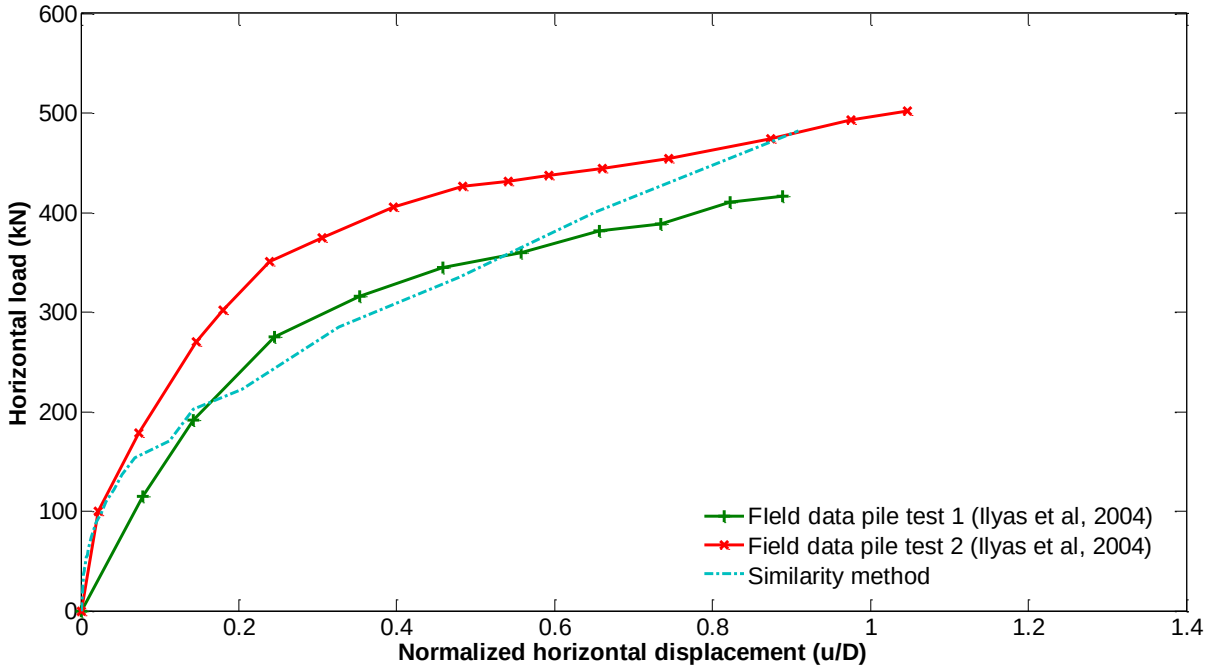

Figure 6.22: Similarity analysis of different laterally loaded pile

6.5 Comparison of different methods for predicting pile displacement

This section shows the validation of field data and centrifuge tests with similarity and energy methods. For a pile under axial load, Figure 6.23 shows that field data validated with an analytical solution and similarity method (using Equation 6.5), and load-displacement curves for two piles loaded axially resulting from two methods were close to field data obtained by Gavin et al. (2008) (all data which used to predict vertical displacement for pile under axial load using the energy method and similarity approach can be found in Section 5.4.2). Moreover, unlike the load-displacement curve estimated from a similarity method, the response of a pile under axial load calculated using an analytical solution was very close to the field data obtained by Farrell et al. (1998) (see Figure 6.24). For a pile loaded laterally, Figures 6.25 and 6.26 show that there is a very good agreement between centrifuge tests carried out by Khemekhem et al. (2010) and Ilyas et al. (2004) and the analytical solution. These results show that the analytical solution is more accurate while the calculations in the similarity method are much simpler.

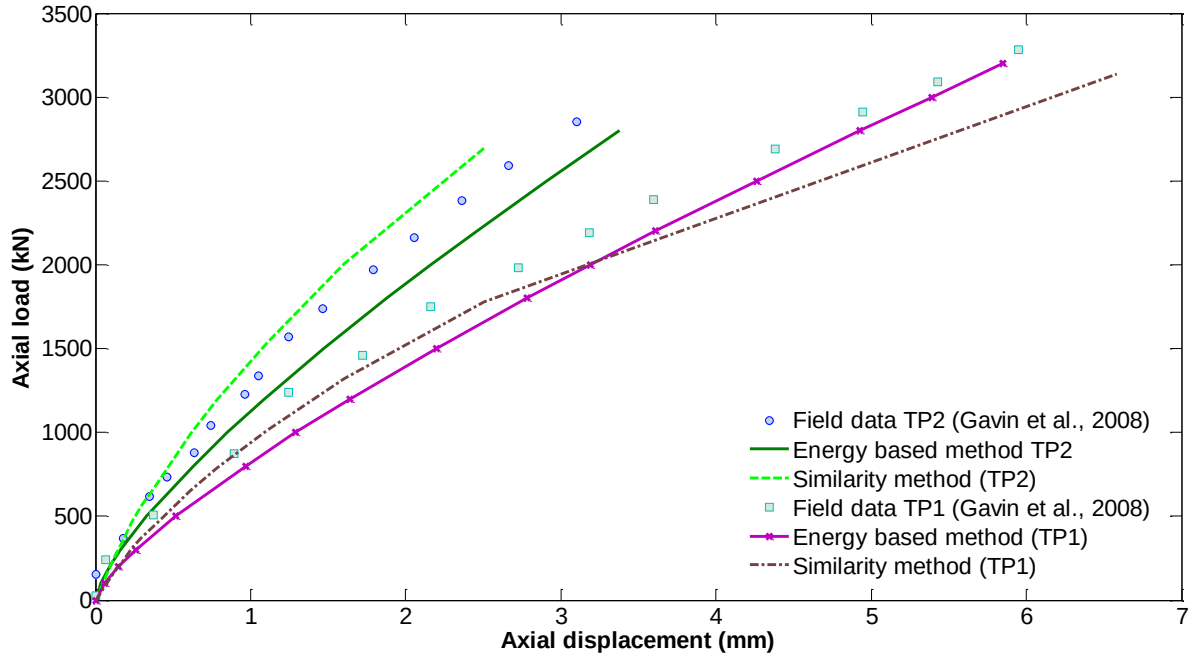

Figure 6.23: Validation similarity method and energy based method with Gavin et al. (2008)

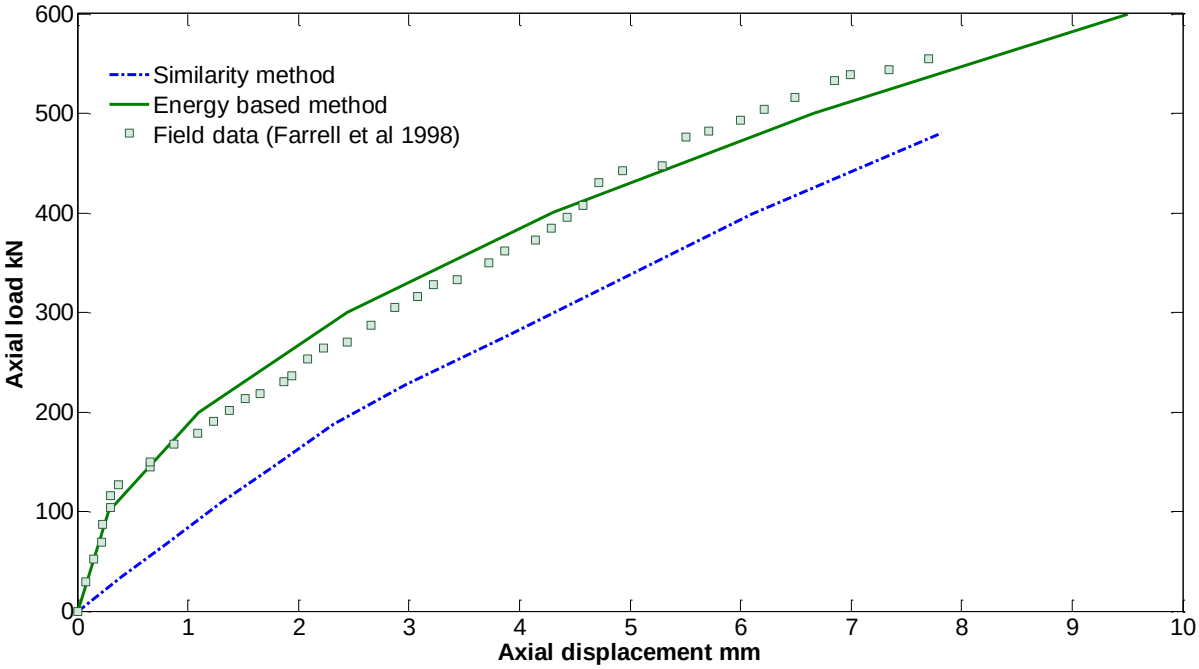

Figure 6.24: Validation similarity method and energy based method with Farrell et al. (1998)

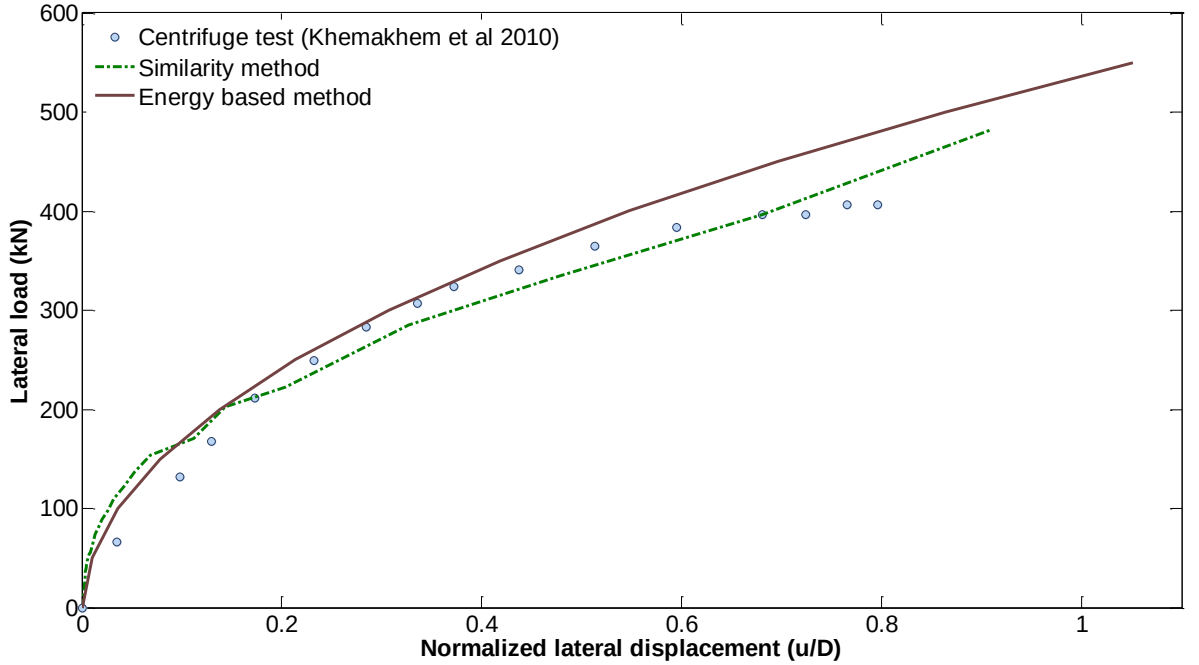

Figure 6.25: Validation with similarity method and energy based method (Khemakhem et al., 2010)

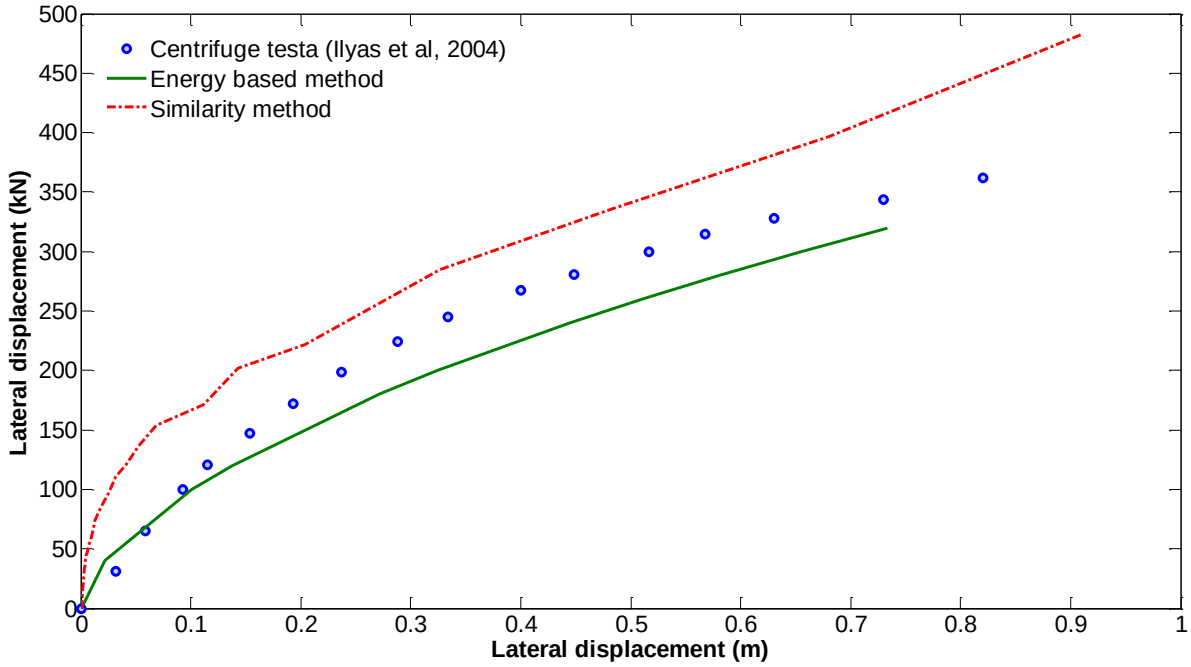

Figure 6.26: Validation with similarity method and energy based method (Ilyas et al., 2004)

6.6 Summary

- A similarity method has been developed for piles in elasto-plastic soil (using Tresca constitutive model), and has been used to derive a load-displacement curve from a triaxial test, where shear strain was related to pile settlement. The strain scaling factors which were derived from the finite element analysis of the pile (with different geometries and loads direction) were used to predict pile displacement (for axially loaded pile $\varepsilon_q = 0.6\frac{\mathrm{v}}{D}$, and for lateral loaded pile $\varepsilon_q = \frac{u}{D}$).

- The deformation of a pile under different loads resulting from the similarity method was compared with three groups of field data and two centrifuge tests. The results show good agreement between previous work and the proposed solution.

- A comparison between the energy based method (derived in Chapters 4 and 5), the similarity approach and previous work has been considered in this chapter. Unlike the similarity method, the displacement-load curve resulting from the energy based

method has been found to fit well with previous work. However, the similarity method is far quicker and simpler than the numerical analysis.

7 Analysis of piles in elasto-plastic Soils

Introduction

Offshore structure vertical piles are regularly used as foundation elements. However, unlike shallow foundations, their bearing capacity under combined loads has not been studied extensively, so solutions for bearing capacity under combined loads will be presented. It is quite common for engineers to use plasticity theory to estimate collapse, while the calculations for displacements are based on elasticity. In previous chapters an extensive analysis were made to predict the static and dynamic response of piles embedded in linear elastic soil and nonlinear elastic soil. However, a new analytical solution for calculating lateral displacements of piles embedded in an elasto-plastic material will also be presented in this chapter.

7.1 Ultimate loads of piles

Piles subjected to pure vertical or horizontal loads have been studied and reported extensively in the literature. However, there is a need to evaluate the effect of combined loading (Achmus & Abdel-Rahman, 2007).

3D finite element analyses have been carried out to determine the shape of the failure envelope for piles under undrained combined (vertical and horizontal) loading. This chapter describes how a Tresca yield criterion with perfect plasticity was adopted. The undrained strength here was assumed to vary linearly with depth.

Displacement-controlled analysis has been conducted to enable observation of post failure condition and hence the accurate identification of the failure envelope. An analysis based on the side probe loading paths (Gourvenec & Randolph, 2003; Martin & Houlsby, 2001; Bell, 1991) has been used to identify the shape of the failure, where each loading path travels around the failure envelope until it reaches a point where normally the failure envelope matches the prescribed displacement ratio. In order to identify the failure envelope in V-H plane (V-H plane means vertical load-horizontal load, where probe test based on first apply

axial load then apply lateral load), vertical displacement is applied first to bring the pile to vertical bearing failure first. Then, translation displacement can be applied until the ultimate lateral load is reached. The translation displacement is applied in order to obtain the complete failure envelope.

7.1.1 Finite element model: geometry and soil conditions

The soil is assumed to be an isotropic material with elasticity and perfect plasticity. The clay is taken to be undrained and is modelled using the Tresca material model. The pile is assumed to be fully-bonded to the surrounding soil and the head of the pile is levelled with the ground surface. The undrained shear strength may vary in a linear relationship with depth (Figure 7.1) according to the following equation: $S_u = S_{u_0} + \psi z$, where S_u and S_{u0} represent the varying undrained shear strength with depth and on the surface, respectively, ψ is the strength gradient with z, $\psi = \kappa S_{u_0}/D$, and κ is the degree of heterogeneity of the soil. The Poisson's ratio of the soil, *v*, is taken to be equal to 0.49, and the ratios between the Young's modulus of the pile and the soil E_p/E_s=1000.

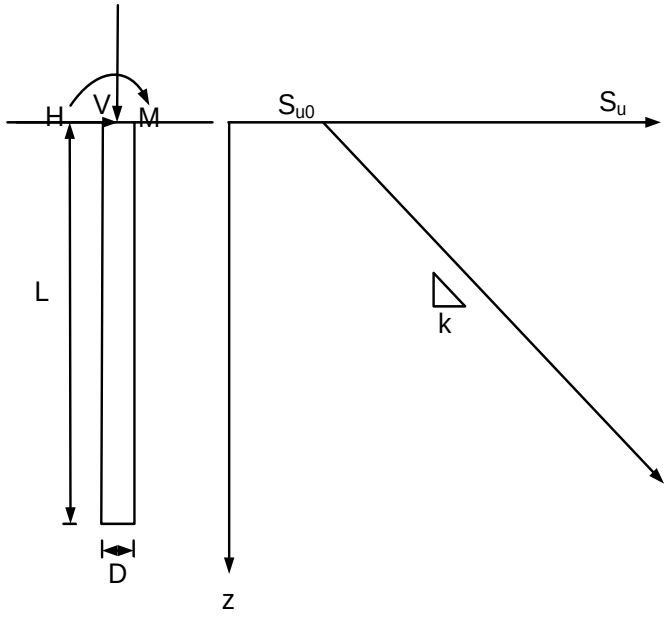

Figure 7.1: Soil and pile conditions

The finite elements analysis has been carried out using ABAQUS 6.10 software. Two finite element meshes for a homogenous soil profile and for a non-uniform profile (the undrained

strength varies with depth) have been used in the analysis, as shown in Figure 7.2. Second order reduced integration elements have been used in the analysis. In the case of a pile with homogenous soil, the mesh consists of 3649 quadratic hexahedral and 354 quadratic wedge elements, and for a pile with different soil properties the mesh consists of 5358 quadratic hexahedral elements.

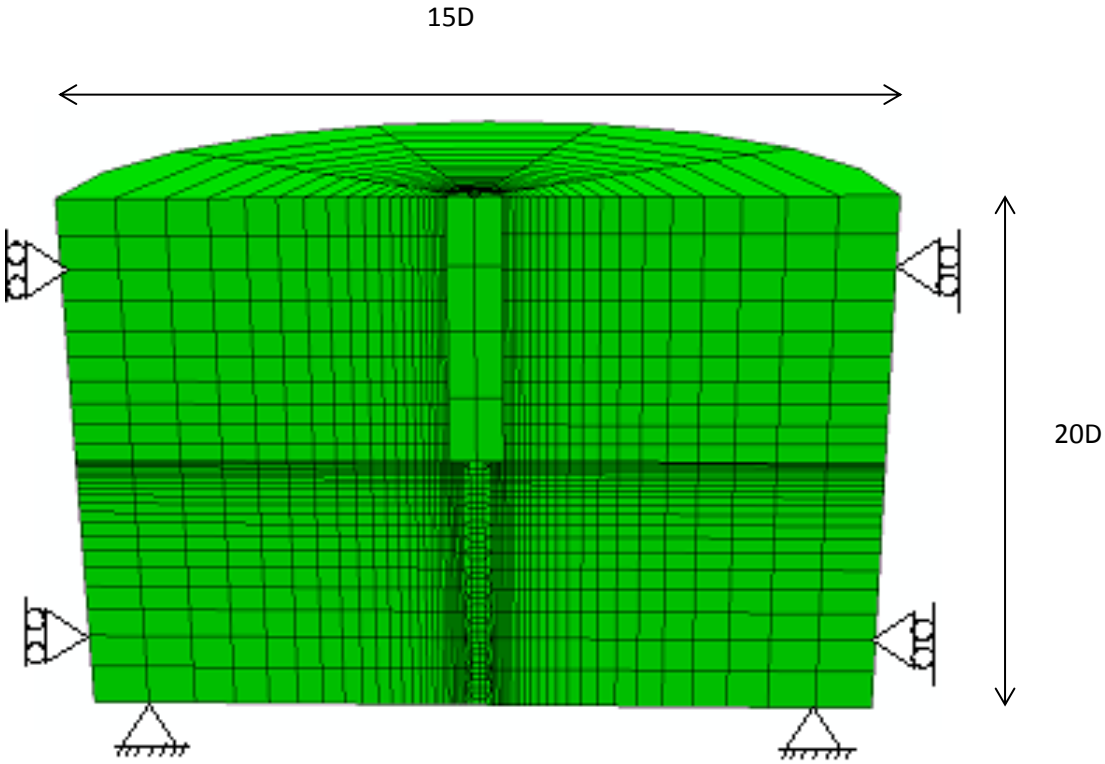

Figure 7.2: Finite element mesh for pile embedded in homogeneous soil

The mesh radius is taken to be equal to 15 D and 20 D depth to ensure that the entire displacement field is contained within the mesh boundary. The mesh under and around the piles is dense due to significant displacement changes in these regions.

7.1.2 Results and discussion

The load path rises due to external loads and displacements. It moves from elastic stiffness to plasticity yielding as a load path approaches the failure envelope. The failure envelope can be reached by applying different values of loads, and the failure envelope shape and size is computed using probe test.

The results for vertical and horizontal loading V-H at moment loading $M_0 = 0$ are shown in Figures 7.3 and 7.4. These results are presented in normalized form with respect to the cross-sectional area of the pile and undrained strength.

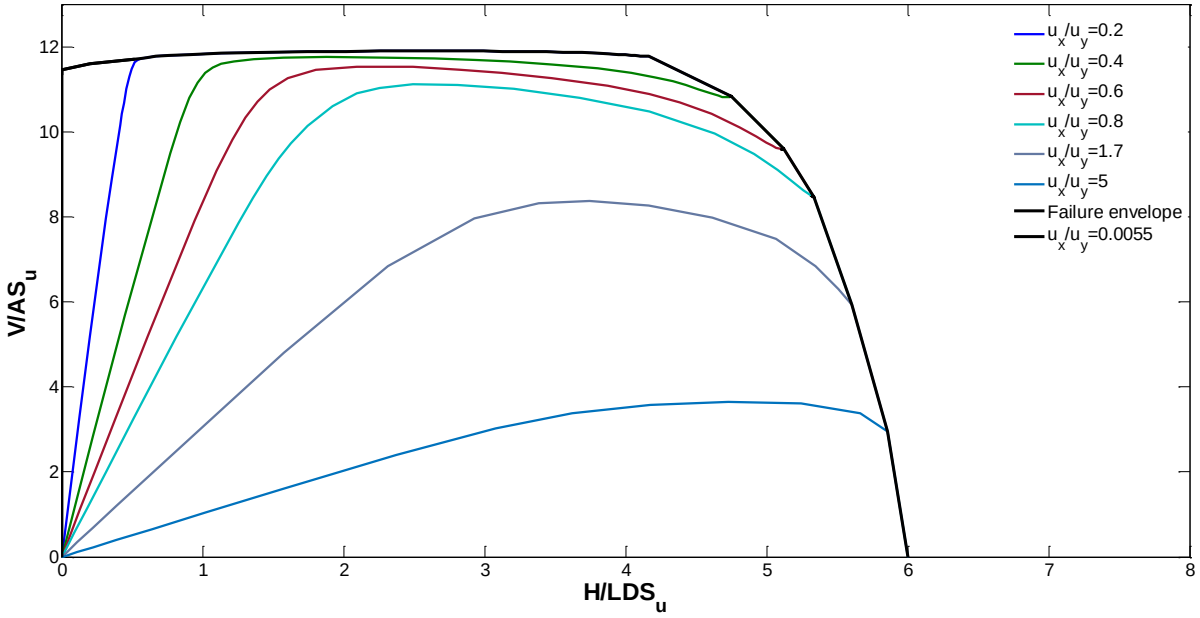

Figure 7.3: Rigid pile in homogeneous soil $^{k\,D}/_{S_u} = 0$

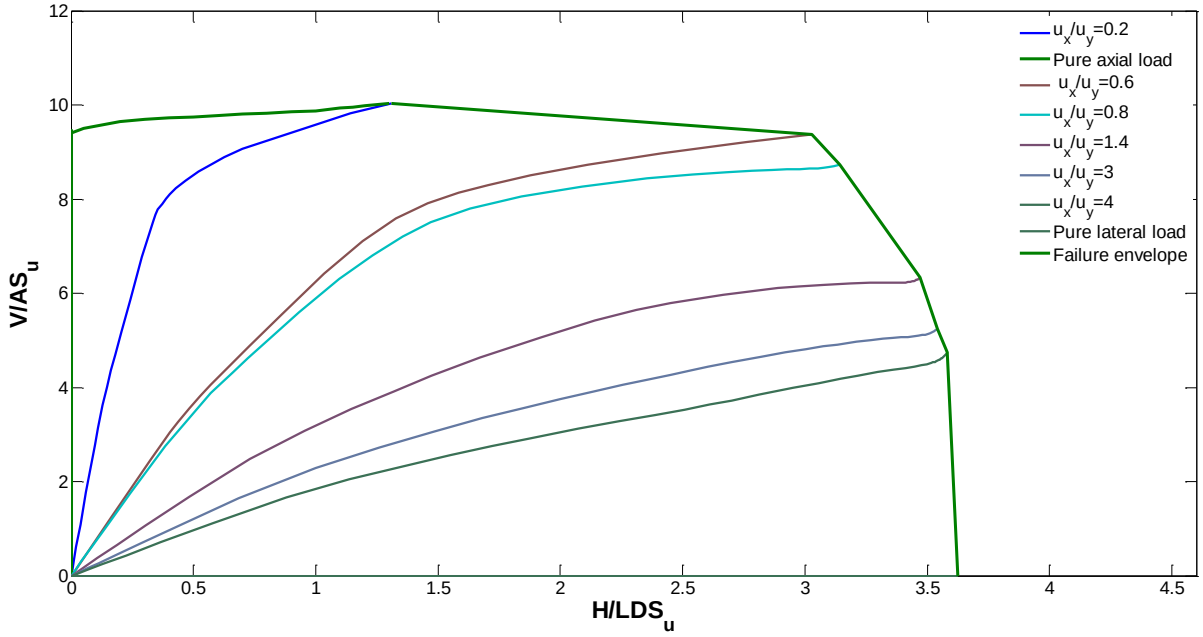

Figure 7.4: Rigid pile in heterogeneous soil $^{k\,D}/_{S_u} = 3$

7.2 Displacement of laterally loaded pile in elasto-plastic soil

In Chapters 3, 4 and 5 an extensive analysis to predict the deformation of laterally and axially loaded pile embedded in different constitutive soils, such as linear elastic soil and nonlinear elastic soil, has been carried out using an analytical solution based on an energy method. Here, a demonstration on how this solution can be extended to elasto-plastic soil is given.

7.2.1 Problem definition

Plane strain conditions are assumed and a plane with strain in z direction is assumed to be equal to zero. This analysis (2D) is used in the case of an axisymmetric pile and while the load is non- axisymmetric (Figure 7.5).

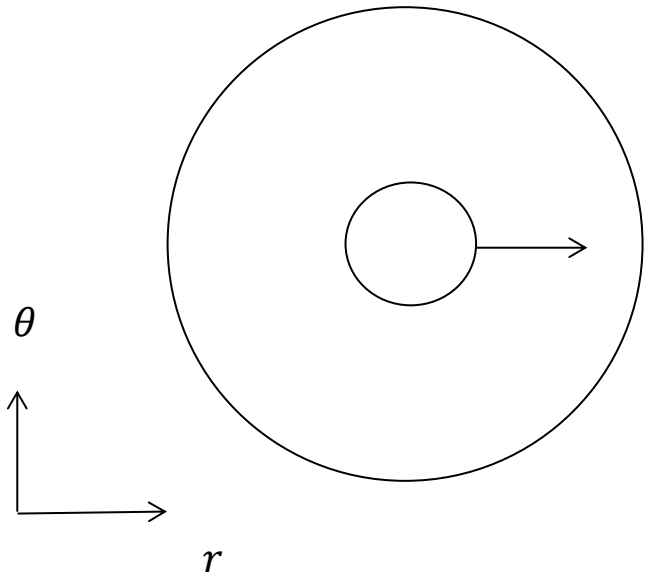

Plan view

Figure 7.5: Laterally loaded pile in elasto-plastic soil

7.2.2 Basic equations

The displacement components in cylindrical coordinates represented by Fourier series are expressed as

$$U = \sum_{k=0}^{L} {u_k}^{(1)}(r)\cos k\theta + \sum_{k=1}^{L} {u_k}^{(2)}(r)\sin k\theta \qquad (7.1a)$$

$$V = -\sum_{k=1}^{L} {v_k}^{(1)}(r)\sin k\theta + \sum_{k=0}^{L} {v_k}^{(2)}(r)\cos k\theta \qquad (7.1b)$$

$$W = 0 \qquad (7.1c)$$

where $U, V \; and \; W$ represent radial, vertical and circumferential incremental displacements, and ${u_k}^{(1)}$, ${u_k}^{(2)}$, ${v_k}^{(1)}$ and ${v_k}^{(2)}$ are the 0^{th} and L^{th} order cosine and L^{th} order sine harmonic coefficients of variables *U* and *V*. The increments of total strain can be found from the first derivative of displacements as

$$\{\varepsilon\} = \begin{Bmatrix} \varepsilon_{rr} \\ \varepsilon_{\theta\theta} \\ \varepsilon_{zz} \\ 2\varepsilon_{r\theta} \end{Bmatrix} = \begin{Bmatrix} \frac{dU}{dr} \\ \frac{1}{r}\left(U + \frac{dV}{d\theta}\right) \\ 0 \\ \frac{1}{r}\frac{dU}{d\theta} + \frac{dV}{d} - \frac{V}{r} \end{Bmatrix} \qquad (7.2)$$

where ε_{ij} denotes a strain component and ε is a total strain.

An elastic strain can be calculated as

$$\varepsilon^e = \varepsilon - \varepsilon^p \qquad (7.3)$$

ε^p is a plastic strain which is defined as

$$\varepsilon_r{}^p = \sum_{k=0}^{L} \hat{\varepsilon}_{rk}{}^{p(1)}(r)\cos k\theta + \sum_{k=1}^{L} \hat{\varepsilon}_r{}^{p(2)}(r)\sin k\theta \tag{7.4a}$$

$$\varepsilon_\theta{}^p = \sum_{k=0}^{L} \hat{\varepsilon}_{\theta k}{}^{p(1)}(r)\cos k\theta + \sum_{k=1}^{L} \hat{\varepsilon}_{\theta k}{}^{p(2)}(r)\sin k\theta \tag{7.4b}$$

$$\varepsilon_z{}^p = \sum_{k=0}^{L} \hat{\varepsilon}_{zk}{}^{p(1)}(r)\cos k\theta + \sum_{k=1}^{L} \hat{\varepsilon}_{zk}{}^{p(2)}(r)\sin k\theta \tag{7.4c}$$

$$\varepsilon_{r\theta}{}^p = -\sum_{k=1}^{L} \hat{\varepsilon}_{r\theta k}{}^{p(1)}(r)\sin k\theta + \sum_{k=0}^{L} \hat{\varepsilon}_{r\theta k}{}^{p(2)}(r)\cos k\theta \tag{7.4d}$$

Equation 7.2 represents the total strain and the elastic strain is calculated as

$$\{\varepsilon^e\} = \{\varepsilon\} - \{\varepsilon^p\} \tag{7.5}$$

Then the stress can be calculated by multiplying the elastic strain vector with the stiffness matrix

$$\{\sigma\} = \begin{Bmatrix} \sigma_{rr} \\ \sigma_{\theta\theta} \\ \sigma_{zz} \\ \sigma_{r\theta} \end{Bmatrix} = [D]\{\varepsilon^e\} = \begin{bmatrix} \lambda+2G & \lambda & \lambda & 0 \\ \lambda & \lambda+2G & \lambda & 0 \\ \lambda & \lambda & \lambda+2G & 0 \\ 0 & 0 & 0 & G \end{bmatrix} \begin{Bmatrix} \dfrac{dU}{dr} - \varepsilon_{rr}{}^p \\ \dfrac{1}{r}\left(U + \dfrac{dV}{d\theta}\right) - \varepsilon_{\theta\theta}{}^p \\ 0 \\ \dfrac{1}{r}\dfrac{dU}{d\theta} + \dfrac{dV}{d} - \dfrac{V}{r} - \varepsilon_{r\theta}{}^p \end{Bmatrix} \tag{7.6}$$

where $[D]$ is the stiffness matrix, and λ and $2G$ are elastic moduli which are assumed to be constant for linear soil.

The total potential energy can be expressed as

$$\prod = F + D \tag{7.7}$$

where F denotes the free energy and D is dissipated energy, which can be rewritten as

$$\prod = \{\sigma\}^T\{\dot{\varepsilon^e}\} + \{\chi\}^T\{\dot{\varepsilon^p}\} \tag{7.8}$$

where χ is the dissipative stress.

Or, if it is written in term of total strain

$$\prod = \{\sigma\}^T\{\dot{\varepsilon}\} + \{\chi - \sigma\}^T\{\dot{\varepsilon^p}\}. \tag{7.9}$$

Since there is no kinematic hardening, the true stresses and the dissipative stresses are equal:

$$\{\chi - \sigma\}^T = 0 \tag{7.10}$$

then Equation 7.8 becomes

$$\prod = \{\sigma\}^T\{\varepsilon\} \tag{7.11}$$

and the free energy can be defined as

$$F = \int_{r_0}^{r_m} r \int_0^{2\pi} \frac{1}{2}\{\sigma\}^T\{\varepsilon^e\} d\theta dr. \tag{7.12}$$

For equilibrium the difference between external and internal energy must be zero

$$\delta\prod = \delta\prod_{int} - \delta\prod_{ext} = 0 \tag{7.13}$$

Similar to the procedure used in previous chapters, the energy equation can be differentiated to obtain the governing equation

$$\delta\prod = \sum \left[A_k(U,V,W)\delta {u_k}^{(1)}\right] + \left[B_k(U,V,W)\delta {u_k}^{(2)}\right] + \left[C_k(U,V,W)\delta {v_k}^{(1)}\right] + \left[D_k(U,V,W)\delta {v_k}^{(2)}\right] = 0 \tag{7.14}$$

The governing equations for deformation can be obtained by collecting the coefficients of δu_k and δv_k

$$\frac{d^2u_k}{dr^2}+\frac{1}{r}\frac{du_k}{dr}-\left(\frac{2+k^2(1-v)-2v}{2(1-v)}\right)\frac{u_k}{r^2}+\frac{k(3-4v)v_k}{2(1-v)r^2}-\frac{k}{2(1-v)}\frac{1}{r}\frac{dv_k}{dr} = {F_{rk}}^p \tag{7.15}$$

$$\frac{d^2v_k}{dr^2}+\frac{1}{r}\frac{dv_k}{dr}-\left(\frac{1+2k^2(1-v)-2v}{(1-v)}\right)\frac{v_k}{r^2}+\frac{k(3-4v)u_k}{(1-2v)r^2}+\frac{k}{(1-2v)}\frac{1}{r}\frac{dv_k}{dr} = {F_{\theta k}}^p \tag{7.16}$$

where

$${F_{rk}}^p=\frac{d{\varepsilon_{rk}}^p}{dr}+\frac{v}{(1-v)}\left(\frac{d{\varepsilon_{\theta k}}^p}{dr}+\frac{d{\varepsilon_{zk}}^p}{dr}\right)+\frac{(1-2v)}{(1-v)}\left(\frac{{\varepsilon_{rk}}^p-{\varepsilon_{\theta k}}^p-{\varepsilon_{r\theta k}}^p}{r}\right) \tag{7.17}$$

$${F_{\theta k}}^p=2\frac{d{\varepsilon_{r\theta k}}^p}{dr}+\frac{2kv}{(1-2v)}\left(\frac{{\varepsilon_{rk}}^p+{\varepsilon_{zk}}^p}{r}\right)+\frac{2k(1-v)}{(1-2v)}\left(\frac{{\varepsilon_{\theta k}}^p}{r}\right)+4\frac{{\varepsilon_{r\theta k}}^p}{r} \tag{7.18}$$

7.2.3 Solution procedure

To solve the above governing equations, an iterative procedure is required. At first, the right hand of Equations 7.15 and 7.16, which represent the plasticity terms, can be taken to be zero (i.e. we start by assuming elastic response). Then the components (u_k and v_k) and the displacements are calculated, and the total strains are calculated using Equation 7.2. The stresses are then calculated from the total strain. If the stresses falls outside the yield surface, corrections to the stresses are needed using Von-Mises material, the yield surface is given by

$$F=\sigma-\sigma_y \tag{7.19}$$

where σ denotes the second stress invariant and σ_y is yield stress. The plastic strain can be estimated as

$$\varepsilon^p=\dot{\lambda}\frac{dF}{d\sigma} \tag{7.20}$$

Using a radial return algorithm, the Lagrangian multiplier λ can be evaluated as

$$\overline{\Delta\lambda} = \frac{q - \sigma_y}{3G} \tag{7.21}$$

dF is the plastic potential function, and $\overline{\Delta\lambda}$ is equal to the deviatoric plastic strain equivalent. From Equation 7.3 we can obtain the elastic strain, and then the stress in Equation 7.5 will be calculated. Once the plastic strain is calculated then the harmonic coefficients are calculated using the fitted method (see the Appendix) and substituted in Equations 7.17 and 7.18 to calculate ${F_r}^p k$ and ${F_\theta}^p k$.

The plastic terms in Equations 7.15 and 7.16 are then updated and the equations are solved for new displacements. These calculations need to be iterated until the difference between the new and old displacements became within a certain tolerance. A flow chart is shown in Figure 7.6.

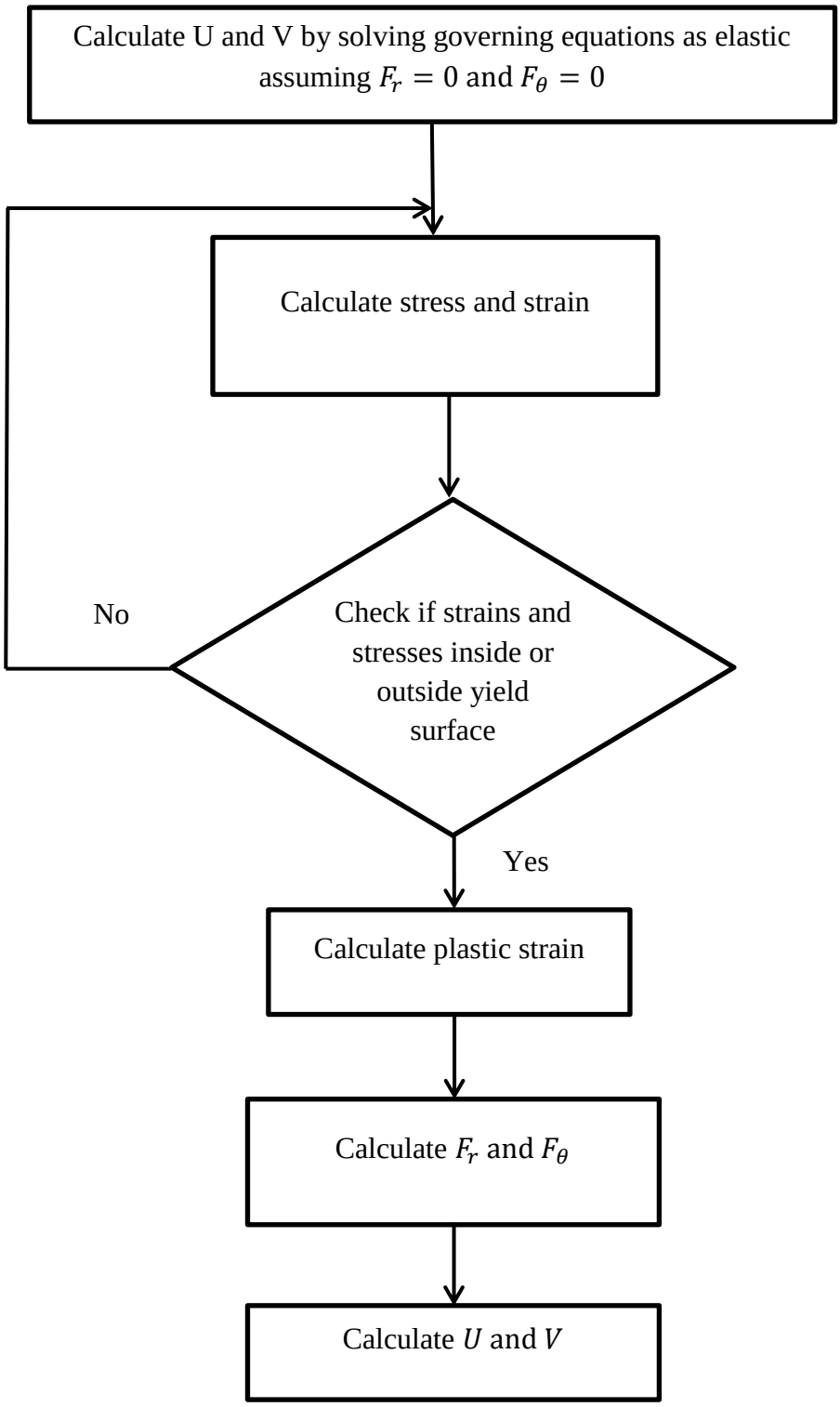

Figure 7.6: Solution flow chart

7.2.4 Results

An analytical solution of a pile under lateral load has been used to estimate the displacement; the pile had a radius of 1 m and was embedded in elasto-plastic soil with soil Young modulus $E_s = 10$ MPa, soil stiffness $G = \frac{E_s}{2(1+\upsilon)}$, elastic modulus $\lambda = \frac{2\,G\,\upsilon}{(1-2\upsilon)}$ and Poisson ratio $\upsilon = 0.499$. Figure 7.7 shows the pile load-displacement curve obtained from the analytical solution fitting well with the finite element results.

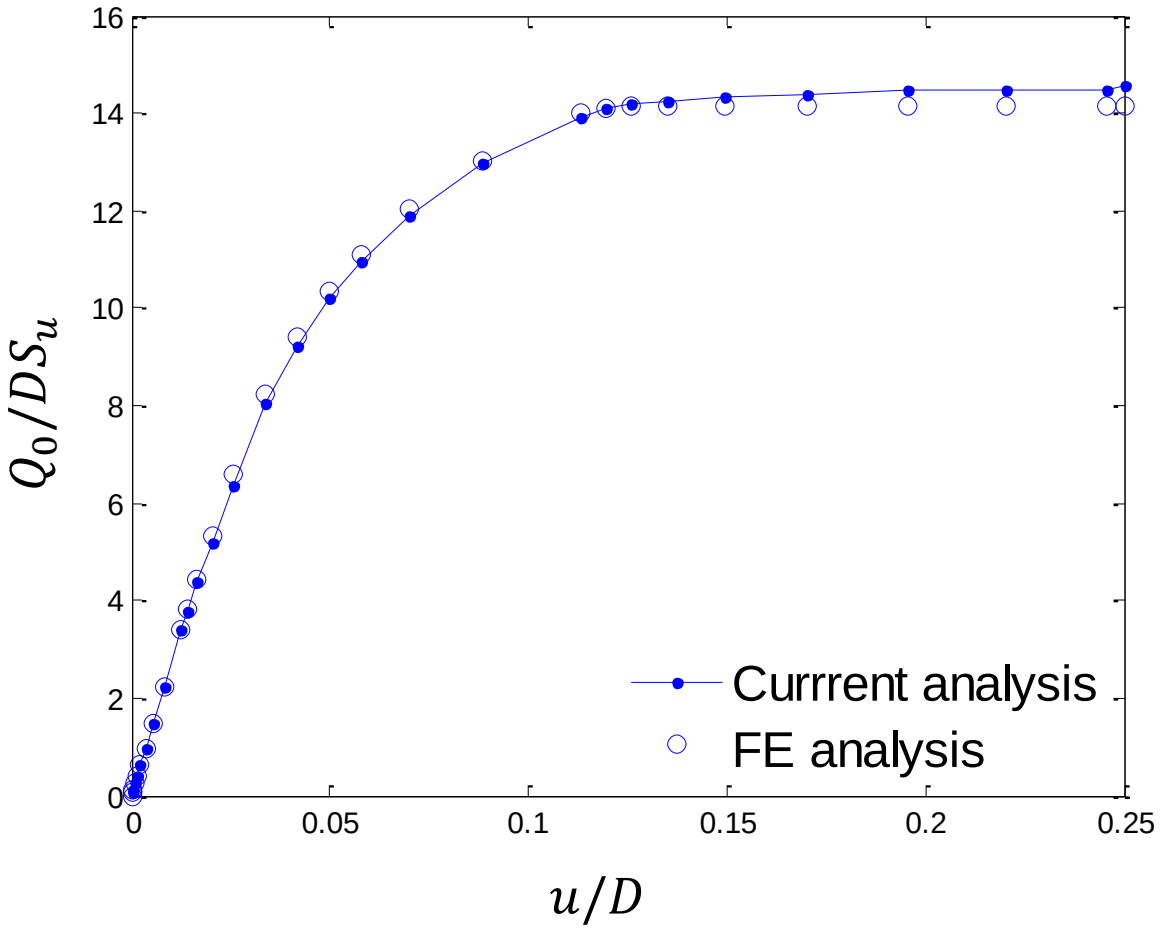

Figure 7.7: The deflection of laterally loaded pile in elasto-plastic

7.3 Summary

- 3D finite element analyses have been carried out to determine the shape of the failure envelope of piles under undrained loading.

- A Tresca yield criterion was adopted in the constitutive model to predict the undrained capacity of the piles.

- 2D energy method analysis has been developed to predict the response of a pile in linear elasto-plastic soil. The results were compared with the finite element analysis.

7.4 Appendix

The fitted method here is suitable to determine the harmonic coefficients, by assuming x is known values, and X represents the unknown harmonic coefficients. Fourier series harmonic coefficients can be estimated by considering variable x which is a function of θ $(x = f(\theta))$. Then x can be given by

$$x = X^0 + X^1 \cos\theta + X^1 \sin\theta + X^2 \cos 2\theta + X^2 \sin 2\theta + \cdots + X^l \cos l\theta + X^l \sin l\theta + \cdots \tag{7.22}$$

Equation 7.22 can be rewritten in matrix form as

$$\begin{Bmatrix} x_1 \\ x_2 \\ x_3 \\ \\ \\ x_{n-1} \\ x_n \end{Bmatrix} = \begin{bmatrix} 1 & \cos\theta_1 & \sin\theta_1 & \cdots & \cdots & \cdots & \cos L\theta_1 & \sin L\theta_1 \\ 1 & \cos\theta_2 & \sin\theta_2 & \cdots & \cdots & \cdots & \cos L\theta_2 & \sin L\theta_2 \\ 1 & \cos\theta_3 & \sin\theta_3 & \cdots & \cdots & \cdots & \cos L\theta_3 & \sin L\theta_3 \\ \cdots & \cdots & \cdots & \cdots & \cdots & \cdots & \cdots & \cdots \\ \\ 1 & \cos\theta_{n-1} & \sin\theta_{n-1} & \cdots & \cos L\theta_{n-1} & & \sin L\theta_{n-1} & \\ 1 & \cos\theta_n & \sin\theta_n & \cdots & \cos L\theta_n & & \sin L\theta_n & \end{bmatrix} \begin{Bmatrix} X^0 \\ X^1 \\ X^1 \\ \\ \\ X^{\frac{n-1}{2}} \\ \\ X^{\frac{n-1}{2}} \end{Bmatrix} \tag{7.23}$$

Equation 7.23 can be rewritten as

$$x = [H]X \tag{7.24}$$

where L denotes the order of Fourier series, x is the vector of known values, X represents the vector of unknown harmonic coefficients and H is the harmonic transformation matrix.

Then we can estimate the harmonic coefficients from the following equations

$$X^0 = \frac{1}{n}\sum_{i=l}^{n} x_i \tag{7.25a}$$

$$X^k = \frac{2}{n}\sum_{i=l}^{n} x_i \cos k(i-l)\,\alpha \tag{7.25b}$$

$$X^k = \frac{2}{n}\sum_{i=l}^{n} x_i \sin k(i-l)\alpha \qquad (7.25c)$$

Figure 7.8 shows the location of x and θ

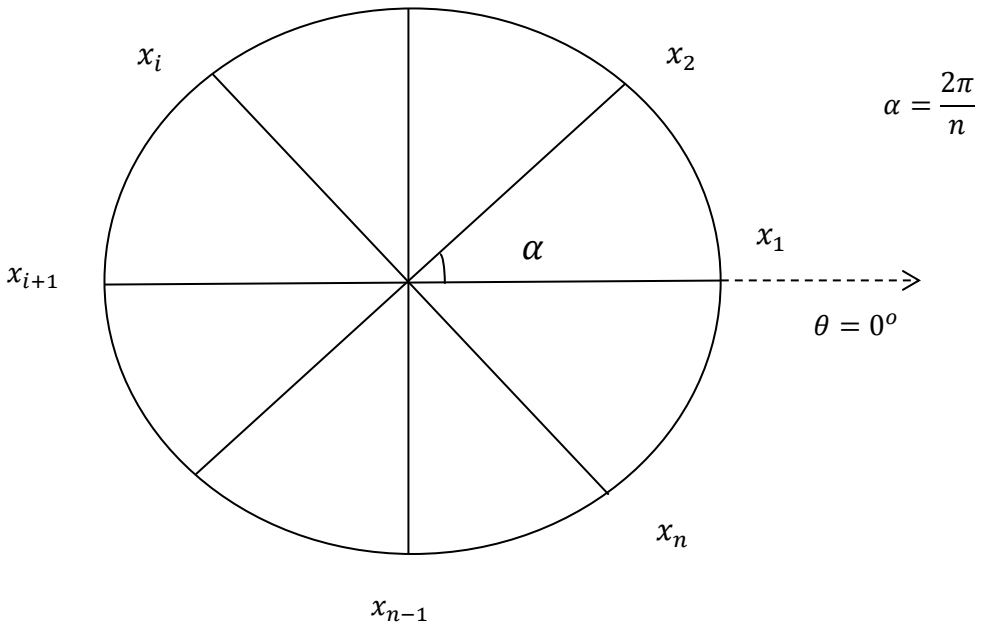

Figure 7.8: Location of value x and θ

8 Conclusions and Further Work

In this thesis, two methods (an energy based method and a similarity method) have been developed to predict pile deformation under different directions for loads (axial, lateral and combined loads), considering different constitutive models for soil. These two new analytical methods have been validated with finite element analysis, centrifuge tests and field data. The finite element analysis to estimate the ultimate load of a pile was used in this thesis, where analysis considers different variations of shear strength with depth and different pile geometries, also the response of pile embedded in elasto-plastic soil and subjected to lateral load was calculated using energy method.

8.1 Achievements

8.1.1 Development of an analytical solution to estimate pile deflection under static and dynamic lateral loads

A simple and quick energy-based analytical method has been developed. This new analytical method represents an extension to the Vlasov method for predicting the displacement of piles under different loading and soil conditions, without the need to conduct complex numerical simulations. A new solution for piles embedded in linear elastic soil, whose stiffness varies with depth, has been developed. This analytical solution can be used in engineering practice providing that appropriate soil stiffness is selected. A new solution for obtaining the dynamic response of laterally loaded piles has also been developed.

Comparison with field data has shown that the presented solution can predict the resonant frequency of piles with reasonable accuracy.

8.1.2 Deformation of piles in nonlinear soil under different types of loads

The energy based method has been extended to analyse piles in nonlinear soil, where the variations of soil stiffness with strain and stress are taken into account. The results have

shown there is good agreement between the proposed analytical method and finite element analyses, field data and centrifuge tests.

Solutions have been developed for different pile loading conditions. These analytical solutions have been developed for monotonically loaded piles as well as piles subjected to loading-reloading cycles. Masing's rule has been used to model soil behaviour during unloading-reloading cycles. A comparison with field data demonstrates the success of the proposed energy-based method.

8.1.3 Prediction of pile deformation using similarity method

In addition to the energy-based method, a simpler method has been developed to predict the displacements of piles. This method is based on the similarity between the stress-strain response of a representative element of soil and the load-displacement curve of the foundation.

A scaling factor has been used to obtain the structural response. A series of nonlinear finite element analyses have been carried out to obtain the scaling factor, which depends on the type of loading, not the geometry of the problem or the boundary conditions. Once the scaling factors are known, then the nonlinear response of the pile is obtained using a simple hand calculation.

The similarity has been validated with field data obtained by Farrell et al. (1998), where the maximum pile head displacement derived from the hand calculation similarity approach was within 15% of the field data

In addition to the methods for calculating displacements of piles, the failure envelope for piles under combined loads has also been investigated. The failure envelope was obtained using 3D finite element (FE) analyses assuming the Tresca yield criterion. Different variations of shear strength with depth were investigated. The failure envelope has been obtained using displacement-controlled analysis and probe-test-type analysis.

8.2 Further work

In this thesis, an analytical solution for pile under dynamic lateral load is developed assuming the soil is linear elastic material. Maheshwari et al. (2005) show that the deformation of piles obtained using linear-elasticity may not be valid for strong excitations. Therefore, the proposed solution need be extended to account for soil nonlinearity. The nonlinear solution for piles under static lateral loads, which is detailed in Chapter 4, can be extended to the case of dynamic loads. Furthermore, the solution for axially loaded pile in nonlinear soil which is in Chapter 5 can also be extended to dynamic loading.

The response of piles embedded in linear elasto-plastic soil subjected to lateral load was calculated using plane strain to simplify the analysis. This solution will not be capable of replicating pile response near the ground surface. These solutions need to be extended to 3D.

In this thesis we only focus on single pile deflection under different external loads, the deformation of a group of piles due to lateral or axial loads is larger than the displacement in single isolated piles (Ilyas et al. (2004); McCabe and Lehane (2006); Basu et al. (2008)). Therefore, this work needs to extend to determine the response of group of piles subjected to different loads.

The response of a group of piles under external loads influences the interaction between individual piles. If piles are placed close to each other the load causes interaction between piles displacement. This interaction leads to increase displacement on the group of piles. For a laterally loaded pile there will be an increase in lateral stresses in the soil near the piles. These zones of high stresses lead to soil yield zones around each pile may lead to an overlap. As a result; it increases the deflection (McVay et al. (1996); Brown et al. (1987)). The response of a group of piles can be calculated by using the energy method (we can use the same procedure in chapters 4 and 5).

Finally, all of the analyses used in this thesis have been related to the response of piles in undrained soil or fully drained soil. In both cases, the analysis is based on total stresses and pore water pressure was not taken into account. These analyses can be extended to take into account the consolidation effect and the development and the dissipation of excess-pore water pressure. Solutions for excess pore water pressure dissipation around a laterally loaded pile

can be obtained by solving Biot's equation of consolidation analytically. The accumulation of excess pore water pressure during cyclic load needs to be taken into account as it plays an important role in the stability and the performance of piles.

MATLAB and Mathematica codes

MATLAB and Mathematica codes were used in this thesis are included on CD, and each file contains programs which used to solve the problem in each chapter.

Reference

Abdel-Rahman, K & Achmus, M. (2006). Numerical modeling of the combined axial and lateral loading of vertical piles. *Proceedings of the 6th European Conference on Numerical Methods in Geotechnical Engineering, Graz, Austria*, pp 1-6.

Allotey, N & El Naggar, H. (2008). A numerical study into lateral cyclic non linear soil- pile response. *Canadian Geotechnical Journal. NRC Reserch Press*, 45, pp 1268-1281.

Anderson, J. B., Grajales, B & Townsend, F. C. (1999). Validation of P-y curves from pressuremeter and dilatometer test at Auburn, Alabama behaviour characteristics of residual soils. *Behavioral Characteristics of Residual Soils, American Society of Civil Engineers,* GSP (92), pp 77-87.

Anderson, J. B., Townsend, F. C & Grajales, B. (2003). Case history evaluation of laterally loaded piles. *Journal of Geotechnical and Geoenvironmental Engineering, American Society of Civil Engineers*, 129 (3), pp 187-196.

Ashour, M & Norris, G. (2000). Modelling lateral soil-pile response based on soil-pile intraction. *Journal of Geotechnical and Geoenvironmental Engineering, American Society of Civil Engineers*, 1265, pp 420-428.

Asik, M. Z & Vallaban, C. V. G. (2001). A simplified model for the analysis of machine foundations on non-saturated elastic and linear soil layer. *Journal of Computers and Structures*, 79, pp 2717-2726.

Atkinson, J. H. (2000). Non-linear soil stiffness in routine design. *Géotechnique*, 50 (5), pp 478-508.

Atkinson, J. H., Richardson, D & Stallebrass, S. E. (1990). Effect of recent stress history on the stiffness of overconsolidated soil. *Géotechnique*, 40 (4), pp 531-540.

Atkinson, J. H & Sallfors, G. (1991). Experimental determination of stress-strain-time characteristics in laboratory and in situ tests. *Proceedings of the 10th European Conference on Soil Mechanics and Foundation Engineering, Florence,* 3, pp 915-956.

Banerjee, P. K. (1978). Analysis of axially and laterally loaded pile groups. Developments in Soil Mechanics, Ed. C. R. Scott, London, Applied Science Publishers.

Banerjee, P. K & Davies, T. G. (1978). The behaviour of axially and laterally loaded single piles embedded in non-homogeneous soils. *Géotechnique,* 28(3), pp 309-326.

Banerjee, P. K., Sen, R & Prezzi, M. (1987). Static and dynamic analysis of axially and laterally loaded piles and pile groups. In Sayed, S. M. (Ed). *Geotechnical Modeling and Applications*, pp 211-243.

Barber, E. S. (1953). Discussion on paper by S. M. Gleser., *ASTM,* STP 154, pp 96-99.

Basack, S & Dey, S. (2011). Pile subjected to lateral cycle loading in sand. *Proceedings of the Indian Geotechnical Conference.* Paper No. N343.

Basack, S & Dey, S. (2012). Influence of relative pile-soil stiffness and load eccentricity on single pile response in sand under lateral cyclic loading. *Geotechnical and Geological Engineering, an International Journal, springer,* 30(2), pp 737-751.

Basu, D., Salgado, R & Prezzi, M. (2009). A continuum- based model for analysis of laterally loaded piles in layered soils. *Géotechnique,* 59 (2), pp 127-140.

Basu, D., Salgado, R & Prezzi, M. (2008). Analysis of laterally loaded piles in multilayered soil deposits. Publication FHWA/IN/JTRP-2008/23. Joint Transportation Research Program, Indiana. Department of Transportation and Purdue University, West Lafayette, Indiana. doi: 10.5703/1288284313454.

Basu, D., Prezzi, M., Salgado, R & Chakraborty, T. (2008). Settlement analysis of piles with rectangular cross sections in multi-layered soils. *Computers and Geotechnics Journal,* 35, pp 563-575.

Basu, D & Salgado, R. (2007). Elastic analysis of laterally loaded pile in multi-layered soil. *Journal of Geomechanics and Geoengineering*. 2 (3), pp 183-196.

Bell, R. W. (1991). The analysis of offshore foundations subjected to combined loading. MSc Dissertation, Oxford University.

Biarez, J & Hicher, P. Y. (1994). Elementry mechanics of soil behaviour. A A Balkema, Rotterdam, The Netherlands.

Bolton, M. D., Sun, H. W & Britto, A. M. (1993). Finite element analyses of bridge abutments of firm clay. *Computers and Geotechnics Journal*, 15, pp 22-245.

Bolton, M. D & Whittle, R. W. (1999). A non-linear elastic perfectly plastic analysis for plane strain undrained expansion. *Géotechnique*, 49 (1), pp 133-141.

Bowles, J. (1997). Foundation analysis and design. McGraw-Hill.

Bransby, M. F & Randolph, M. F. (1998). Combined loading of skirted foundations. *Géotechnique*, 48(5), pp 637- 655.

Bransby, M. F. & Springman, S . M. (1996). 3D finite element modelling of pile groups adjacent to surcharge loads. *Journal of Computers and Geotechnics*, 19 (4), pp 301-324.

Bransby, M. F. (1999). Selection of p–y curves for the design of single laterally loaded piles. *International Journal for Numerical and Analytical Methods in Geomechanics*, 23(15), pp 1909-1926.

Brinch Hansen, J. (1970). A revised and extended formula for bearing capacity. *Danish Geotechnical Institute Bulletin*, 28, pp 5-11.

Broms, B. B. (1981). Pre-cast Piling Practice. Thomas Telford, London.

Broms, B.B. (1964a). Lateral resistance of piles in cohesive soils. *Journal of the Soil Mechanics and Foundation Division, American Society of Civil Engineers*, 90(SM2), pp 27-63.

Broms, B.B. (1964b). Lateral resistance of piles in cohesionless soils. *Journal of the Soil Mechanics and Foundation Division, American Society of Civil. Engineers*, 90 (SM3), Proc. Paper 3825, May, pp 123-159.

Brown, D. A., Shie, C. & Kumar, M. (1989). P–y curves for laterally loaded piles derived from three-dimensional finite element model. *Proceeding of the 3rd Intternational Symposium on Numerical Models in Geomechanics (NUMOG III), Niagara Falls*, pp 683-690.

Brown, D. A., Reese, L. C. & O'Neill, M. W. (1987). Cyclic lateral loading of a large-scale pile group. *Journal of Geotechnical Engineering, American Society of Civil Engineers*, 113(11), pp 1326-1343.

Budhu, M & Davies, T. G. (1987). Analysis of laterally loaded piles in soft clay. *Journal of Geotechnical Engineering, American Society of Civil Engineers*, 114, pp 21-39.

Budhu, M & Davies, T. G. (1988). Nonlinear analysis of laterally loaded piles in cohesionless soil. *Canadian Geotechnical Journal*, 24, pp 289-296.

Burland, J. B. (1990). 30th Rankine lecture- on the compressibility and shear-strength of natural clays, *Géotechnique*, 40(3), ISSN: 0016-8505, pp 329-378.

Burland, J. B., Rampello, S., Georgiannou, V. N & Calabresi, G. (1996). A laboratory study of the strength of four stiff clays. *Géotechnique*, 46(3), pp 491-514.

Butterfield, R & Ticof, J. (1979). Design parameters for granular soils (discussion contribution). *Proceeding of the 7th International Conference Soil Mechanicand Foundation. Engineering*, Brighton, 4, pp 259-261.

Butterfield, R & Banerjee, P. K. (1971). The elastic analysis of compressible piles and pile groups. *Géotechnique*, 21 (1), pp 43-60.

Carter, J. P & Kulhawy, F.H. (1992). Analysis of laterally loaded shafts in rock. *Journal of Geotechnical Engineering*, 118(6), pp 839-855.

Comodromos, E. M & Papadopoulou, M. C. (2012). Response evaluation of horizontally loaded pile groups in clayey soils. *Géotechnique,* 62(4), pp 329-339.

Coulomb, C. A. (1773). Sur une application des r´egles de Maximis et Minimis a quelques probl´emes de statique relatifs ´a l'Architecture. Acad. Roy. des Sciences Memoires demath. et de physique par divers savans, 7, pp 343-382.

Cox, A. D., Eason, G & Hopkins, H. G. (1961). Axially symmetric plastic deformation in soils. *Proceedings of the Royal Society of Londo,*. A0 254, pp 1-45.

Cox, W. R., Reese, L. C & Grubbs, B. R. (1974). Field testing of laterally loaded piles in sand. *Journal of the Geotechnical Engineering Division American Society of Civil Engineers*, 120 (5), pp 816-837.

Das, Y. C & Sargand, M. H. (1999). Forced vibrations of laterally loaded piles. *International Jornal of solid and structures*, 36, pp 4975-4989.

Dasari, G. R. (1996). Modelling the variation of soil stiffness during sequential construction. PhD thesis, University of Cambridge.

Davies, M. P. (1987). Lateral loaded pile behaviour using in-situe testing method. M.Sc Thesis. University of British Columbia Canada.

Davis, E. H & Booker, J. R. (1973). The effect of increasing strength with depth on the bearing capacity of clays. *Géotechnique,* 23(4), pp 551-563.

Davisson, M. T & Robinson, K. E. (1965). Bending and buckling of partially embedded piles. *Proceeding of the 6th international conference soil mechanics and foundation engineering*, 2, pp 253-246.

Drnevich, V. P & Massarsch, K. R. (1979). Sample disturbance and stress-strain behavior. *ASCE Journal of Geotechnical Engineering Division*, 105 (GT9), pp 1001-1016.

Drucker, D. C., Greenberg, H. J & Prager, W. (1952). Extended limit design theorems for continuous media. *The Quarterly Journal of Mechanics and Applied Mathematics*, 9, pp 381-389.

Elhakim, A. F. (2005). Evaluation of shallow foundation displacements using soil small-strain stiffness. PhD Thesis. Georgia Institute of Technology. GA. USA.

El-Marsafawi, H., Han, Y. C & Novak, M. (1992). Dynamic experiments on two pile groups. *Journal of the Geotechnical Engineering Division, American Society of Civil Engineers*, 118 (4), pp 576-592.

Farrell, E. R., Coxon, P., Doff, D. H & Priedhomme, L. (1995a). The genesis of brown boulder clay of Dublin. *Quarterly Journal of Engineering Geology*, 28, pp 143-152.

Farrell, E. R., Bunni, N. G & Mulligan, J. (1988). The bearing capacity of Dublin black boulder clay. *Transactions of the Institution of Engineers of Ireland*, 112, pp 77-104.

Farrell, E., Lehane, B & Loopy, M. (1998). An instrumented driven piles in Dublin boulder clay. *Journal of the Geotechnical Engineering Division,* 131, pp 233-241.

Fleming, K., Weltman, A., Randolph, M & Elson, K. (2008). Piling Engineering, 2nd edition, Taylor & Francis. UK.

Fleming, K., Weltman, A., Randolph, M & Elson, K. (1985). Piling Engineering Surrey University Press, London.

Gavin, K., Cadogan, D & Towmey, L. (2008). Axial resistance of CFA piles in Dublin Boulder Clay. *Proceeding of the Institution of Civil Engineers, Geotechnical Engineering*, 161 (GE4), pp171-180.

Georgiadis, K., Sloan, S. W & Lyamin, A. V. (2013). Undrained limiting lateral soil pressure on a row of piles. *Journal of Computers and Geotechnics*, 54, pp 175-184.

Gieser, S. M. (1953). Lateral Load Tests on Vertical Fixed-head and Free-Head Piles. *ASTM*, STP 154, pp 75-93.

Gourvenec, S. (2007). Failure envelopes for offshore shallow foundations under general loading. *Géotechnique*, 57(9), pp 715-728.

Gourvenec, S & Barnett, S. (2011). Undrained failure envelope for skirted foundations under general loading . *Géotechnique*, 61(3), pp 263–270.

Gourvenec, S & Randolph, M. (2003). Effect of strength non-homogeneity on the shape of failure envelopes for combined loading of strip and circular foundations on clay. *Géotechnique*, 53(6), pp 575-586.

Gunn, M. J. (1992). The prediction of surface settlement profiles due to tunnelling. *Predictive soil mechanics, Proceedings of the Wroth Memorial Symposium, Oxford*, pp 304-316.

Gunn, M. J. (1993). The prediction of surface settlement profiles due to tunneling,Predictive soil mechanics, Houlsby and Schofield (eds.), *Proceedings of the Wroth Memorial Symposium, Thomas Telford, London*, pp 304-314.

Guo, W. D & Lee, F. H. (2001). Load transfer approach for laterally loaded piles. *International Journal for Numerical and Analytical Methods in Geomechanics*,25, pp 1101-1129.

Guo, W. D. (2006). On limiting force profile, slip depth and lateral pile response. *Journal of Computers and Geotechnics*, 33(1), pp 47-67.

Guo, W. D. (2009). Nonlinear response of laterally loaded piles and pile groups. *International Journal for Numerical and Analytical Methods in Geomechanics*, 33(7), pp 879-914.

Haldar, S & Sivakumar Babu, G. L. (2012). Response of vertically loaded pile in clay: aprobabilistic study. *Journal of Geotechnical and Geological Engineering*, 30(1), pp 187-196.

Haldar, S. & Sivakumar Babu, G. L. (2009). Design of laterally loaded piles in clay based on cone penetration test data: reliability approach. *Géotechnique*, *59(7)*, pp 593-607.

Hardin, B. O. (1978). The nature of the stress-strain behaviour of soils. *Earthquake Engineering and Soil Dynamics, American Society of Civil Engineers,* 1, pp 3-9.

Hardin, B. O & Drnevich, V. P. (1972). Shear modulus and damping in soils: design equations and curves. *Journal of the Soil Mechanics and Foundations Division, American Society of Civil Engineers,* 98(SM 7), pp 667-692.

Heidari, M., Jahanandish, M., El Naggar, M. H & Ghahramani, A. (2013). Nonlinear cyclic behaviour of laterally loaded pile in cohesive soil. *Canadian Geotechnical Journal*. doi: 10.1139/cgj-2013-0099.

Hibbeler, R. C. (2010). Engineering mechanics dynamics. New Jersy.USA, Person Prentice Hall.

Houlsby, G. T & Puzrin, A. M. (1999). The bearing capacity of a strip footing on clay under combined loading. *Proceedings of the Royal Society of London,* A 455, pp 893-916.

Houlsby, G. T & Wroth, C. P. (1983). Calculation of stresses on shallow penetrometers and footings. OUEL Report No. 1503/83, (Soil Mechanics Report No. SM041/83), Department of Engineering Science, University of Oxford.

Houlsby, G. T & Wroth, C. P. (1991). The variation of shear modulus of a clay with pressure and overconsolidation ratio. *Journal of Soils and Foundations,* 31 (3), pp 138-143.

Ilyas, T, Leung., C. F, Chow., Y. K & Budi, S. S. (2004). Centrifuge model study of laterally loaded pile group in clay. *Journal of Geotechnical and Geoenvironmental Engineering American Society of Civil Engineers,* 130 (3), pp 274-283.

Jardine, R. J., Symes, M. J & Burland, J. B. (1984). The measurement of soil stiffmessin the triaxial apparatus. *Géotechnique,* 34 (3), pp 323-340.

Kaynia, A. M. (1982). Dynamic behavior of pile groups. *Proceeding of the 2nd International conference on numerical method in offshore piling, Austen, Tx*, pp 509-532.

Kezdi, A. (1975). Pile foundations. Handbook of foundation Engineering, Winterkorn and Fang Eds, Van Nostrand, New York, pp 556-600.

Khemakhem, M., Chenaf, N., Garnier, J., Rault, G., Thorel & Dano, C. (2010). Static and cyclic lateral pile behaviour in clay. *Proceeding of the International Conference on Physical Modelling in Geotechnics, ICPMG, Zurich*, 2, pp 953-958.

Klar, A & Frydman, S. (2002). Three-dimensional analysis of lateral pile response using two-dimensional explicit numerical scheme. *Journal of Geotechnical and Geoenvironmental Engineering, American Society of Civil Engineers*, 128 (9), pp 775-784.

Koutsoftas, D. C & Ladd, C. C. (1985). Design strengths for an offshore clay. *Journal of the Soil Mechanics and Foundations Division, American Society of Civil Engineers*, 111 (3), pp 337-355.

Kulhawy, F. H & Mayne, P. W. (1990). Manual on estimating soil properties for foundation design, Report No. EL-6800, Electric Power Research Institute, Palo Alto, CA.

Lambe, T. W & Whitman, R. (1969). Soil mechanics. Joun Wiley & Sons, Inc., New Yourk. NY.

Lee, K. L. (1968). Buckling of partially embedded piles in sand. *Journal Soil Mechanics and Foundation Division American Society of Civil Engineers*, 94(SMl), pp 255-270.

Lee, J., Prezzi, M & Salgado, R. (2013). Influence of axial loads on the lateral capacity of instrumented steel model piles. *International Journal of Pavement Research and Technology*, 6(2), pp 80-85.

Lee, K-M & Xiao, Z. R. (1999). A new analytical model for settlement analysis of a single pile in multi-layered soil. *Journal of Soils and Foundations*, 39(5), pp 131-143

Lehane B. M., Jardine R. J & McCabe B, A. (2003). Experimental investigation of pile groups subjected to cyclic tension loading UK Health and Safety Executive, Research Report.

Lehane, B. M., Jardine, R. J & McCabe, B. A. (2003). Pile group tension cyclic loading:Field test programme at Kinnegar N. Ireland. Report.

Lehane, B. M., Phillips, D. M., Paul, T. S & Horkan, E. (1999). Instrumented piles subjected to combined vertical and lateral loads. *Proceeding of the Eurpian Conference on Soil Mechanins and Foundation Engineering, Amestrdam,* 2, pp 1145-1150.

Lehane B. M., McCabe B. A & Jardine R.J. (2003). One-way axial cyclic tension loading of driven piles in clay. *Proceedings of the BGA International Conference on Foundations, Dundee*, pp 493-406. doi: 10.1680/fiodap.32446.

Liu, Q., Deng, F& He, Y. (2014). Transverse seismic kinematics of single piles by a modified Vlasov model. *International Journal for Numerical and Analytical Methods in Geomechanics*. DOI: 10.1002/nag.2286.

Lo Presti, D. C. F., Jamiolkowski, M., Oronzo, P & Cavallaro. (1996). Rate and creep effect on the stiffness of soils. *Poceeding of the Measuring and Modeling Time Dependent Soil Behavior,* pp 166-180.

Long, M & Menkiti, C. O. (2007). Geotechnical properties of Dublin boulder clay. *Géotechnique,* 57 (7), pp 595-611.

Looby, M., Farrell, E & Lehan, B. (1995). Driven piles in boulder clay-design and practice. *Transaction of The Institution of Engineers of Ireland,* 119, pp 89-106. (IEI Civil Prize).

Maheshwari, B., Truman, K., Gould, P. & El Naggar, M. (2005). Three-dimensional nonlinear seismic analysis of single piles using finite element model: effects of plasticity of soil. *International Journal Geomechanics,* 5(1), pp 35-44.

Martin, C. M. & Houlsby, G. T. (2001). Combined loading of spudcan foundation on clay: numerical modelling. *Géotechnique,* 51(8), pp 687-699.

Masing, G. (1926). Eigenspannungen und verfestigung beim Messing. *Proceedings of the 2nd International Congress of Applied Mechanics, Zurich, Switzerland,* pp 332-335.

Matlock, H. & Reese, L. C., (1961), Foundation analysis of offshore pile supported structures., *Proceeding of the 5th International Conference Soil Mechanicand Foundation Engineering*, 2, pp 91-97.

Matlock, H. & Reese, L. C. (1960). Generalized solutions for laterally loaded piles. *Journal of Soil Mechanics and Foundation Division American Society of Civil Engineers*, 86 (SM5), pp 63-91.

Menaldi, J. L., Rofman, E & Sulem, A. (2001). Optimal control and partial differential equations in Honour of Professor Alain Bensoussan's 60th Birthday. *IOS Press, Amsterdam*, pp 414-423.

McCabe, B. A & Lehane, B. M. (2006). Behaviour of axially loaded pile groups driven in clayey silt. *Journal Geotechnical and Geoenvironmental Engineering, American Society of Civil Engineers*, 132 (3), pp 401-410.

McClelland, B & Focht, J. A. (1956). Soil modulus for laterally loaded piles. *Journal of Soil Mechanics and Foundation Division American Society of Civil Engineers*, 82 (SM4), pp 1049-1063.

McGann, C. R., Arduino, P & Mackenzie-Helnwein, P. (2011). Simplified procedure to account for a weaker soil layer in lateral load analysis of single piles. *Journal of Geotechnical and Geoenvironmental Engineering*, 138(9), pp 1129-1137.

McVay, M. C., Shang, T. I & Casper, R. (1996). Centrifuge testing of fixed-head laterally loaded battered and plumb pile groups in sand. *Geotechnical Testing Journal*, 19(1), pp 41-50.

Meyerhof, G. G. (1951). The ultimate bearing capacity of foundations. *Géotechnique*, 2 (4), pp 301-332.

Meyerhof, G. G. (1953). The bearing capacity of foundations under eccentric and inclined loads. *Proceeding of the 3rd International Conference Soil Mechanicand Foundation. Engineering, Zurich*, 1, pp 440-445.

Mindlin, R. D. (1936). Force at a point in the interior of a semi-infinite solid. *Journal of Physics*. 7, pp 195-202.

Moller, I. F & Christiansen, T. (2011). Laterally loaded monopile in dry and saturated sand - static and cyclic loading experimental and numerical Studies. MSC. Aalborg University Esbjerg.

Ng, C. W. W & Zhang, L.M. (2001). Three-dimensional analysis of performance of laterally loaded sleeved piles in sloping ground. *Journal of Geotechnical and Geoenvironmental Engineering, American Society of Civil Engineers*, 127 (6), pp 499-509.

Osman, A. S., Yeow, H. C & Bolton, M. D. (2004). Estimation of undrained settlement of shallow foundations on London clay. *Proceedings of 2nd international conference on structures and foundations failure, Singapore*, 2-4 August, pp 443-454.

Osman, A. S., White, D. J., Britto, A. M & Bolton, M. D (2007). Simple prediction of the undrained displacement of a circular surface foundation on non-linear soil. *Géotechnique*, 57 (9), pp 729-737.

Osman, A. S., White, D. J., Britto A. M & Bolton, M. D. (2007). Non-linear displacement of shallow foundations on undrained clay. *Géotechnique*, 57(9), pp 729-737.

Phillips, D. T. P & Lehane, B. M. (2004). The response of driven single piles subjected to combined loads. *Proceedings of the Fifth International Conference on Case Histories Geotechnical Engineering*. New York, paper No 1.17.

Phillips, D. M & Lehane, B. M. (1998). The lateral capacity of an instrumented pile in glacial till. *Proceeding of the VII International Conference on Piling and Deep foundations, Vienna*, 5, pp 131-136.

Potts, M, D & Zdravkovic, L. (1999). Finite element analysis in geotechnical engineering theory. Thomas Telford. London. UK.

Poulos, H. G. (1971 b). Behavior of laterally loaded piles: II pile groups. *Journal of the Soil Mechanics and Foundation Division, American Society of Civil Engineers*, 97(SM5), pp 733-751.

Poulos, H. G. (1980). Settlement of single piles in non-homogeneous soil. *Journal of Geotechnical Engineering devision, American Society of Civil Engineers,* 105(5), pp 627-641.

Poulos, H. G & Davis, E. H. (1968). The settlement behavior of single axially loaded incompressible piles and piers. *Géotechnique,* 18(3), pp 351-371.

Poulos, H. G. (1971a). Behaviour of laterally loaded piles: I-Single Piles. *Journal of the Soil Mechanics and Foundation Division, American Society of Civil Engineers,* 97(SM5), pp 711-731.

Poulos, H. G. (1971c). Discussion on load-deformation mechanism for bored piles. by R. D. Ellison, E. D'Appolonia, & G. R. *Thiers. Journal of the Soil Mechanics and Foundation Division, American Society of Civil Engineers*, 97(SM12), pp 881-879

Poulos, H. G. (1974). Analysis of pile groups subjected to vertical and horizontal loads. *Austalian Geomechanics Journal,* G4(1), pp 26-32.

Poulos, H. G. (1980). An approach for the analysis of offshore pile groups. *Proceedings of the International Conference Numerical methods in offshore piling, London,* pp 119-126.

Poulos, H. G & Davies, T. G. (1980). Pile foundation analysis and design. W. S. Inc.

Puzrin, a., Frydman & Talesnick, M. (1995). Normalized nondegrading behavior of soft clay under cyclic simple shear loading. *Journal of Geotechnical engineering*, (121), pp 836-843.

Pyke, R. (1979). Nonlinear soil models for irregular cyclic loading. *Journal of Geotechnical Engineering Division, American Society of Civil. Engineers*, 105 (6), pp 715-726.

Randolph, M. F. (1998). Modelling of offshore foundations part 2: Anchoring Systems, *Australian Geomechanics*, 33(3), pp 3-15.

Randolph, M. F. (1981). The response of flexible piles to lateral loading. *Géotechnique,* 31(2), pp 247-259.

Randolph, M.F & Wroth, C. P. (1978). Analysis of vertical deformation of vertically loaded piles. *Journal of Geotechnical Engineering, American Society of Civil Engineers,*104(12), pp1465-1488.

Randolph, M. F & Houlsby, G. T. (1984). The limiting pressure on a circular pile loaded laterally in cohesive soil. *Géotechnique*, 43(4), pp 613-623.

Randolph, M. F. & Puzrin, A. M. (2003). Upper bound limit analysis of circular foundations on clay under general loading. *Géotechnique*, 53(9), pp 785-796.

Reese, L. C. and W. F. Van Impe (2001). Single piles and pile groups under lateral loading. London,UK, Taylor&Francis Group Plc.

Reese, L. C. (1971). The analysis of piles under lateral loading. *Proceedings of the Symposium on Ineraction of of Structure and Foundoundation, University of Birmingham, Birmingham, England,* pp 206-218.

Richart, F. E., Hall, J. R & Woods, R. D. (1970). Vibration of soils and foundations. Englewood Cliffs: Prentice-Hall.

Russo, G. (2004). Full-scale load test on instrumented micropiles. *Proceedings of the Institution of Civil Engineers: Geotechnical Engineering*, 157(3), pp 127-135.

Sadd, M. H. (2005). Elasticity theory, applications and numerics Oxford. UK. Elsevier.

Salencon, J. & Pecker, A. (1995a). Ultimate bearing capacity of shallow foundations under inclined and eccentric loads. Part I: Purely cohesive soil. *European Journal of Mechanics,* A 14(3), pp 349-375.

Salencon, J. & Pecker, A. (1995b). Ultimate bearing capacity of shallow foundations under inclined and eccentric loads. Part II: Purely cohesive soil without tensile strength. *European Journal of Mechanics*, A 14(3), pp 377-396.

Salgado, R., Prezzi, M & Seo, H. (2007). Advanced modeling tools for the analysis of axially loaded piles, *Proceedings of the International Workshop on Recent Advances in Deep Foundations (IWDPF07).* Ed. by Kikuchi, Otani, Kimura & Morikawa.

Salgado, R., Tehrani, F. S., Prezzi, M. (2014). Analysis of laterally loaded pile groups in multi-layered elastic soil. *Journal of Computers and Geotechnics*, 62, pp 136-153.

Sen, R., Davies, T. G & Banerjee, P. K. (1985). Dynamic behavior of axially and laterally loaded piles and pile groups embedded in inhomogeneous soil. *Journal of Earthquake Enginerring and Structural Dynamics,* 13(1), pp 53-65.

Seo, H., Basu, D., Prezzi, M & Salgado, R. (2009). Load-settlement response of rectangular and Ccircular piles in multilayered soil. *Journal of Geotechnical and Geoenvironmental Engineering*, 135 (3), pp 420-430.

Seo, H. & Prezzi, M. (2007). Analytical solutions for a vertically loaded pile in multilayered soil. *Geomechanics and Geoengineering An International Journal,* 2 (1), pp 51-60.

Shield, R. T. (1955). On the plastic flow of metals under conditions of axial symmetry. *Proceedings of the Royal Society of London*. A 233, pp 267-287.

Stallebrass, S. E. (1990). The effect of recent stress history on the deformation of overconsolidated. PhD Thesis, City of University.

Stallebrass, S. E & Taylor, R. N. (1997). The development and evaluation of constitutive model for the prediction of ground movements in overconsolidated clay. *Géotechnique*, 47(2), pp 235-253.

Sun, K. (1994). A numerical for laterally loaded piles. *Journal* of *Computer and Geotechnics*, 16, pp 263-289.

Taiebat, H. A. & Carter, J. P. (2000). Numerical studies of the bearing capacity of shallow foundations on cohesive soil subjected to combined loading. *Géotechnique,* 50(4), pp 409-418.

Taiebat, H. A. & Carter, J. P. (2002a). A failure surface for the bearing capacity of circular footings on saturated clays. *Proceedings of the 8th International Symposium NUMOG VIII, Rome*, pp 457-462.

Taiebat, H. A. & Carter, J. P. (2002b). Bearing capacity of strip and circular foundations on undrained clay subjected to eccentric loads. *Géotechnique*, 52(1), pp 61-64.

Taiebat, H. A & Carter, J. P. (2010). A failure surface for circular footings on cohesive soils. *Géotechnique*, 60(4), pp 265-273.

Timoshenko, S.P. & Goodier, J.N. (1987). Theory of elasticity. 3rd edition, McGraw- Hill.

Tresca, H. (1869). Mémoire sur le poinçonnage et la théorie mécanique de la deformation References des métaux, Comptes rendus hebdomadaires des Séances de l'Académie des Sciences, Paris, 68, pp 1197-1201.

Trochanis, A.M., Bielak, J. & Christiano, P. (1991). Three-dimensional nonlinear study of piles. *Journal of Geotechnical Engineering, American Society of Civil Engineers*, 117 (3), pp 429-447.

Ukritchon, B., Whittle, A. J. & Sloan, S. W. (1998). Undrained limit analysis for combined loading of strip footings on clay. *Journal of Geotechnical and Geoenvironmental Engineering, American Society of Civil Engineers,* 124(3), pp 265-276.

Vallabhan, C. V. G. & Das, Y. C. (1991a). Modified Vlasov model for beams on elastic foundations. *Journal of Geotechnical Engineering, American Society of Civil Engineers,* 117(6), pp 956-966.

Vallabhan, C.V.G. & Mustafa, G. (1996). A new model for the analysis of settlement of drilled piers. *International Journal of Numerical and Analytical Methods in Geomechanics*, 20, pp 143-152.

Vardanega, P. J. & Bolton, M. D. (2011b). Strength mobilization in clays and silts. *Canadian Geotechnical Journal,* 48(10) , pp 1485-1503.

Verruijt, A. & Kooijman, P. A. (1989). Laterally Loaded Piles in a Layered Elastic Medium. *Géotechnique*, 39(1), pp 39-46.

Vesic, A. S. (1963). Bearing capacity of deep foundation in sand, Highway Research Record, *National Academy of Sciences, National Research Council*, 39, pp 113-151.

Vlasov, V. Z & Leont'ev, N. N. (1966). Beams, plates and shells on elastic foundations. Jerusalem: Israel Program for Scientific Translations.

Von Mises, R. (1913). Mechanik der festen Körper im plastisch-deformablen Zustand. Narchrichten von der Königlichen Gesellschaft der Wissenschaften zu Göttingen, Mathematisch-physikalische Klasses, pp 582-592.

Vucetic, M. (1994). Cyclic threshold shear strains in soils. *Journal of Geotechnical and Geoenvironmental Engineering*, 120 (12), pp 2208-2228.

Winkler, E. (1867). Die Lehre Von Elastizitat und Festigkeit. 1st Edn., H. Dominicus, Prague.

Wood, D. M. (1990). Soil behaviour and critical state soil mechanics. Cambridge unversity press.

Wood, D. M. (2004). Geotechnical modelling. Spon Press. Tylor & Francis Group.

Wood. L. A. (1979). A program for the analysis of laterally loaded pile Groups, Sheet Piles and Diaphragm Walls., *Proceedingsof the 1st International Conference on Engineering Software, Southampton University*, 1.4, pp 614-632.

Yamashita, S., Hori, T. & Suzuki, T. (2003). Effects of fabric anisotropy and stress condition on small strain stiffness of sands. *Proceedings of the Deformation Characteristics of Geomaterials*, 1, pp 187-194. (Proc. Lyon), Swets and Zeitlinger, Lisse.

Zhang, L., Ernst, H & Einstein, H. H. (2000). Nonlinear analysis of laterally loaded rock-socketed shafts. *Journal of Geotechnical and Geoenvironmental Engineering, American Society of Civil Engineers*, 126 (11) pp 955-968.